Mass spectrometric studies of the biological fate of platinum-based drugs and selenium supplementation in cancer chemotherapy

Sarah Elizabeth Taylor

Doctoral Thesis

Submitted in Partial Fulfilment of the Requirements for the Award of Doctor of Philosophy of Loughborough University

“If we knew what it was we were doing, it would not be called research, would it?”

Albert Einstein

Abstract

Platinum-based drugs are an important group of alkylating-like agents which are used in cancer chemotherapy treatment. Cisplatin and oxaliplatin in particular are still commonly used today and are the focus of this thesis. As with most chemotherapy drugs, the efficacy of these drugs are limited by toxicity as well as tumour resistance, and therefore by increasing our understanding of these areas it is hoped to one day achieve personalised chemotherapy.

The use of ICP-MS in the study of bio-sciences is still relatively new, however it has the ability to provide robust, fast and accurate methods for the quantification of platinum in biological samples. The research presented here utilised mass spectrometry in the study of the formation of Pt-DNA adducts in the clinical samples, the binding of oxaliplatin to short peptides and the effect of selenium supplementation on oxaliplatin in colorectal cancer cell lines.

A comparison in the number of Pt-DNA adducts in saliva and leukocyte samples obtained from patients undergoing Pt-based chemotherapy demonstrated a lack of correlation between the two sample types. Samples were taken pre- and post-treatment and analysed via SF-ICP-MS and significant inter-patient variability was observed as expected. In both leukocyte and saliva samples, not only was Pt from previous chemotherapy cycles observed, but Pt was detected in the DNA in both sample types 1 hour after treatment. However a lack of correlation between platinum levels seen in the blood and saliva, combined with unexpected difficulties obtaining patient adherence to the saliva sampling protocol, indicated that saliva does not at present offer a reliable alternative to leukocytes for this assay.

The binding of oxaliplatin to short nitrogen and sulfur rich peptides was investigated. Platinum binding to the peptides was observed and no significant differences in the level of binding were observed between the range of N and S rich peptides studied in this investigation. Partly due to the inability to reproduce biological conditions in this study, oxaliplatin was observed as a whole molecule, and furthermore dimers and multimers were also observed.

The effect of selenium supplementation on the total cellular uptake of platinum was investigated in cultured cells via ICP-MS and LA-ICP-MS. It was observed that selenium decreased the amount of Pt taken up by the cancer cells. This was seen in analysis of populations of cells as well as by single cell analysis. Furthermore, while problems were encountered measuring selenium in subcellular experiments, the effect of selenium on the subcellular distribution of platinum as well as the number of Pt-DNA adducts could be determined.

Key Words

Pt-based drugs, oxaliplatin, cisplatin, Pt-DNA Adducts, platinum, selenium, MSA, clinical samples, cell culture, ICP-MS, ESI-MS.

Acknowledgments

I would like to thank Loughborough University for providing me with the funding to be able to carry out this research, and special thanks go to Professor Barry Sharp and Dr Helen Reid for giving me the opportunity to work with them and for guiding me through my PhD. I couldn't have got here without your support and guidance.

I would also like to acknowledge and express my gratitude to Dr George D. D. Jones, Dr Anne Thomas, Dr Joanna Wood, Dr Karen Bowman and all of my collaborators at the University of Leicester and the Leicester Royal Infirmary, Dr Tamer Shoeib at the American University in Cairo and to Dr Aref Zayed, Dr John Pugh, Dr Claire Camp and Carl Cooper who all contributed to this work. A lot of this would not have been possible without you.

I'd also like to thank some of the staff in the Department who have helped over the years, in particular Mark Weller and Trevor Brown for your technical knowhow. And a special mention to David Hinds (Thermo) for all the ICP-MS advice over the years.

On a personal level, I would like to dedicate this thesis in particular to my mother, Laura-Jane Taylor (1956-2008), for everything she did for me and without whom I wouldn't be the person I am today. You are missed every day, and I hope that I have made you proud.

My deepest thanks also go to my dad, for his unwavering support and belief in me over the years, and for the endless supply of tea during my writing up to keep me going. Thank you for everything you have done for me. To Derek and Lynette and all of my friends, thank you for your support.

I would also like to express my thanks to all my friends in the department, your friendships have kept me going these last few years. In particular I'd like to thank Dave and Pez for their all of their help and for all the laughs, good times and trips to Nandos. To Grant and Tharwat for your friendships and the many hours of entertainment you provided me. Special thanks to Amy Managh, whose interesting baking and unique insights into just about everything has kept me sane and amused over the last 3 years. To the second floor analytical groups, in particular Caitlyn, Neil, Aadi and Liam for the many hours of entertainment at lunch and the many drinks. And finally, to Darren for being there and keeping me going through this final phase of my PhD.

Thank you to you all.

Table of Contents

Table of Figures

List of Tables

Glossary

2D	Two dimensional
5-FU	5-Fluorouracil
AAS	Atomic absorption spectroscopy
APCI	Atmospheric pressure chemical ionisation
APPI	Atmospheric pressure photo ionisation
Bev	Bevacizumab
CAM	Complementary and alternative medicine
CID	Collision induced dissociation
Cis/etop	Cisplatin and etopside
CisPt	Cisplatin
CPS	Counts per second
CRM	Charge residue model
ctDNA	Calf thymus deoxyribonucleic acid
Da	Daltons
DACH	Diaminocyclohexane
DF	Dilution factor
DI	Deionised
DNA	Deoxyribonucleic acid
ECX	Epirubicin, cisplatin and capecitabine
ELISA	Enzyme-linked immunosorbent assay
EOX	Epirubicin, oxaliplatin and capecitabine
ESA	Electrostatic analyser
ESI	Electrospray ionisation
ESI-MS	Electrospray ionisation mass spectrometry
Eu	Europium
FACS	Fluorescence-activated cell sorting
FCS	Foetal calf serum
FDA	Food and drug administration
FOLFOX	5-fluorouracil, folinic acid and oxaliplatin
GSH	Glutathione
HR	High resolution
HR-ICP-MS	High resolution inductively coupled plasma mass spectrometry
ICP-MS	Inductively coupled plasma mass spectrometry

IEM	Ion evaporation model
LA	Laser ablation
LA-ICP-MS	Laser ablation inductively coupled plasma mass spectrometry
LIT	Linear ion trap
LR	Low resolution
MR	Medium resolution
MS	Mass spectrometry
MSA	Methaneseleninic acid
MSC	Methylselenocysteine
m/z	Mass to charge ratio
N	Nitrogen
OxPt	Oxaliplatin
P	Phosphorus
PBS	Phosphate buffered saline
ppb	Parts per billion
ppm	Parts per million
ppt	Parts per trillion
Pt	Platinum
Pt-DNA adduct	Platinum-based drug adduct with DNA
QMS	Quadrupole mass spectrometers
RF	Radio frequency
RSD	Relative standard deviation
S	Sulfur
Se	Selenium
SEM	Secondary electron multiplier
SeMet	Selenomethionine
SIM	Single ion monitoring
SF-ICP-MS	Sector-field inductively coupled plasma mass spectrometry
TOFMS	Time of flight mass spectrometer
WBC	White blood cell

1. Introduction

1.1 Objectives

It is estimated that cancer now affects more than one in three people during the course of their lifetime.[1] Such a prevalent disease is therefore naturally the subject of extensive research worldwide with the aim of both preventing and curing the disease. Platinum-based anti-cancer drugs are among the most widely used in cancer chemotherapy treatments. While very effective, they are not without their limitations, including extensive side effects and the development of drug resistance. This thesis focuses on the use of platinum-based anti-cancer drugs, specifically oxaliplatin and cisplatin, and their interaction with DNA and proteins within the body.

Three main objectives were set out to further our understanding on the way Pt-based drugs work. The first of these objectives was to investigate if the use of saliva was a viable alternative to blood for the investigation of Pt-DNA adducts in clinical patient samples. The work performed to achieve this is presented in Chapter 2. In this work, a method previously utilised to measure Pt-DNA adduct levels in patient leukocyte samples was modified and adapted for the use in both blood leukocyte and saliva samples, with the aim of providing an alternative, more patient friendly and non-intrusive sampling technique for patients receiving Pt-based chemotherapy with the ultimate aim of providing clinicians with up-to date analysis of the level of adduct formation in patients.

The second objective was to investigate the interaction of oxaliplatin with proteins found in the cytosol. It has been established that only a small amount (approximately 1%) of the Pt-drug given to a patient reaches the ultimate physiological target, the DNA, and is it theorised there are multiple 'platinum sinks' within the cell where platinum binds, thus potentially reducing the amount reaching the DNA.[2–4] While the nuclear fraction within a cell only receives around 9% of the platinum, around 70% is found within the cytosol of the cell, making the cytosolic proteins very likely binding sites for the platinum[5]. In this work it was hoped to discover if there were potentially binding sites on proteins where binding of platinum was favoured over others, or if the binding was more uniform. The work carried out to achieve this objective is described in Chapter 3.

The third objective was to investigate the effect of selenium on oxaliplatin, as detailed in Chapter 4. While there is some evidence to suggest that selenium has some cancer-preventative properties at high enough concentrations, there has only been limited research into the effect

that selenium has on Pt-based drugs, despite many cancer patients taking herbal and vitamin supplements during treatment. In this work the effect on the level of Pt-DNA adducts was investigated caused by the presence of selenium at different concentrations, as well as the effect on the sub-cellular distribution of both platinum and selenium, and finally a competitive binding study was performed using a ubiquitous cytosolic protein.

In the subsequent sections of this chapter, the history, use and importance of Pt-based drugs and selenium supplementation will be explored in more detail, alongside a review of the main instrumentation used in the study of these areas during this research primarily sector-field inductively coupled plasma mass spectrometry (SF-ICP-MS) and electrospray ionisation linear ion trap mass spectrometry.

1.2 Cancer Chemotherapy

Cancer is, by definition, the uncontrolled growth of abnormal cells within the human body with the ability to migrate and invade other tissues around the body.[6] There are currently three main forms of treatment for cancer, chemotherapy, radiotherapy and surgery, which are often used in conjunction with each other. And while over half of cancer patients currently receive chemotherapy treatment, the exact treatment a patient will receive is determined on an individual basis.

Cancer chemotherapy works by killing cells by the use of chemicals which interfere and interrupt the process of cell division with the aim of causing cell apoptosis. By destroying the cancerous cells the aim is not only to stop the growth of the tumour but also to prevent metastasis (the spread of cancer from where it started (primary site) to other parts of the body). While in many cases it can be very effective, cancer chemotherapy is not without its problems. One of the primary drawbacks is the extensive range of side effects frequently experienced by patients, often caused by chemotherapy damaging non-cancerous cells as well as the cancerous, resulting in side effects that range from nausea, neuropathy, neutropenia and hair loss.[7] As the level of side effects experienced by patients can result in lowering the dosage for the next treatment, or even in many cases the termination of treatment due to the severity of the side effects, one of the primary aims of ongoing cancer research worldwide is the development of new more effective chemotherapy drugs which kill less healthy cells and which will induce minimal side effects.

Chemotherapy can be prescribed to patients either as part of a curative or a palliative regime. While the curative aims at ridding the patient of all cancerous cells so that the patient can be considered to be in remission, palliative care is designed to help to address symptom management or to extend life expectancy without significantly reducing or totally removing the cancer already present. As previously mentioned different treatment approaches are often used in conjunction with one another. Adjuvant chemotherapy is when chemotherapy is given after surgery has been performed to remove the tumour with the aim of killing any remaining cancerous cells to prevent cancer reoccurrence.

It is difficult to date the first treatment of cancer with drugs as herbal medicines and other concoctions have been used in the past. The first chemotherapy drugs were originally based on mustard gas after it was observed that soldiers exposed to it died due to bone marrow damage and as a result Nitrogen mustard, an alkylating agent, was first used in 1942 to treat lymphoma patients with limited success.[7] Since then the understanding of the mechanisms and mode of

action of chemotherapy drugs has increased enormously and has resulted in the development of many highly effective chemotherapy drugs.

1.2.1 Platinum-based chemotherapy drugs

1.2.1.1 History of platinum-based chemotherapy drugs

Platinum-based chemotherapy drugs are an important type of anti-cancer drug as they are currently used in about half of all chemotherapy treatments.[8] The possibility of using platinum-based complexes in cancer chemotherapy was first uncovered by Dr Barnett Rosenberg at Michigan State University in the late 1960's. He made the discovery by accident when investigating the effect of applying a magnetic or electric field on cell division with the use of platinum electrodes (which were believed to be inert) and observed some unexpected electrolysis products. These electrolysis products were analysed and found to contain two active complexes; the neutral *cis*-isomer $[Pt(II)(NH_3)_2Cl_2]$ (cisplatin) and a platinum(IV) analogue, *cis*-diammineteterachloroplatinum(IV). In 1968 cisplatin (*cis*-diamminedichloroplatinum(II)) was observed to cause tumour regression in mice and by 1971 was used to treat patients even though it wasn't approved by the US Food and Drug Administration (FDA) until 1978.[7,9] Since then it has become of the most widely used cancer chemotherapy drugs worldwide.

The discovery of cisplatin resulted in a great deal of research into platinum-based drugs for use in cancer chemotherapy and as a result thousands of platinum complexes were synthesised with the aim of creating a drug which was safe for patients and which would hopefully reduce the severity of the nephrotoxicity (damage to kidneys) caused by cisplatin. While thousands of platinum derived complexes have been synthesised, to date, only two have been approved for use on patients worldwide; carboplatin (which was introduced as a second generation analogue of cisplatin in the 1980's) and oxaliplatin. Oxaliplatin (see Figure 1), which is one of the primary drugs of interest in the work presented in this thesis, consists of a platinum centre which is bound to two bidentate ligands, a diaminocyclohexane (DACH) ligand and an oxalate ion. The structures of these platinum-based drugs can be seen in Figure 1, which also details some of the other platinum-based drugs which made some progression in clinical testing.

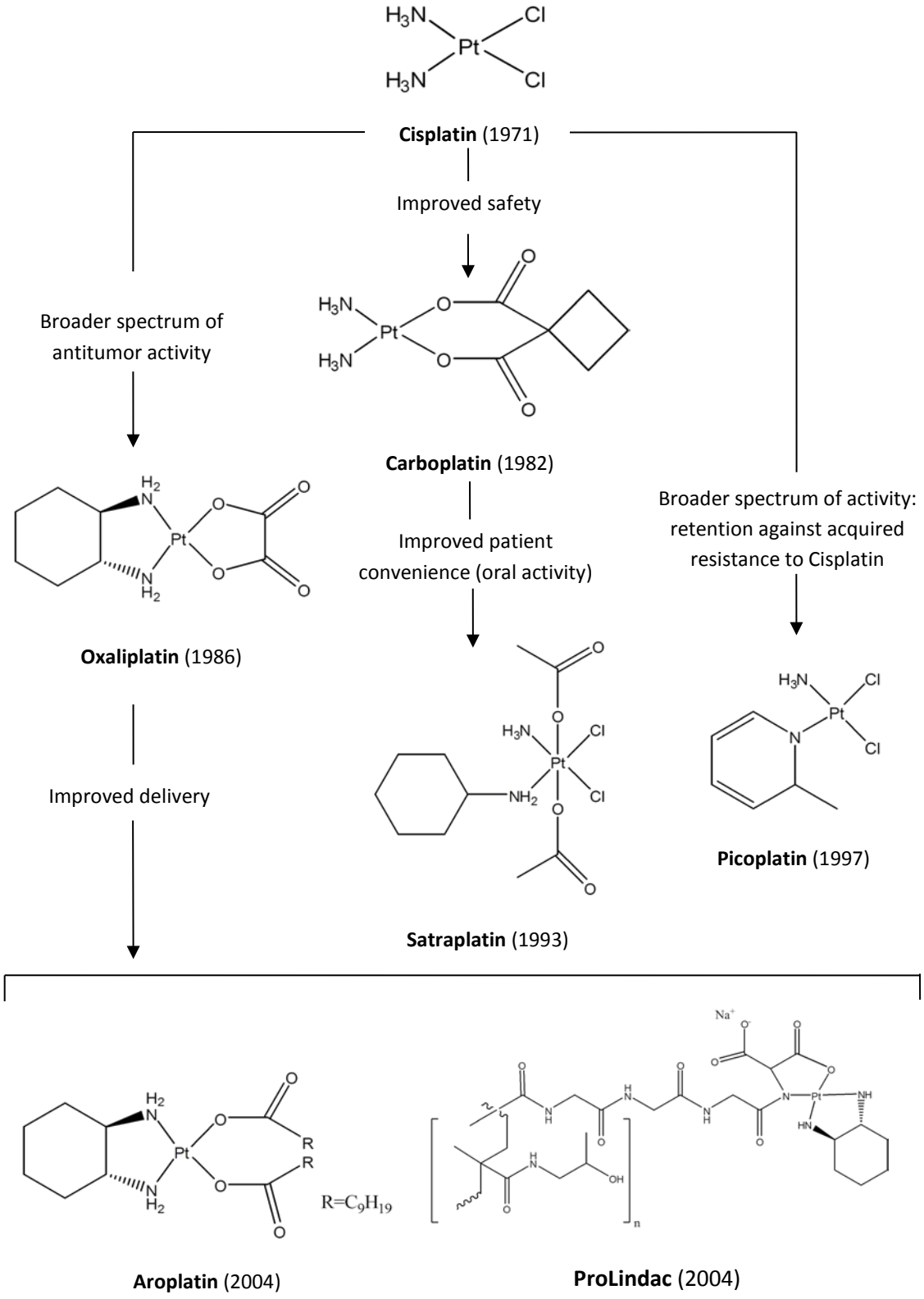

* Note: The dates provided are the dates when each drug was first administered to patients.

Figure 1 - The development stages of platinum-based chemotherapy drugs. Used with permission. [9]

1.2.1.2 Clinical use of platinum-based chemotherapy drugs

While some of the drugs detailed in the previous section have now been available for decades they are still commonly used today. Cisplatin is still commonly used in the treatment of ovarian, testicular, cervical, head, neck and lung cancers, while oxaliplatin is used in the treatment of colorectal cancer. [10–14] Combination treatments, such as FOLFOX (a combination of Folinic acid, 5-fluorouracil and oxaliplatin), have increased the efficacy and reduced some side effects, and are now common place.

In clinics, dosage of such drugs are calculated based on two factors; body surface area and kidney function. Treatment tends to be given over a number of cycles (as determined by research and clinical trials for each drug combination regime) which are typically two to four weeks apart. By spacing the treatment cycles out this allows time for the normal healthy cells to recover. Currently oxaliplatin can be administered up to 85 mg/m^2 on a two weekly cycle, or if a three weekly cycle is used dosage can be increased to 130 mg/m^2. Cisplatin is typically administered every three to four weeks at a dosage level between 50 and 70 mg/m^2.[15–17]

Currently dosage levels are calculated per person based on their body surface area and kidney function, with the ability of adjusting the dose between chemotherapy cycles, much of the current research is aimed at identifying a means of creating a more personalised chemotherapy regime. The need for this has been known for a long time due to large inter-patient variability in both response to treatment as well as toxicities being observed in multiple studies; however it is only now that the possibility of individualised chemotherapy treatments is truly being investigated.

1.2.1.3 Mode of action

In recent years the understanding of the mechanism of action of platinum-based anti-cancer drugs has grown, however there is still some uncertainty. Both cisplatin and oxaliplatin work by acting as complexing agents for DNA, and the generally accepted mode of action is the covalent binding of the drug to the DNA forming Pt-DNA adducts, which in turn distort the helical structure of the DNA signalling cell cycle arrest and causing cell apoptosis if the level of damage is too great to repair.[9,16]

Cisplatin, for example, is taken up by the cells by passive diffusion and copper transporters. Cisplatin is introduced into the body intravenously before entering the cells. In order to become activated, a neutral cisplatin molecule will become aquated upon entering a cell via the loss of two chlorine atoms (see Figure 2). This hydrolysis, and activation, of cisplatin does not happen

easily in the blood stream due to high concentration of chloride ions, however it is easily performed within the cell due to lower concentrations (below 100 mM).[5,18,19]

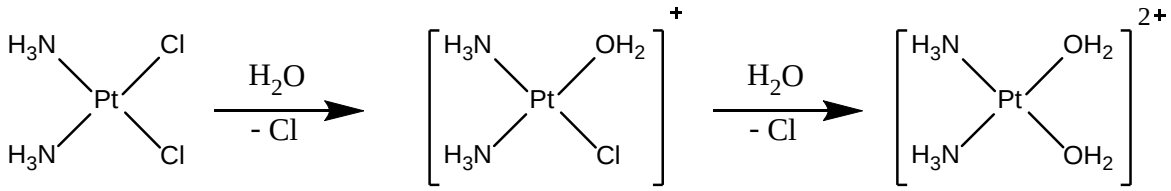

Figure 2 - Hydrolysis of cisplatin

Once inside the cell the activated cisplatin can bind to a multitude of ligands found within the cell. While the primary physiological target is the DNA, the binding to other ligands goes some way in accounting for the limited amount of platinum which reaches the DNA to form Pt-DNA adducts. When binding to DNA, cisplatin binds primarily to the N7 position of the imidazole ring of purine bases, primarily guanine (G) and adenine (A) to a lesser extent.[9] This binding can occur as either mono- or bi-functional adducts (i.e. via one or both leaving groups).[20] Studies have shown that the vast majority of the adducts formed are intra-strand crosslinks (adducts) between adjacent base pairs on the same DNA strand (1,2 intra-strand adducts), with around 60-65% of the total adducts formed between adjacent G-G base pairs, while A-G intra-strand adducts make up about 20-25% of the total adduct formed. Other less common adducts recorded include the 1,3 intra-strand G-G adduct (~2%), monofunctional guanine adduct (~2%) and G-G inter-strand adduct (~2%).[9] It is these crosslinks/adducts that distort the structure of the DNA which result in cell cycle arrest, and if the repair cannot be completed due to high enough levels of damage, cell apoptosis occurs.[21,22] The primary adducts are summarised in Figure 3.

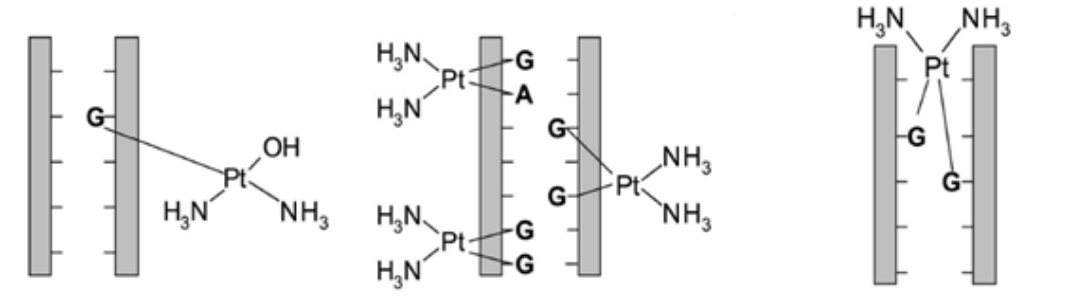

Monoadduct

Intrastrand crosslinks (1,2-d(GG), 1,2-d(AG), 1,3(GG)

Interstrand crosslink

Figure 3 - Cisplatin adduct formation with DNA. Used with permission. [10]

Oxaliplatin works in a very similar way, primarily differing in the loss of an oxalate group before becoming aquated.[10,23,24] As it is inherently less stable at high chloride concentrations (such as that found in the blood) when compared to cisplatin, oxaliplatin first undergoes a ligand exchange where the oxalate ligand is replaced by two chloride ions forming [Pt(DACH)(Cl_2)]. It is this complex which then penetrates the cell to become hydrolysed forming $[Pt(DACH)(H_2O)_2]^{2+}$, which in turn binds with the DNA to form adducts. While there is some evidence suggesting that oxaliplatin forms fewer adducts than cisplatin, it was found that it distorted the DNA strands to a greater degree thus resulting in it being equally as potent and effective.[10]

1.2.1.4 Side effects

Cisplatin, while being the oldest of the platinum-based chemotherapy drugs, is still commonly used today, particularly for the treatment of testicular and ovarian cancers, as well as cancers of the neck and lung. However, it has two primary limitations; drug toxicity and tumour resistance. Drug toxicity can be defined as the adverse effects experienced by patients undergoing a drug treatment. The three most common side effects reported by patients undergoing cisplatin chemotherapy are nephrotoxicity (kidney damage), ototoxicity (problems with the ear and hearing) and neuropathy (nerve damage, often experienced as a numbness), with are experienced by approximately 20-41%, 23-50% and 30-62% of patients respectively for each of the side effects.[10] Due to the severe side effects as detailed above, cisplatin is administered in small doses to try and limit such toxicities.[17]

One of the primary advantages of carboplatin over cisplatin was the significant reduction in nephrotoxicity reported. Furthermore, reductions in number of patients experiencing ototoxicity (around 1% of patients) as well as neuropathy (6-25%) were also reported.[10] However, an increase in reported cases of myelosuppression (decrease in bone marrow activity often leading to neutropenia) was higher than with cisplatin; a reported 20-40% at the standard dose, but increasing up to 90% at higher doses.

The primary side effect experienced with oxaliplatin is neuropathy, with the other side effects detailed above being experienced only rarely. While neuropathy is experienced in around 95% of all patients immediately after treatment, it is only experienced by 15% of patients on a cumulative or chronic basis.[10] Therefore the peripheral neuropathy is considered to be the dose limiting side effect of oxaliplatin.

While Pt-drugs are presently still frequently used there is a continuous need for the development and improvement of chemotherapy drugs not only in an attempt to alleviate the level of side effects but also to tackle the problem of tumour resistance (both acquired and intrinsic

resistance). Furthermore, there is great interest in improving patient care at point of care by attempting to understand and potentially predict individual patient responses. Currently patients receive a standardized dose calculated by measuring the body surface area and kidney function of the patient, and while this dose is often reduced between cycles due to toxic side effects experienced by patients, it is estimated that around 40% of patients receive an unsuitable or inappropriate dose or drug.[25] Consequently currently there is an aim to be able to achieve personalised chemotherapy doses, with the aim of ultimately improving patient care dramatically.

Consequently currently there is a desire to be able to achieve personalised chemotherapy doses, with the aim of ultimately improving patient care dramatically.

1.3 Selenium supplementation

The use of supplements, such as dietary antioxidants, during chemotherapy and radiation therapy remains a controversial issue despite years of research investigating their efficacy and safety. While several randomised clinical trials have shown some evidence that administration of antioxidants with chemotherapy or radiation treatments can reduce some treatment related side effects, however some data suggested the tumour as well as healthy cells were protected from oxidative damage while other data has contradicted this.

Selenium is just one of the many antioxidants under investigation by researchers. At present the characterisation of the interaction between selenium and chemotherapy drugs is still limited and unclear. The work presented below outlines the use, dosage and possible effects of using selenium as well as previous trials conducted.

1.3.1 Selenium

Selenium is a trace element found within the body, being used within the body for functions from immune defence, metabolism and body growth, as well as being researched for its potential role in disease prevention, such as cancer. Selenium was first discovered by Jons Jakobs in 1817, however it was believed to be toxic to humans up until the 1950's, and it wasn't until the 1970's that the link between selenium deficiency and diseases, such as Keshan disease, was made.[26–28]

The human body obtains the selenium it requires from food, with some of the richest sources being garlic, onions and brazil nuts, with the average nutritional intake found to be between 50-350 µg per day.[29,30]

Selenium has many functions within the body, and can be found in around 30 different known selenoproteins, with selenium being found primarily in the form of L-selenomethionine and L-selenocysteine.[27] These selenoproteins have various roles within the body (see Table 1). The role of selenium within cells is primarily associated with oxidative metabolism, and in particular glutathione peroxides (and potentially selenoproteins P and W) which exhibit antioxidant properties. These antioxidant properties reduce the damaging reactive oxygen species to harmless products via coupling their reaction with the oxidation of glutathione. [27]

Table 1 - Selenoproteins and selenoenzymes and their functions. Used with permission. [28]

Selenoprotein	Function
Glutathione peroxidises, GPx, (GPx1, GPx2, GPx3 and GPx4)	Antioxidant enzymes: remove hydrogen peroxide, lipid and phospholipid peroxides (thereby maintaining membrane integrity, modulating eicosanoid synthesis, reducing inflammation and the likelihood of propagation of further oxidative damage to biomolecules such as lipids, lipoproteins and DNA).
(Sperm) mitochondrial capsule selenoprotein	Form of glutathione peroxidase (PHGPx): shields developing sperm cells from oxidative damage and later polymerises into a structural protein required for stability/motility of mature sperm.
Iodothyronine deiodinases	Production of active thyroid hormone T3, from thyroxine, T4.
Selenophosphate synthetase, SPS2	Required for the biosynthesis of selenophosphate, the precursor of selenocysteine, and therefore for Selenoprotein synthesis
Selenoprotein P	Found in plasma and associated with endothelial cells against damage from peroxynitrate.
Selenoprotein W	Needed for muscle function.
Prostate epithelial selenoprotein (15kDa)	Found in epithelial cells of the ventral prostate. Seems to have a redox function (resembles PHGPx).
DNA-bound spermatid selenoprotein (34kDa)	Glutathione peroxidise-like activity. Found in stomach and in nuclei of spermatozoa. May protect developing sperm.
18kDa selenoprotein	Important selenoprotein found in kidney and large number of other tissues.

1.3.2 Selenium and cancer

Selenium is believed to have a role within the prevention of some diseases; however it has also been investigated in relation to cancer prevention as well as the effect of taking it during treatment for cancer.

The first attempt at investigating the relationship between selenium and cancer incidence levels was made by Shamberger *et al*.[31] where it was observed that areas of higher selenium in crops within the USA had a lower rate of cancer mortality, thus sparking an interest and resulted in further research in both animal and human populations. Further epidemiological studies in multiple countries followed this initial study, reaffirming the results.[32–34]

From epidemiological studies, the interest in selenium spread to work with small animals, and to date over 100 investigations into the relationship between cancer incidence and selenium levels have been performed on animals. A review by Whanger[35] concluded that two-thirds of the studies showed a significant reduction in the number of tumours observed. In fact, it was found that in half of the studies reviewed, reductions of 50% or more were observed when selenium levels were larger than the control samples.

The results from the animal and epidemiological studies gave sufficient positive results to warrant the progression onto clinical trials. By 2004 8 human trials had taken place, 7 of which showed that selenium supplementation had a positive effect and an overall reduction in levels of cancer incidence.[35] These studies also discovered that on average cancer patients tended to have slightly lower levels of selenium when compared to the healthy control groups.[32,36] In China, the results from three separate clinical trials supported the concept of selenium as a cancer preventative agent; the first study utilised a selenium-enriched yeast (200 mg Se per day) and recorded a reduction in cancer incidence over a two year period, the second added 15 ppm (as Na_2SeO_3) to salt resulting in incidence of liver cancer decreasing from 54.8 to 34.5 per 100,000 people over a 6 year period, while the third study again used selenium-enriched yeast (50 mg per day) along with β-carotene and vitamin E and saw a slight reduction in total cancer mortality.[32,37]

Clinical trials and animal studies such as those discussed above indicate that it is possible that a link between the level of selenium and incidence of cancer exists, and further large scale studies are still being carried out. However, having already established that selenium has some efficacy in the prevention of some types of cancer, the next step was to determine how it provided this protection. There are many forms of selenium, and the bioavailability of selenium is dependent on the chemical form, which in turn determines where in the body the selenium is found. It is thought that the chemical transformation of selenium is an important step in the chemo-preventative action of selenium. As a result, many different selenium compounds have been used in trials (both human and animal) in an attempt to determine the most effective form.

Selenomethionine (SeMet), which is found in enriched yeasts and cereal grains, as well as Se-methylselenocysteine (SeMCYS), which is the primary seleno-compound found in plants, garlic and broccoli are just two of the forms which have been investigated. From this research it was found that SeMCYS was the most effective form at reducing mammary tumours, however, its efficacy against other cancer types was not determined in the same study. [35]

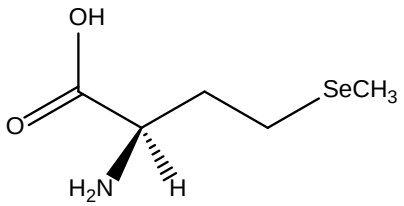

Selenomethionine (SeMet)

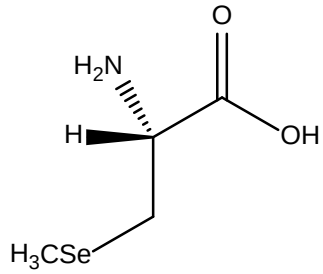

Methylselenocysteine (MSC)

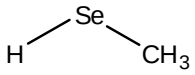

Methylselenol

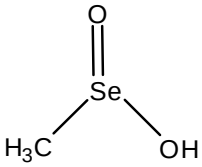

Methaneseleninic Acid (MSA)

Figure 4 - Structures of seleno-compounds of interest

The SELECT trail (Selenium and Vitamin E Cancer Prevention Trial)[38] chose selenomethionine (Figure 4), while a lower homolog of SeMet, methylselenocysteine (MSC) was used in another study and was found to double mammary tumorigenesis suppression in rodents when compared to SeMet (50% reduction compared to 20%).[35,39,40] Other trials have identified methylselenol as a potentially very important metabolite in cancer prevention, however due to its high reactivity precursors such as MSC and MSA (see Figure 4) have been used to create methylselenol endogenously. [32,40–43]

Theories as to how selenium provides a level of cancer prevention are still being investigated, however one theory is that selenium blocks the clonal expansion of transformed lesions (the ability to reduce cell proliferation of transformed clones). [40] In one study, MSC, while being tested on early stage mammary carcinogenesis, was found to block clonal expansion and increased cell apoptosis by nearly 3 fold.[40] However, the use of MSC in *in vitro* studies highlighted the high concentrations required, and as a result, a different seleno-compound was investigated; methaneseleninic acid (MSA) (Figure 4), which required only µM concentrations to generate methylselenol endogenously. Furthermore, one study found that MSA inhibited the growth of human premalignant breast cells, with a 5 fold increase in the level of apoptosis after 24 hours.[40,42,43]

Supranutritional levels of selenium have frequently been associated with the chemopreventive actions observed, reportedly up to around 10 times the level of selenium required to prevent selenium deficiency or to allow the correct function of selenoenzymes.[40,44] The mechanism by which selenium aids in the prevention of cancer is still unclear; however the results from studies suggest that it could be via two main routes - as part of antioxidant enzyme mechanisms and as part of anti-carcinogenic metabolites. Figure 5 shows the different modes, based on dose, by which selenium can work as a chemopreventative agent.

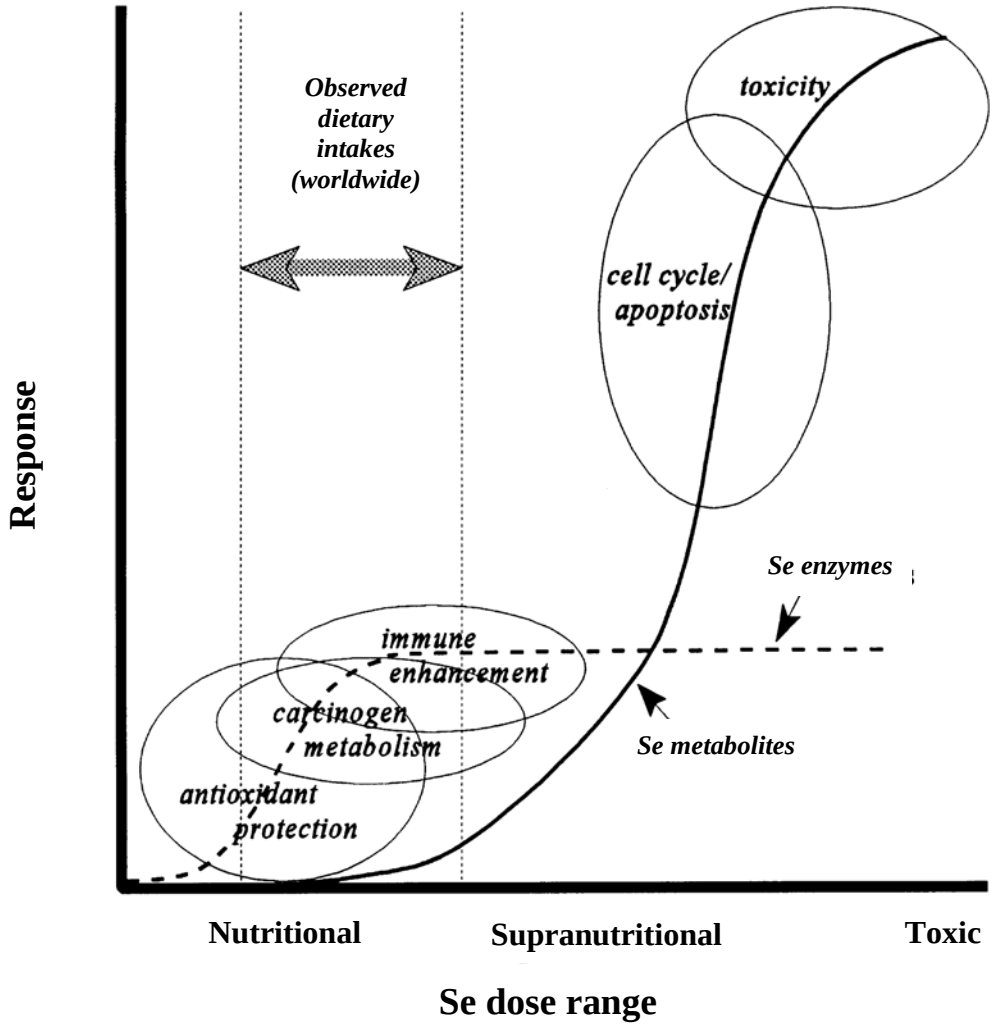

Figure 5 - A suggested model for the two-stage role selenium plays in cancer prevention. Used with permission. [32]

While the majority of current literature suggests that selenium works as chemopreventative agent by acting as an antioxidant, some research suggests that it could also work a pro-oxidant. Drake[45] proposed that sodium selenite and MSA oxidise thiol-containing substrates resulting in pro-oxidative apoptosis of cells.

While the studies to date have presented some varied results and there is still a lot unknown about which form of selenium is best and how it works, the majority of research has shown a reduction on the incidence of cancers. While research also suggests that selenium is most effective at early stages of carcinogenesis or as a cancer preventative agent, the interactions between selenium and platinum-based drugs has to be investigated. [40]

Due to the possibility of selenium having a role in cancer prevention, it is also frequently taken by patients during the course of chemotherapy or radiotherapy with the hope that it will be beneficial to them. In fact, one European study carried out over 14 countries determined that an average of 35.9% (ranging from 14.8 – 73.1%) of cancer patients were taking some form of complementary or alternative medicine.[46] This ranged from vitamins and minerals, such as selenium, to medicinal teas and homeopathy. Due to the large number of patients taking supplements during the course of their treatment it is vital to have an understanding of the interactions of these supplements and the chemotherapeutic drugs to ensure they do not interfere with the treatment or cause the patients harm.

It has been theorised that selenium supplements could aid in the reduction of some toxicities associated with platinum-based chemotherapy drugs. Platinum-based chemotherapy drugs are well documented to induce a range of side effects and toxicities, for example, cisplatin, one of the most extensively investigated drugs, primarily causes toxicity via the formation of free radicals (e.g. hydroxyl radical) which cause oxidative damage. Antioxidants, such as selenium and vitamins E and C, in theory have the ability to combat this damage. However, studies have shown that levels of antioxidants in the plasma drop significantly during treatment with cisplatin.[27,47–50]

Olas *et al*.[51] investigated the effect of administering selenium during treatment with cisplatin, and reported a reduction in toxicity with an apparent lack of inhibitory effect on the anti-tumour properties of the drug. Weijil *et al*.[48] reported similar findings and it was shown that high selenium, vitamin C and vitamin E plasma levels corresponded to a decrease in ototoxicity and nephrotoxicity caused by cisplatin. However, not all patients had a high level of the supplements in their plasma and it was unclear whether this was due to poor compliance or from inadequate dosage levels. Another study gave ovarian cancer patients selenium over 3 months and observed a rise in the level of white blood cells as well as a reduction in some side effects, including loss of appetite and hair loss.[52]

Similar results were also observed in another cisplatin study where it was found that selenium could be used to reduce nephrotoxicity and leukopenia.[53] Patients were given 4000 µg of Se per

day over the course of either their first or second cycles, and the level of nephrotoxicity was determined via enzymes in urine. It was also found that the levels of white blood cells were higher when selenium was used, however optimal dosage requirements still needed further investigation.[53]

Studies such as these have shown that taking supplements during platinum-based chemotherapy can potentially provide some relief from the side effects and a reduction in the toxicity, however, in most studies selenium was given in combination with other antioxidants and is therefore difficult to determine how much of these benefits were caused by selenium alone.

There have also been significantly less studies investigating the effect of selenium with other platinum-based drugs, such as oxaliplatin. Furthermore, there is still a lot of uncertainty as to whether the supplements bind to or have any interaction with the drugs which could result in lower levels reaching the tumours. [54–56] Additionally, there is still a lot of uncertainty as to how selenium may reduce toxicity resulting from the platinum-based drugs. While it is believed that the toxicity of some of the drugs is linked to specific oxidative metabolites of valproic acid, VPA, due to the formation of hydrogen peroxide and hydroxyl radicals, each drug works slightly differently and has a tendency to cause varying side effects, and therefore a lot more research into the matter is required.[57] Analytical techniques such as ICP-MS can now be used to study the effect of selenium in new ways by taking direct measurements and studying the pharmacokinetic pathways of the various selenium compounds under investigation.

1.4 ICP-MS

Inductively coupled plasma mass spectrometry (ICP-MS) is a highly sensitive analytical technique used for the determination of trace metals, by the introduction of a sample into a plasma where it is desolvated, atomised and ionised. Following which the resulting ions are extracted through a vacuum interface before being separated according to their mass to charge ratio (*m/z*) and detected.

Previously other atomic spectrometric techniques, such as atomic absorption spectrometry (AAS), were used for the detection and analysis of clinical and biological samples.[58–60] ICP-MS is not without limitations, especially in relation to biological samples. Spectral and non-spectral interferences are some of the major limitations, and as biological samples often have very complicated matrices this can cause problems such as the formation of polyatomic ions.[61,62] Spectral interferences arise from atomic or molecular ions having a similar nominal mass as the analyte or analytes of interest. Some interferences can also be induced from the plasma gas or solvents used during analysis.

Biological samples tend to contain a relatively high concentration of organic species which can cause a multitude of spectral interferences. Matrix interferences arise from a combination of ionisation energy and plasma conditions as well as the sample matrix.[63] However, it is worth noting that a lot of the polyatomic interferences found in biological samples can be overcome by utilising an ICP-MS with a medium and high resolution capability.[61,64] Furthermore, there are several methods which enable for the correction of non-spectral interferences such as internal standardisation, standard addition and matrix-match methods.[61–64] Despite its limitations, ICP-MS is considered such a valuable technique as it has the ability to offer a wide linear range, low detection limits for most elements, lesser interferences, speed, high throughput and a high level of precision.[65] Moreover, while ICP-MS is most commonly used for solution based work via sample nebulisation, it can also be coupled with other chromatographic techniques, such as HPLC, and laser ablation.[66–69] For the reasons detailed above, ICP-MS is an ideal technique for the quantification of the low levels of Pt observed in clinical and other biological samples.[70] The basic instrumentation of ICP-MS is discussed briefly in the sections below.

1.4.1 ICP-MS instrumentation

There are 4 major parts to a SF-ICP-MS instrument, as utilised in the research presented in this thesis; sample introduction, plasma, vacuum interface and the mass analyser and detector region (see Figure 6), and which are described in the following sections.

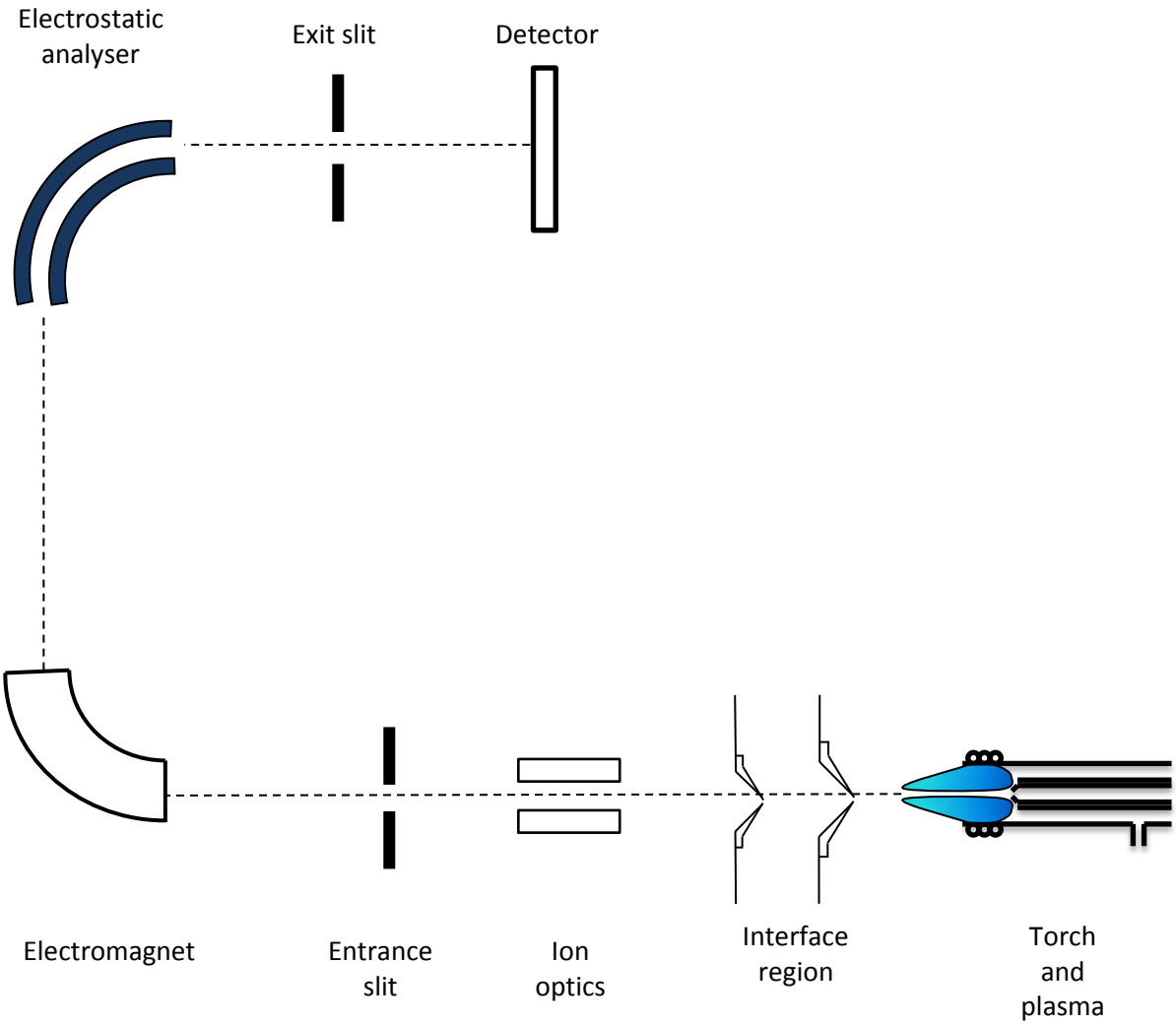

Figure 6 - Schematic diagram of a SF-ICP-MS with reverse Nier-Johnson geometry

1.4.1.1 Sample introduction

Various different interfaces have been developed to allow the introduction of solid, liquid and gaseous samples into an ICP-MS. The primary focus of this work was the use of a nebuliser and spray chamber to introduce a liquid sample into the system. In this set up, a peristaltic pump is also used to ensure constant flow of the sample. The nebuliser utilises a high velocity gas (typically argon with a flow rate between 0.5-1 L min^{-1}) to aspirate a solution into a fine aerosol. The spray chamber is used to sort the droplets by size via gravity, with droplets around 5 µm or larger getting separated out and taken to waste, and consequently only around 1-2% of the sample enters into the plasma. The spray chamber also aids in the creation of a smoother sample to be transported to the plasma, as some pulsing can occur at the nebuliser. The aerosolised sample produced in the section of the ICP-MS is transported to the plasma by a flow of argon gas. In this set up a sample uptake flow rate can be set to an appropriate value for the work. While typical flow rates can be around 1 mL min^{-1}, significantly lower rates, such as 20 µL min^{-1} can also be used. Lower flow rates such as this are highly useful when only a limited amount of sample is available, which is often the case with clinical samples.[71]

One of the primary ways to introduce a solid sample in to an ICP-MS is via laser ablation (LA). Laser ablation utilises a laser beam (typically from a Nd:YAG laser) to generate an aerosol containing nanometer and micrometer sized particulates of the sample. [72]

1.4.1.2 The plasma – formation and ion generation

The plasma, which is an ionised gas that is overall neutral, is where the sample is ionised. The plasma is formed using an inert gas inside a quartz torch. Argon is typically used as it is cheap and relatively abundant, and furthermore has the ability to excite and ionise most elements due to its relatively high ionisation potential. The gas passes through three concentric tubes within the torch (see Figure 7). The inner tube, the injector, carries the sample aerosol, or sample gas, to create a central sample channel through the plasma, sometimes referred to as the 'punch through', and is used to deliver the sample into the plasma itself. The middle tube contains the plasma or auxiliary gas, whose main function is to prevent the plasma from making contact with the injector. Typical auxiliary gas flows are between 0.5 and 1.2 L min^{-1}. The outer tube contains the cool gas, which has a typical flow rate of 15-20 L min^{-1}, which is designed to cool the outer parts of the torch to ensure that the plasma shape is maintained.

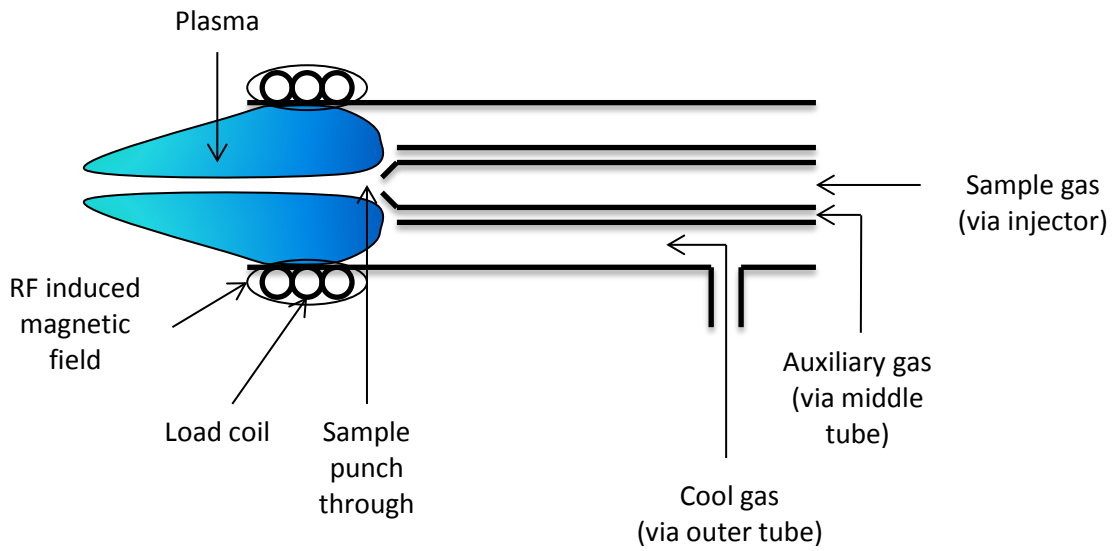

Figure 7 - Schematic diagram of an ICP-MS torch

In order to create the plasma, firstly the argon gas is allowed to flow through the torch where a high spark voltage (a Tesla spark) is introduced. This strips electrons from the argon atoms, which are then accelerated using a magnetic field from a radio frequency (RF) coil which surrounds the torch. The accelerated electrons ionise the argon gas via collisions between the electrons and the argon atoms, resulting in a chain reaction which forms the ICP discharge. The plasma will be maintained as long as the RF field is present.

The cool gas destabilises the base of the plasma allowing the sample gas to 'punch through' the base of the plasma and introduce the sample, via the injector, directly into the centre of the plasma. Due to the conditions and temperature (6000-8000 K) within the plasma, as the sample passes through it becomes desolvated, atomised and ionised, before being introduced into the mass spectrometer via the vacuum interface region. Almost the entire sample is transformed into singly charged atomic ions, and with the ionisation efficiency of most elements in the plasma close to 100%, it makes an ICP-MS a highly valuable analytical technique.[68,69,71]

1.4.1.3 The interface region

The plasma, and ionisation of the sample, is at atmospheric pressure (760 Torr), however as mass spectrometers require reduced pressure (10^{-6} Torr) an interface region is required in the ICP to allow the movement of ions between the two different pressures. This is arguably one of the most crucial areas within the instrument.

The interface region operates at around 3-4 Torr via the use of a roughing pump. In order to allow for the reduction in pressure between the plasma and mass spectrometer regions, two cones, the sampler and skimmer, are placed in the interface region (see Figure 8). The ions generated from the plasma move from atmospheric pressure, through the sampler cone, into an area of reduced pressure (3-4 Torr). Due to entering an area with a lower pressure, the ions expand and increase in velocity, exceeding the speed of sound forming a supersonic jet called the zone of silence.[73] The sample then begins to slow (mach disk) and is forced through a second cone, the skimmer cone, and into an area of even lower pressure. The sampler cone typically has an orifice of around 1 mm whereas the skimmer cone has a smaller orifice around 0.8 mm in diameter. The cones are typically made from nickel or platinum as they are designed to be resistant to corrosive liquids, such as acids, commonly used in ICP-MS.

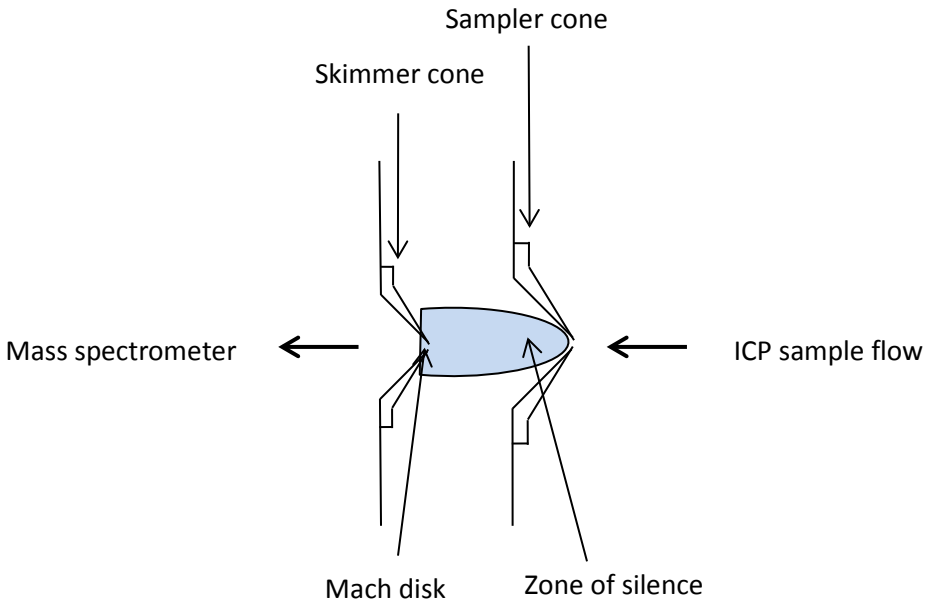

Figure 8 - Schematic drawing of the cone interface region

1.4.1.4 The mass analyser and detector

There are three main types of mass analysers used in ICP-MS; the quadrupole, the time of flight and the double-focussing magnetic sector. While the quadrupole (QMS) is perhaps the most common due to its speed, lower price and robustness, it only has the ability to be operated in a low resolution mode, and thus is unsuitable for the measurement of certain sample types. Time of flight mass spectrometers (TOFMS) separate ions based on their kinetic energy (which is directly proportional to its mass and velocity), and while all masses can be monitored simultaneously, sensitivity can be a problem due to ions only being injected in short nanosecond bursts as opposed to a continuous stream. As only a magnetic sector ICP-MS was utilised in the work presented in this thesis, only this form will be discussed in more detail here.

There are two designs used in magnetic sector instruments, the forward (or standard) and reverse Nier-Johnson design. In a reverse Nier-Johnson instrument the magnetic analyser is placed before the electrostatic analyser (ESA) whereas in a forward instrument the ESA is placed before the magnetic analyser. The ICP-MS used in this work was a Thermo Element 2 XR, a high resolution sector field ICP-MS, utilising a reverse Nier-Johnson (see Figure 6).

Upon exiting the skimmer cone, the ion beam is focused and accelerated via the ion optics into the mass analyser housing, where samples are separated according to their *m/z* ratio. The ion optics also ensure that no photons, particulates or neutral species enter the mass analyser and detector, as this would cause larger backgrounds and signal instability. The originally circular ion beam becomes rectangular as they are focussed and enters, through a slit, into the magnetic sector of the instrument. The slit can be used to control mass resolution (low, medium or high) by adjusting the width of the slit, and thus the ion beam dispersion. The magnetic sector generates a field perpendicular to the ion beam, but parallel to the slit, causing the ions to deviate from the path and follow a curved trajectory. The magnetic sector is dispersive with respect to ion energy and mass (momentum), allowing for separation of ions by the *m/z* ratio as ions separate out and follow different angles of curvature within the magnetic sector. By keeping the radius of the magnetic sector constant and varying the field strength, the ions of varying *m/z* can be focused onto an intermediate slit, thus stopping the transmission of any ions of higher or lower *m/z* than the desired analyte.

However ions of the same mass can differ in kinetic energy (due to formation position in the plasma), and thus have a different curvature through the magnetic sector, resulting in peak broadening and loss of resolution. Therefore to overcome this, a second mass analyser, an electrostatic analyser (ESA), is used. This electrostatic sector is dispersive with respect to ion

energy only, and not mass. The ESA utilises two curved plates with opposing voltages placed either side of the ion beam causing the ions to deviate into a curved path. The inner plate has a negative polarity applied to it resulting in the attraction of the positively charged ions towards it, while the outer plate repels the ions due to its positive charge.[74] By using a combination of the magnetic and electrostatic sectors, where the energy dispersion is equal in magnitude but opposite in direction, it allows for the focussing of ions based on the *m/z* ratio.

Upon exiting the ESA housing, the ion beam passes through a third slit, the exit slit, and enters the detector region. The Element XR contains two detectors, a Secondary Electron Multiplier (SEM) and a Faraday Cup. Before entering the SEM the ion beam comes into contact with a conversion dynode, resulting in an electron being ejected from it. This electron goes on to hit the first of 18 dynodes comprising the SEM, resulting in the ejection of one or more electrons. The dynodes are laid out to allow the electrons to follow a zig-zag path through the SEM causing an exponential growth in the number of electrons, and as a result the original signal is amplified.

If all of the dynodes are used, this is denoted as the counting mode of the detector and can be used to detect up to $5x10^6$ counts per second (cps), but when only a few dynodes are required in the amplification of the signal, this allows for detection between $5x10^6$ and $1x10^7$ cps, and is referred to as the analogue mode. If an even higher count rate is required (up to 1.5 $x10^7$ cps), the Faraday cup can be utilised. Once ions enter the Faraday cup they strike a metal detector plate. As the ions become neutralised, a current is generated and the change in potential is measured, and the current is directly proportional to the number of ions. The detection mode will be dependant of the count rate.

As previously mentioned, one of the major advantages of the SF-ICP-MS is the ability to switch between the three resolutions; low, medium and high. Resolution is defined as the ability of the instrument to separate one mass peak from another, and is calculated using the equation below:

$$R = \frac{m}{\Delta m}$$

Where *R* is the resolution, *m* is the mass of the analyte of interest, and *Δm* is the peak width of the mass at 5% peak height. For the Element XR ICP-MS the resolutions are given as approximately 300 for low, 3000 for medium and 10,000 for high.[74] While the higher resolutions allow for greater separation of peaks, the trade-off is that as the ion beam becomes smaller (due to size of the slit) the number of ions transmitted is reduced, and thus a reduction in sensitivity is experienced.

With the change in resolution a change in peak shape is also experienced. Low resolution peak shapes are trapezoidal (i.e. flat topped) while medium and high resolutions become Gaussian. As a result, the precision at low resolution is deemed to be very high due to the flat topped nature of the peaks, and consequently the relative standard deviation (RSD) values tend to be in the range of 0.01-0.05% in low resolution. Due to the more Gaussian peak shapes observed in medium and high resolutions the precision does decrease, however and RSD values of around 0.1% can be achieved.[75]

One of the primary advantages of using a SF-ICP-MS for biological work as presented in this thesis is the ability to resolve elements such as ^{31}P from polyatomic interferences. This is particularly useful when the sample of interest contains a large amount of ^{31}P such as DNA (which is composed of roughly 10% P) and phospholipids and peptides. In order to separate ^{31}P from common interferences, such as $^{15}N^{16}O$ a resolution of around 1455 is required, and thus on this instrument it is possible to measure ^{31}P with medium resolution.[76]

1.5 Electrospray ionisation mass spectrometry

One of the downsides of ICP-MS technology is the loss of all structural data within the plasma, and thus while elemental data can be obtained, structural elucidation and molecular weight information for compound identification is lost. Therefore, the use of molecular mass spectrometry techniques such as electrospray ionisation mass spectrometry (ESI-MS) can be used instead.

There are a multitude of molecular mass spectrometers available which have the ability to analyse a variety of biological materials, including single quadrupole, triple quadrupole, time of flight (TOF) and ion trap mass spectrometers. Linear ion trap (LIT) mass spectrometers are sensitive and highly versatile, and also have the advantage of being able to perform tandem mass spectrometric experiments. Due to its high mass range (made possible by the multiple charging of molecules by ESI) and resolution, linear ion trap mass spectrometry is ideal for the study of biomolecules such as peptides and proteins. A Thermo-Finnigan LTQ (a linear ion trap mass spectrometer) with an electrospray ionisation source (ESI) was used, and therefore the instrumentation of this shall be discussed in more detail below.

1.5.1 LTQ Instrumentation

The major components of a linear ion trap instrument are the ion source (ESI in this case), the ion optics, the mass analyser and the detector (see Figure 9), each of which are described briefly below.

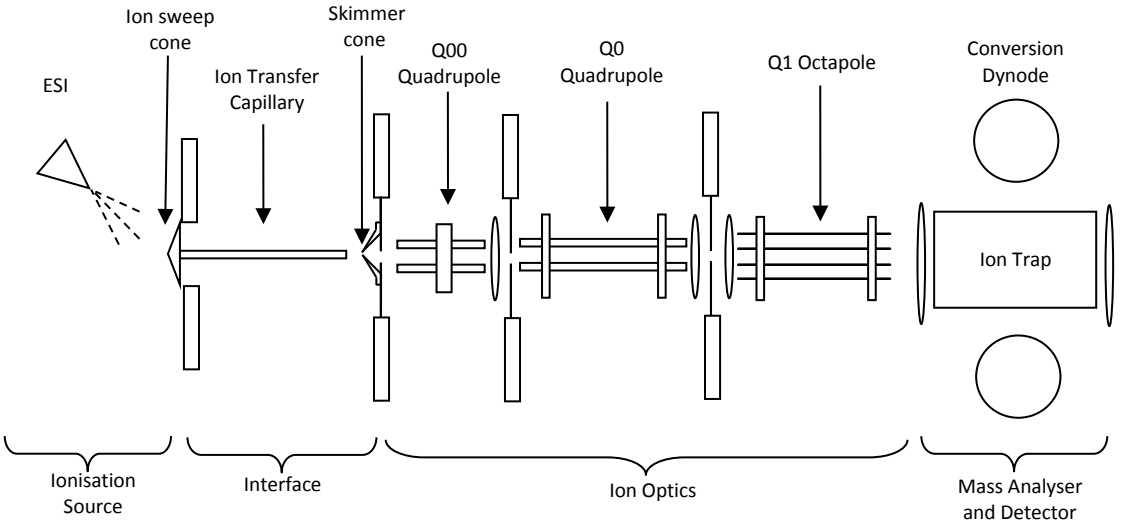

Figure 9 - Schematic diagram of a linear ion trap mass spectrometer[77]

1.5.1.1 Ionisation – Electrospray ionisation

Linear ion trap mass spectrometry is commonly used in combination with electrospray ionisation (ESI), which is a powerful technique for the production of intact ions. Other techniques such as atmospheric pressure chemical ionisation (APCI) and atmospheric pressure photo ionisation (APPI) can also be used, however they tend to be utilised when small low polarity compounds are of interest, whereas ESI is suitable for polar compounds of a larger molecular weight range. [77] As only ESI was used in the work presented in this thesis, only this will be discussed further.

ESI is a soft ionisation technique, and thus produces very limited fragmentation of molecules within the sample, making it an ideal ionisation technique for biological samples. It has been shown that larger biomolecules such as proteins can produce multiply charged ions allowing them to be determined on instruments with lower mass range capabilities. Furthermore, due to the soft ionisation, it is useful for analysis of ligand-protein complexes. [78,79]

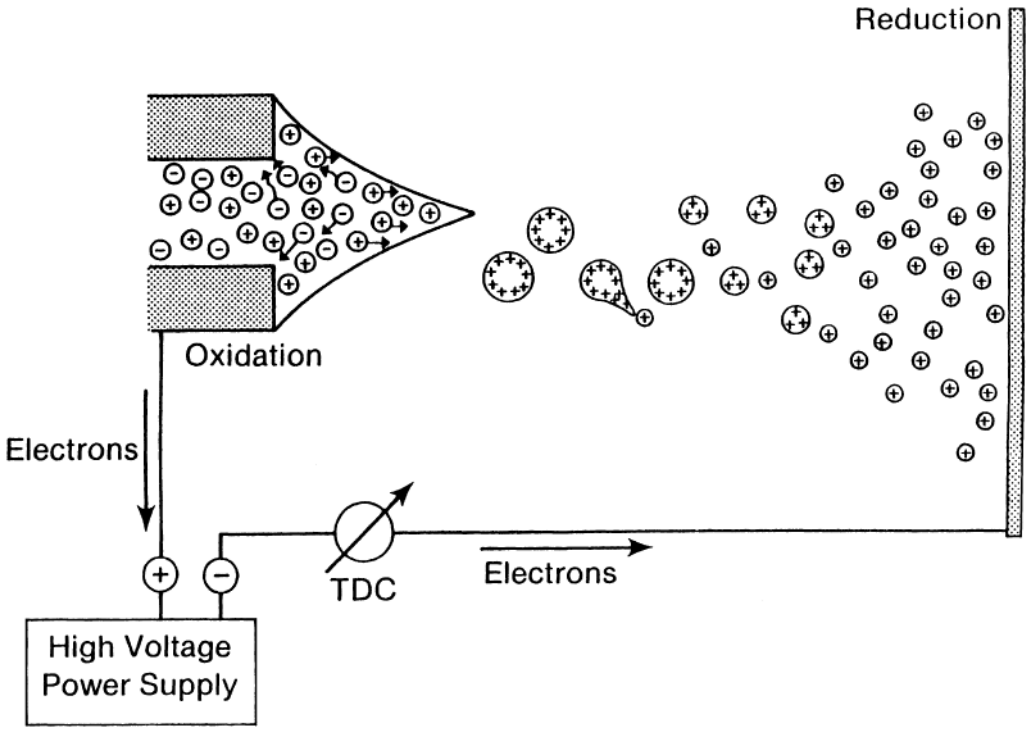

Figure 10 - Principles of electrospray ionisation droplet formation. Used with permission. [80]

Electrospray ionisation creates ions at ambient pressure by passing an analyte through a capillary tube on to which a strong electric potential is applied. The analyte is usually dissolved in a mixture of water and organic solvent (often methanol), with another chemical added to aid ionisation, typically formic or acetic acid for positive ionisation or ammonia for negative. The sample is introduced at a slow flow rate through a needle, on which the strong electric potential is applied. The applied potential, which can be positive or negative depending on the mode of ionisation

desired, results in the formation of an ion enriched cone (known as a Taylor cone) at the tip of the needle, as shown in Figure 10.

The electrically charged sample droplets are released from the Taylor cone and evaporate and decrease in size due to the flow of nitrogen gas, resulting in an increase in the charge density. As the charge density increases, the charges begin to repel each other to a greater extent resulting in the division of the droplets in to more numerous smaller droplets, and an equilibrium is reached when the forces of surface tension and ion repulsion within the droplet are equal (the Rayleigh limit). This process continues until individual sample ions enter the gas phase.[78,79,81]

The mechanism by which gaseous ions are formed is still widely debated, and two alternate models have been suggested for the formation of gaseous ions from the condensed phase; the ion evaporation model (IEM) and the charge residue model (CRM) (see Figure 11). In both models as solvent droplets reach the Rayleigh limit they undergo a number of fission events resulting in the formation of smaller droplets as mentioned above, and it is after this point that the theories separate. The charge residue model (CRM) considers the distribution of ions within each solvent droplet to be even and thus it suggests that continuous cycles of droplet evaporation and the Rayleigh limit being reached and subsequent solvent fission until each droplet contains only a single analyte ion. It is theorised that this droplet containing a single ion then completely evaporates resulting in the deposition of the analyte into the gaseous phase.

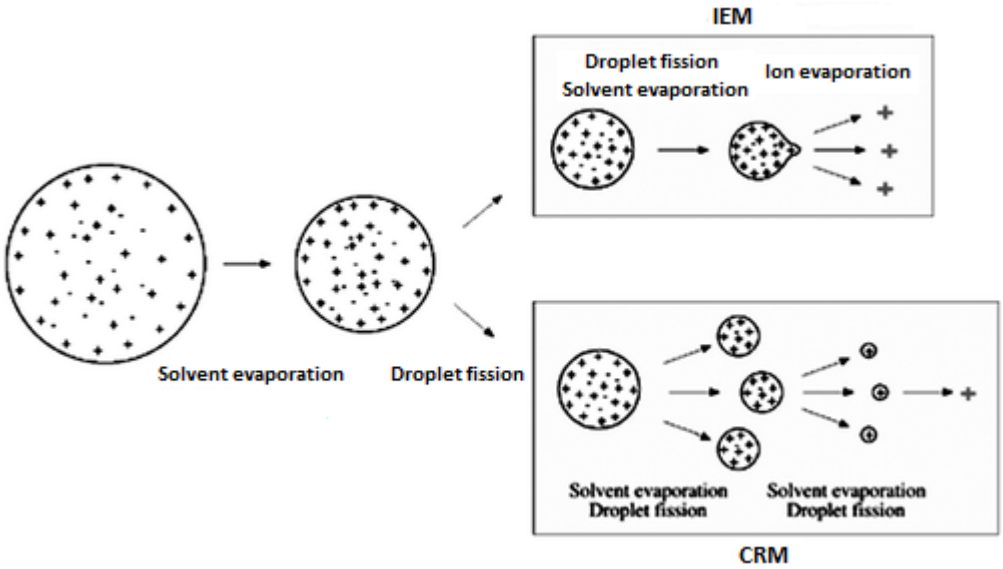

Figure 11 - The two models for gas-phase ion generation by ESI; the ion evaporation model (IEM) and the charge residue model (CRM). Used with permission. [82]

The ion evaporation model (IEM) assumes that the shape of the droplet will vary and thus affect the distribution of the ionised analytes within the droplet. The IEM mechanism proposes that if the droplet is not spherical the ions will be unevenly distributed, and thus the ions could be closer in proximately to each other at a point on the surface of the droplet than in the middle. Therefore the charge distribution at the surface point could exceed the solvation forces and thus be released as individual ions in the gaseous phase from the droplet.

1.5.1.2 Interface region and ion optics

The ions produced in the ESI source are transported using a heated ion transfer capillary which is seated behind the ion sweep cone. The capillary is heated to aid in any remaining desolvation of the ions that may be required. This interface region works at approximately 1 Torr and allows the ions to be transported efficiently to the skimmer which acts as a gate between this region of medium pressure to the lower pressure of the ion optics and detector.[77]

The LTQ ion optics consist of two sets of quadrupoles (Q00 and Q0) and one octapole (Q1) (see Figure 9) which act as guides and focus the ions towards the mass analyser. A gate lens is located before the Q1 octapole which controls when ions are allowed into the ion trap.

1.5.1.3 Ion trap

The LTQ employs a 2D ion trap analyser, which utilises an oscillating electric field to trap ions. It consists of two pairs of rods that create a hollow space in the centre in which the ions are trapped. The rods are divided into three sections to allow different voltages to be applied along the ion trap, enabling the trap to move the ions towards the centre. In two of the opposing rods, the exit rods, a small slit allows for ions to be released for detection.[77]

When conducting a full mass spectrum scan all ions are collected in the trap and then ejected and detected. If single ion monitoring (SIM) is required, the ions are collected in the trap before altering the voltages allowing only a single *m/z* to be released through the exit rods for detection. In the tandem MS mode (MS/MS or MS^n mode), ions are isolated as above, however the ions are then excited via the application of voltages, causing them to collide with a gas (typically helium) resulting in fragmentation. The daughter or product ions are then ejected towards the detector. If multiple fragmentation steps are required (MS^n) then the isolation and excitation steps can be repeated before the ejection step.

1.5.1.4 Detectors

This system uses two off-axis ion detection systems, each of which is composed of a conversion dynode and an electron multiplier. Ejected ions hit the surface of the conversion dynodes which have a positive or negative potential applied to them depending on acquisition mode (negative potential is applied when detecting positive ions), resulting in the release of electrons which in turn encounter the electron multiplier.[77] The electron multipliers amplify the signal which is then recorded and the signals displayed on the computer screen.

1.6 Summary

The sections above have summarised some of the theory and instrumentation that formed the basis of this research. There have been a great number of advances in recent years in progressing not only our understanding of Pt-based anti-cancer drugs and supplementation but also in the development of analytical instrumentation. This has enabled us to detect lower levels of trace elements in biological samples, making research such as this possible. The work presented in the following chapters is aimed at addressing the objectives outlined in Section 1.1, and each of the three main work streams has been split into separate chapters.

2. A comparison of blood and saliva as a source of DNA for the investigation of Pt-DNA adducts in patients undergoing Pt-based chemotherapy

2.1 Introduction

As outlined in Chapter 1, the use of Pt-drugs in the field of cancer chemotherapy is extensive due to its efficacy at destroying cancer cells via the formation of Pt-DNA adducts. It is these adducts which have been the subject of much research and which are the main focus of this chapter.

While the level of cytotoxicity caused by Pt-DNA adducts is of primary interest, they can also aid in the understanding of drug uptake, repair, resistance and toxicity/side effects.[83–88] However, while increasing our understanding in these areas is very beneficial, it is at the clinical stage where there is a limited understanding of how the level of Pt-DNA adducts affects each patient individually. Many studies in several fields have highlighted the issue that there is great inter-patient variability and how a patient will respond to treatment is dependant of a range of factors, and include some host-specific factors. [5,89–91] Some research studies have indicated that there is a relationship between the levels of Pt-DNA adducts formed and the patient's response, tumour resistance, drug toxicity and overall clinical outcome. [5,92–97]

As useful as the determination of Pt-DNA adduct levels in patients can be there are many problems associated with their detection and quantification. One of the primary issues associated with the quantification of Pt-DNA adducts is the low levels found both *in vitro* and *in vivo*. More than 90% of the drug administered during treatment will bind to blood proteins resulting in it being inactive in the treatment of the cancer,[98,99] and only around 1% of the Pt drug will ever reach and bind with the DNA to form adducts,[3,4] while the rest of the drug binds to proteins in the cytoplasm and cell membrane and other higher affinity biomolecules within the cell, and consequently very sensitive techniques are required for the determination of adducts in human cells.

Typical Pt-DNA adduct levels in leukocytes have been reported in the range of 1-7 Pt adducts per 10^6 nucleotides for oxaliplatin and cisplatin, [5,100,101] and as the amount of clinical sample obtained is usually limited, detection of Pt-DNA adducts has proved problematic in the past. The Comet assay and ICP-MS are amongst the most frequently used techniques however other methods include AAS, immunoassays (e.g. ELISA assay) and post-labelling assays. [88,102–108] However due to

limitations in sample quantity, some of these techniques are only useful when conducting experiments *in vitro*.

ICP-MS, being a highly sensitive technique, has proved to be very useful in the determination of Pt-DNA adducts. While as a technique it proves a speedy and robust method for determination of adducts at low levels found in clinical samples, it too is not without its drawbacks. Unfortunately all structural data is lost and therefore only the overall level of Pt associated with the DNA can be measured, and cannot be further divided into the level of different adducts formed.

In this research project a Thermo Element 2 XR, which is a high resolution SF-ICP-MS was used in investigating the level of Pt-DNA adducts in clinical samples. Previous work on the quantification of Pt-DNA adducts to that presented in this chapter has been performed at Loughborough University. This work lead to the development of a fast, sensitive and robust ICP-MS assay which can be applied to *in vivo* Pt-DNA adduct formation. The first researcher in the group at Loughborough University to investigate Pt-based drugs was Dr Peter Winship.[109] In his research, the Pt-DNA adducts of both cisplatin and oxaliplatin in calf thymus DNA (ctDNA) was successfully measured down to levels of 1 Pt per 500,000 nucleotides using a quadrupole ICP-MS, however his work was performed entirely on ctDNA where it was possible to use large quantities of DNA (around 1000 µg of DNA) which is simply not obtainable from clinical samples.

Dr Samantha Kerr[110] followed on this work using a high resolution SF-ICP-MS, and was therefore able to lower the limit of detection of platinum, as well as significantly reduce the level of matrix effects observed when analysing whole DNA and overcoming the problematic viscosity of DNA solutions by refining sample preparation methods and introducing a sample digestion process (outlined in Section 2.3.7). As a result of this work, it was possible to measure Pt doses in as little as 130 µg of DNA with excellent results, and some success was had at levels as low as 12 µg of DNA.

Her work lead onto the application of these methods on clinical samples by Dr Aref Zayed.[111] During his research not only did he refine the assay and apply the use of the digestion procedure to clinical samples, but added the use of an internal standard (europium) to increase the reliability of the data.

The progression of this work within the research group has been towards the overall aim of developing a robust and rapid technique for the quantification of Pt-DNA adducts in clinical samples with the aim of being able to determine the level of adducts during and between cycles

in order to better predict and influence the outcome of chemotherapy by adjusting and personalising doses on a patient to patient basis.

As discussed above, the work by Zayed[111] included a study where the level of Pt-DNA adducts was measured in leukocytes obtained from patients undergoing Pt-based chemotherapy treatment. His work uncovered some interesting observations, including the significant inter-patient variability, evidence of significant repair in some patients 24 hours post infusion and ability to see some correlation between adduct levels of toxicity and outcome experienced by patients. As well as the adduct level after 24 hours showing significant levels of repair in some patients, a low level of carryover of platinum between cycles was also observed. This work highlighted some important issues for further investigation; specifically how adduct levels change in the hours and days following Pt-drug infusion. Some studies have shown a peak in adduct formation around 6 hours after infusion, [103] therefore not only were the hours immediately post infusion desirable to investigate but also how the levels changed and decreased between cycles.

While there is some debate about the use of healthy cells (such as patient leukocytes) over cancerous tumour tissues, tumour tissues are not easy to obtain, and furthermore, as this project is primarily interested in the toxicity experienced by patients (where the effect of the drugs on healthy cells plays an important role) and how this varies over time, the use of leukocytes was deemed to be a suitable study material. However, the work by Zayed was not without its limitations, with the primary problem being obtaining the clinical samples themselves. To obtain blood leukocyte samples, trained personnel are required and furthermore in order to prevent the movement or change of platinum within the blood sample prior to analysis, the leukocytes have to be extracted as quickly as possible, which is a time consuming process. However the biggest challenge was obtaining the samples at times which were convenient for patients, and consequently an investigation into adduct formation levels over many hours and days post-infusion using leukocyte samples would prove to be highly difficult unless a patient was hospitalised.

Therefore, the main aim of the work presented in this chapter was to investigate the possibility of the use of an alternative biological sample which would be less intrusive and a more patient friendly means for the analysis of adduct levels. Saliva was chosen as it has been shown to be a viable alternative source of DNA for various applications[112,113] and most importantly it can be obtained non-intrusively and does not require the presence of trained personnel to obtain the sample and can therefore be done in the privacy of a patient's home. Consequently the work presented in this chapter was designed to aid in achieving this goal. Firstly, method development

is discussed followed by the application of these methods to clinical samples from patients undergoing Pt-based cancer chemotherapy treatment.

2.2 Experimental design

In order to investigate the possibility of using saliva as an alternative to leukocytes for determining the number of Pt-DNA adducts in clinical patient samples with the ultimate aim of carrying out a study of the level of adducts over an extended time period, a trial experiment was set up to determine the correlation of adduct levels in blood and saliva in a small number of patients undergoing Pt-based chemotherapy.

Firstly, ethical approval was obtained from the Leicestershire and Rutland Research Ethics Committee allowing the collection of both blood and saliva samples from patients undergoing Pt-based chemotherapy. A total of 10 patients were wanted for this initial trial, from which both saliva and blood samples would be obtained.

A commercially available saliva kit (OG-500 kit obtained from Oragene) was chosen for the use in this investigation for the collection of saliva for several reasons. Firstly, it has been used successfully in previous DNA studies in other fields, and secondly because the use of the kit does not require the presence of trained personnel to obtain the samples, and could therefore be used in the privacy of a patients home, while allowing the DNA to be kept stable for extended periods of time before the DNA had to be extracted.[114–118]

Blood and saliva samples were taken pre- and 1 hour post infusion, which would allow for a direct comparison in the level of Pt-DNA adducts at these time points. These time points were chosen primarily for patient convenience. A further saliva sample was taken 24 hours post infusion, and where possible a blood sample was also taken at this point, however this was usually not feasible unless a patient was hospitalised in the days following their treatment.

DNA was then extracted from these samples, digested and were analysed via SF-ICP-MS to determine the Pt-DNA adduct levels, the details of which are given in the following sections. This investigation was not designed to be statistically powered, but rather as a proof of concept experiment before a larger scale experiment would take place.

2.3 Methodology

Some of the methodology used in this chapter was developed by previous members of this research group and adapted for use on the samples presented.[109–111] These methods are outlined and referenced below where appropriate; however some further method development was required, the details of which are also presented in the following sections.

2.3.1 Patient sampling – patient criteria and ethics

As previously stated, ethical approval was granted by the Leicestershire and Rutland Research Ethics Committee. Following this, patients were recruited at Leicester Royal Infirmary by Dr Anne Thomas and Dr Joanna Wood, who obtained informed consent from the patients undergoing Pt-based chemotherapy. Following this approximately 15 to 20 mL of blood and 2 mL of saliva were collected from the patients immediately prior to treatment and 1 hour post treatment. A further 24 hour post treatment sample was also obtained for the saliva, and where possible, blood sample.

The patients recruited in this trial were all suffering from cancers of the gastro-intestinal system and were on palliative care, and were on different Pt-based chemotherapy treatment regimes and on different cycles. Full details of patient treatments are given in Table 30 (Appendix A), however briefly they included FOLFOX (5-fluorouracil, folinic acid and oxaliplatin), FOLFOX and Bev (bevacizumab), EOX (epirubicin, oxaliplatin and capecitabine), ECX (epirubicin, cisplatin and capecitabine) and Cis/etop (cisplatin and etopside).

2.3.2 Collection of saliva samples from patients

Saliva samples were collected using a commercially available saliva collection kit, OG-500 (Oragene, Ontario, Canada). Following the manufacturers recommendations, patients were kindly asked to abstain from eating food, drinking anything, smoking or chewing gum for 1 hour prior to donating a saliva sample.

The OG-500 kits contain a sample collection tube which is marked to indicate how much sample is required (2 mL). A small funnel supplied is attached to the top of the collection tube allowing easier donation of saliva sample. Patients were encouraged to allow saliva to pool naturally at the front of their mouths and allow it to pass into the funnel as opposed to attempting to force the production of saliva.

Having filled the sample tube with 2 mL saliva (excluding bubbles), the lid of the funnel was snapped shut, allowing the release of a stabilising solution (2 mL) into fresh saliva sample, producing a final sample with a volume of 4 mL. The funnel was then removed and a simple, but secure, screw cap replaced it, ensuring the sample did not leak out of the tube. The tube was then inverted repeatedly for 5 seconds to ensure proper mixing of the saliva and stabilising solution.

While the exact chemical breakdown on the stabilising solution is not known due to it being proprietary information, it is known that the DNA is stabilised by causing the cells to lyse. Oragene have conducted experiments to show that the DNA collected is stable for up to at least 5 years from collection. [118]

While the pre- and 1 hour post-infusion samples were donated while patients were in the hospital, the 24 hour post infusion sample was donated by the patients while at home. They were offered free secure posting or could bring the sample with them to their next appointment.

The stabilised saliva solutions were stored upright at room temperature (as per manufacturer's instructions[119]) until the DNA extraction was performed.

2.3.3 DNA extraction from saliva

PrepIT.L2P solution was purchased from Oragene (Ontario, Canada) for the purpose of extracting the DNA from the OG-500 saliva collection kits. The manufacturer's protocol was followed and was conducted as follows.[119] Firstly, to ensure the DNA is properly released from the cells a heat-treatment step was required, and therefore all samples were incubated in air at 50°C overnight. The full 4 mL of sample was then transferred to a 15 mL Falcon tube and 160 µL of PrepIT.L2P solution was added. To ensure complete mixing, the sample was vortexed for a few seconds. At this stage the sample became turbid as cell debris was precipitated out. The samples were then incubated on ice for 10 minutes, allowing for complete precipitation of the cell debris.

Samples were then centrifuged at room temperature at 15000 x *g*, following which the clear supernatant was carefully collected using a pipette being careful not to disturb the pellet (which contained the impurities). The supernatant was placed in a clean 15 mL Falcon tube where 2.4 mL of 99% ethanol (BioUltra pure, purchased from Sigma Aldrich, Poole, UK) was added before being mixed gently by inversion. The added ethanol triggered the DNA precipitation, and the samples were allowed to stand for 10 minutes to allow full precipitation. The DNA at the point was usually visible as small clump of fibres.

The samples were centrifuged again at room temperature for 5 minutes at 15000 x *g* and the resultant supernatant was disposed of. The remaining DNA pellet was washed once with 70% ethanol and after ensuring that all ethanol was removed the remaining DNA pellet was dissolved in 200 µL distilled water. The manufacturer recommends TE as a DNA storage buffer (10 mM Tris-HCl, 1 mM EDTA, pH 8.0), especially for longer term storage, however to keep contaminants and lower backgrounds for the ICP-MS analysis distilled water was chosen for this study. While water is not an ideal storage medium for DNA as it will evidentially result in the breakdown of DNA over time, for the purposes of this investigation where the DNA is digested prior to analysis and no structural information of DNA is required, this was not a major concern. However, having ensured that the DNA was fully dissolved, the DNA was quantified using UV absorbance at 260 nm and 280 nm before the sample was stored at -20°C before digestion and subsequent analysis via SF-ICP-MS.

2.3.4 Collection of blood samples from patients

Blood samples were taken from patients immediately prior and 1 hour post infusion by either Dr Joanna Wood or one of the nurses working on the Chemotherapy Suite at Leicester Royal Infirmary. The samples were taken in vials containing potassium EDTA (SARSTEDT, Germany) as an anti-coagulant (with final concentration being 1.2-2 mg EDTA/ mL of blood). To prevent further movement or change of the Pt-based chemotherapy drugs within the blood samples, the leukocytes were extracted from the whole blood samples as quickly as possible, with the whole process usually being completed within 2 hours of the sample being taken.

2.3.5 Leukocyte isolation

In order to extract the leukocytes from the whole blood samples, Ficoll-Paque PLUS (GE Healthcare, Chalfont, UK) was used. The blood samples were transferred into a 50 mL Falcon tube and equal volume of room temperature RPMI 1640 media was added (purchased from Sigma Aldrich, Poole, UK). The mixture was mixed well using a pipette.

To four clean 50 mL tubes, 12 mL Ficoll-Paque PLUS was added. Very carefully, and ensuring no mixing occurred, approximately 10 mL of the blood/media mixture was added on top of the Ficoll-Paque PLUS. The samples were then centrifuged at 20°C for 30 minutes at 1700 rpm, using a low or no break setting. The resulting fractions are depicted in Figure 12.

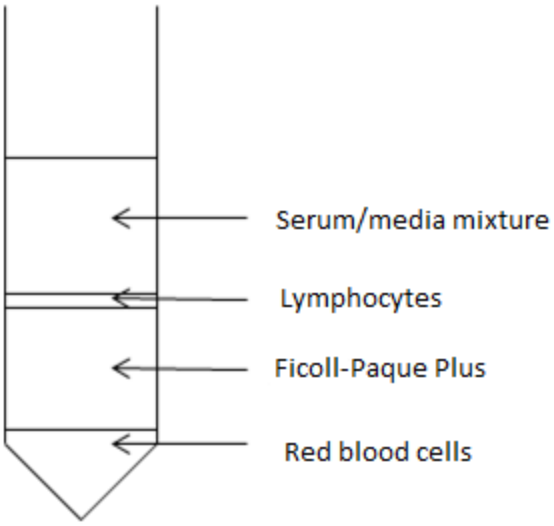

Figure 12 – Layers obtained during the isolation of leukocytes from whole blood using Ficoll-Paque PLUS

The leukocyte layers for each sample were very carefully collected using a clean Pasteur pipette and washed using RPMI 1640 media. A haemocytometer and microscope was used to provide a cell count which was in turn used to re-suspend the leukocyte samples in fresh RPMI 1640 media containing 20% FCS (Foetal calf serum) and 10% DMSO to a final concentration of around 4-5 million cells per mL. The isolated leukocyte samples were then frozen at -80°C until DNA extraction was to be performed.

2.3.6 DNA extraction from leukocytes

DNA was extracted from the leukocytes using the QiaAmp DNA Blood Mini Kit purchased from Qiagen (Crawley, UK). While this kit can be used for the manual extraction of DNA, in this case an automated DNA extraction system, a QIAcube (Qiagen, Crawley, UK) was used in an attempt to reduce hands-on preparation time as well as reduce human error and human introduced contamination while extracting DNA from clinical samples.

The DNA Blood Mini Kit was used as per the manufacturer's instructions, with only a couple of minor modifications, including changing the final elution buffer to distilled water and adding in an RNase clean up step. An overall outline of the extraction procedure is detailed below.

The frozen leukocyte samples were thawed and washed with PBS before being placed into the QIAcube where the DNA extraction process was completed. The overall extraction process consists of 4 main stage; lysing of cells, binding of DNA to silica membrane, washing and elution. Firstly, in the lysis step, Buffer AL and protease enzyme are added to the sample, which is heated, to break down the cells to allow access to the DNA from within the nucleus. While the exact

chemical breakdown of the Qiagen buffers are not known due to it being proprietary information, the lysis buffer is known to contain Chaotropic salts which destabilise hydrogen bonds and hydrophobic interactions resulting in the disruption of the interactions of nucleic acids and water which in turn prepares for the binding of the DNA to the membrane. The lysis buffer is also believed to contain a detergent causing protein lysis and solubilisation.

The next step is to separate the DNA from remaining cell material and to bind the DNA to the silica-based membrane. This is achieved by the addition of ethanol and when the sample is loaded onto the column and centrifuged, the DNA binds well to the membrane and the remaining impurities from the lysate are removed.

A wash step aids in the purification of the DNA. During this step any further residual proteins or salts on the membrane are washed way using buffers AW1 and AW2. The first wash (buffer AW1) uses a low concentration of Chaotropic salts to remove remaining proteins, while the second wash (buffer AW2) uses ethanol to remove remaining salts. All of the ethanol must be completely removed before the DNA elution step so the membrane, which is housed in a column, is centrifuged until dry.

Finally, during the elution step, the DNA is hydrated using buffer AE (this was exchanged for distilled water in this investigation) and is released from the membrane. A final elution volume of 200 µL was set. As discussed previously, water is not a suitable storage media for DNA long term, but for the purposes of this investigation was preferable. A small aliquot of the DNA was then quantified using UV absorbance at 260nm and 280 nm before being stored at -20°C for analysis via SF-ICP-MS.

2.3.7 Sample preparation

A digestion method originally described by Yamada et al.[120] and modified by Kerr[110] was used for the extracted DNA samples for both blood and saliva. This method has also previously been used and validated for DNA from leukocytes by Zayed[111].

This digestion procedure was accomplished by the addition of 0.8 volume of ultrapure 70% nitric acid (Romil, Cambridge, UK) to 1 volume of sample and heated at 70°C for one hour. Before use, the small Eppendorf vial lids were pierced using a sterile needle to prevent pressure build up during heating. Following this one hour heating with nitric acid, 0.8 volume of ultrapure 30% hydrogen peroxide (Sigma Aldrich, Poole, UK) was added to each sample and heated for a further 4 hours at 70°C.

Following this, the digested sample was evaporated to dryness while being heated at 70°C and under a gentle stream of oxygen free nitrogen gas. This evaporation to dryness was carried out on a TurboVap Concentration Workstation (Biotage, Uppsala, Sweden).

The dry sample was reconstituted to 350 µL prior to analysis on SF-ICP-MS using 2% nitric acid (HNO_3) containing 0.5 ppb europium (^{153}Eu). The use of europium as an internal standard for Pt and P was previously validated by Zayed.[111]

The digestion procedure is used to solve the viscosity problem of DNA solutions associated with thin auto sampler tubing as found in this instrumental set up. Furthermore it also was found to lower the background and reduce matrix effects.[110,111]

2.3.8 Instrumentation

Having reconstituted the digested DNA samples as above, the samples were analysed using sector-field inductively coupled plasma mass spectrometry (SF-ICP-MS) (Thermo Scientific, Element 2 XR, Bremen, Germany). This instrument can be set up to aid lower or higher sample flow rates, as well as other variables. In this case, the instrument was set up to accommodate a flow rate of approximately 80 µL/min. This was achieved by attaching a PFA nebuliser (PFA-ST Elemental Scientific, Omaha, USA) and a Cyclonic spray chamber (Glass Expansion, Victoria, Australia). As an autosampler was used, a low flow (80 µL/min) probe was utilised (Elemental Scientific, Omaha, USA). Nickel sampler and skimmer cones were used throughout this work (ICPMS cones Ltd., Chester, UK).

A method previously developed by Zayed to measure the three elements of interest, ^{153}Eu (LR), ^{195}Pt (LR) and ^{31}P (MR) was used.[5,111] This method measured 13 passes per run and 3 runs per sample. The data obtained via SF-ICP-MS was used to calculate the level of Pt associated with DNA (Pt-DNA adducts) as detailed in the next section.

The ICP-MS nebuliser gas flows and torch positions were tuned every day to optimise conditions and maximise signal intensity, however typical conditions are summarised in Table 2.

Table 2 – Typical operating conditions for analysis via SF-ICP-MS

Parameter	Setting
Radio frequency (RF) power	1215 W
Cool gas flow rate	15.50 L min^{-1}
Auxiliary gas flow rate	0.95 L min^{-1}
Nebuliser (sample) gas flow rate	1.0 L min^{-1}
Sampler cone	Nickel
Skimmer cone	Nickel
Detection mode	Triple mode
Low resolution	^{153}Eu, ^{195}Pt
Medium resolution	^{31}P

2.3.9 Quantification of DNA from UV absorbance

During this investigation, the DNA was quantified via two methods; UV and ICP-MS. An experiment was performed by Zayed as part of his research to determine if ICP-MS could be used to accurately quantify DNA.[111] His experiments were successful and found that DNA quantification via ICP-MS was actually more reliable and reproducible than UV as the Pt and P measurements were more robust against matrix effects and thus produced consistent data. In this investigation, both UV and ICP-MS were used to quantify DNA to ensure the results corroborate, however the final calculation of Pt-DNA adducts will be performed using the data obtained from the ICP-MS.

To measure DNA concentration and purity via UV analysis, the absorbances of the DNA samples was measured at 260 and 280 nm. The samples were diluted with water to provide readings between 0.1 and 1 to ensure that the readings fell within the linear range defined by Beers law. In order to calculate the concentration of DNA in the solution, the following equation was used:

$$DNA\ \mu g/\mu l\ = \frac{A260\ x\ DF\ x\ 50}{1000}$$

In the equation above A_{260} is the absorbance measured at 260nm and DF is the dilution factor. The equation is based on a 50 µg/ml sample of double-stranded DNA which has an absorbance of 1 at 260 nm. The DNA purity can be calculated using the ratio of A_{260}/A_{280}, where the absorbance ratio should be between 1.6-1.8 (1.6 is ideal).

2.3.10 Quantification of DNA via ICP-MS

To be able to quantify the number of Pt-DNA adducts formed via ICP-MS, the P and Pt concentrations had to be calculated from the data obtained from the ICP-MS. Firstly this information was used to calculate the number of Pt atoms per nucleotide by the use of the following equations.

While investigating the number of Pt-DNA adducts formed, two methods were investigated. Firstly, by taking the P and Pt concentrations calculated from the ICP-MS data, the number of Pt atoms per nucleotide was calculated by using the following equations:[109,111]

$$Pt\ per\ nucleotide = \frac{Number\ of\ Pt\ atoms\ per\ litre}{Number\ of\ nucleotides\ per\ litre}$$

$$No.of\ nucleotides\ per\ litre = \frac{P\ concentration\ \ (\mu g/L)}{1000}\ x\ \frac{0.001}{30.974}\ \ x\ Avogadros\ constant$$

Alternatively, the UV data in conjunction with the Pt data obtained from the ICP-MS data could be used. To do this, an adjustment to the above formula for the calculation of the number of number of nucleotides per litre would be changed to:

$$No.of\ nucleotides\ per\ litre = \frac{DNA\ concentration\ (mg/L)\ x\ 0.001}{307.61}\ \ x\ Avogadros\ constant$$

Where 307.61 is the average molecular weight of a nucleotide polymerised in a DNA molecule.

2.4 Saliva method development

The DNA extraction, digestion and analysis methods detailed above in Section 2.3 were previously used and validated on clinical patient leukocyte samples by Zayed.[5,111] As the ICP-MS assay contained several sample preparation steps, including the harsh acid digestion, the overall assay from start to finish was investigated to ensure that a high recovery and reproducibility was obtained.

Firstly, an investigation was performed by Zayed where the digestion procedure, evaporation and reconstitution was performed and analysed via ICP-MS using platinum standards at a range of concentrations. The level of Pt recovery and relative error was found to be good, and the investigation was extended to look at a Pt-based drug being digested with and without the presence of ctDNA. This brought to light an issue of slight signal enhancement, thought to be caused by DNA matrix effects. This was overcome by the introduction of europium as an internal standard.

This method was later used successfully on patient leukocytes[5,111], however to ensure that the experiment design (as detailed at the start of this chapter), aim and outcome would not be compromised by the unknown interaction or degradation of platinum based chemotherapy drugs in saliva, a stability study was conducted.

According to the manufacturer, the DNA from a saliva sample stored within an Oragene OG-500 saliva collection kit is stable for at least 5 years at room temperature, but could also be stored in the freezer if the user required[119], however to ensure that this was the case, and that the platinum in the sample, in particular the Pt-DNA adducts, would be stable as well, a 12 month stability test was performed.

2.4.1 Experimental design

Firstly, to determine the stability of Pt-DNA adducts within saliva sample stored within an Oragene OG-500 kit, a yearlong stability study was set up. A set of sampling time points were chosen to allow storage of samples for 0 days (immediate), 1 week, 2 weeks, 1 month, 2 months, 3 months, 6 months, 9 months and 12 months. At each of these time points a healthy volunteer would donate 2 mL of saliva having not drunk or eaten anything for the previous hour. The sample was then spiked with 100 µL of oxaliplatin ($8.64E^{-7}$M) and left for 1 hour to allow the Pt-drug to interact with the DNA before the stabilising solution in the lid of the OG-500 kits was added in and the sample inverted to ensure proper mixing. The sample was then stored upright at

room temperature until analysis was performed. All samples, including procedural blanks were analysed at the same time.

2.4.2 Methodology

The DNA from the saliva was extracted, digested, evaporated and reconstituted as per the methods described in Section 2.3.

The ICP-MS was tuned in both low and medium resolutions to optimise signal intensity on the day of analysis and the instrument set up and analysis method described in Section 2.3 was utilised in this investigation.

Previous work in this research group has shown that while overall background Pt and P levels are low, digested samples over non-digested samples have a slightly higher background; however it is still significantly lower than the levels measured in samples. To ensure that this was the case with the saliva samples, digested water blank as well as saliva blanks (no added platinum) were analysed.

2.4.3 Results and discussion

The ICP-MS calibration data for platinum (^{195}Pt) using europium (^{153}Eu) as an internal standard (Figure 13) shows excellent linearity. For each sample the platinum concentration was calculated in ppb based on the calibration graph, and the theoretical platinum concentration based on level of oxaliplatin added and the recovery was calculated as a percentage (see Table 3 and Figure 14).

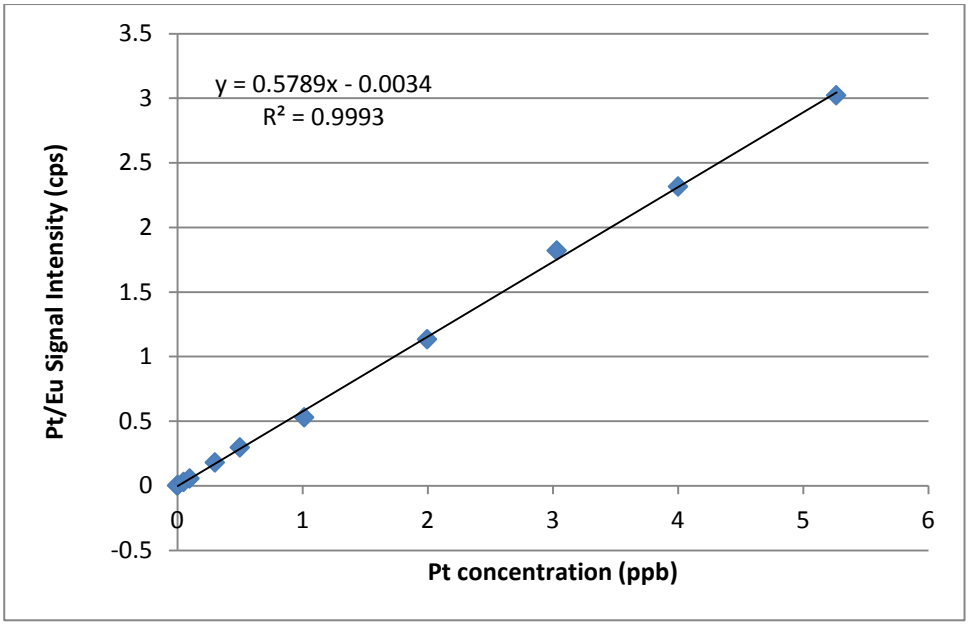

Figure 13 - Pt calibration graph using ^{153}Eu as an internal standard

Table 3 - Platinum recovery in saliva stability study

Time point	Measured Pt (ppt)	Pt spike concentration (ppb)	Recovery (%)
Water blank 1	2.56	0.00	-
Water blank 2	2.95	0.00	-
Saliva blank 1	3.93	0.00	-
Saliva blank 2	3.84	0.00	-
Immediate	48.24	4.23	1.14
1 week	43.43	4.20	1.04
2 week	40.77	4.23	0.96
1 month	43.12	4.21	1.02
2 month	41.63	4.23	0.98
3 month	36.62	4.25	0.86
6 month	34.60	4.21	0.82
9 months	40.51	4.26	0.95
12 months	36.69	4.35	0.84

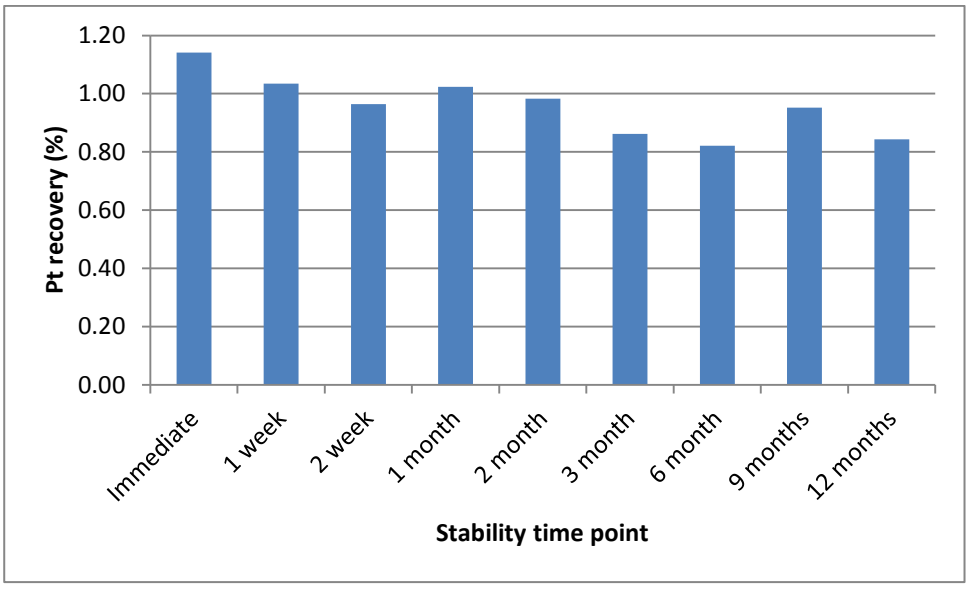

Figure 14 - Platinum recovery in saliva stability study

While at first glance the platinum recovery seems very low (around the 1% mark), this was to be expected. Previous work has shown that within cell cultures the sub-cellular fractionation of cells has shown that only around 9-17% of all cellular proteins can be found within the nuclear fraction of the cell, depending on the cell type, and furthermore only around 9% of Pt-based drugs exposed to cell cultures ends up in the nuclear fraction, however in patient leukocyte samples this value increased to the range of 20-26%.[5,111]

While these values are significantly higher than the recoveries observed in this experiment, this can be explained as the values stated for the nuclear fraction includes not just DNA, but proteins found within the nuclear fraction. Furthermore, previous research has suggested that only around 1% of the Pt given to patients reaches the DNA.[3,4,71] This is in approximate agreement with the results observed in this experiment.

The level of platinum recovery observed was not the primary aim of this experiment however, as no matter how low the recovery of platinum observed in the DNA, the main aim of this experiment was to observe if the levels of recovery changed over time that the kits could be stored for. As can be seen from Figure 14 and Table 3 the levels of Pt recovery over the 12 month period remained relatively stable.

Ensuring drug stability over time within the OG-500 kits was essential as the primary aim of the comparison of Pt-DNA adduct levels in blood and saliva is to establish if there is a correlation between the two measurements or not and for that to be achieved the samples had to be kept as uniform as possible. Therefore, while the ICP-MS results for the measured Pt concentrations showed a low level of Pt when compared to the spike level, the results were quite consistent and stable. This combined with the observation of very low background levels of Pt observed in both the digest blank (water blanks) as well as the DNA extraction blanks is a positive indication for the suitability of the OG-500 kits in the clinical study.

2.4.4 Conclusion

The recovery and stability were determined to be within an acceptable range and it was concluded that the OG-500 saliva kits would be stable enough for the purpose of the investigation into the comparison on the level of Pt-DNA adducts in saliva and blood.

2.5 Comparison of Pt-DNA adducts in patient leukocyte and saliva samples

2.5.1 Results and Discussion

The collection of samples of both blood and saliva for this trial proved to be very problematic. As is often the case when working with human samples a level of patient drop out was experienced. Patients were entitled to withdraw consent from the trial at any point and there were 5 incidences where not all samples were obtained as the patients withdrew from the study.

However, there were some specific problems associated with each form of sampling. Firstly, with regard to blood samples, as was anticipated very few patients were willing to donate a 24 hour blood sample due to the inconvenience of having to return to the hospital the day following their treatment. Considering the patients' poor health this was completely understandable and in the end only one patient of the final 23 patients sampled was able to donate a 24 hour blood sample.

In contrast, and proving that for patients' saliva was a much more patient-friendly sampling technique, nearly all patients provided a 24 hour saliva sample. However, problems were experienced in gaining patient compliance with the sampling protocols. While initially the aim was to obtain a sample set from 10 patients, due to problems collecting correct saliva samples, in total 23 patients were recruited for this study before 10 complete sample sets had been obtained.

The most common problem encountered while collecting saliva samples was patients not providing a full 2mL saliva sample. While this in theory would not cause a problem with the quality of the DNA provided, it could result in a lower yield of DNA being recovered and no replicate analysis being possible. The second most common issue found with this sampling technique was the failure to add all or some of the stabilising solution contained within the kit. If no or little stabilising solution was added there was potential for sample degradation or movement in Pt within the sample to occur, which would affect the results of this experiment. On occasions samples would be returned to the lab short of the final 4 mL sample and it was impossible to know if the sample was small due to there being too little saliva donated or whether not all of the stabilising solution was added.

The final, and least common, problem encountered in saliva sampling was the failure to swap the funnel to the leak free screw cap lid after donating sample and addition of stabilising solution. This resulted in either the complete loss and/or contamination of the sample and those samples

were therefore useless. A full list of all samples taken (both complete and incomplete) is shown in Table 29 (Appendix A).

As it was uncertain whether or not all of these problems would affect the final result, samples were continued to be collected to ensure 10 complete and correct sets. Below the results from the 10 complete sample sets are analysed first, before looking at all of the samples obtained.

2.5.1.1 Comparison of Pt-DNA adducts in 10 complete sample sets

The patients from whom 10 complete blood and saliva sample sets were obtained were from patient numbers 34, 35, 39, 48, 49, 50, 51, 53, 54 and 55. The results for these 10 complete sample sets were run in 4 batches on the ICP-MS (2 batches for each blood and saliva). For each batch a calibration graphs for both phosphorus (^{31}P) and platinum (^{195}Pt) using europium (^{153}Eu) as an internal standard were produced. While all calibration graphs pertaining to this section can be found in Appendix A, all of which showed excellent linearity, an example of a P and Pt calibration graph for the blood samples is shown below (Figure 15 and Figure 16).

The calibration graphs and the raw intensity data (cps) for the elements measured were then used to calculate the number of Pt-DNA adducts per 10^6 nucleotides for both blood and saliva samples from all 10 patients. Three replicates were obtained for the blood samples (the leukocyte samples were split into aliquots prior to DNA extraction); while two replicates were run for the saliva samples (the extracted DNA sample dissolved in water was mixed thoroughly then split into two equal aliquots). The results from this as summarised in Table 4, Figure 15 and Figure 16.

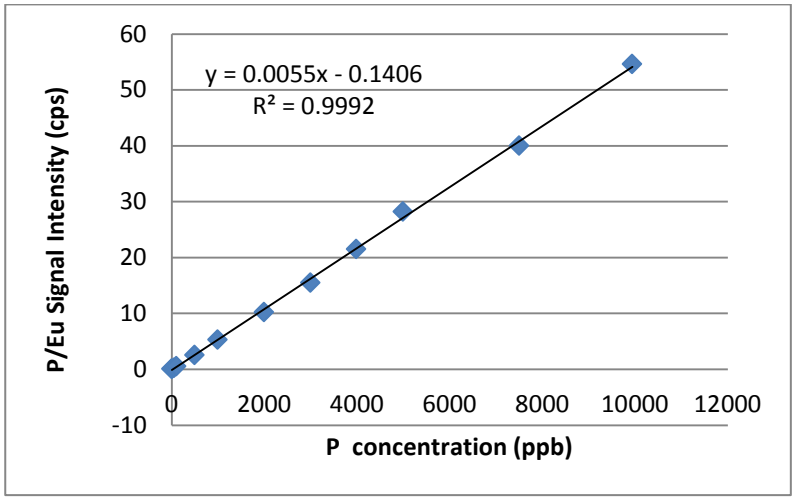

Figure 15 - Example Phosphorus Calibration Graph

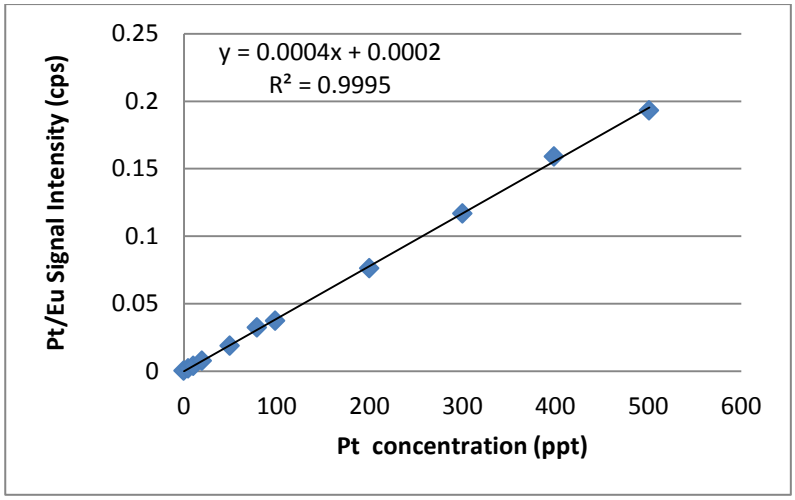

Figure 16 - Example Platinum Calibration Graph

Table 4 - Pt-DNA adduct data obtained from 10 patient blood and saliva samples

Patient ID	Time point	Average number of Pt-DNA adducts (per 10^6 nucleotides)	
		Blood	Saliva
34	Pre	0.21	0.45
	1 Hour	4.10	5.60
	24 Hour	5.10	6.22
35	Pre	0.42	0.39
	1 Hour	3.84	3.74
	24 Hour	-	2.36
39	Pre	0.56	0.59
	1 Hour	3.35	4.44
	24 Hour	-	1.43
48	Pre	0.38	0.76
	1 Hour	5.32	3.34
	24 Hour	-	2.78
49	Pre	0.65	1.17
	1 Hour	7.11	4.24
	24 Hour	-	3.24
50	Pre	0.13	0.29
	1 Hour	4.53	4.00
	24 Hour	-	1.57
51	Pre	0.28	0.76
	1 Hour	3.35	3.04
	24 Hour	-	5.35
53	Pre	0.44	0.60
	1 Hour	3.35	3.17
	24 Hour	-	3.99
54	Pre	0.27	0.68
	1 Hour	1.68	5.81
	24 Hour	-	6.47
55	Pre	0.37	0.37
	1 Hour	2.87	4.07
	24 Hour	-	4.16

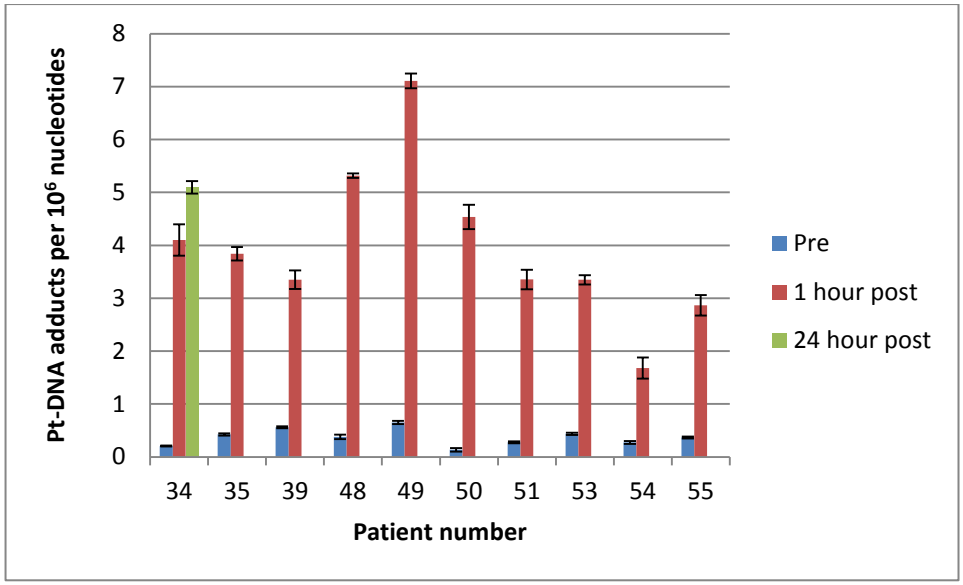

Figure 17 - Number of Pt-DNA adducts formed in pre- and post-infusion leukocytes samples in patients. Error bars produced 2x standard deviation, *n*=3

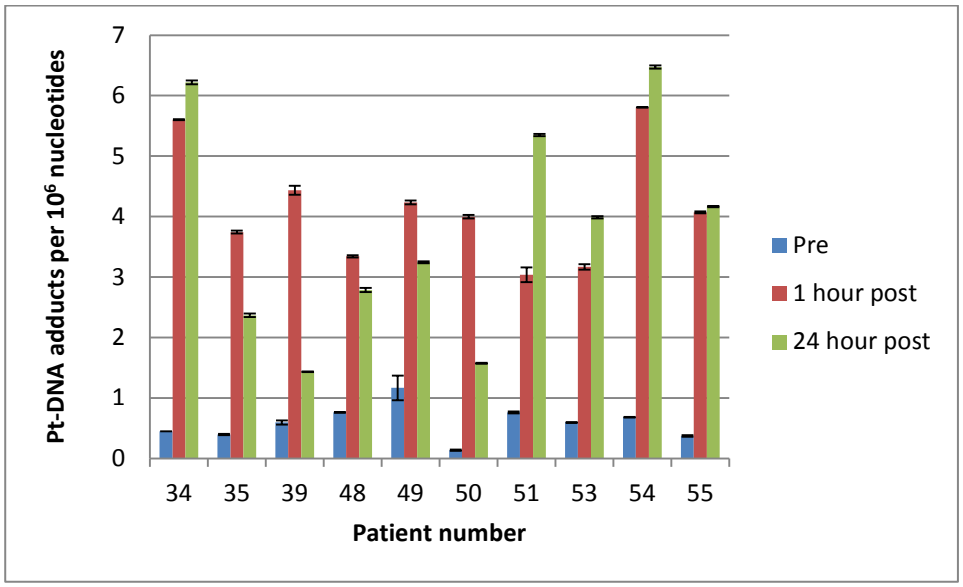

Figure 18 - Number of Pt-DNA adducts formed in pre- and post-infusion saliva samples in patients. Error bars represent range of samples

Figure 17 and Figure 18 show the average number of Pt-DNA adducts measured in the blood and saliva samples respectively for all 10 patients at the different sampling time points. The error bars shown were calculated either as two times the standard deviation of the replicates or represent the range of the results. With the exception of patient number 34, no 24 hour blood samples could be obtained, and therefore only the pre- and 1 hour post-infusion data is presented for the blood samples from the remaining patients. To enable an easier visual comparison between the two data sets, they were combined onto one graph (see Figure 19).

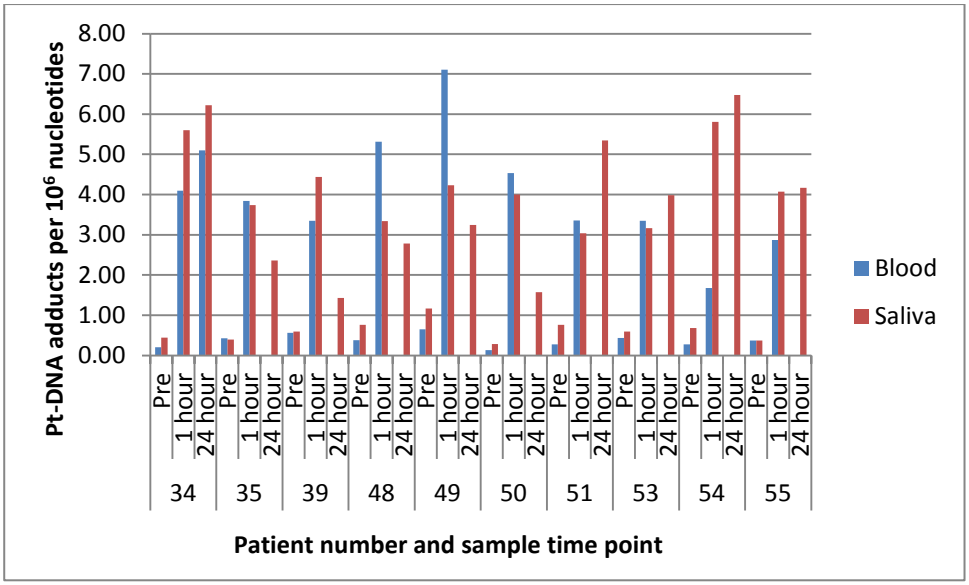

Figure 19 - Comparison of Pt-DNA adduct formation levels in saliva and leukocyte patient samples

Figure 17, Figure 18 and Figure 19 show very clearly that it is possible to measure Pt-DNA adducts in blood and saliva samples obtained from clinical patients. However, a comparison of the level of Pt-DNA adducts in both blood and saliva samples from the same patients at the same time point showed a poor correlation between the two sample types.

However, one positive observation is that the adduct levels recorded in saliva were of a similar level (i.e. same order of magnitude) as measured in the blood samples. With the exception of patient 54, the range of adducts per 10^6 nucleotides recorded was within a factor of 2 at the 1 hour time point. This is suggestive that with further method development and adjustments that saliva could be a viable alternative to blood sampling. While a visual inspection of the adduct levels between sample types indicated poor or no correlation, correlation scatterplots for pre-infusion and 1 hour post-infusion were drawn to aid in assessing the correlation for the two sample types (see Figure 20 and Figure 21). As only one 24 hour blood sample was obtained, no comparison between the 24 hour samples could be drawn.

Pearson correlation coefficients were calculated for the data sets presented; as shown in Figure 20 and Figure 21 and Table 5. While there is some correlation between the pre-infusion samples for the blood and saliva samples ($r = 0.6143$), there is no correlation (or in fact a slight negative correlation, $r = -0.2598$) between the 1 hour post infusion blood and saliva samples.

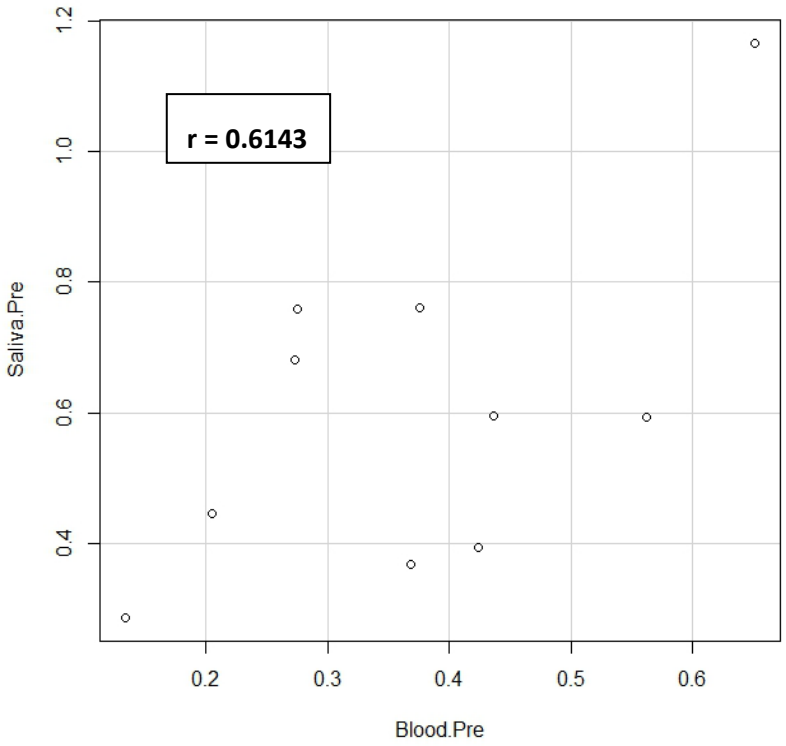

Figure 20 - Scatterplot showing the correlation between the pre-infusion samples from blood and saliva samples

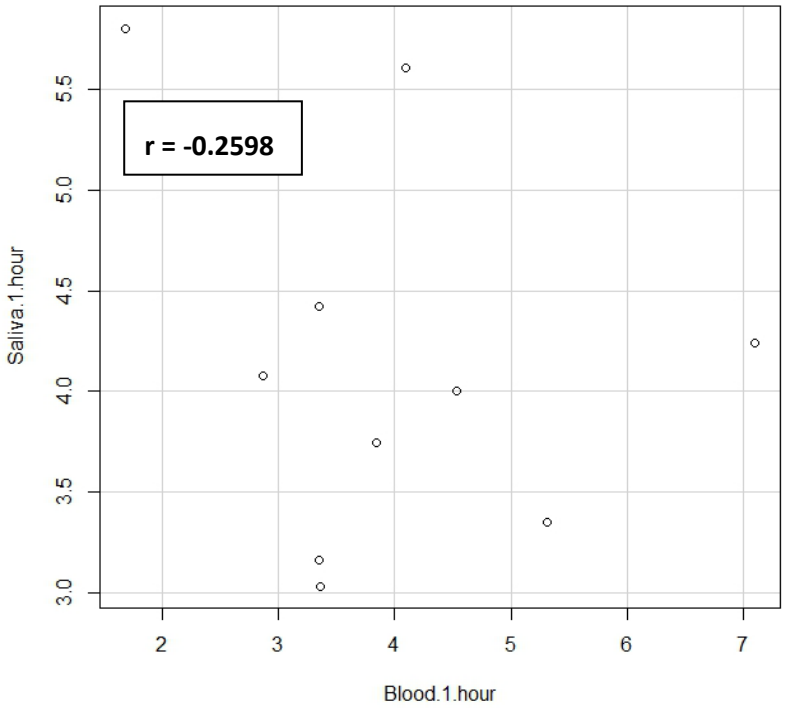

Figure 21 - Scatterplot showing the correlation between the 1 hour post-infusion samples from blood and saliva samples

Table 5 - Pearson correlation coefficient values for complete patient data set

	Blood Pre	Blood 1 Hour	Saliva Pre	Saliva 1 Hour
Blood Pre	1.0000	0.4054	0.6143	-0.2019
Blood 1 Hour	0.4054	1.0000	0.5272	-0.2598
Saliva Pre	0.6143	0.5272	1.0000	-0.0884
Saliva 1 Hour	-0.2019	-0.2598	-0.0884	1.0000

Reasons for the lack of correlation require further investigation, however, studies have shown that DNA obtained from saliva does not originate exclusively from buccal epithelial cells as once thought and is instead a mixture of a range of cells. This mixture of cell types can be dependent on such factors as the condition of the mouth. One study found that saliva frequently contains a significant quantity of leukocyte cells. In this study, the number of leukocyte cells in saliva has been measured and varied greatly from 2 to 136,000 cells/mL to $1.1x10^6$ cells/mL where a patient has had an inflamed oral cavity.[121,122] Oral mucositis, which is a side effect of chemotherapy experienced by some chemotherapy patients, can result in sores and ulcers leading to an increased level of blood in the mouth. Theoretically if a higher level of leukocytes were present in the saliva samples the correlation between the two sample types should be better, however the extent of oral mucositis was not fully known for the patient group in this investigation and therefore the number of leukocytes in each sample remains unknown. Other potential reasons for the lack of correlation were also considered, such as a potentially different mechanism of uptake of platinum by buccal cells compared to blood cells, as well as the possibility of different types of leukocytes within the two sample types which could act differently. On top of this there is also the potential for DNA contamination from bacterial organisms from within the mouth. However without further knowledge of the samples contents no firm conclusions could be made.

It is therefore feasible that the lack of correlation observed in this study could potentially be due, at least in part, to the unknown and variable mixture of cells and leukocyte contamination level in each saliva sample. Unfortunately, the level of leukocyte contamination and mixture of cells was unknown for these samples and without this knowledge further data analysis on these samples was not possible. Any future studies would have to employ the use of cell sorting on saliva samples before DNA extraction was performed to see if any better correlation could be obtained.

In this investigation cell sorting was not an option as the saliva collection kits (OG-500) prevented such a step and the stabilising solution added to preserve the sample induced cell lysis. A cell sorting procedure, such as flow cytometry, would have to be performed on a fresh DNA sample, thus potentially coming across the issue of having to analyse the sample immediately which was

one of the inconveniencies of blood sampling, however would still remain a less intrusive and more patient friendly sampling technique.

While a lack of correlation was observed in the 1 hour post-infusion samples, a significantly higher level of correlation was observed in the pre-infusion samples. All 10 of the patients in this part of the study had already received at least one previous cycle of chemotherapy, and consequently had a very low level Pt-DNA adduct level in their pre-infusion samples. Due to the fact that these levels are low (typically lower than 0.5 Pt-DNA adducts per 10^6 nucleotides), even if the actual number of adducts were not exactly the same between sample types, they were at least closer to each other, resulting in a higher level of correlation observed.

While investigating the correlation between the Pt-DNA adduct levels was the primary aim of this investigation, the data set presented also highlighted some other interesting insights. Firstly a significant amount of inter-patient variability was observed. Speculated reasons for this variation are two-fold. Firstly, the 10 patients in this study were receiving different doses of varying combination treatments for various types of cancer (these details are summarised in Table 6, however full details can be found in Appendix A). Secondly, large variation in human and other biological studies is not uncommon, particularly when considering the mixture of gender and age as in this study. When this is considered in relation to Pt-DNA adduct formation, it is suggestive that patient-specific factors play a role in how a patient is affected by and how effective the cancer chemotherapy treatment is.[123–126]

Previous studies have shown some, often limited, correlation between adduct levels and toxicities experienced by patients.[5,86,94,96,127] Toxicities are graded according to the Common Toxicity Criteria (CTC), and any grade 3/4 toxicities observed during the course of chemotherapy were recoded (see Appendix A), however in this study, no particular correlation between adduct levels and grade 3/4 toxicities were noted. Furthermore, as a mixture of adjuvant and non-adjuvant patients (i.e. mixture of metastatic and non-metastatic patients) were recruited for this trial, it is difficult to compare survival data.

Table 6 - Patient regiment and cycle numbers

Patient	Regiment	Cycle	Cancer Type	Dose Reduction (cycle number)	Toxicity reported
34	EOX	4	Adeno carcinoma oesophagus	75 % (3 onwards)	-
35	FOLFOX and Bev	10	Colorectal cancer	75% (2 onwards)	Diarrhoea cycle 1
39	FOLFOX and Bev	8	Colorectal cancer	70% (4 onwards) 0% (10 onwards)	Neuropathy cycle 3
48	FOLFOX	2	Colorectal cancer	75% (3 onwards)	Neutropenia and neuropathy cycle 2
49	FOLFOX and Bev	7	Colorectal cancer	80% (4 onwards) 75% (8 onwards) Stopped cycle 12	Neuropathy cycle 3
50	FOLFOX	2	Colorectal cancer	75% (2 onwards) 50% (7 onwards) 0%(8)	Neuropathy cycle 1
51	FOLFOX and Bev	11	Colorectal cancer	-	-
53	ECX	53	Gastric oesophageal junction cancer	-	-
54	Cis / etop	3	Small cell oesophagus	85% (4 onwards)	Deterioration in hearing cycle 3
55	EOX	2	Gastric	75% (2 onwards) 50% (4 onwards)	Fatigue, diarrhoea, neutropenia, vomiting, neuropathy cycle 1

As previously mentioned, a low number of Pt-DNA adducts were observed in each pre-infusion sample measured in this part of the study. This was not surprising as none of these 10 patients were on their first cycle. This carry-over effect of platinum in patients between cycles has been observed before, and shows that at least a low level of platinum stays within the blood stream (and other bodily cells, such as saliva) between cycles which are typically two to three weeks apart.[5] This phenomenon has a lot of potential for future investigation as it is unclear what, if any, effect the number of Pt-DNA adducts persisting in the body between cycles has on patient response or side effects experienced.

Another key observation from these results was the rapid appearance of platinum within the saliva samples as was evident by the increase in the level of Pt-DNA adducts as seen in the 1 hour-post saliva samples compared to the pre-infusion samples. While this was expected in the blood samples (see Figure 17), given that the treatment is administered intravenously, and thus is visible at measurable levels at the first post-treatment sample time point, it is evident from Figure 18 that the platinum also reaches the DNA within the saliva within a 1 hour time period. Even

though the results of this work showed a poor correlation between the two sample types, the rapid movement of platinum into the saliva is a positive observation for the possibility of using saliva as a research sample for this type of work.[112]

From Figure 18 it can also be noted that that in some cases the number of adducts measured at the 24 hour time point had increased when compared to the 1 hour post-infusion sample, where as in other patients the level had decreased. This could potentially be evidence of repair of the DNA, or potentially due to instability of the guanine adducts. Guanine adducts (which comprise of large percentage of adducts formed, see Chapter 1) are labile and can undergo depurination. And therefore the stability of the adducts and the repair efficiency may be the key factors resulting in inter-patient variability. While this effect has been seen in leukocyte samples previously, some studies have suggested that adduct levels are at their highest around 6 hours post drug infusion.[5,71,100] While in this study it would have been possible to collect a saliva sample at 6 hour post-infusion time point, it would not have been feasible to collect a corresponding blood sample to compare it to, and thus would not have helped in determining whether saliva is a viable alternative to leukocytes.

2.5.1.2 Comparison of Pt-DNA adducts in the 13 remaining incomplete sample sets

As previously discussed, in total 23 patients were recruited for this study before a final of 10 complete patient sets were obtained. A sample set was determined to be incomplete if one or more of the samples were missing (either blood or saliva) or if too little sample was provided. When samples containing too little saliva sample were returned it wasn't always clear whether this was because the patients had just donated less saliva than we had asked for (which would result in a lower yield of DNA) or whether the stabilising solution had not been added (and therefore the sample would not have been stable). Thus it was decided not to include such samples in the complete data sets described above, but rather to analyse them as part of the 'incomplete' sets, using the preparation and analysis methods detailed in Section 2.3.

The calibration graphs for the remaining blood and saliva samples (patient numbers 33, 36, 37, 38, 40, 41, 42, 43, 44, 45, 46, 47 and 52) are shown in Appendix A. The results of these are outlined below (Table 7, Figure 22, Figure 23 and Figure 24).

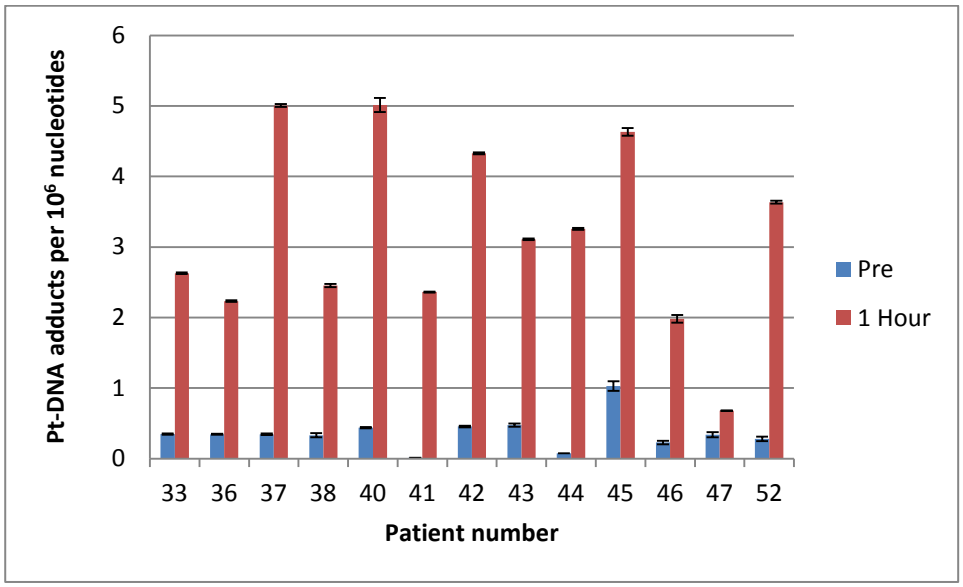

Figure 22 - Number of Pt-DNA adducts formed in pre- and post-infusion leukocytes samples in incomplete patient sample sets. Error bars produced 2x standard deviation, *n*=3

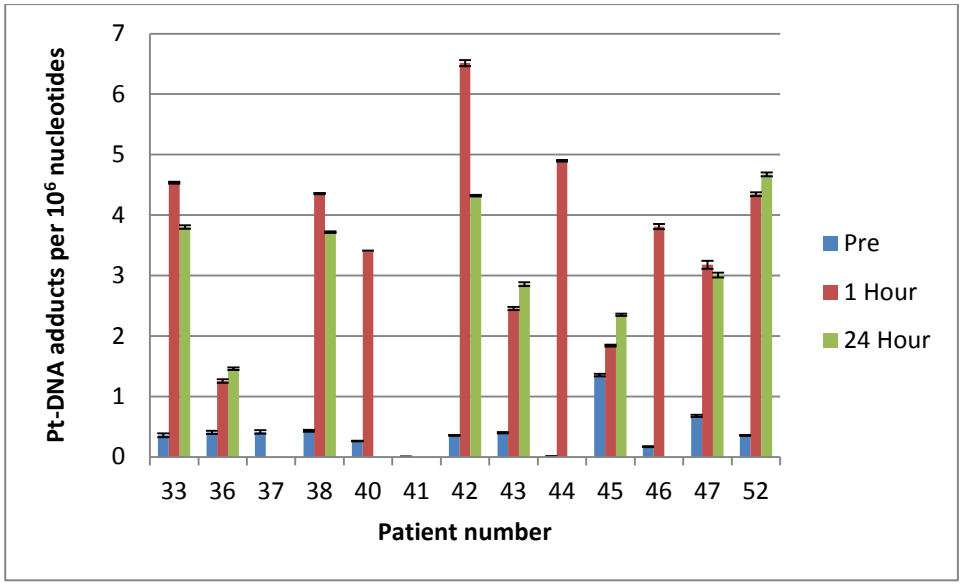

Figure 23 - Number of Pt-DNA adducts formed in pre- and post-infusion saliva samples in incomplete patient sample sets. Error bars represent the range of samples

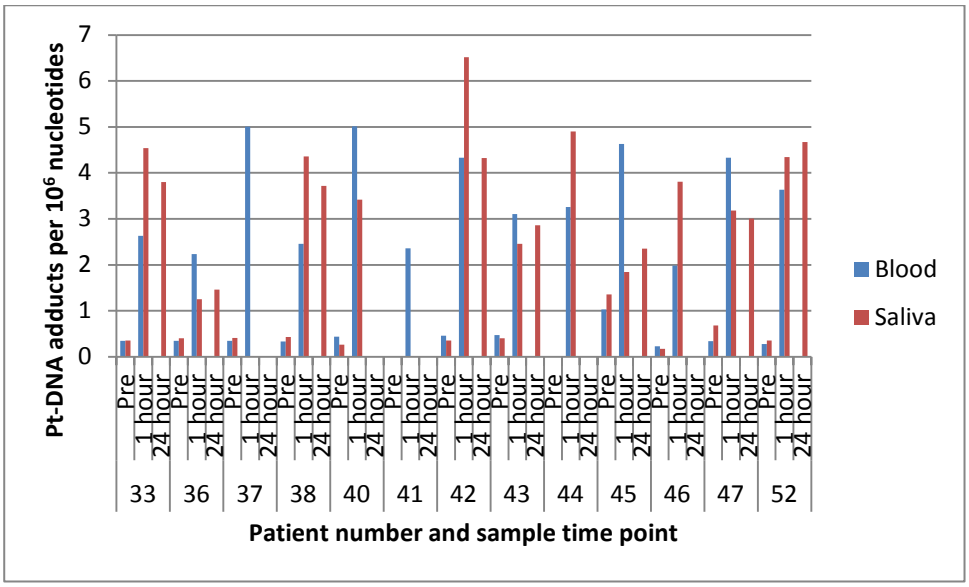

Figure 24 - Comparison of the number of Pt-DNA adducts formed in pre- and post-infusion leukocytes and saliva samples in incomplete patient sample sets

Table 7 - Average Pt-DNA adduct formation in 13 incomplete patient blood and saliva sets

Patient ID	Time point	Average adducts (per 10^6 nucleotides)	
		Blood	Saliva
33	Pre	0.35	0.36
	1 Hour	2.63	4.54
	24 Hour	-	3.80
36	Pre	0.34	0.40
	1 Hour	2.23	1.25
	24 Hour	-	1.46
37	Pre	0.34	0.41
	1 Hour	5.01	-
	24 Hour	-	-
38	Pre	0.33	0.43
	1 Hour	2.45	4.36
	24 Hour	-	3.71
40	Pre	0.44	0.26
	1 Hour	5.01	3.41
	24 Hour	-	-
41	Pre	0.01	0.01
	1 Hour	2.36	-
	24 Hour	-	-
42	Pre	0.46	0.35
	1 Hour	4.33	6.51
	24 Hour	-	4.32
43	Pre	0.47	0.40
	1 Hour	3.11	2.46
	24 Hour	-	2.86
44	Pre	0.01	0.01
	1 Hour	3.26	4.90
	24 Hour	-	-
45	Pre	1.03	1.35
	1 Hour	4.63	1.84
	24 Hour	-	2.35
46	Pre	0.23	0.17
	1 Hour	1.98	3.81
	24 Hour	-	-
47	Pre	0.34	0.68
	1 Hour	4.33	3.18
	24 Hour	-	3.01
52	Pre	0.28	0.35
	1 Hour	3.63	4.34
	24 Hour	-	4.67

These results were treated in the same way as the complete sample sets were and the scatter plots and Pearson correlation coefficients were calculated (see Figure 25 and Table 8).

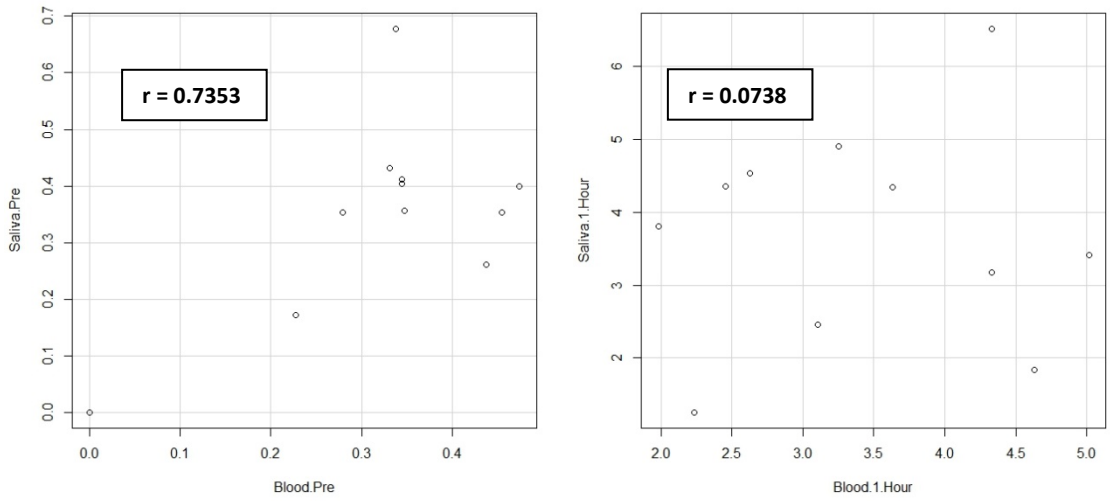

Figure 25 - Scatter plots comparing the adduct levels in both blood and saliva levels in pre- and 1 hour post infusion time points

Table 8 - Pearson correlation coefficient values for incomplete patient data set

	Blood Pre	Blood 1 Hour	Saliva Pre	Saliva 1 Hour
Blood Pre	1.0000	0.4047	0.7353	-0.1754
Blood 1 Hour	0.4047	1.0000	0.3336	0.0738
Saliva Pre	0.7353	0.3336	1.0000	-0.3032
Saliva 1 Hour	-0.1754	0.0738	-0.3032	1.0000

For the pre-sample scatterplot and Pearson correlation coefficient calculation patient number 45 was removed from the calculation. This was due to an error occurring during sample donation which resulted in the pre-infusion sample only being taken immediately at the end of the treatment and the 1 hour post infusion sample being taken 1 hour after that, and therefore the pre- sample was not a true reflection of the pre-infusion adduct levels.

When examining the correlation coefficients measured in the incomplete sets, slightly better correlation was observed in both pre- and 1 hour post-infusion samples. While the condition and stability of some of these saliva samples is unclear and therefore does question some of these results, there are some potential explanations for the slight differences in results observed.

Firstly, in this second set of samples there were 3 patients on their first cycles of treatments. These patients by definition should only have had background levels of platinum in their samples, resulting in the very low (virtually zero) number of adducts per 10^6 nucleotides. As one of these patients was patient number 45 where the pre- sample was taken late this sample can be

discounted when making these observations. The two remaining first cycle samples were below the LLOQ of 0.2 adducts per 10^6 nucleotides as determined by Zayed.[111] These very low results likely aided the correlation as the difference between the two recorded values was noticeably smaller.

The reason for the slight change in correlation in the 1 hour post-infusion samples (from a slightly negative correlation to virtually no correlation) is unclear, however when considering how great human variation is and the potential error associated with some of the stability of the saliva samples, this change seems very slight and not of great significance.

2.6 Conclusions

This chapter described the application of an ICP-MS assay to the quantification of Pt-DNA adducts in both blood leukocyte and saliva samples in patients receiving platinum based chemotherapy drugs. While this assay had previously been successful in the determination of Pt-DNA adducts in leukocyte samples, it was for the first time successfully used in determining the number of adducts in saliva samples as well.

This work aimed to be able to directly compare adduct levels in two different sample types from the same patients in order to determine whether saliva DNA (which can be obtained less invasively and is thus a more patient friendly technique) could be used as an alternative to leukocyte sampling for the determination of adduct formation. To do so, leukocyte and saliva samples were obtained from patients both pre- and 1 hour post-infusion with an additional 24 hour post-infusion saliva sample being obtained. While the initial aim was to collect 10 sample sets for comparison of adduct levels, problems encountered in gaining patient compliance with the saliva sampling protocol resulted in a total of 23 patients sets being acquired before a set of 10 complete sets were eventually obtained. The lack of patient adherence to the sampling protocol, as detailed in the sections above, was an unforeseen difficulty and is something that would need to be addressed if saliva was to become a viable alternative sampling technique for this application.

A direct comparison of the 10 complete (and 13 incomplete sets) was performed but while a limited correlation was observed between the adduct levels in blood and saliva pre-infusion samples, a lack of correlation was observed in the 1 hour post-infusion samples. Possible reasons for this were discussed, however it was concluded that a feasible explanation was the unknown mixture of cell types found in the saliva samples as well as a potentially different uptake mechanism for other types of cells.

While a direct comparison could be made for the pre- and 1 hour post-infusion time points, it had been hoped to be able to collect a few 24 hour blood samples to compare the 24 hour post infusion saliva samples, however unfortunately only one patient was able to donate a 24 hour blood sample. While unfortunate, this was not wholly unexpected and does reinforce the idea that more patient friendly and less intrusive sampling methods, such as saliva, would help in the study of adduct levels over extended periods of time when patients are not in hospital. One positive observation from the saliva sampling was the high yield of DNA collected. In clinical

sampling often sample size can be a limiting factor, however while the DNA yield from saliva between patients was variable, more DNA was extracted from the saliva than the leukocytes.

The number of participants in this study was small and consequently only limited statistical data can be obtained from it. Only 10 patients were chosen from the outset for this investigation as this experiment was not designed to be statistically powered but rather act as a proof of concept that saliva could be a viable alternative to blood sampling. Had this investigation yielded positive results, a further more extensive study could have been carried out using a greater number of patients and further time points to aid in the understanding on how adduct formation over time is correlated to patient outcome and side effects, with the ultimate aim of eventually creating an *ex-vivo* test for predicting toxicity and aiding in personalised chemotherapy doses.

Overall this work has shown that not only was it possible to determine the level of Pt-DNA adducts in DNA obtained from both white blood cells and saliva clinical samples using ICP-MS, but that it was also possible to observe platinum from previous chemotherapy cycles in both sample types. Significant inter-patient variability as well as some evidence of repair between the 1 and 24 hour time points was observed. The purpose of this investigation was to determine whether saliva could be used as a less invasive and more patient friendly sampling technique for the measurement of Pt-DNA adducts. DNA adducts were quantified, but the correlation found between sample types was poor, leading to the conclusion that while saliva showed promise as a technique for DNA extraction, it is not at present a viable alternative to blood sampling for the quantification of Pt-DNA adducts.

3. The binding of Pt-based chemotherapy drugs to cytosol proteins

3.1. Introduction

Colorectal cancer is one of the four most commonly diagnosed cancers worldwide and as it has long been considered to be moderately resistant to chemotherapy. As a result new drugs and combination treatments, as well as other ways to improve the efficacy of the drugs, are constantly being investigated.[128,129] Oxaliplatin, often in combination with 5-fluorouracil, is still widely used in the treatment of colorectal cancers.[13,129,130]

Previous studies have discovered that only about 1% of the platinum drugs reach the DNA, and furthermore that the cytosol is the largest 'sink' for platinum-based drugs, such as that demonstrated in Figure 26. [4,5,131]

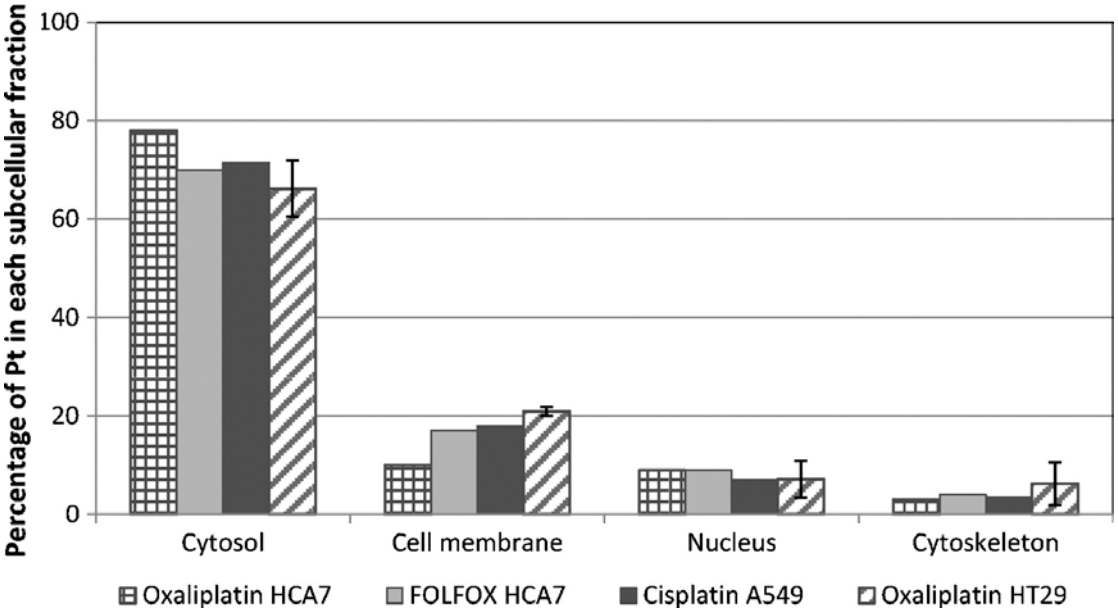

Figure 26 - Percentage of platinum found in the different sub-cellular fractions of various colorectal cancer cell lines following treatment with the Pt-based drugs indicated. Used with permission. [5]

It is the binding of Pt-drugs, such as oxaliplatin, to proteins found in the cytosol of colorectal cancer cells that is the primary focus of this chapter. By investigating the potential binding sites on proteins found within the cytosol of cells it was hoped to identify the preferred binding sites of oxaliplatin.

Pt- drugs, such as oxaliplatin and cisplatin, are known to bind in particular to ligands which are nitrogen and sulfur rich, and therefore short peptide sequences rich in sulfur and nitrogen were chosen for this investigation.[4,132–134] Once oxaliplatin has entered the cell, the intracellular

environment has to be considered, in particular the sulfur-containing nucleophiles, as oxaliplatin has been found to exhibit a higher reactivity towards sulfur-containing compounds than cisplatin.[132] The analysis of both nitrogen and sulfur rich peptides were of interest as there is evidence to suggest that the binding of oxaliplatin to nitrogen is not only possible, but energetically competitive to the binding with sulfur.[134]

3.2 Experimental design

The overall aim of this section of work was to identify which, if any, proteins and peptides in the cytosolic fraction have a higher affinity for binding with platinum-based anti-cancer drugs. As a step towards achieving this aim, this section of work identified potential target peptides and by modelling their interaction with oxaliplatin it was hoped to result in the identification of specific targets of oxaliplatin which could be further investigated.

Previous attempts to carry out a tryptic digest of the cytosol from cells exposed to oxaliplatin and to directly identify Pt-peptides using HPLC-ICP-MS had been made within this research group. The results were not reproducible and therefore the top-down approach was temporarily abandoned in favour of a bottom-up approach starting with simple peptides, such as glutathione[134] and carnosine[135], and then moving on to sequences that were represented in proteins that had been identified as having altered abundances in cancer patients. A fellow researcher within the group at Loughborough University, Dr Claire Camp, had previously identified a list of cytosolic proteins of interest, which was used as a basis for this work.[136] Firstly a literature search was conducted searching for proteins and peptides up-regulated in cancer patients. Proteins were then chosen based on a search using the Uniprot database using the search criteria of human, cytosol and colon, resulting in a few proteins being chosen which had also been cited in related journal articles. [5,9,15,84,136–152] Short peptide fragments from these proteins were then chosen by undergoing a theoretical tryptic digest using ExPASy peptide cutter before residues of an appropriate length which were rich in either nitrogen or sulfur were chosen for analysis, these being the potential primary binding sites for oxaliplatin.

The following short peptides were chosen for analysis:

- Sulfur rich: GCMR, AMMK, MSMK, MMTK, MCAAR, CVK
- Nitrogen rich: NNIK, ENQK, QHEK, YRPR

The fragmentation and full mass spectrum of each peptide was analysed, before the binding of the peptides with oxaliplatin was measured immediately after mixing and at 24 hours.

3.3 Methodology

The peptides listed above in Section 3.2 were synthesised by and purchased from Generon (Maidenhead, UK). Each peptide (3mM) was dissolved in 50:50 MeOH:H_2O with 0.1% formic acid, before a full mass spectrum was obtained. Following this, oxaliplatin was added to the solution in a 2:1 mM ratio (peptide: oxaliplatin) before being analysed again immediately after mixing and at 24 hours. The oxaliplatin, formic acid, HPLC grade water and methanol were all purchased from Sigma Aldrich (Poole, UK).

The samples were analysed primarily on an LTQ linear ion trap mass spectrometer with an electrospray ionisation source, with some also being analysed on an 'Orbitrap' high resolution Q-Exactive fourier transform mass spectrometer (Thermo Electron, San Jose, CA, USA). The Q-Exactive was equipped with a Tri-Versa NanoMate ESI chip nanospray (Advion, New York, USA).

The LTQ was operated in the positive mode at 5.20 kV and 260°C, having been calibrated prior to use as per the manufacturer's recommendations. The resolving powers achieved were in the order of 1500 while the upper instrumental error limit in measurements was 0.2 m/z units. The LTQ auto-tune function was used following this to obtain lens, quadrupole and octapole voltages for maximum transmission of the ions of interest. Helium gas was used as a buffer gas within the ion trap (at approximately 10^{-3} Torr) to improve the trapping efficiency as well as the collision gas for collision induced dissociated experiments (CID).

Samples were introduced into the instrument at the rate of 10 μL min^{-1} into the electrospray source which utilised nitrogen as a nebulising gas. Auxiliary and sheath gases were tuned daily to enable maximum signal transmission.

3.4 Results and Discussion

The 10 peptides were analysed as detailed in Section 3.3. Full mass spectra were generated in positive ion mode for the peptide and oxaliplatin mixtures performed without allowing any incubation time. The mixture was stored at room temperature and analysed again after 24 hours to ensure that no significant alterations to the predominant peaks occurred. This data, along with analysis of the full peptides only can be found in Appendix B.

3.4.1 Nitrogen rich peptides

Analysis of the four nitrogen rich peptides (NNIK, ENQK, QHEK, YRPR) is presented below. The structures of these four peptides are shown in Figure 27.

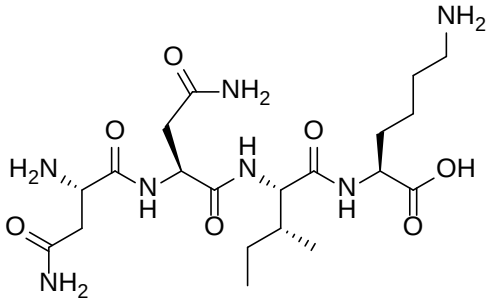

Peptide 1 - NNIK

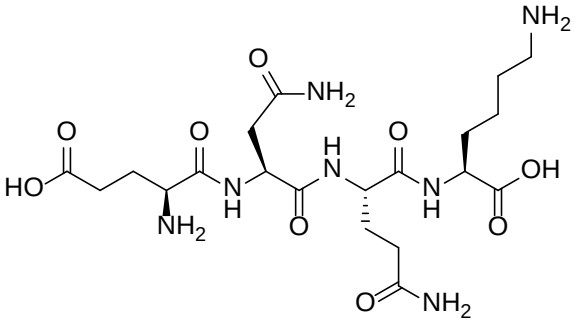

Peptide 2 - ENQK

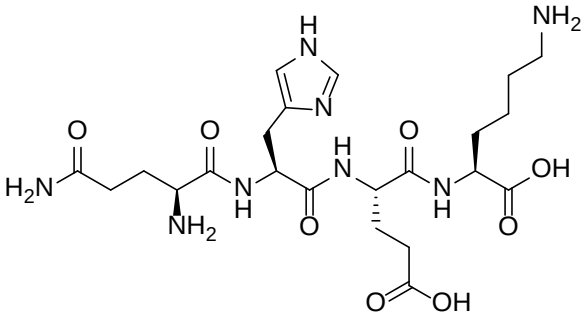

Peptide 3 - QHEK

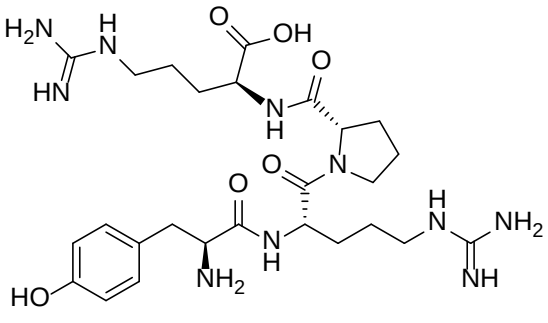

Peptide 4 – YRPR

Figure 27 – Structures of the four nitrogen rich peptides

The first peptide analysed was NNIK. The full mass spectrum is shown in Figure 28 and the main peaks assigned in Table 9.

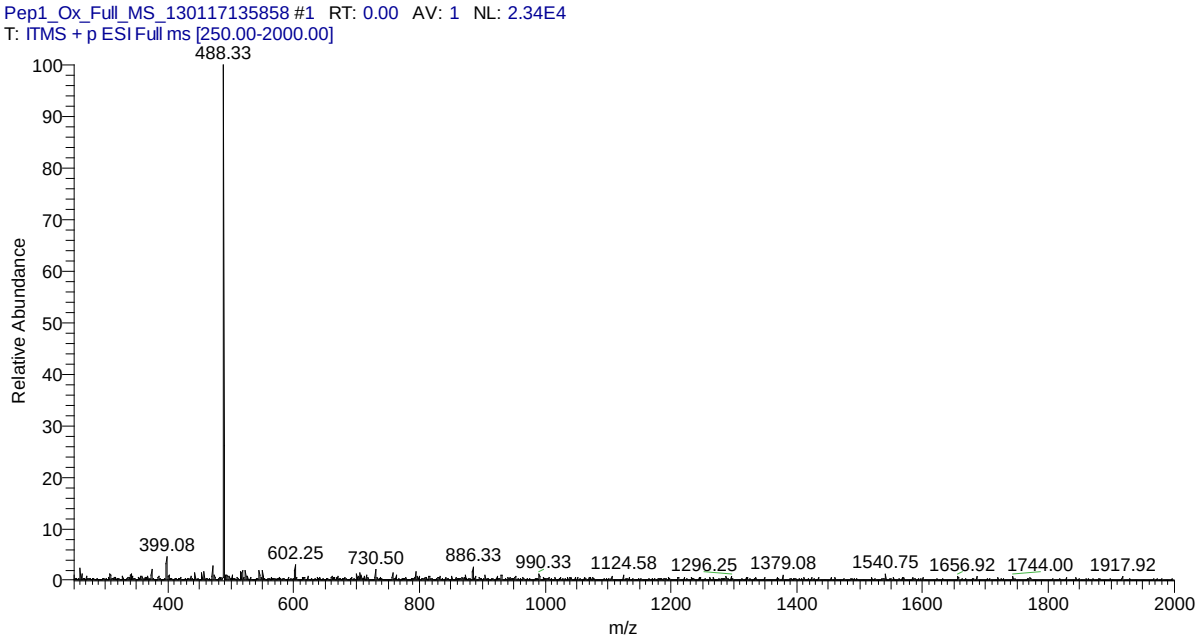

Figure 28 – Full mass spectrum for peptide 1 (NNIK) and oxaliplatin

Table 9 – Peak assignments for peptide 1 (NNIK) and oxaliplatin

Most abundant isotope *m/z*	Assignment
399.08	$[OxPt + H]^+$
488.25	$[NNIK + H]^+$
602.25	$[(NNIK+N) + H]^+$
794.92	$[(OxPt)_2 + H]^+$
886.33	$[NNIK+ OxPt + H]^+$

*N denotes the amino acid asparagine

As can be seen from Figure 28 the base peak was peptide 1 (NNIK) on its own (*m/z* 488.3), with a small peak observed for oxaliplatin as the second largest peak. A small peak was observed at *m/z* 886.3, which was assigned as the peptide and oxaliplatin complex, indicating that while some binding occurred, this binding was not strong as plenty of free oxaliplatin remained. When compared to the spectrum of that obtained 24 hours later (Figure 92, Appendix B), while a few new peaks were observed, the primary peak of interest (*m/z* 886) did not appear to be significantly larger. This pattern was seen with the other peptides described later in this chapter, and can therefore be concluded that the binding between the peptides and oxaliplatin are not altered significantly with a 24 hour incubation time.

A significantly lower signal intensity was observed in all of the spectra for $[OxPt+H]^+$ relative to those of the peptides. Some potential reasons for this are as follows. Firstly, the ratio of peptide: oxaliplatin was in favour of the peptide, using a 2:1 ratio, and therefore being at a higher concentration to begin with, a larger intensity signal would be expected. Secondly, the ionization efficiency of the species may not be equivalent, and furthermore as the signal for oxaliplatin is split over a larger isotopic range when compared to that of the peptides, it is feasible to suggest this as a potential reason for the smaller observed signals for oxaliplatin and oxaliplatin-peptide complexes. Additionally, work by Shoeib *et al.*[134] investigated the interaction between oxaliplatin and the protein glutathione and observed a similar trend and theorised another potential reason for the lower oxaliplatin signal was due to the two ligands not competing equally for proton sources within the solution. With the aid of computer modelling they reported that glutathione had a higher proton affinity than oxaliplatin (255.3 and 233.5 kcal mol^{-1} at 298K respectively). Glutathione is a small, tri-peptide protein found abundantly within the cytosol, and is similar in size and structure to many of the peptides studied in this chapter, and it is plausible to suggest that the peptides used in this study have a higher proton affinity than that of oxaliplatin.[153] Computational analysis for two peptides presented in this chapter were performed by collaborators at the American University in Cairo, the results of the modelling are presented in Section 3.4.3.

Another interesting observation noted from the spectrum of peptide 1 (and subsequent spectra of the remaining peptides below) is the presence of whole/intact oxaliplatin as opposed to what is considered to be the biologically active form (oxaliplatin minus the oxalate group). This could potentially be accounted for by the difference in biological conditions which enable the oxalate group to leave when compared to the acidic solution used in this experiment (replicating biological conditions was beyond the scope and possibility of this study). Additionally, the formation of a $[peptide + OxPt + H]^+$ species forming before the dissociation of the oxalate ligand has been seen in previous studies where other biological materials were used, namely glutathione and carnosine.[134,135] And furthermore, there has been some reports in the literature of Pt-drugs remaining intact even in biological environments.[154,155]

Aside from the peaks of interest (peptide only, oxaliplatin and peptide-oxaliplatin complex), in the study of each peptide several other species were observed, usually with significantly lower abundances, and which have been assigned in the respective tables. These ions were usually protonated dimers and multimers of oxaliplatin, multimers of the peptides and several different combinations of the peptide and oxaliplatin species. Some of these minor peaks were poorly

resolved, but were assigned where possible based on theoretical isotopic patterns and *m/z* observed.

While the assignment of most peaks by *m/z* and isotope pattern correlated well, some exceptions were found relating to the oxaliplatin and oxaliplatin-peptide peaks. A typical theoretical [OxPt + H]$^+$ pattern is shown in Figure 29, where the three largest (but similar in intensity) peaks are at *m/z* 398, 397 and 399. However in some of the experimental data, while the observed *m/z* range for oxaliplatin [OxPt + H]$^+$ was correct the most abundant peak was not at *m/z* 398. The reason for this remains unclear, however as the relative abundance of the three main peaks at *m/z* 397, 398 and 399 are similar it is possible that a slight problem with the mass calibration occurred. However, this effect was seen only intermittently and was most probably due to an instrumental issue that has now been resolved. For example, in peptide 2 (ENQK), the immediate measurement of the peptide/oxaliplatin solution produced the most abundant peak at *m/z* 397, but the same solution measured 24 hours later observed the oxaliplatin most abundant peak at *m/z* 398.

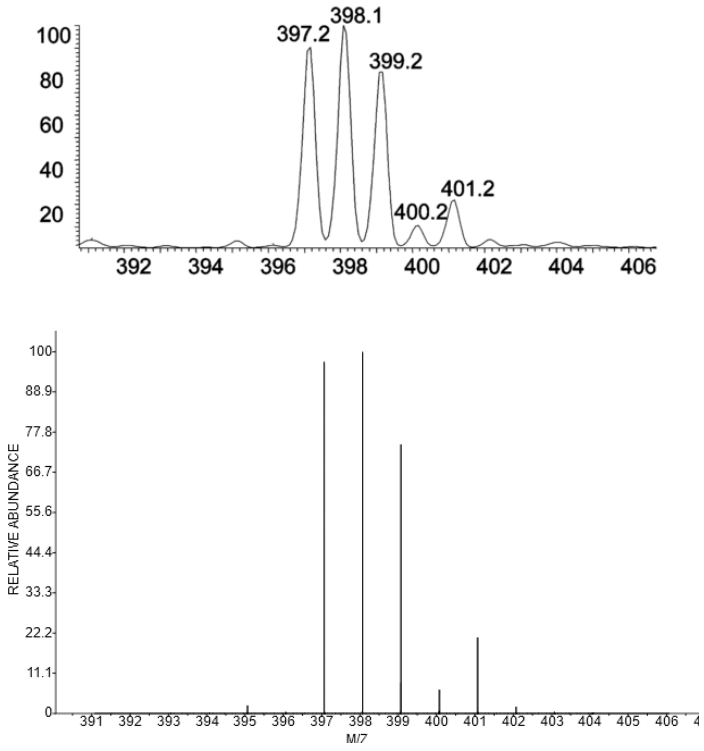

Figure 29 – Theoretical isotope pattern of protonated oxaliplatin in stick and peak profiles

To investigate the possibility of a calibration issue, where possible, left over samples were run on high resolution Q-Exactive fourier transform mass spectrometer. For example, the full mass spectrum at high resolution of peptide 1 (NNIK) is shown in Figure 30. As can be seen, the mass of

the free oxaliplatin $[OxPt + H]^+$ is now at the correct *m/z* of 398, and by comparing to the theoretical pattern can be identified as oxaliplatin (Figure 31).

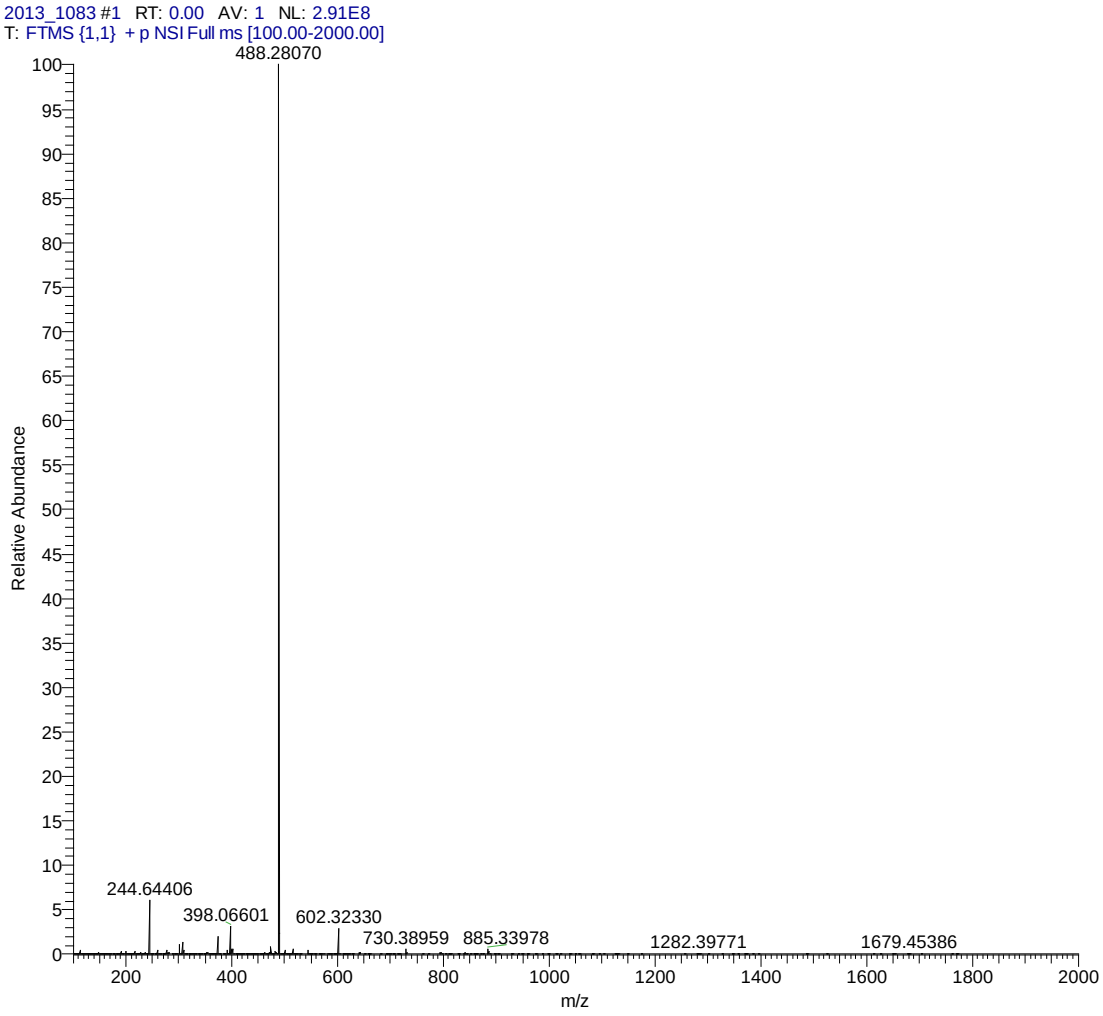

Figure 30 - Orbitrap spectrum of peptide 1 (NNIK) and oxaliplatin

Table 10 – High resolution Orbitrap data peak assignments for peptide 1 (NNIK) and oxaliplatin

Most abundant isotope *m/z*	Assignment
398.07	$[OxPt + H]^+$
488.28	$[NNIK + H]^+$
602.32	$[(NNIK+N) + H]^+$
885.33	$[NNIK+ OxPt + H]^+$

*N denotes the amino acid asparagine

As can be seen from Figure 30 and Table 10, the oxaliplatin and oxaliplatin and peptide (*m/z* 398 and 885 respectively) are at the correct *m/z* now when compared to the original LTQ data.

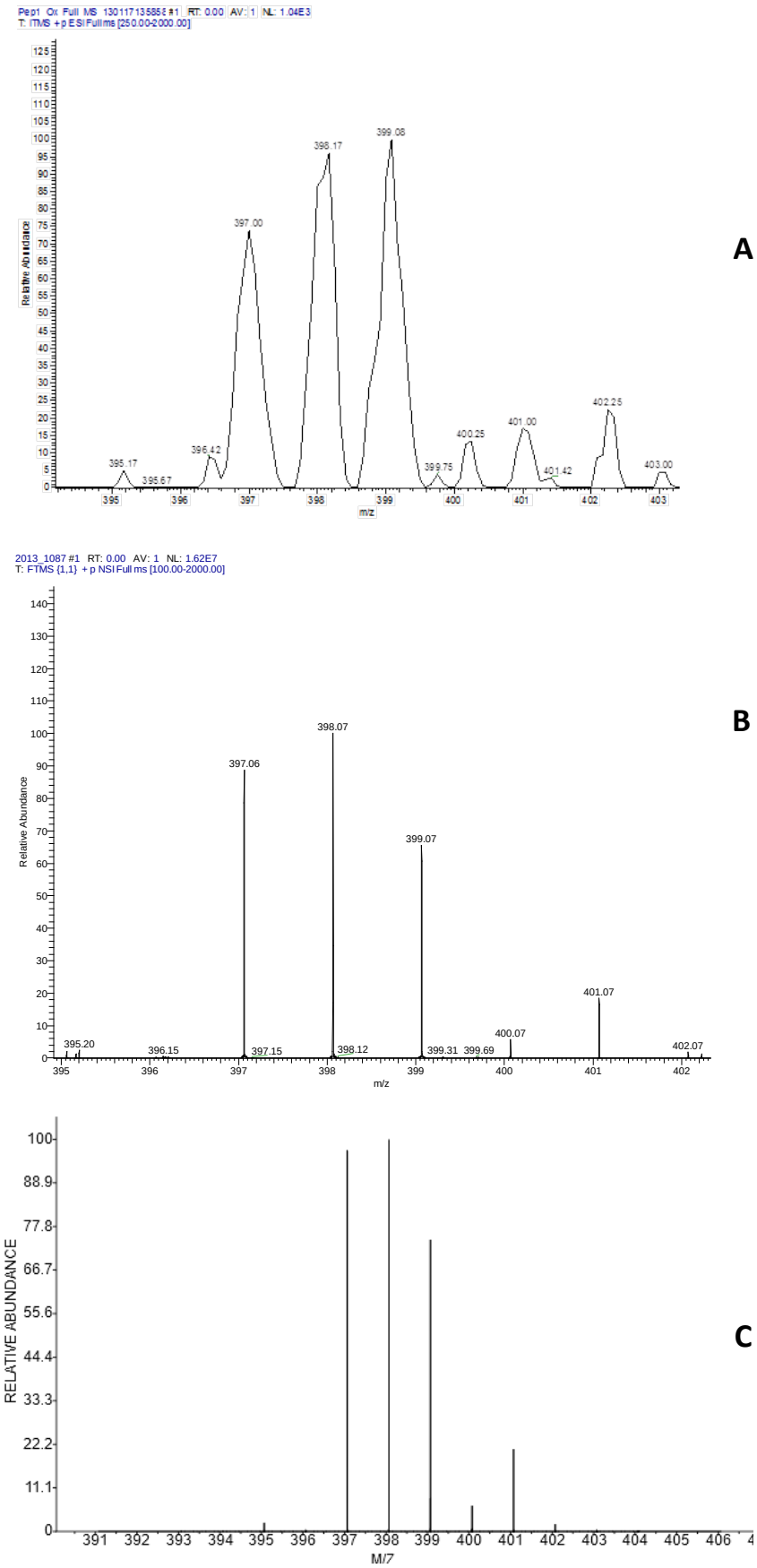

Figure 31 - Comparison of experimental data (A – LTQ, B - Orbitrap) and theoretical peak profile (C) for oxaliplatin as seen in peptide 1 (NNIK) samples

As can be seen in Figure 31, the peak profile obtained for peptide 1 (NNIK) from the initial LTQ work (label A) was not a perfect match for the theoretical (label C), as the relative peak heights for the 3 most abundant peaks (*m/z* 397, 398 and 399) were incorrect, potentially due to an instrumental error. However when the high resolution data was obtained (panel B) it is a correct match with the theoretical isotopic profile, and thus can confidently be assigned as oxaliplatin.

The high resolution data obtained made it possible to assign peaks with confidence (especially with the nitrogen rich peptides where the intermittent instrumental problem was observed) and compare isotopic peak profiles more easily. This was done for the remainder of the peptides, some examples for peptide 1 (NNIK) are shown below.

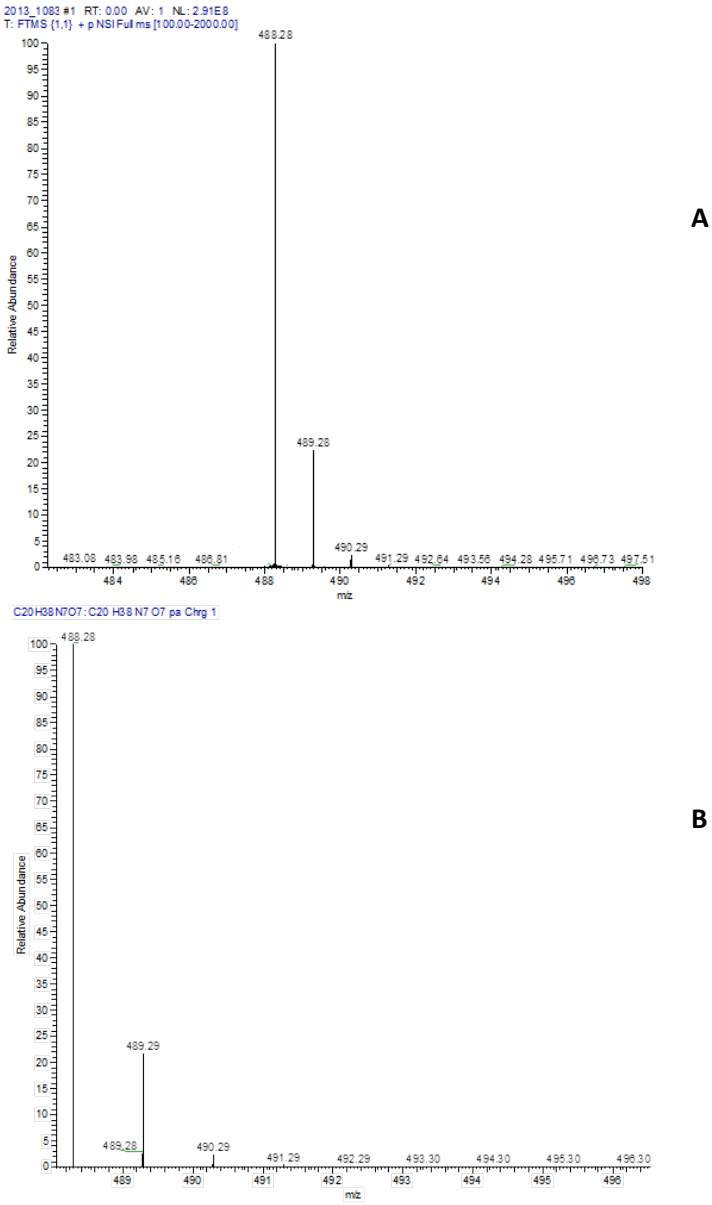

Figure 32 - Comparison of experimental (A) and theoretical (B) peak profiles of m/z 488 $[NNIK + H]^+$

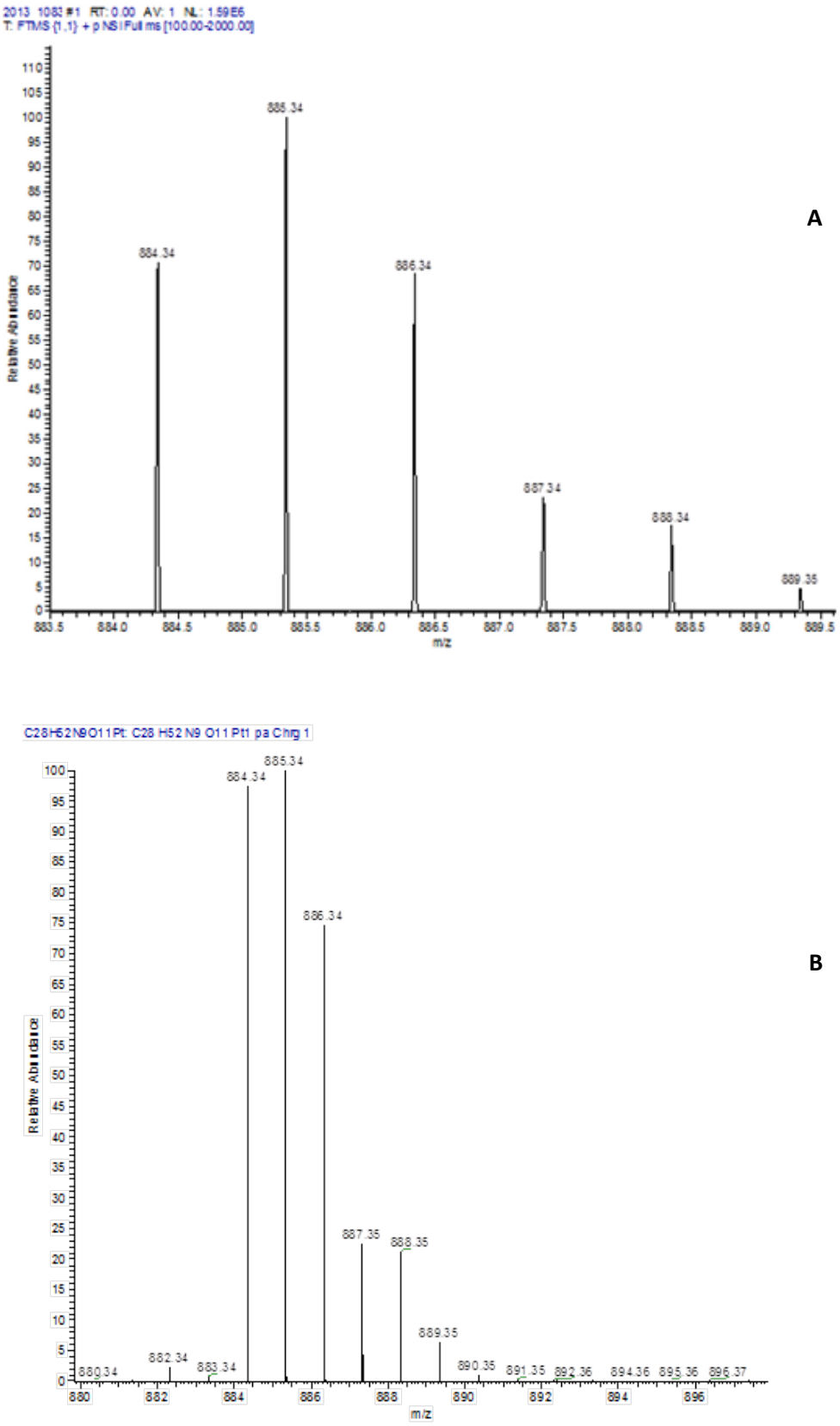

Figure 33 - Comparison of experimental (A) and theoretical (B) peak profiles of m/z 885 [NNIK + OxPt + H]$^+$

In the case of peptide 2 (Figure 34 and Table 11), the base peak was the protonated peptide $[ENQK + H]^+$ at *m/z* 518, and the main peptide and oxaliplatin complex was observed at *m/z* 916. Several dimer and multimer complexes were also observed.

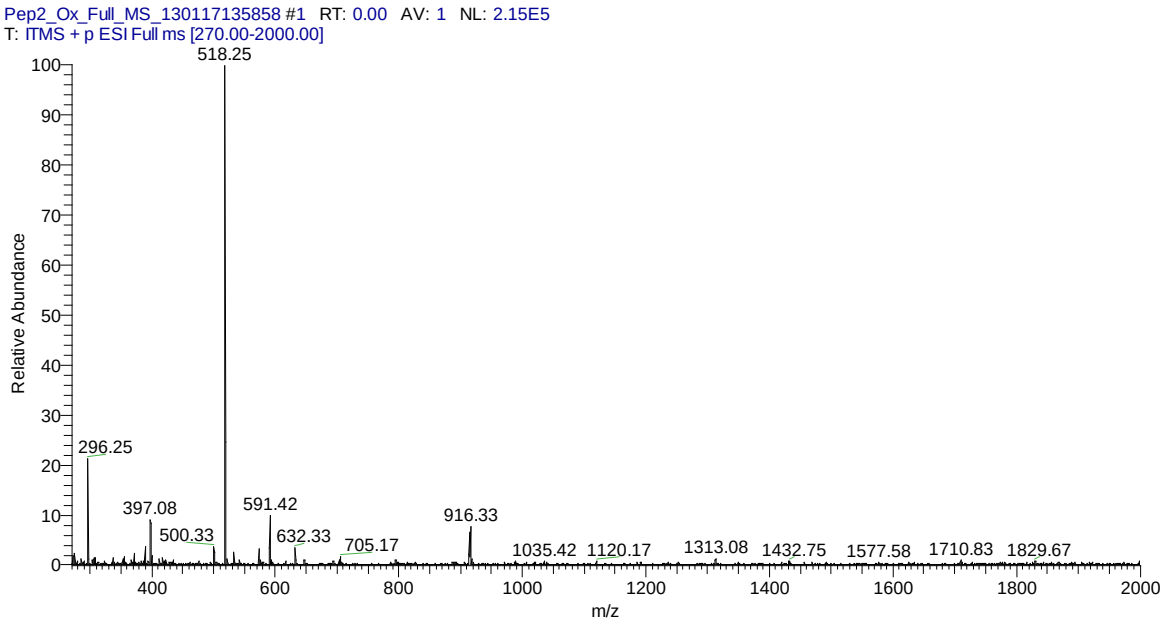

Figure 34 - Full mass spectrum for peptide 2 (ENQK) and oxaliplatin

Table 11 - Peak assignments for peptide 2 (ENQK) and oxaliplatin

Most abundant isotope *m/z*	Assignment
296.25	$[ENQK + C_4H_{11}N + 2H]^{2+}$
397.08	$[OxPt + H]^+$
518.25	$[ENQK + H]^+$
591.42	$[ENQK + C_4H_{11}N + H]^+$
632.33	$[ENQK + (ENQK\text{-}C_4H_{11}N) + H]^+$
916.33	$[ENQK + OxPt + H]^+$
1035.42	$[(ENQK)_2 + H]^+$
1313.08	$[ENQK + (OxPt)_2 + H]^+$
1432.75	$[(ENQK)_2 + OxPt + H]^+$
1710.83	$[ENQK + (OxPt)_3 + H]^+$
1829.67	$[(ENQK)_2 + (OxPt)_2 + H]^+$

Peptide 3, QHEK, (Figure 35 and Table 12), the base peak was the protonated peptide $[QHEK + H]^+$ at *m/z* 541, and the main peptide and oxaliplatin complex was observed at *m/z* 938 as expected. Several dimer and multimer complexes were also observed.

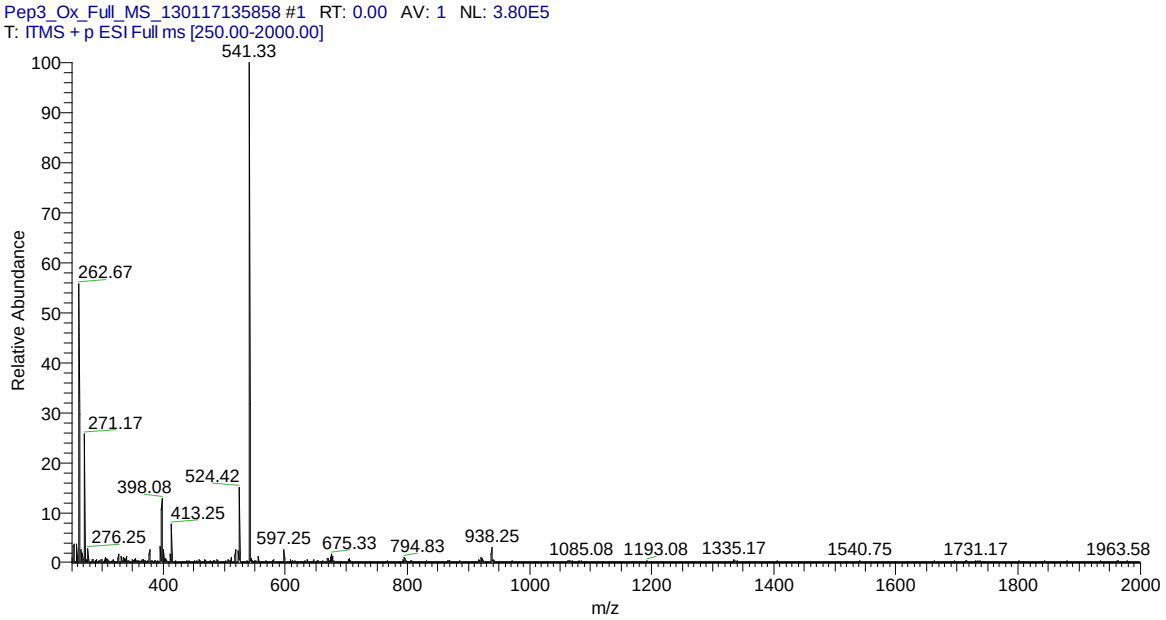

Figure 35- Full mass spectrum for peptide 3 (QHEK) and oxaliplatin

Table 12 - Peak assignments for peptide 3 (QHEK) and oxaliplatin

Most abundant isotope *m/z*	Assignment
262.67	$[QHEK - NH_3 + 2H]^{2+}$
271.17	$[QHEK + 2H]^{2+}$
398.08	$[OxPt + H]^+$
413.25	$[(HEK) + H]^+$
524.42	$[QHEK - NH_3 + H]^+$
541.33	$[QHEK + H]^+$
794.83	$[(OxPt)_2 + H]^+$
938.25	$[QHEK + OxPt + H]^+$
1085.42	$[(QHEK)_2 + H]^+$
1193.08	$[(OxPt)_3 + H]^+$
1335.08	$[QHEK + (OxPt)_2 + H]^+$
1478.92	$[(QHEK)_2 + OxPt + H]^+$
1731.17	$[QHEK + (OxPt)_3 + H]^+$
1879.67	$[(QHEK)_2 + (OxPt)_2 + H]^+$

Peptide 4, YRPR, (Figure 36 and Table 13), the base peak was the protonated peptide $[YRPR + H]^+$ at *m/z* 591, and the main peptide and oxaliplatin complex was observed at *m/z* 989. Several dimer and multimer complexes were also observed.

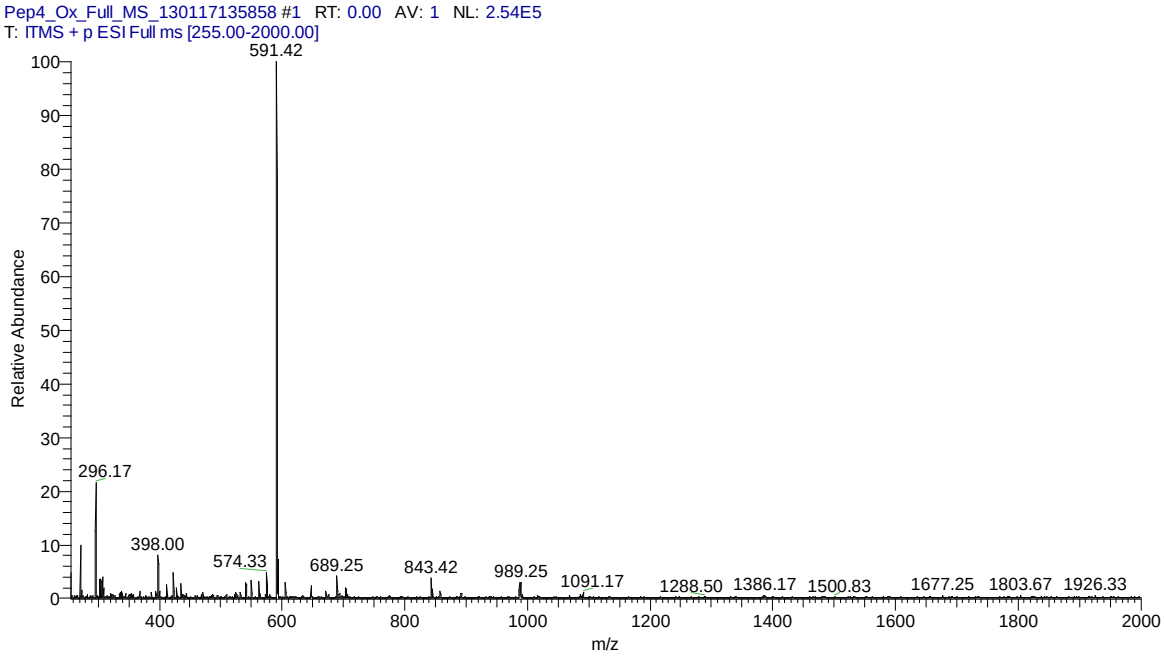

Figure 36 - Full mass spectrum for peptide 4 (YRPR) and oxaliplatin

Table 13 - Peak assignment for peptide 4 (YRPR) and oxaliplatin

Most abundant isotope *m/z*	Assignment
296.17	$[YRPR + 2H]^{2+}$
398.00	$[OxPt + H]^+$
574.33	$[(YRPR\text{-}OH) + H]^+$
591.42	$[YRPR + H]^+$
794.00	$[(OxPt)_2 + H]^+$
989.25	$[YRPR + OxPt + H]^+$
1386.17	$[YRPR + (OxPt)_2 + H]^+$
1579.75	$[(YRPR)_2 + OxPt + H]^+$

3.4.2 Sulfur rich peptides

Analysis of the six sulfur rich peptides (GCMR, AMMK, MSMK, MMTK, MCAAR, CVK) is presented below. The structures of these six peptides are shown in Figure 37.

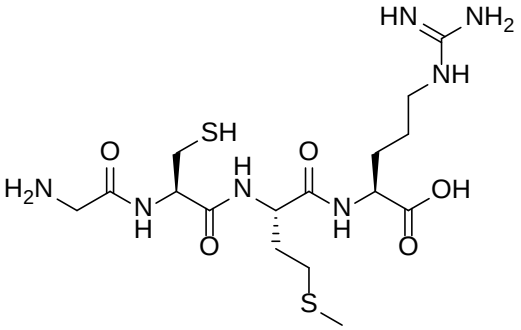

Peptide 5 – GCMR

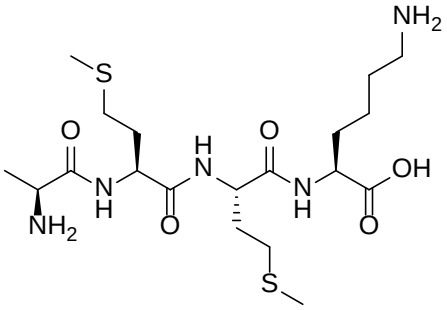

Peptide 6 - AMMK

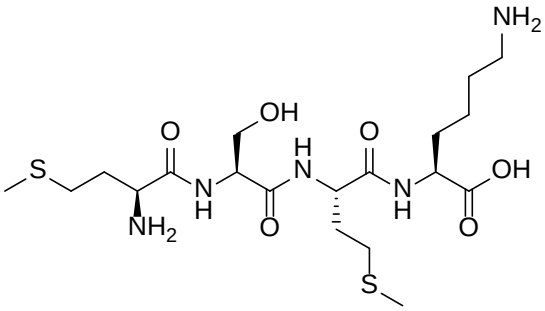

Peptide 7 - MSMK

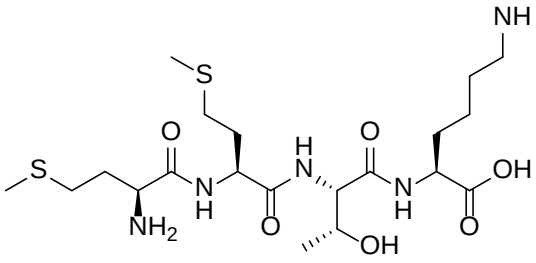

Peptide 8 – MMTK

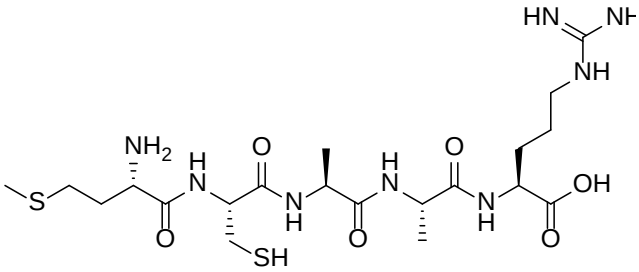

Peptide 9 – MCAAR

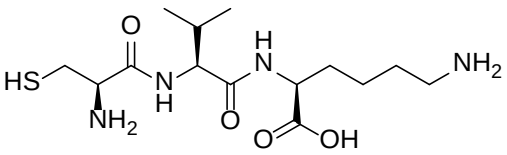

Peptide 10 – CVK

Figure 37 – Structures of the six sulfur rich peptides

The data collected for the first of the sulfur rich peptides (Peptide 5), GCMR, is presented below (Figure 38 and Table 14).

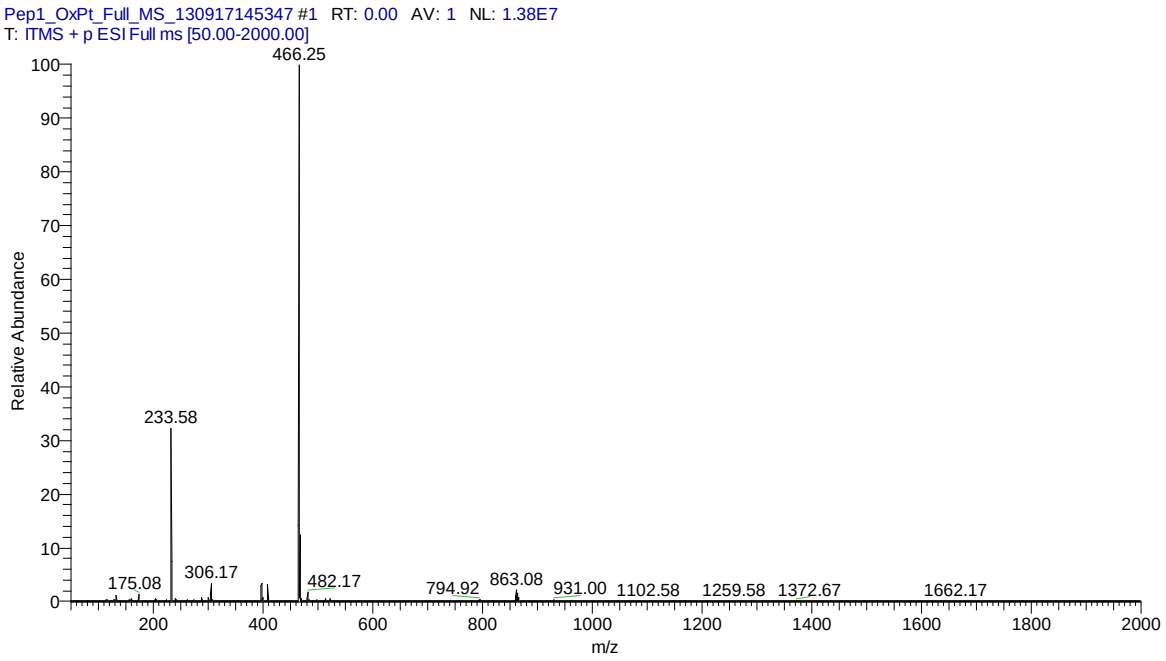

Figure 38 - Full mass spectrum of peptide 5 (GCMR) and oxaliplatin

Table 14 - Peak assignments for peptide 5 (GCMR) and oxaliplatin

Most abundant isotope *m/z*	**Assignment**
175.08	$[R + H]^+$
233.58	$[GCMR + 2H]^{2+}$
398.08	$[OxPt + H]^+$
409.25	$[(GCMR\text{-}G) + H]^+$
466.25	$[GCMR + H]^+$
482.17	$[GCMR + NH_2 + H]^+$
794.92	$[(OxPt)_2 + H]^+$
863.08	$[GCMR + OxPt + H]^+$
931.00	$[(GCMR)_2 + H]^+$
1259.58	$[GCMR + (OxPt)_2 + H]^+$
1330.08	$[(GCMR)_2 + OxPt + H]^+$
1726.25	$[(GCMR)_2 + (OxPt)_2 + H]^+$

Again the oxaliplatin did not bind strongly to the peptide, with unbound oxaliplatin being observed in the solution, and the peptide-oxaliplatin complex (*m/z* 863) being less than 5% of the relative intensity of the base peak. Furthermore, dimer and multimer complexes were also observed at low intensity.

Peptide 6, AMMK, showed evidence of unbound oxaliplatin and a small peak of the peptide-oxaliplatin complex (*m/z* 877). A large amount of the peptide dimer (*m/z* 240) was observed as well the protonated peptide (*m/z* 480).

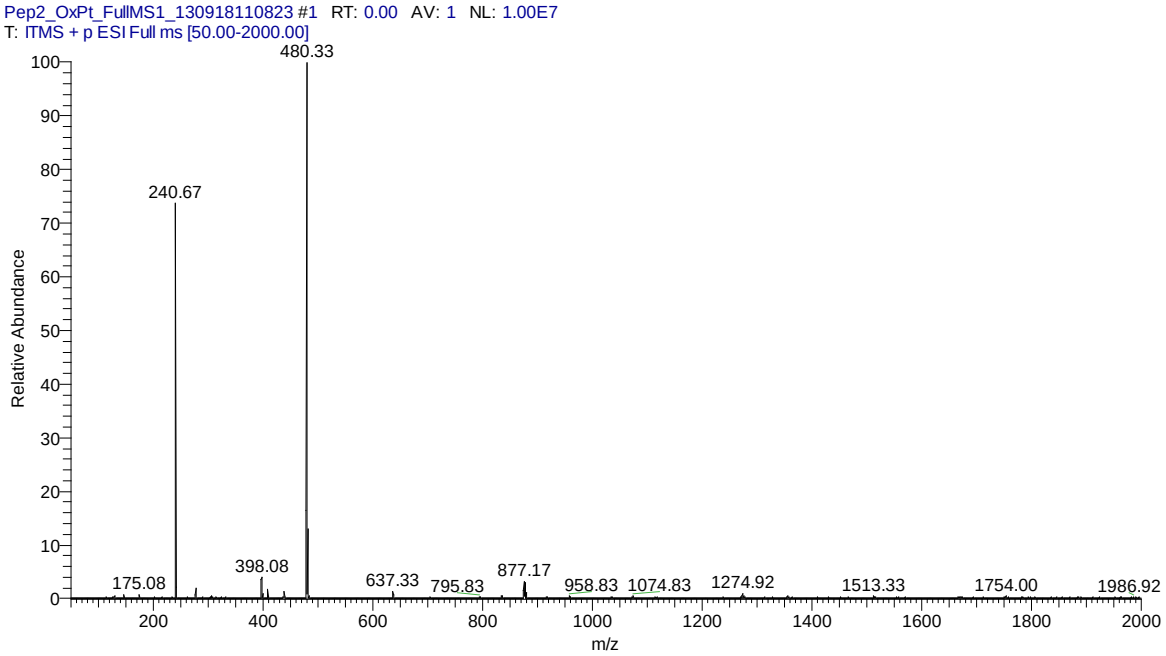

Figure 39 - Full mass spectrum for peptide 6 (AMMK) and oxaliplatin

Table 15 - Peak assignments for peptide 6 (AMMK) and oxaliplatin

Most abundant isotope *m/z*	Assignment
240.58	$[AMMK + 2H]^{2+}$
398.08	$[OxPt + H]^{+}$
480.33	$[AMMK + H]^{+}$
637.33	$[AMMK + (OxPt)_2 + 2H]^{2+}$
795.83	$[(OxPt)_2 + H]^{+}$
877.17	$[AMMK + OxPt + H]^{+}$
958.75	$[(AMMK)_2 + H]^{+}$
1035.08	$[AMMK + (OxPt)_2 + 2H]^{2+}$
1274.92	$[AMMK + (OxPt)_2 + H]^{+}$
1356.83	$[(AMMK)_2 + OxPt + H]^{+}$
1672.92	$[AMMK + (OxPt)_3 + H]^{+}$
1754.00	$[(AMMK)_2 + (OxPt)_2 + H]^{+}$

When compared to the spectrum obtained 24 hours later (Appendix B), it is clear that no significant increase in the peptide-oxaliplatin complex was present at *m/z* 877.

Peptide 7, MSMK, yielded a base peak of the peptide at *m/z* 496, and a small peptide-oxaliplatin peak at *m/z* 893, with several dimer and multimer complexes also being observed (Figure 40 and Table 16).

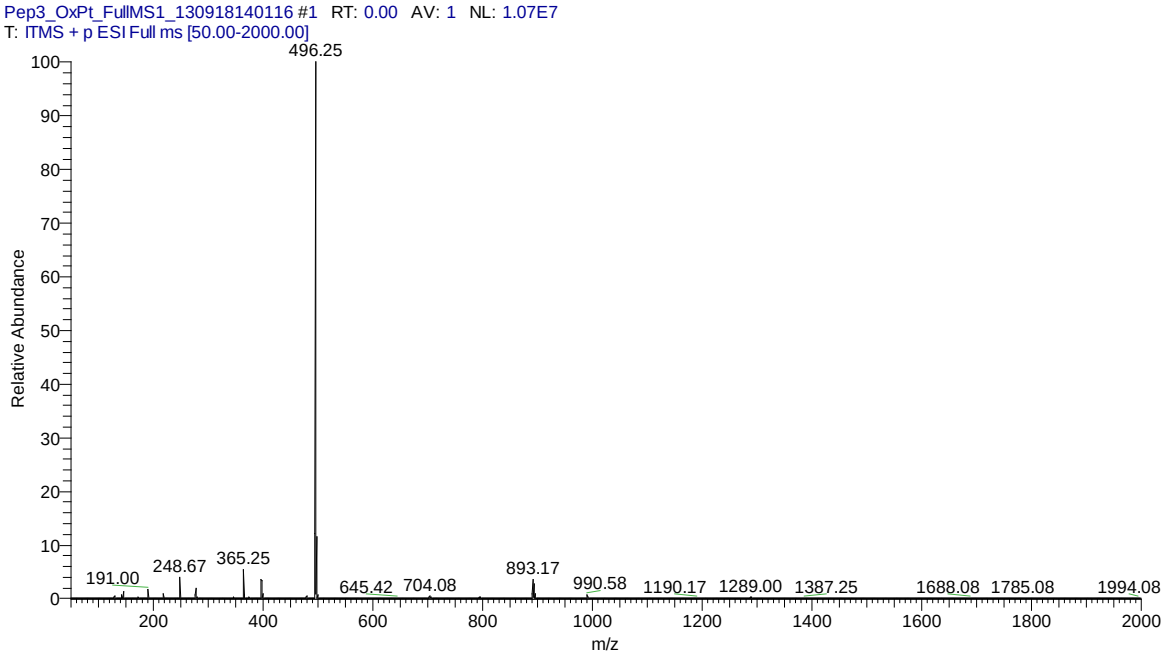

Figure 40 - Full mass spectrum of peptide 7 (MSMK) and oxaliplatin

Table 16 - Peak assignments for peptide 7 (MSMK) and oxaliplatin

Most abundant isotope *m/z*	Assignment
248.67	$[MSMK + 2H]^{2+}$
365.25	$[(SMK) + H]^{+}$
398.17	$[OxPt + H]^{+}$
496.33	$[MSMK + H]^{+}$
794.83	$[(OxPt)_2 + H]^{+}$
893.17	$[MSMK + OxPt + H]^{+}$
990.58	$[(MSMK)_2 + H]^{+}$
1289.00	$[MSMK + (OxPt)_2 + H]^{+}$
1387.22	$[(MSMK)_2 + OxPt + H]^{+}$
1785.08	$[(MSMK)_2 + (OxPt)_2 + H]^{+}$

Peptide 8, MMTK, as shown in Figure 41 and Table 17, yielded a base peak of the peptide at *m/z* 510 as well as a large dimer peak (*m/z* 255), and a small peptide-oxaliplatin peak at *m/z* 907. Again the presence of unbound oxaliplatin was observed (*m/z* 398).

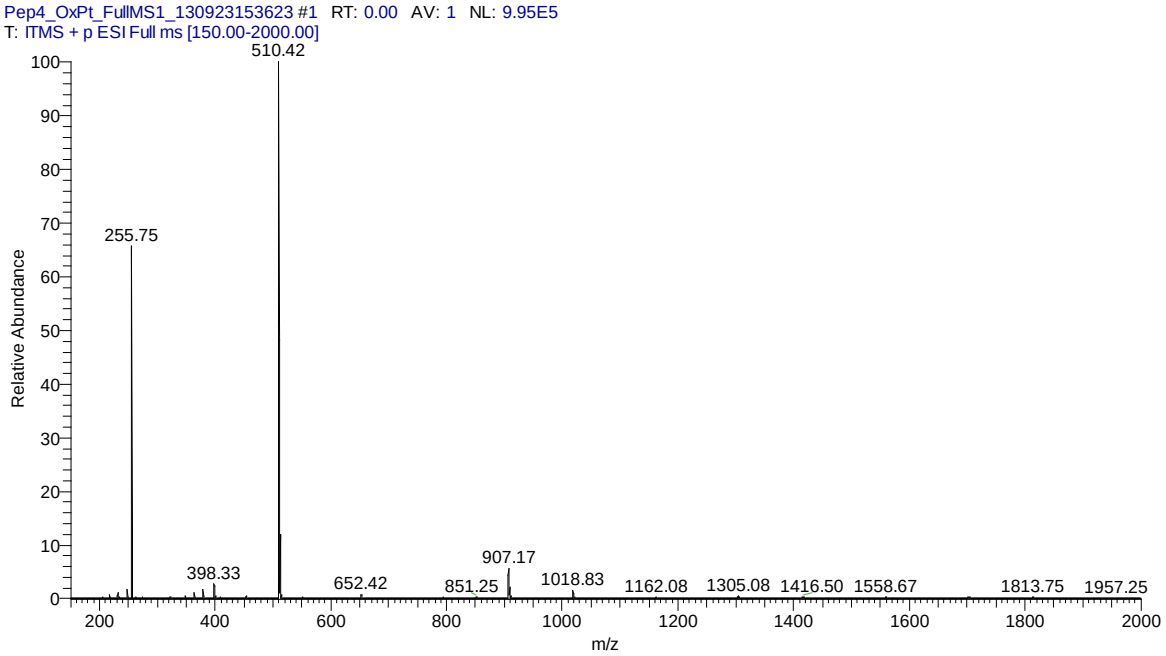

Figure 41- Full mass spectrum of peptide 8 (MMTK) and oxaliplatin

Table 17 - Peak assignment for peptide 8 (MMTK) and oxaliplatin

Most abundant isotope *m/z*	Assignment
255.75	$[MMTK + 2H]^{2+}$
379.33	$[(MTK) + H]^{+}$
398.33	$[OxPt + H]^{+}$
454.17	$[MMTK + OxPt + 2H]^{2+}$
510.33	$[MMTK + H]^{+}$
907.17	$[MMTK + OxPt + H]^{+}$
1018.83	$[(MMTK)_2 + H]^{+}$
1305.08	$[MMTK + (OxPt)_2 + H]^{+}$
1416.50	$[(MMTK)_2 + OxPt + H]^{+}$

Peptide 9, MCAAR, yielded a base peak of the peptide at *m/z* 551 as well as a large dimer peak (*m/z* 276), and a small peptide-oxaliplatin peak at *m/z* 948. Again the presence of unbound oxaliplatin was observed (*m/z* 398) as well as several peptide and oxaliplatin dimer complexes (Figure 42 and Table 18).

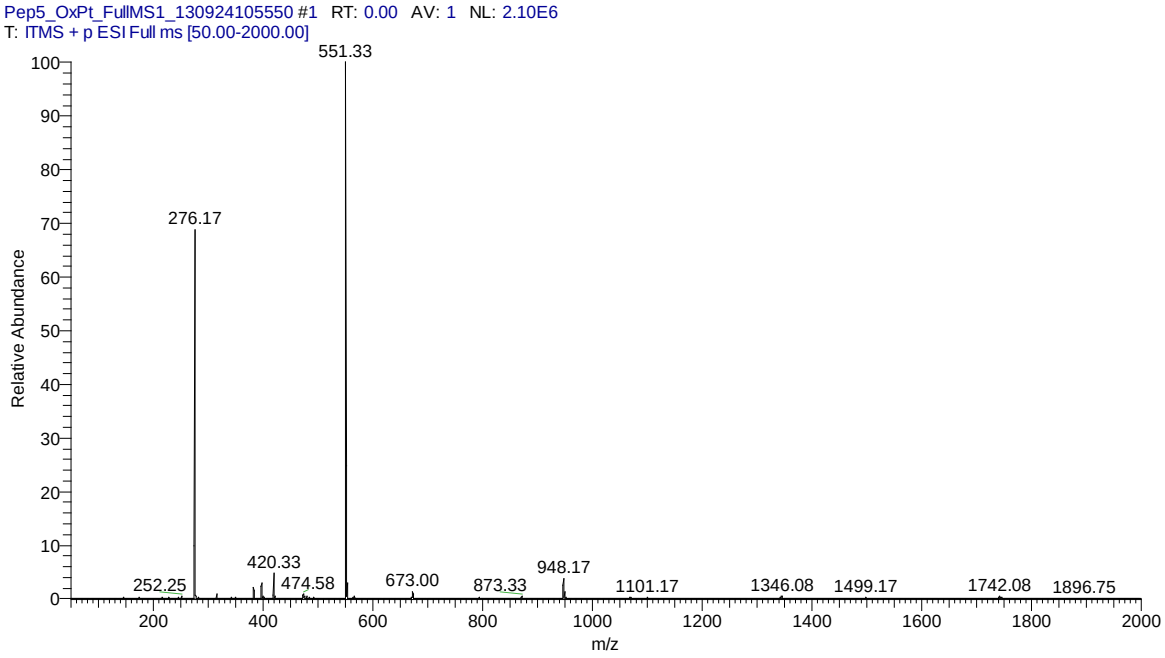

Figure 42 - Full mass spectrum of peptide 9 (MCAAR) and oxaliplatin

Table 18 - Peak assignment for peptide 9 (MCAAR) and oxaliplatin

Most abundant isotope *m/z*	Assignment
276.17	$[MCAAR + 2H]^{2+}$
398.17	$[OxPt + H]^{+}$
420.33	$[CAAR + H]^{+}$
551.33	$[MCAAR + H]^{+}$
673.00	$[MCAAR + (OxPt)_2 + 2H]^{2+}$
948.17	$[MCAAR + OxPt + H]^{+}$
1101.17	$[(MCAAR)_2 + H]^{+}$
1346.08	$[MCAAR + (OxPt)_2 + H]^{+}$

Peptide 10, CVK, yielded a base peak of the peptide at *m/z* 349 as well as a large dimer peak (*m/z* 175). A peptide-oxaliplatin peak was observed at *m/z* 746 as well as several peptide and oxaliplatin dimer complexes (Figure 43 and Table 19).

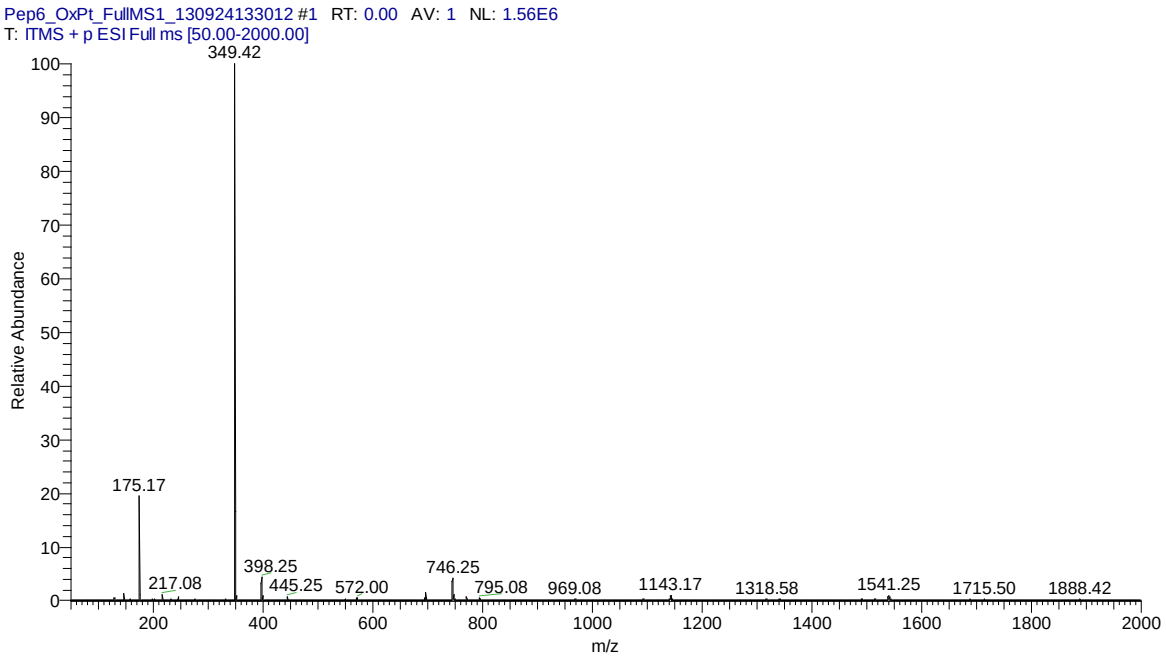

Figure 43 - Full mass spectrum of peptide 10 (CVK) and oxaliplatin

Table 19 - Peak assignment for peptide 10 (CVK) and oxaliplatin

Most abundant isotope *m/z*	Assignment
175.17	$[CVK + 2H]^{2+}$
349.42	$[CVK + H]^{+}$
398.25	$[OxPt + H]^{+}$
572.00	$[CVK + (OxPt)_2 + 2H]^{2+}$
697.17	$[(CVK)_2 + H]^{+}$
746.25	$[CVK + OxPt + H]^{+}$
795.08	$[(OxPt)_2 + H]^{+}$
1094.83	$[(CVK)_2 + OxPt + H]^{+}$
1143.17	$[CVK + (OxPt)_2 + H]^{+}$
1541.25	$[CVK + (OxPt)_3 + H]^{+}$

3.4.3 Computational modelling of peptide-oxaliplatin interactions

Based on the results presented in the previous two sections, it was felt that further investigation of the binding to both sulfur and nitrogen rich peptides was required. Two peptides were chosen for computational modelling to further investigate the interactions between the peptides and oxaliplatin, one from the nitrogen rich category and one from the sulfur rich category; peptide 3 (QHEK) and peptide 5 (GCMR) respectively.

This computer modelling work was done by Dr Tamer Shoeib at the American University in Cairo based on the previously obtained experimental data.

All molecular orbital calculations were performed using GAUSSIAN09W. Structures were optimized without symmetry constraints by means of Hartree-Fock (HF) level of theory. The most energetically favoured conformations were further optimized by means of density functional theory (DFT) employing the hybrid Becke's three-parameter exchange functional and the correlation functional from Lee, Yang and Parr (B3LYP).[156–158] Optimizations at all levels of theory made use of the pseudo potential LANL2DZ basis set. The computational tractability of this theoretical method makes it suitable for calculations of systems containing relatively large number of heavy atoms such as those in this study. Much more important however are the results of DFT calculations in systems involving transition metals, which are in many cases in better agreement with experimental data than those obtained from Hartree–Fock (HF) calculations.

The modelled interactions of these peptides are presented below.

3.4.3.1 Nitrogen rich peptide – QHEK

The structure of peptide 3 (QHEK) is shown in Figure 44 without the presence of oxaliplatin.

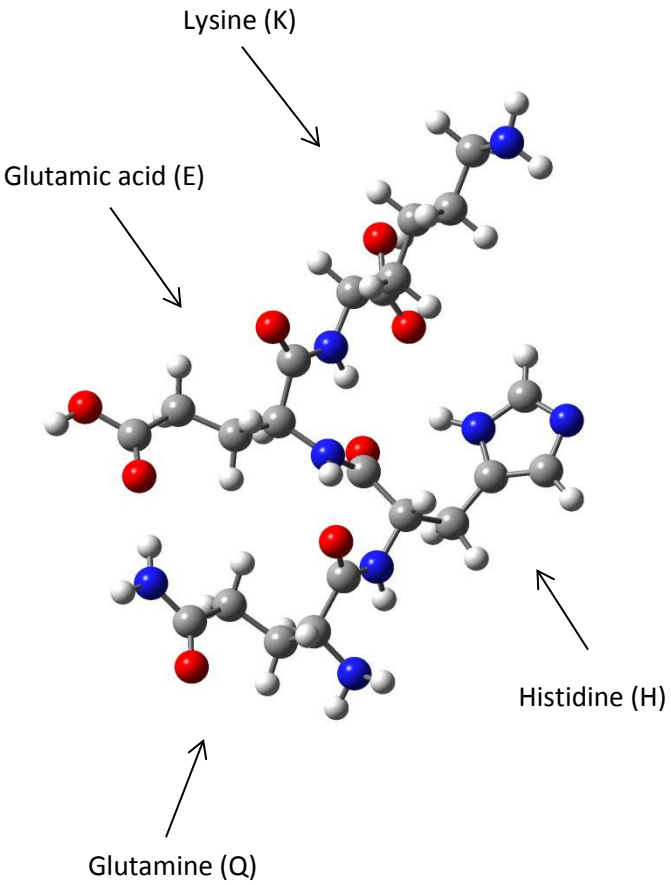

Figure 44 - Structure of peptide 3 (QHEK)

This structure was then modelled with oxaliplatin and the following favoured structures for binding were determined (see Figure 45 and Figure 46). The relative free energy for these four modelled structures were also calculated to determine which was the most favourable. This data is shown in Table 20.

Table 20 - Relative free energy values for peptide 3 (GHEK) and oxaliplatin structures

Structure	Relative free energy (Kcal/mol)
QHEKOxPtB	0
QHEKOxPtA	5.6
QHEKOxPtC	5.6
QHEKOxPtD	12.4

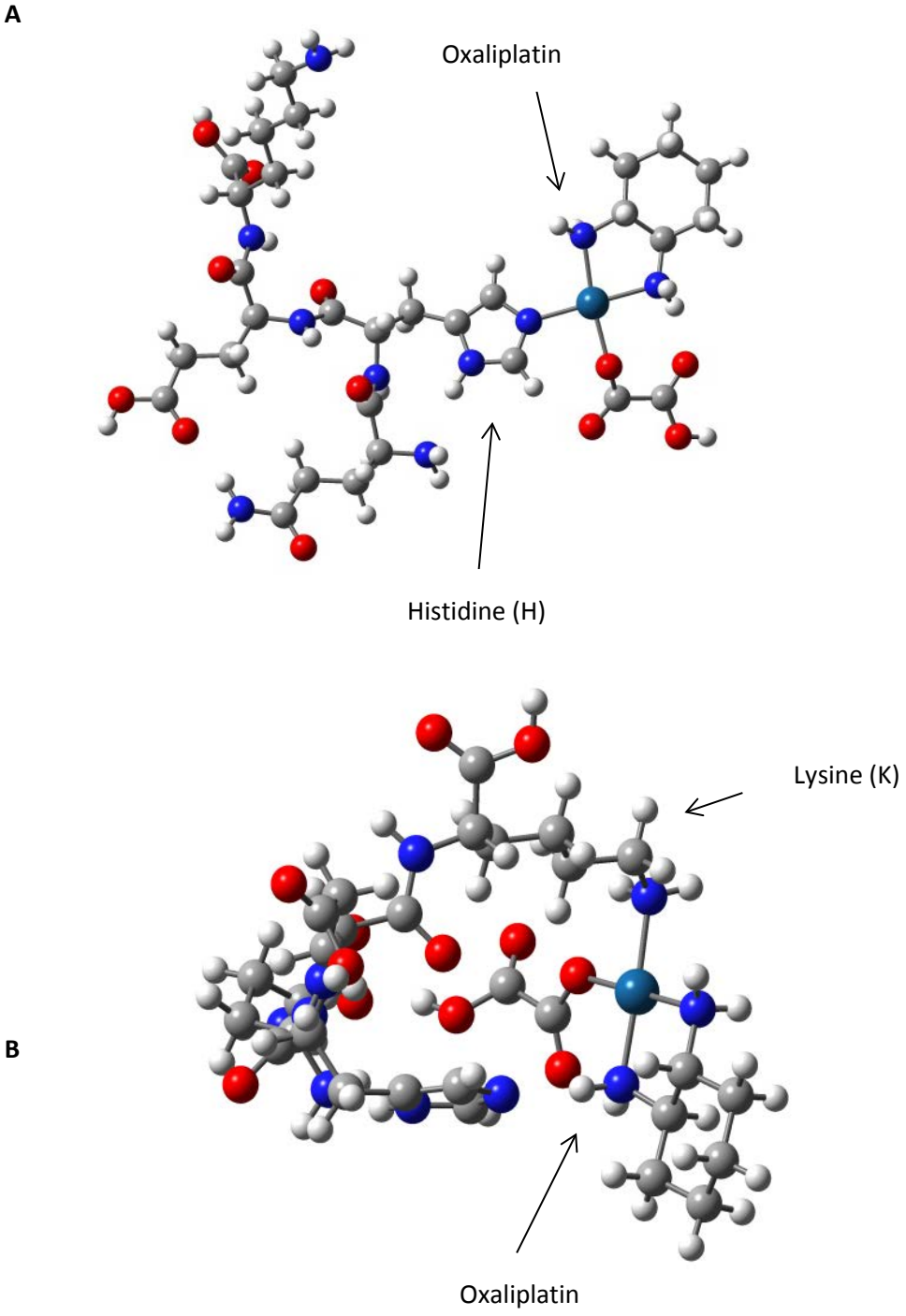

Figure 45 - Peptide 3 (QHEK) and oxaliplatin binding possibilities A-B

C

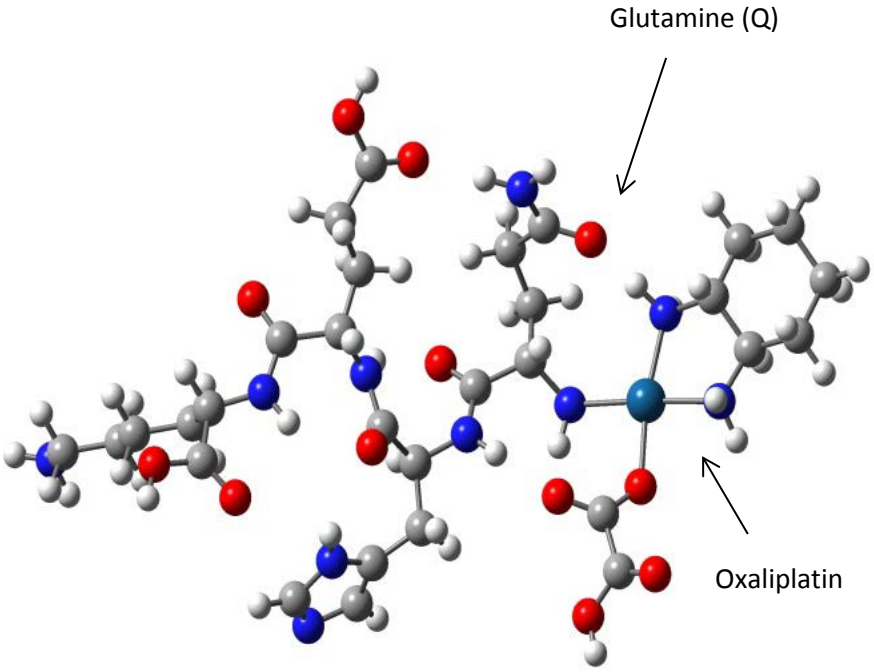

D

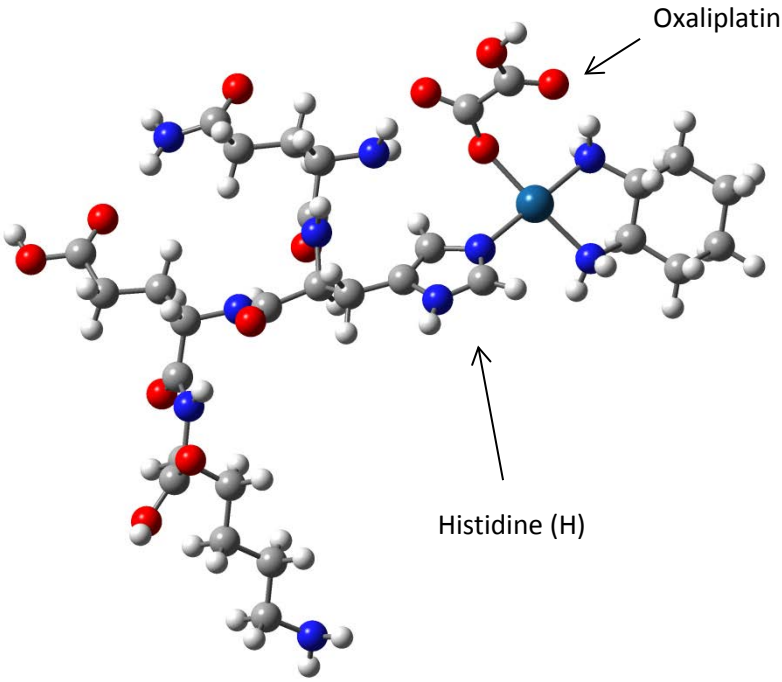

Figure 46 - Peptide 3 (QHEK) and oxaliplatin binding possibilities C-D

Oxaliplatin binds to peptide 3 on a N in the aromatic ring of histidine in structures A and D, while in structure B, the oxaliplatin binds to the terminal nitrogen of the lysine (K) amino acid, and in structure C binds to a N at the end of the chain in the glutamine. Table 20 shows that structure B is the most favourable structure with the lowest energy, followed by structures A and C which are equal in energy, and structure D being the highest in energy. However, the energy differences between the lowest three energy structures are small (5.6 Kcal/mol) (approximately the strength of a hydrogen bond) and therefore all four structures are possible and could have been found within the experimental data presented in Section 3.4.1.

As no sulfur was present within the peptide no conclusions can be drawn about competitive binding of oxaliplatin to N or S binding sites, however it is clear that within the structure of this peptide certain nitrogen's were favoured more than others.

3.4.3.2 Sulfur rich peptide – GCMR

Peptide 5 (GCMR) was chosen for modelling as it contains both N and S binding sites, and thus any preferential binding of oxaliplatin to N or S could be investigated. The structure of peptide 5 (GCMR) is shown in Figure 47 without the presence of oxaliplatin.

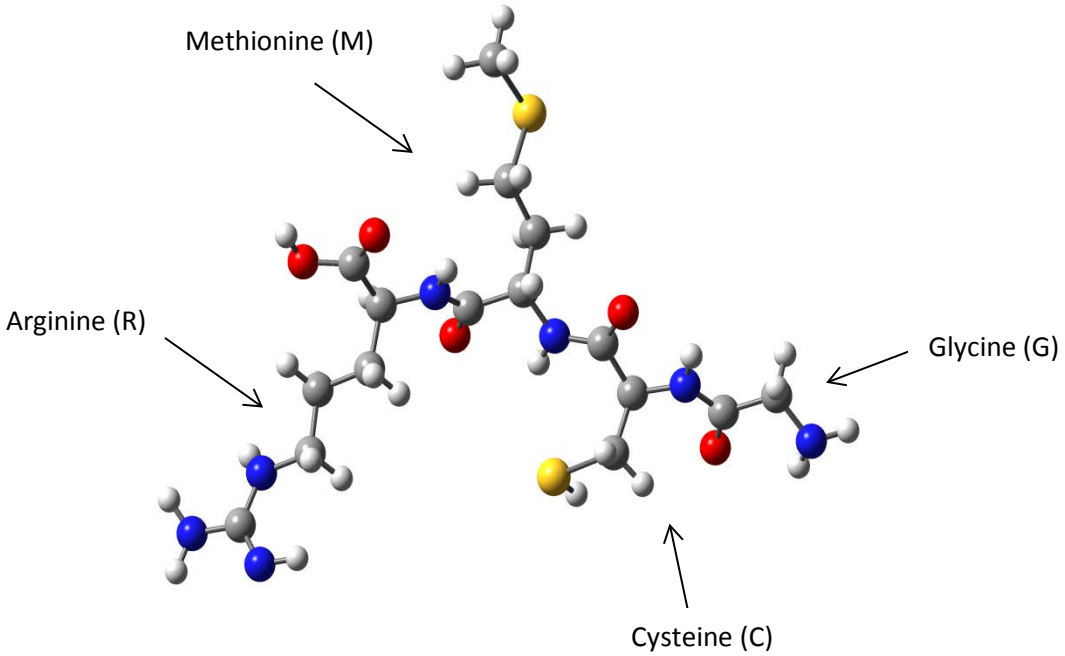

Figure 47 - Peptide 5 (GCMR) and oxaliplatin binding possibilities A-D

This structure was then modelled with oxaliplatin and the following favoured structures for binding were determined (see Figure 48, Figure 49 and Figure 50). The relative free energy for these five modelled structures were also calculated to determine which was the most favourable. This data is show in Table 21.

A

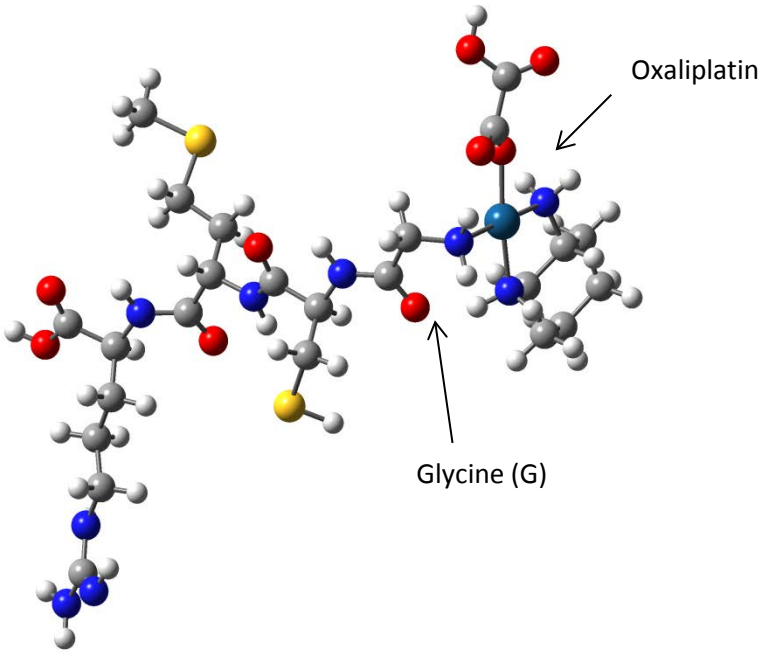

B

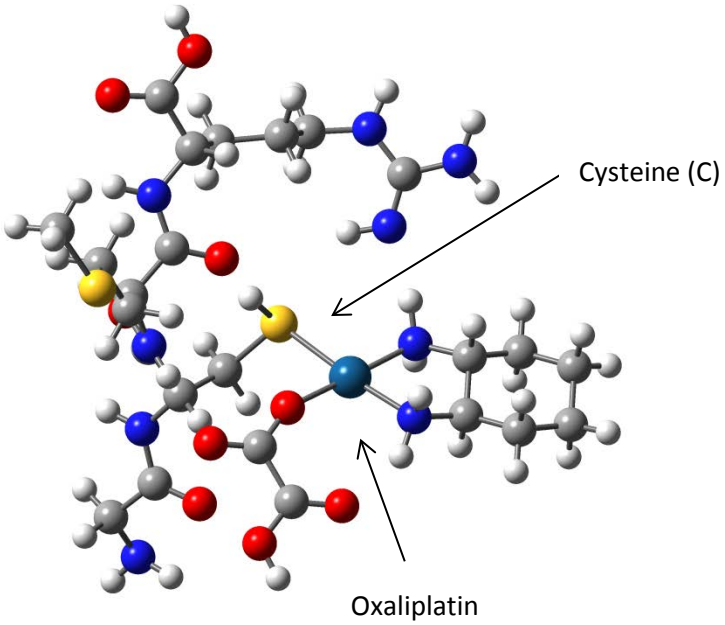

Figure 48 - Peptide 5 (GCMR) and oxaliplatin binding possibilities A and B

C

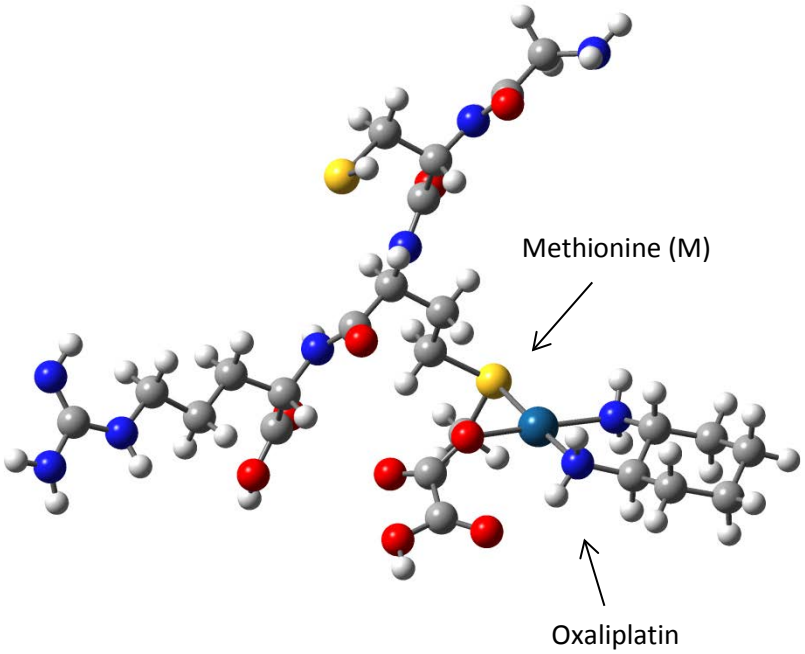

D

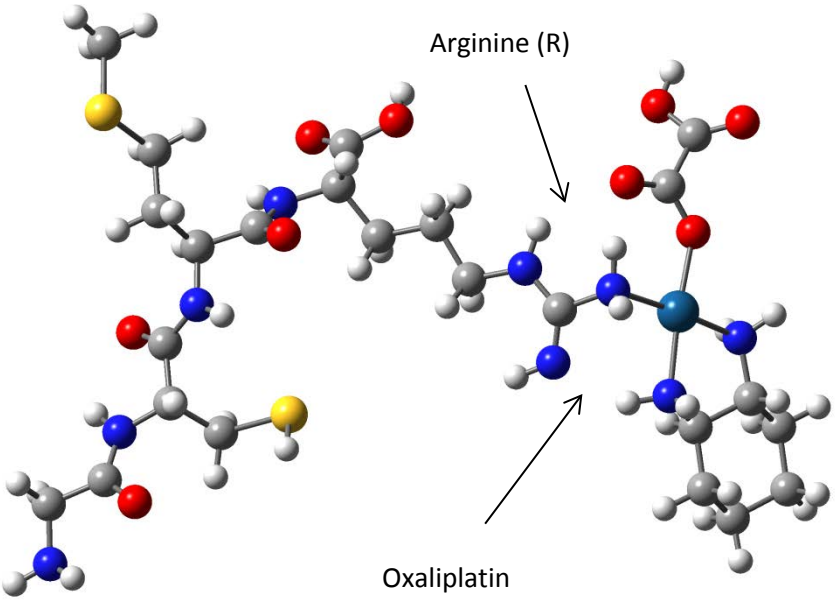

Figure 49 - Peptide 5 (GCMR) and oxaliplatin binding possibilities C and D

E

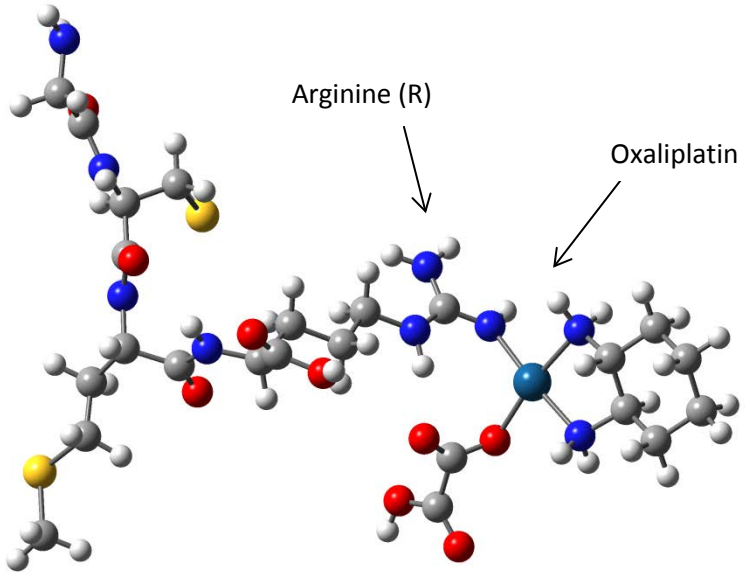

Figure 50 - Peptide 5 (GMCR) and oxaliplatin binding possibility E

Table 21 - Relative free energy values for peptide 5 (GCMR) and oxaliplatin structures

Structure	Relative free energy (Kcal/mol)
GCMROxPTE	0.0
GCMROxPtA	12.0
GCMROxPtD	17.7
GCMROxPtB	19.5
GCMROxPtC	35.3

The modelling work for peptide 5 (GMCR) showed that binding of oxaliplatin to both N and S binding sites is possible. Oxaliplatin binds to peptide 5 (GCMR) at the terminal N of glycine (G) in structure A, the S of cysteine (C) in structure B, the S of methionine (M) in structure C and the terminal nitrogen's of arginine (R) in structures D and E. Table 21 shows that structure E is the most favourable structure with the lowest energy, followed by structure A then structure D then structure B, with only a minor energy difference between D and B. Structure C is significantly higher in energy and therefore less favourable. When comparing the structures and the relative

free energy, it is clear that the three lowest energy structures (E, A and D) have oxaliplatin binding to a terminal nitrogen, while the two highest energy structures are where the oxaliplatin is bound to a S. However, the difference in energy between structures D and B (N and S binding sites respectively) is very small and both are certainly possible to have been found within the experimental data presented in Section 3.4.2.

3.4.3.3 Modelling summary

Platinum is a soft acid, and therefore is theoretically more likely to bind to a soft base (such as sulfur) compared to a hard base (such as nitrogen). However the experimental data produced in this chapter investigated this and found little/no significant differences in the level of binding observed between the two sites.

Computer modelling further backed up the experimental data showing that binding to nitrogen binding sites is not only possible, but in some cases could be more favourable and lower in energy than binding to sulfur sites on the peptides.

3.5 Conclusions

Binding to both nitrogen and sulfur rich peptides was observed as has been previously reported.[134] However, no significant differences in level of binding was observed between the ranges of peptides studied in this investigation which was unexpected as binding to sulfur would be expected to be preferred over nitrogen (HSAB theory). Computational modelling on two peptides has shown that not only does oxaliplatin bind to both nitrogen and sulfur binding sites, but that in some cases binding to nitrogen could in fact be slightly more favourable than binding to sulfur. However in most cases the energy differences between the different binding possibilities were relatively small and therefore binding to both N and S sites is likely, and thus confirms the results seen in the experimental portion of this chapter.

As discussed in the sections above, binding between the peptides and oxaliplatin was observed. When no incubation was allowed, oxaliplatin was seen in its unbound form as well as in various peptide-oxaliplatin complexes. In all cases unbound oxaliplatin was also seen at the 24 hour time point, however in some cases the relative intensity was slightly smaller, suggesting that no major time constraint played a role in this investigation.

Reasons as to the lower signal intensity observed for oxaliplatin were discussed and were supported by available current literature. Not only was the ratio of peptide:oxaliplatin in favour of the peptide with a 2:1 ratio, and with oxaliplatin having a larger isotopic range than the peptides, this again would reduce the relative intensity of the peaks observed. Additionally, previous computational studies have highlighted the fact that there is a discrepancy between the proton affinities of short tri-peptides and that of oxaliplatin, where oxaliplatin had a lower proton affinity than that of the peptides.

Although this study was not able to reproduce biological conditions due to the complexity of biological matrices, and as a result the binding of oxaliplatin was observed as a whole molecule (as opposed to binding after the loss of the oxalate group), it was shown that oxaliplatin can and did bind to both S and N binding sites. Oxaliplatin bound primarily in the form of a peptide-oxaliplatin complex, however, several other species at lower abundances were observed as well, suggesting that the binding of oxaliplatin was spread out over these peptide dimers and multimers. However it worth noting that the ratio of oxaliplatin to peptide utilised in these experiments were significantly higher than would be found in biological conditions, and as such oxaliplatin is not likely to bind as dimers or multimers within the body.

Overall, the work detailed in this chapter has shown that there is a large excess of potential binding sites for platinum. Binding to both sulfur and nitrogen binding sites are common and

consequently no species or functionality was found to dominate. Had one binding site been preferential, possibilities would have arisen to allow for therapeutic intervention via the modification of that species to ultimately improve the targeting of the Pt-based drug to the DNA.

4. Determination of the effect of selenium on the cellular distribution and uptake of oxaliplatin in cell cultures

4.1 Introduction

Every year millions of people worldwide are diagnosed with cancer, with the four most common types being breast, prostate, colorectal and lung cancers.[128,159] As previously discussed in Chapter 1 treatment options are primarily limited to surgery, radiotherapy and chemotherapy, however many patients undergoing treatment will take supplements during this time, many of which are not prescribed by their doctors. In fact, one study of over 14 different European countries revealed that 35.9% of the 956 cancer patients questioned in the study were taking/receiving some form of complementary or alternative medicine, including vitamins and minerals (including selenium), herbal medicines, homeopathy and medicinal teas.[46] Furthermore, this study found that the number of patients taking supplements varied significantly between different countries, ranging from 14.8% to 73.1%, with England and Scotland averaging around 29%.[46]

While a range of supplements are taken by patients, selenium in particular was chosen for study in this investigation as there is some evidence to suggest that it has some cancer-preventative properties (as detailed in Chapter 1), and furthermore there is potential for it to bind to glutathione, an abundant cytosolic protein where it is thought that Pt binds, which could potentially free up more Pt-drug to bind to the DNA within the nucleus, the ultimate physiological target. It is well characterised that glutathione bonds platinum-based chemotherapy drugs as well as selenium. It has been hypothesised that if selenium is used as a supplement in chemotherapy that the selenium-glutathione bonding may result in a reduction in platinum-glutathione binding, freeing the platinum to bind at other sites.

While the most effective form of selenium for cancer prevention is still under investigation, a metabolism pathway (Figure 51) was constructed to aid in the understanding of how selenium compounds break down within the body and hopefully provide an insight into which form of Se provided the best protection against cancer. Research studies identified methylselenol as an important metabolite, however due to problems relating to its high reactivity, methaneseleninic acid (MSA, CH_3SeO_2H) could be used to generate methylselenol endogenously, and therefore this was selected for use in this investigation.[29,42,43,160–163]

Due to the large numbers of patients taking such supplements and the limited knowledge of if/how they affect or interact with the anti-cancer drugs, the work detailed in the rest of this chapter was dedicated to furthering the understanding on how selenium affects the efficacy of

the platinum based anti-cancer drug oxaliplatin. Some initial work was performed as part of a Master's degree research project before continuing and extending the project as part of this PhD.[164] The main results from this investigation are summarised at the start of the results section to provide background for the rest of the work performed. Furthermore, a Masters student, Carl Cooper, also contributed some data towards this work, done in collaboration with the author of this thesis.[165] The contributions from these projects are detailed in the relevant sections below.

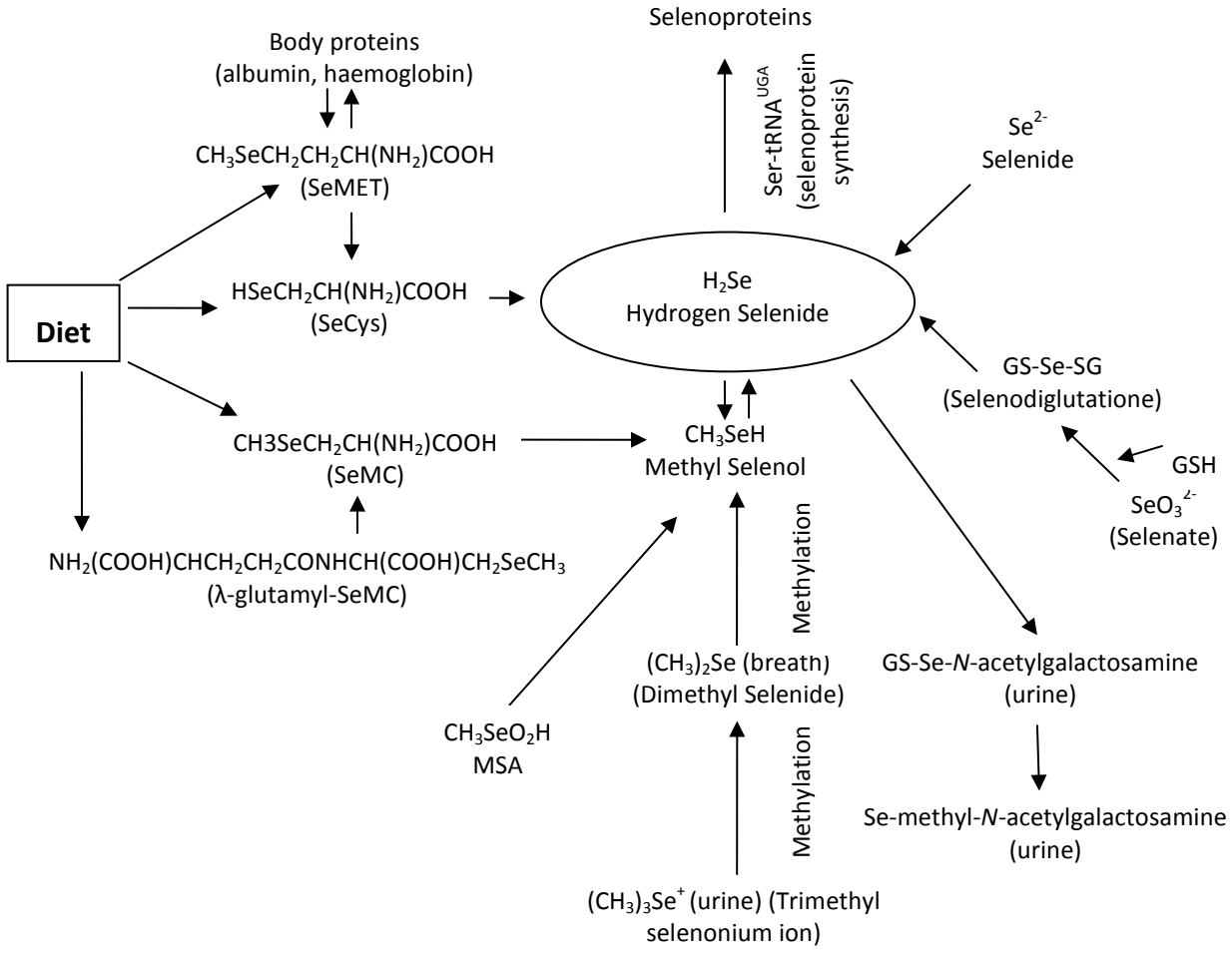

*Note: MSA provides a direct route to methyl selenol, an active anti-carcinogenic form of Se.

Figure 51 – Metabolism pathway of selenium. Used with permission. [29]

Therefore, the main aim of the work presented in this chapter was to further the understanding of how Se effects and interacts with Pt-based anti-cancer drugs. Throughout this chapter a colorectal cancer cell line (HT-29) was chosen for use, and as oxaliplatin is still commonly used in the treatment of colorectal cancer, it was therefore chosen as the Pt-based drug of choice for this work.[166,167]

The work detailed in the following sections aimed to investigate various aspects of the effect that Se had on the Pt-based drugs, ranging from the effect of Se on the subcellular distribution of platinum, the number of Pt-DNA adducts formed as well as the effect on the total cellular uptake of platinum, to the competitive binding of selenium and oxaliplatin.

4.2 Effect of MSA on oxaliplatin in cell cultures

4.2.1 Introduction

This section of this chapter can be divided into four main sections. By exposing the human colorectal cancer cell line (HT-29) to MSA and/or oxaliplatin, several different experiments could be performed. Firstly, by using cells exposed to MSA or oxaliplatin and MSA and oxaliplatin together and extracting the DNA, the number of Pt-DNA adducts could be measured to investigate if Se had an effect, either positive or negative.

Secondly, as previously mentioned, only around 1% of the platinum drugs that penetrate the cell will form adducts with DNA, but little is known about the other major platinum binding sites within the cell.[2–4,111] And furthermore, previous work within this research group has shown that around 70% of platinum exposed to cultured cells can be found within the cytosolic fraction, while around 17% and 4% were observed in the membrane and cytoskeletal fractions respectively and finally around 9% was measured in the nuclear fraction.[5,111] Therefore, by applying this sub-cellular fractionation experiment on cells that were exposed to MSA as well as oxaliplatin, the effect of Se on the sub-cellular distribution of oxaliplatin could be determined.

Thirdly, a piece of work is presented where were whole cells exposed to different combinations and doses of MSA and oxaliplatin to determine if selenium has an impact on the amount of Pt taken up by the cell as a whole. And finally, an attempt at single cell analysis was made using the whole cells exposed to Se and oxaliplatin as described above to determine the distribution within a population of cells.

4.2.2 Methodology

4.2.2.1 Cell culture

The human colorectal cancer cell line (HT-29) used in these experiments were obtained from colleagues at the University of Leicester, but were originally purchased from the American Type Culture Collection (USA).

The cells were taken out of long term storage (ampoules stored under liquid nitrogen) and were rapidly thawed in a water bath at 37°C for 1-2 minutes before being transferred to a cell culture flask (150 cm^2) which already contained cell culture growth media (RPMI 1640 media purchased from Sigma Aldrich, Poole, UK) pre-warmed to 37°C. The flask was subsequently placed in a 37˚C incubator with 5% CO_2 atmosphere. Cells stored under liquid nitrogen have to be stored in media containing DMSO to prevent damage to the cells however once thawed it is damaging to the cells and therefore while diluting the DMSO with cell culture media helps to eliminate the DMSO, the media needs to be replaced after 24 hours with fresh media (containing 10% FCS).

The HT-29 cell line grows adherently and therefore once the cell line had fully recovered from being resurrected from storage (typically 1-2 weeks), the HT-29 cell lines were sub-cultured until sufficient cells were obtained for the experiments detailed above at which point the cells could be exposed to/treated with the oxaliplatin and/or MSA before being harvested.

Drug treatment of cells was performed as follows. Firstly, flasks were examined under a microscope to ensure around 70% confluent, following which the old media was removed from each flask and replaced with either 30 mL fresh media or 30 mL fresh media doped with the desired concentration of MSA and/or oxaliplatin (both purchased from Sigma Aldrich, Poole, UK). For some experiments the MSA and oxaliplatin were added simultaneously, while in later experiments cells were exposed to/grown in MSA for 24 hours before removing all MSA containing media and replacing it with fresh media containing only oxaliplatin. Unless otherwise stated, cells were exposed to the drugs for 1 hour in the incubator before fresh media was placed into the flasks and cells were allowed to recover for either 1 hour or 24 hours. These recovery time points were chosen based on work reported in previous studies and the hours when access to the cell culture laboratory was acceptable.[5,103,111]

At the end of the appropriate recovery time point the cells were harvested, cell counted and aliquoted for each experiment to be carried out; typically 5 million cells per each cell partitioning experiment and 10 million for DNA extraction.

Cell harvesting was performed as follows. Firstly, cell growth media was removed from the flask and the remaining monolayer of cells was washed with PBS (20 mL for 150 cm^2 flasks) to ensure all remaining media was removed from the cells. Following the PBS wash, around 5 mL of Trypsin/EDTA (Sigma Aldrich, Poole, UK) was added to aid in the removal of the cells from the flask. With the added trypsin, the flasks were returned to the incubator for about 5 minutes to allow the trypsin to detach the cells from the flask. Flasks were examined under a microscope to ensure that the majority of cells had been detached, following which 15 mL of media was added to each flask to dilute and deactivate the trypsin. The cell suspensions were transferred into labelled universal flasks and centrifuged for 5 minutes at 1500 rpm to form a cell pellet. The supernatant was then removed and the cells re-suspended in 5 mL media so that a cell count using a haemocytometer could be performed. Briefly, 10 µL of the cell suspension was added to an equal volume of trypan blue (Sigma Aldrich, Poole, UK) before pipetting the mixture under cover slip of haemocytometer and cells in each quadrant were counted and this related back to the number of cells in the original suspension by use of the following equation:

$$Number\ of\ cells\ per\ ml = \frac{Dilution\ factor\ x\ total\ cells\ in\ all\ squares}{Number\ of\ squares}\ x\ 10000$$

The cell suspension was spun down again (5 minutes, 1500 rpm) and could be re-suspended to an appropriate volume of PBS to allow easy aliquoting for subsequent experiments.

4.2.2.2 DNA extraction

The DNA extraction was performed manually unlike the automated extraction described in Section 2.3. The overall principal is similar, where a Genomic-tip/column utilises anion-exchange technology to extract purified high-molecular weight DNA from biological samples.[168] Lysis buffers are used to denature proteins (e.g. nucleases, histones and DNA-binding proteins). DNA binds to the resin within the column due to specific pH and low-salt conditions provided by the buffers while allowing other cell constituents to pass through the column for removal. When a high salt buffer is added to the column, DNA is eluted off the column for use in further experiments or analysis.

DNA extraction was performed using the Qiagen Blood and Cell Culture DNA Midi Kit (Qiagen, Crawley, UK) following the manufacturers guidelines which are outlined below:[168]

1. 2 mL ice cold Buffer C1 and 6 mL ice cold distilled water was added to each 10-20 million cell aliquot of harvested cells after drug exposure and recovery times and mixed thoroughly by inverting the tube several times. Buffer C1 causes cell lysis while stabilising and preserving the nuclei.
2. This mixture was incubated on ice for 10 minutes before being centrifuged at 4°C for 15 minutes at 3000 rpm after which the supernatant was discarded.
3. 1 mL of Buffer C1 and 3 mL distilled water (both ice cold) was added to each sample, which was then mixed thoroughly on a vortex which also aided in re-suspending the pelleted sample. This wash step aims to remove all residual cell debris from the nuclear pellet.
4. Samples were then centrifuged for 15 minutes at 4°C at 3000 rpm following which the supernatant was discarded.
5. Buffer G2 (5 mL) was added to each sample while ensuring that the nuclei were completely re-suspended with the aid of a vortex. This buffer lyses the nuclei and denatures proteins.
6. Protease enzyme solution (95 µL) was added to each sample and was then incubated at 50°C for 60 minutes. The Proteinase K in combination with buffer G2 removes all bound proteins from the DNA.
7. One column (Qiagen genomic tip 100/G) was equilibrated for each sample by allowing 4 mL of Buffer QBT to filter by gravity through each column. Once equilibrated a sample mixture was loaded onto the column (after being vortexed briefly to ensure thorough mixing) and was then allowed to pass through the column with the run off being collected into a waste container.
8. Buffer QC was used to wash the sample to remove all remaining contaminants (3 x 5 mL) and allowed to pass through the column via gravity.
9. To elute the DNA off of the column, 5 mL Buffer QF (pre-warmed to 50°C) was added to the column and the resulting solution collected into a clean tube. The DNA was precipitated with the addition of 3.5 mL of isopropanol (room temperature), and aided by the gentle inversion of the tube. The DNA was then spooled using a pipette tip and moved to a clean, labelled Eppendorf tube containing 200 µL of distilled water. To ensure the DNA was fully dissolved, the samples were heated at 55°C for 2 hours.

4.2.2.3 Cell partitioning

Cell partitioning on cultured cells was performed using a ProteoExtract® Subcellular Proteome Extraction Kit (Merck, Watford, UK). This kit contained buffers which when added in sequence to cells resulted in four subcellular compartments being solubilised and extracted which could then be individually analysed. The four subcellular fractions, in order of extraction, are the cytosolic fraction (containing primarily cytosolic proteins), the membrane and organelles, the nuclear faction and finally cytoskeletal matrix.[169]

After harvesting the confluent cells after drug exposure as detailed in the Section 4.2.2.1, an aliquot containing 5 million cells was spun down to form a pellet and the supernatant discarded. From this point, the manufacturers' protocol for the extraction was followed and is detailed below.[169]

1. Buffer 1 (1 mL x *n*, where *n* is the number of samples) was mixed with Protease Inhibitor Cocktail (5 µL x *n*). 1 mL of this resulting mixture was added to each cell pellet. Thorough mixing was required to ensure full re-suspension of the cells.
2. This resulting mixture of Buffer 1 and cells was incubated on ice for 10 minutes with shaking using a rotary shaker to prevent formation of cell clumps.
3. Samples were centrifuged at 1000 *g* for 10 minutes at 4°C, after which 1 mL of supernatant was removed to a clean pre-labelled Eppendorf tube (Fraction 1 – cytosol) and stored on ice.
4. Buffer 2 (1 mL x *n*) was mixed with Protease Inhibitor Cocktail (5 µL x *n*), following which 1 mL was added to each cell pellet (left over from previous step). Sample was re-suspended and then incubated on ice for 30 minutes with gentle shaking.
5. Samples were centrifuged at 6000 *g* at 4°C for 10 minutes following which the resulting 1 mL of supernatant (Fraction 2 – cell membrane) was transferred to a clean pre-labelled tube and stored on ice.
6. Buffer 3 (0.5 mL x *n*) was mixed with Protease Inhibitor Cocktail (5 µL x *n*) and Benzonase Nuclease (1.5 µL x *n*), following which 0.5 mL was added to each cell pellet (left over from previous step). Sample was re-suspended and then incubated on ice for 30 minutes with gentle shaking.
7. Samples were centrifuged at 7000 *g* at 4°C for 10 minutes following which the resulting 0.5 mL of supernatant (Fraction 3 – nuclear fraction) was transferred to a clean pre-labelled tube and stored on ice.

8. Buffer 4 (0.5 mL x *n*) was mixed with Protease Inhibitor Cocktail (5 µL x *n*), of which 0.5 mL was immediately added to each cell pellet (left over from previous step). Sample was re-suspended thoroughly and labelled as Fraction 4 (cytoskeletal).
9. All four fractions for each sample were then stored at -20°C until needed.

The protease inhibitor cocktail provided with the kit prevented any protein degradation during the extraction of each of the four subcellular fractions while the benzonase nuclease enzyme removed nucleic acids.

4.2.2.4 Digestion

The acid digestion, based on the method of Yamada *et al*.[120] which was modified by Kerr[110] as described in Section 2.3 was used for this work.

4.2.2.5 Spinning cells onto slides

To perform laser ablation ICP-MS (LA-ICP-MS) on cultured cells approximately 50,000 cells in 0.5 mL media were spun down onto Polysine slides (Thermo Fischer Scientific, Loughborough, UK). To do this the cell aliquots were taken after cells had been harvested and counted. The cells were left in suspension and stored on ice before being spun down within a few hours onto slides. To do this a special cyto bucket rotor fitted with a chamber and filter card (DJB Labcare, Newport Pagnell, UK) was used in a Hettich Universal 320R centrifuge (Sigma Aldrich, Poole, UK). The cell aliquots were thoroughly mixed and placed into the slanted chamber with a pre-labelled slide and spun at 500 x *g* for 5 minutes to allow the cells to be spread over the surface of the slide while removing the media onto the filter card. Once spun onto the slides, the cells were stable and could be analysed by LA-ICP-MS at a later stage.

4.2.2.6 Instrumentation

The instrumentation set up used in the work presented in this chapter is very similar to that as described in Section 2.3, however slightly different methods and sets ups were used as detailed below.

For the solution based work, the SF-ICP-MS was set up for a slightly higher flow rate than used in Section 2.3. A PFA nebuliser (Elemental Scientific, Omaha, USA) and a Cyclonic spray chamber (Glass Expansion, Victoria, Australia) were used, along with a 100 µL min^{-1} auto-sampler probe (Elemental Scientific, Omaha, USA) and nickel sampler and skimmer cones (ICPMS cones Ltd., Chester, UK).

Samples evaporated to dryness using the above digestion methods (Section 4.2.2.4), were reconstituted in 400 µL of 2% nitric acid with 1 ppb europium added as an internal standard for Pt and P.

An ICP-MS method was utilised which measured 4 elements of interest; either ^{78}Se (LR) or ^{82}Se (LR), ^{153}Eu (LR), ^{195}Pt (LR) and ^{31}P (MR) was used. While ^{80}Se is the most abundant isotope (49.7%), this isotope could not be used due to spectral interferences with the $^{40}Ar_2$ peak.[170,171] Previous work investigated different isotopes of selenium; in particular ^{77}Se and ^{78}Se and their relative responses and given that ^{78}Se has the higher natural abundance (23.6% as opposed to 7.6%) and it yielded a better response, this isotope was initially chosen and was used for the first few experiments detailed below, before a move to ^{82}Se was made (abundance 9.2%) for all further work due to a lower background being observed.[164,165]

As stated in Section 2.3, nebuliser gas flows and torch position were tuned daily, and typical conditions were shown in Table 2.

For the laser ablation (LA-ICP-MS) work a commercially available laser ablation system, UP-213 (Electro Scientific Industries, Cambridgeshire, UK), was connected to the SF-ICP-MS (Thermo Scientific, Element 2 XR, Bremen, Germany). The laser system was fitted with a low volume, tear-drop shaped cell as described by Horstwood *et al*.[172] High purity helium was used as the ablation gas with a flow rate around 0.55 L/min. Argon sample gas (at a flow rate of 0.9 L/min) was introduced and mixed with the helium using a Y-piece between the ablation cell and the ICP-MS. NIST 611 glass was used to tune the system for maximum ^{238}U signal intensity while maintaining the Th/U ratio around 1. Typical operating conditions for LA-ICP-MS analysis are shown in Table 22.

Table 22 – Typical operating conditions for analysis via LA-ICP-MS

Parameter	Setting
Radio frequency (RF) power	1260 W
Cool gas flow rate	15.50 L min^{-1}
Auxiliary gas flow rate	0.95 L min^{-1}
Sample gas flow rate	0.90 L min^{-1}
Ablation gas flow rate	0.55 L min^{-1}
Sampler cone	Nickel
Skimmer cone	Nickel
Laser spot size	30 µm
Repetition frequency	1 Hz (single shot)
Laser power setting	100 %
Laser fluence	26 J cm^{-2}

4.2.3 Results and Discussion

4.2.3.1 Cell partitioning and formation of Pt-DNA adducts in cultured cells

This work built on and extended work carried out as part of the author's previous MChem project.[164] To aid in providing suitable background to the work performed a short summary of the previous work carried out is provided below, before progressing onto the new work.

In the first experiment conducted, four different drug exposure conditions were set up using HT-29 cells; control (no oxaliplatin or MSA), 50 µM oxaliplatin only, 20 µM MSA only and 50 µM oxaliplatin and 20 µM MSA. Replicates flask were prepared, and enough cells for use in both Pt-DNA adduct formation experiments as well as cell partitioning were grown, as shown in Figure 52.

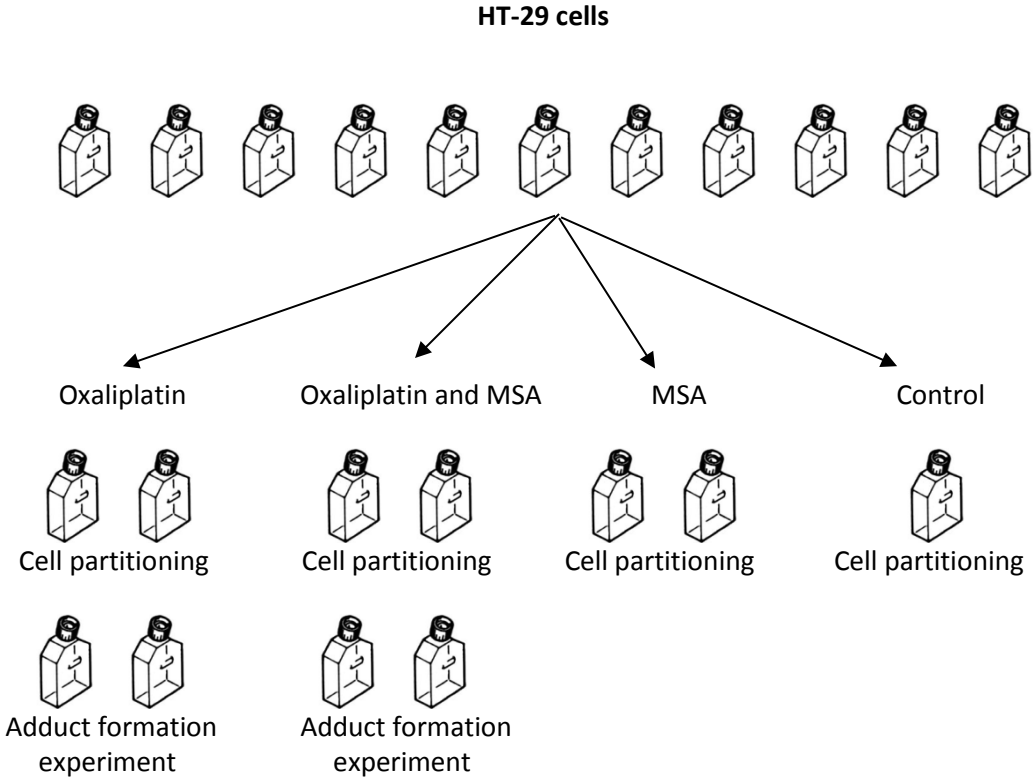

Figure 52 – *In vitro* treatment of cell lines with 50 µM oxaliplatin and 20 µM MSA

These drug doping concentrations were chosen for several reasons. A 20 µM MSA concentration was chosen based on work by Goenaga-Infante *et al*.[161] while a 50 µM oxaliplatin concentration was chosen based on previous work by Zayed *et al*. [111] with the aim of extending and comparing against this work. This dosage level is higher than what would be considered to be a clinically relevant concentration to compensate for the short incubation time (1 hour) when compared to the extended periods of time a drug can circulate around the body in a clinical patient.

Cells were exposed to the drugs, allowed to recover and were harvested before either having the DNA extracted from them or being cell partitioned as described in Section 4.2.2.

The results obtained showed good linearity from the calibration graphs for all elements and good reproducibility was observed for the Pt response. Unfortunately, difficulties were experienced in observing Se in the samples, usually recording only background levels and therefore only the Pt data was examined further.

For determining the subcellular distribution of platinum, the amount of Pt (nanograms (ng) per million cells) was calculated, and when combining the data for all 4 fractions, the percentage of Pt in each fraction could be expressed. While two flasks were prepared for each condition, from which 3 replicates were prepared, this data was averaged out and condensed to form Figure 53.

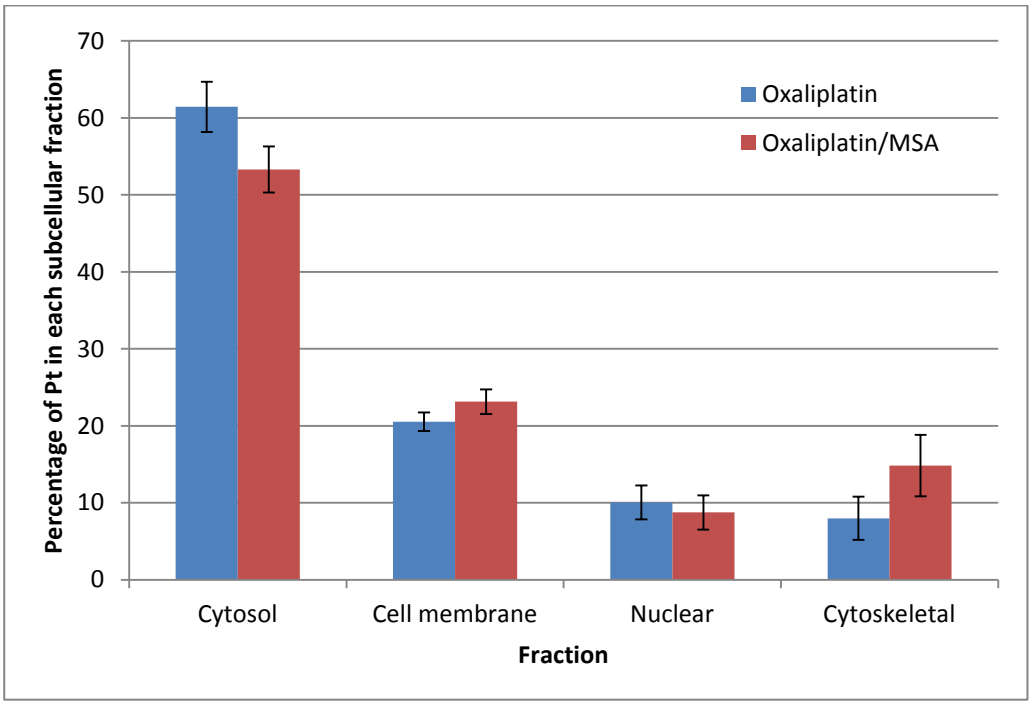

Figure 53 - Percentage of Pt determined in each subcellular fraction in HT-29 human colorectal cancers after exposure for 1 hour to 50uM OxPt and 20uM MSA (error bars calculated using 2x standard deviation, *n*=6)

The error bars were produced by calculating two times the standard deviation, but it is worth noting that biological samples are renowned for larger variation, and therefore a larger error is to be expected.[173] Even though Se was not successfully measured, Figure 53 still allowed for a comparison of Pt position within the cell with and without the cells being exposed to MSA.

Firstly, when looking solely at the distribution of Pt within a cell, a similar trend to that reported by Zayed was observed where a very high level of Pt was observed within the cytosolic fraction when compared to the protein content.[111] It was speculated that the presence of other non-protein molecules (such as glutathione) that reside within the cytosol and have a high binding

affinity for Pt-based drugs could be the reason for this, as well as the possibility of some free/unbound drug still lingering within that fraction.[5,111,174]

When directly comparing the Pt distribution with and without the presence of Se, while it appears that a slight shift in the Pt from the cytosol to the cytoskeleton and cell membrane was observed, this shift was not considered to be statistically significant. Furthermore, and most importantly, the level of Pt reaching the nuclear fraction appears to be unaltered, suggesting that the Se supplementation had not altered the amount of drug reaching the nuclear fraction containing the DNA.

The Pt-DNA adduct information obtained yielded similar results. Figure 54 shows the average number of Pt-DNA adducts formed under the two conditions, and while it appeared that a small decline in the number of Pt-DNA adducts formed when MSA was present, this shift was not determined to be large enough to be statistically conclusive.

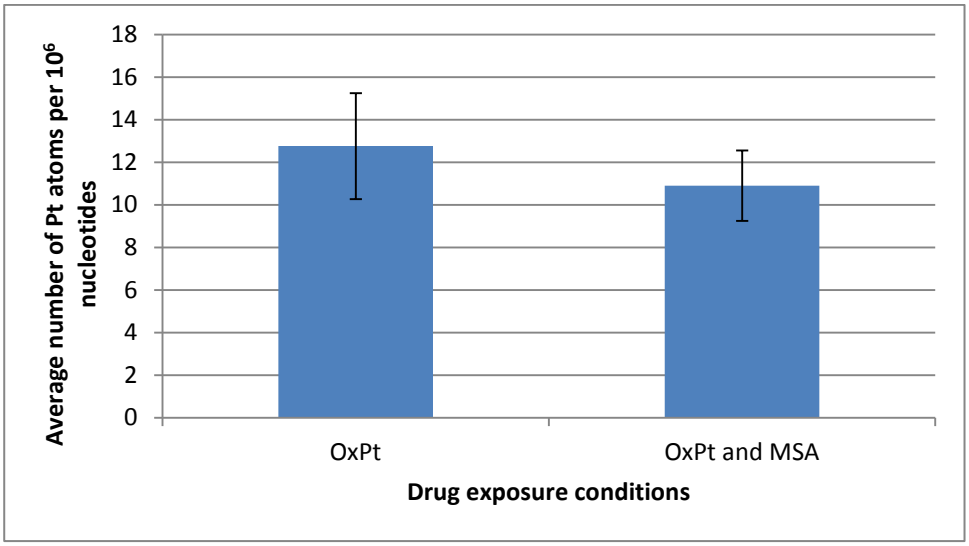

Figure 54 – Number of Pt-DNA adducts formed in HT-29 cells exposed to 50 µM oxaliplatin and 20 µM MSA for 1 hour with 1 hour recovery (error bars produced 2x standard deviation, *n*=6)

The experiment detailed above was repeated, with a couple of adjustments. Firstly a 100 µM MSA concentration was introduced as well as repeating the experiment at 20 µM, and a 24 hour recovery time point as well as the previously used 1 hour was used. Both a 1 and 24 hour recovery time points were chosen for the study of the formation and repair of adducts for two reasons, firstly as these correlate to when the collection of patient samples was usually possible (see Chapter 2) and secondly due to practical limitations and access to the cell culture laboratory.

Even with this increased selenium level problems were still experienced when trying to determine the level of Se in the samples, however the selenium's effect on Pt-DNA adducts could still be observed (see Figure 55).

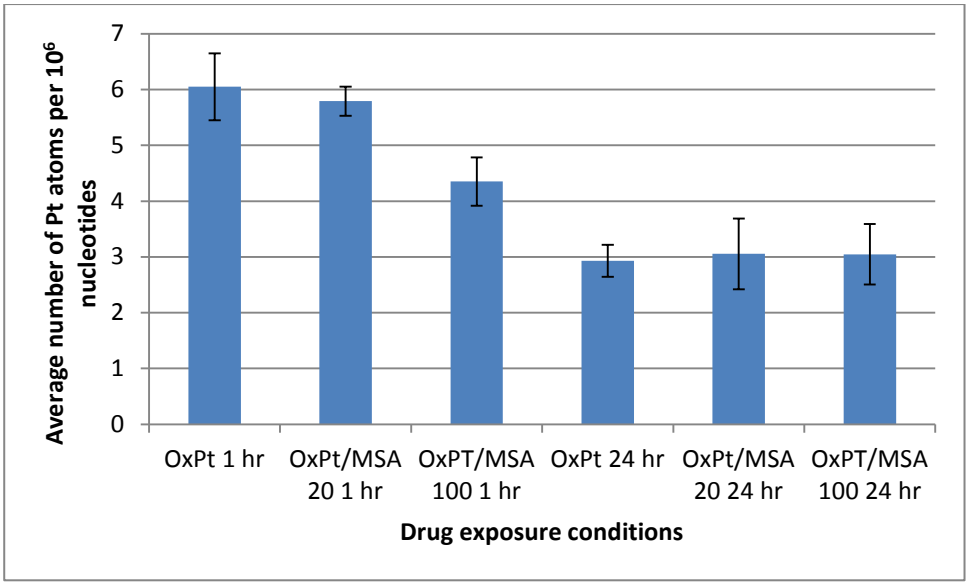

Figure 55 - Number of Pt-DNA adducts formed in HT-29 cells exposed to 50 µM oxaliplatin and either 20 or 100 µM MSA for 1 hour with 1 and 24 hour recovery. Error bars produced 2x standard deviation, n = 4.

As Figure 55 shows, a drop in the number of adducts formed at the highest selenium dosing level was observed following just a 1 hour recovery period, however, when examining the 24 hour recovery data little difference was observed, indicating that Se at high enough doses could retard the amount of Pt reaching the DNA initially, but this effect could be negated over a longer time period.

The work summarised above highlighted issues for further study, and consequently the topic was revisited. Some of the work detailed below was done in collaboration with an MChem student, Carl Cooper.[165]

As well as wanting to repeat the above experiments to ensure their validity and accuracy, other adjustments to the experimental design were made, primarily the growth of the cells in media containing MSA for 24 hours prior to exposure to oxaliplatin as opposed to doping the cells with both drugs simultaneously to better simulate the scenario of patients taking selenium supplements every day. Furthermore, this would remove the possibility of the any Pt-Se interaction outside of the cells which could affect the Pt uptake by the cells.

One of the problems found in the first set of experiments was the inability to accurately record the selenium concentration. It was theorised that the problems associated with measuring the selenium previously could have been due to the harsh conditions experienced by the samples under the acid digestion conditions used, and that the selenium was being lost due to its volatility. Therefore selenium recovery using different isotopes was investigated using ctDNA as part of an MChem project.[165] Briefly, replicate solutions of ctDNA were spiked with MSA before being digested using the method detailed in Section 4.2.2.4 and analysed via ICP-MS. Cooper[165]

reported that while ^{78}Se provided good recovery data, it was ^{82}Se that produced the best response, with recoveries averaging 102%. Therefore as ^{82}Se was determined to be the best isotope for future analysis, despite being low in abundance (9.2%), the lowest background was achieved with this isotope.[165,170]

Based on the results detailed above, a second attempt at measuring both Se and Pt in cultured cells was made to determine the effect of Se on the subcellular distribution of Pt-based anti-cancer drugs. A similar experimental design was set up with one flask being prepared for DNA extraction and one for cell partitioning for each exposure condition (control, 20 µM MSA, 50 µM oxaliplatin and 20 µM MSA and 50 µM oxaliplatin). As previously mentioned, cells were exposed to MSA for 24 hours once confluent before being exposed to oxaliplatin (if necessary) in fresh media for 1 hour before being allowed to recover for either 1 or 24 hours.

Unfortunately, problems and errors were encountered during both the DNA extraction as well as the cell partitioning experiments and for the most part the results had to be discarded. The extraction of DNA encountered problems when loading the sample on to the columns. The columns appeared to be overloaded and consequently some samples were lost and from others only a limited amount of DNA was recovered. Therefore, unfortunately, not enough data was obtained to enable a good comparison to the work previously conducted.

The cell partitioning experiment had limited success. The 1 hour recovery data was compromised by the accidental addition of a contaminating buffer, however data was obtained for the 24 hour recovery experiment (see Figure 56).

The subcellular distribution was slightly different from that seen previously with a lower percentage being recorded in the cytosol and higher in the cytoskeleton. However without the presence of the 1 hour data it was unclear as to whether the results observed were due to the 24 hour recovery or whether an error occurred.

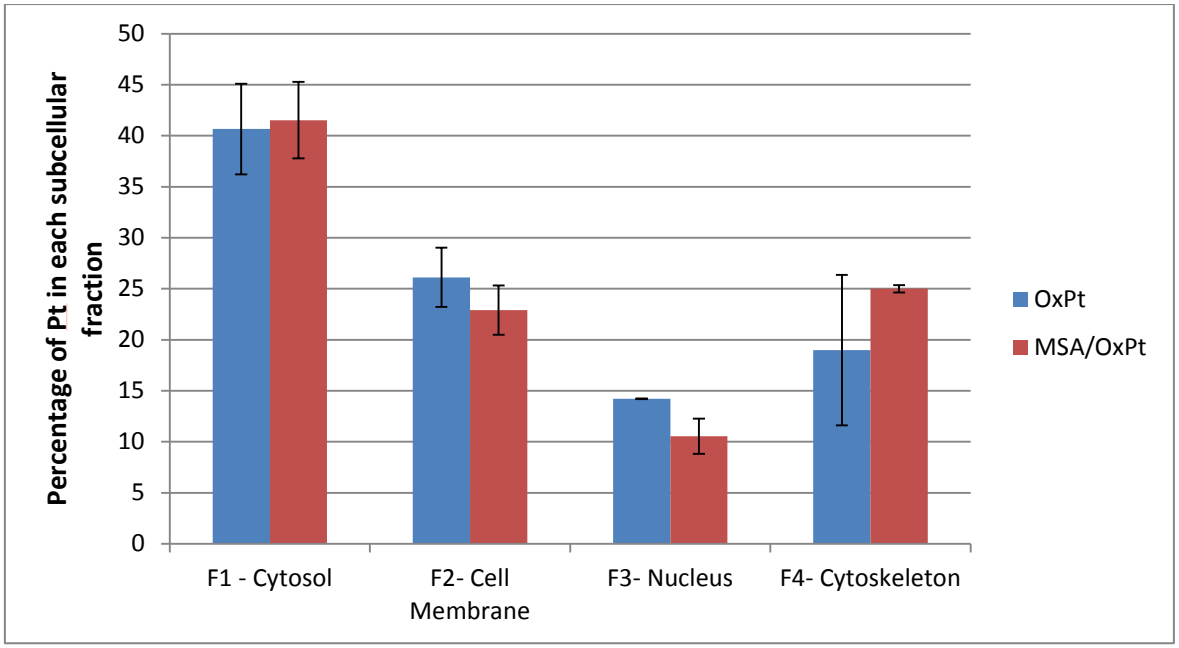

Figure 56 - Percentage of Pt determined in each subcellular fraction in HT-29 human colorectal cancers after exposure for 1 hour to 50uM OxPt and 20uM MSA with 24 hour recovery. Error bars produced using 2x standard deviation, n = 4.

Even though the data obtained in this work was incomplete and largely had to be discarded, in some of the whole cell pellet samples (designed to be used as part of a mass balance experiment for the cell partitioning) selenium was successfully measured (it was not seen in the DNA samples or in the partitioning fractions), which would lead on to the next piece of work.

4.2.3.2 Whole cell analysis

As detailed in the previous section, limited success at measuring the effect of Se on Pt-based drugs within the cell has been obtained. Having ruled out the digestion procedure as the reason for the lack of selenium signal, it was theorised that the selenium was potentially lost during either the DNA and cell partitioning experiments. As a result it was decided to investigate an earlier stage in the process, and therefore the uptake of Pt by whole cells and the possible effect of Se on this uptake was investigated.

In total, 15 flasks (150 cm^2) of HT-29 cells were prepared where the effect of 3 different concentrations of MSA on the total cellular uptake of Pt-based drugs could be investigated (see Table 23). Three different MSA concentration levels were chosen (25, 50 and 75uM) in order to provide a larger Se concentration range which was hoped to allow the successful measurement of Se as well as Pt (oxaliplatin exposure concentration was kept constant at 50 µM). One flask for each condition was set up, from which replicates could be obtained.

Table 23 – Number of flasks and conditions set up for investigating the effect of Se on the uptake of Pt on whole cells

Condition	1 hour recovery	24 hour recovery
Control	1	-
MSA	3	3
Pt	1	1
MSA and OxPt	3	3

* Note: 1 flask of each MSA concentration (25, 50 and 75 µM) was prepared.

The HT-29 cells were grown in RPMI 1640 media (as per Section 4.2.2.1) until around 70% confluent at which point the used media was removed and fresh growth media doped with MSA was placed into the flasks. The flasks were placed back into the incubator and allowed to grow in the presence of MSA for 24 hours before adding fresh media (containing 50 µM oxaliplatin if required) and left for 1 hour before fresh media was once again put into every flask and left for either 1 or 24 hours to recover.

After the desired recovery time has passed, cells were harvested (see Section 4.2.2.1) and pelleted down in to three aliquots of 5 million and one 10 million cell aliquot (where possible) for solution analysis via ICP-MS, while a 50,000 cell aliquot (diluted in approximately 0.5mL media) was taken for analysis via LA-ICP-MS (see Section 4.2.3.3).

Cells were digested as in Section 4.2.2.4 and reconstituted to a final volume of 500 µL of 2% nitric acid with 0.5 ppb Eu as an internal standard. The calibration graphs showed good linearity (see Figure 57 as an example and Appendix C) and the data obtained allowed for the calculation of the

concentration of Pt and Se per million cells for all conditions, as displayed in Table 24 and Figure 58 and Figure 59.

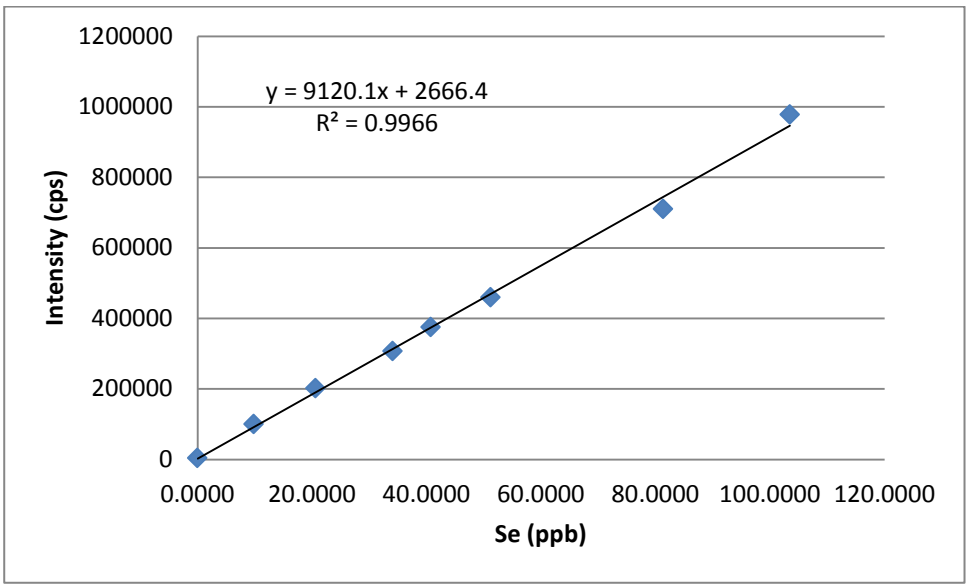

Figure 57 – ^{82}Se calibration graph for Se determination in whole cultured cells

Table 24 – Average concentration per million cells of Pt and Se measured in cultured cells exposed to oxaliplatin and/or MSA

Sample name	Pt (ppb) per million cells	RSD	Se (ppb) per million cells	RSD
Control	0.058	0.012	0.865	0.152
Pt 1 hr	6.711	0.452	0.866	0.028
25uM MSA 1 hr	0.080	0.047	5.966	0.489
50uM MSA 1 hr	0.055	0.012	8.132	0.575
75uM MSA 1 hr	0.055	0.013	9.269	0.476
25uM MSA + Pt 1 hr	4.777	0.151	6.260	0.248
50uM MSA + Pt 1 hr	5.047	0.192	7.134	0.196
75uM MSA + Pt 1 hr	4.554	0.245	9.606	0.292
Pt 24 hr	4.687	0.410	0.855	0.019
25uM MSA 24 hr	0.054	0.013	4.871	0.108
50uM MSA 24 hr	0.054	0.013	7.686	0.366
75uM MSA 24 hr	0.056	0.015	8.515	0.297
25uM MSA + Pt 24 hr	2.745	0.266	5.226	0.248
50uM MSA + Pt 24 hr	3.401	0.107	6.705	0.461
75uM MSA + Pt 24 hr	3.447	0.302	6.746	0.292

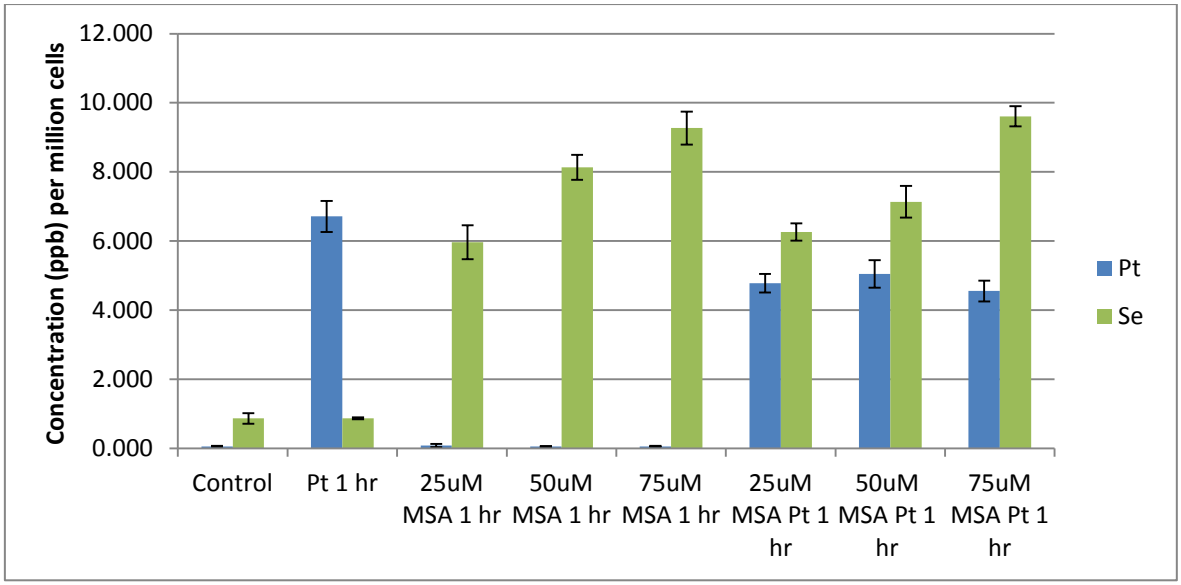

Figure 58 – Concentration of Pt and Se per million cells in 1 Hour recovery and control samples. Error bars produced 2x standard deviation, n = 3.

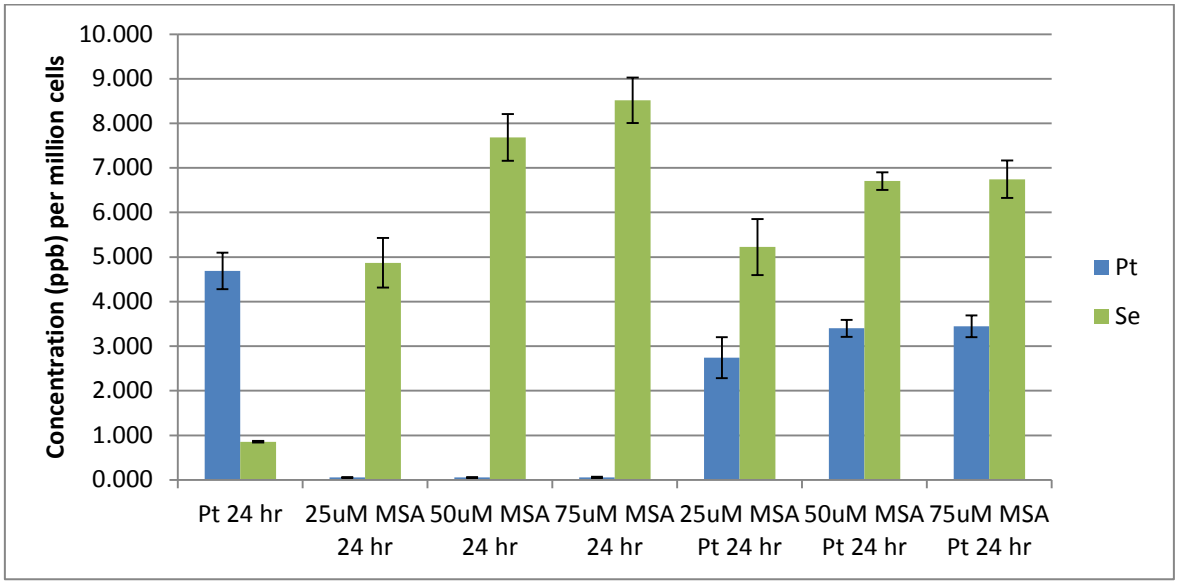

Figure 59 – Concentration of Pt and Se per million cells in 24 Hour recovery samples. Error bars produced 2x standard deviation, n = 3.

The error bars shown in the figures above were calculated using twice the standard deviation of the replicates. To aid in the direct comparison of Pt and Se levels at the different recover time points, Figure 60 was produced.

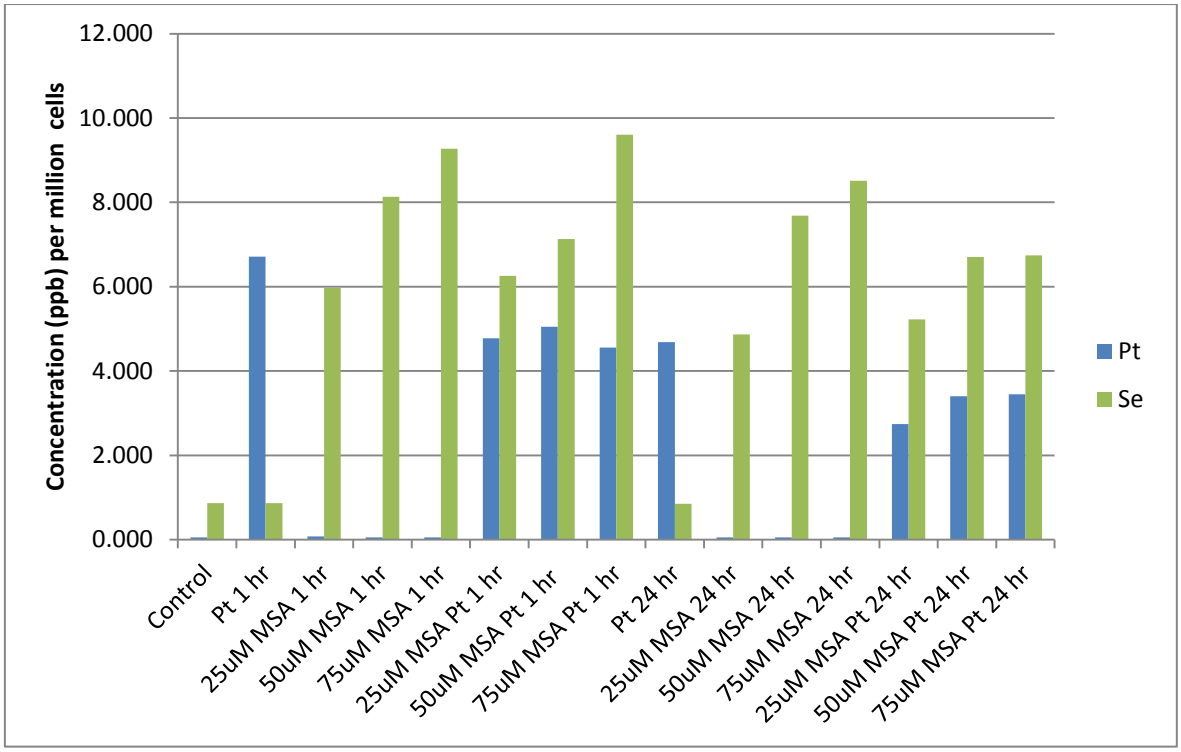

Figure 60 – Concentration of Pt and Se per million cells in all samples (control, 1 hour and 24 hour recovery samples)

The first noticeable observation from Figure 58, Figure 59 and Figure 60 is the successful measurement of both Pt and Se. Even at the 25 µM MSA dosing level (the level closest to the 20 µM used in previous experiments) Se above background was clearly measured, reinforcing the theory that the Se was being lost in both the DNA extraction and cell partitioning. Furthermore, the growing of the cells in MSA for 24 hours prior to dosing with oxaliplatin seems to have aided in the quantification of Se.

There was however a significantly higher level of Se observed in the control cells than Pt. This was to be expected for two main reasons. Firstly, even though ^{82}Se had the lowest background level of interferences of the isotopes measured in previous experiments the background was still significantly higher than that observed for ^{195}Pt. And secondly, selenium is a trace element naturally found within the body and can be found in many selenoproteins and therefore a higher background level of Se would be expected.[171,175,176] However, the concentrations determined in the MSA dosed cells were significantly higher than the background (observed in digest blank samples and control cells) and therefore can be assumed to be a real measurement of selenium.

It is also evident that the selenium uptake by the cells does not linearly correlate with the amount of selenium used to dose the cells. While it can be seen that the Se levels did increase with the dosage levels, particularly evident at the 1 hour recovery time point, the measured Se level does

not rise by the same amount at each dosage jump (i.e. the concentration increase between 25 and 50 µM does not equal that observed between 0 and 25 µM). This could suggest that the cells only have a limited uptake capacity for MSA. However, as the MSA dosage level is increased the Se concentrations observed did increase as well. Unfortunately as a result of the high MSA concentrations used to dose the cells, a greater number of cells were observed to have become detached from the flask overnight (the HT-29 cell line is an adherent cell line) as well as a slight increase in the ratio of dead: live cells as determined during the cell counting step, suggesting that using any significantly higher doses within a cell culture experiment could result in too high a concentration of dead cells to be considered a viable experiment. This effect did become progressively more pronounced as the concentration of MSA was increased.

When comparing the level of Pt taken up by the cells, it is possible that a level of repair (or efflux of Pt from the cells) has occurred between the 1 and 24 hour oxaliplatin only samples. This effect has been seen before when examining the number of Pt-DNA adducts formed (as seen in Chapter 2 and in studies such as those by Zayed and Almeida).[103,111] While this data does not provide information of the number of adducts, it is possible that this reduction in platinum levels after 24 hours recovery could correspond to a decrease in the number of Pt-DNA adducts.

It is also clear that the MSA did have an effect on the level of Pt taken up by the cells. At the 1 hour time point the level of Pt drops by approximately 1-2 ppb per million cells compared to the oxaliplatin only 1 hour samples. At the 24 hour time point, again Pt levels are lower in the samples containing MSA compared to those which did not indicating that repair occurred both with and without MSA being present. While the presence of MSA did reduce the amount of Pt taken up by the cell, the decrease in Pt taken up by the cells at each of the three MSA concentrations were not significantly different. The cells used in this investigation were exposed to MSA for 24 hours, before being washed and fresh media added for the dosage with oxaliplatin. This was done to remove the possibility of Pt-Se interactions outside of the cell reducing the uptake of platinum.

Furthermore, MSA (as well as the Pt) levels had fallen at the 24 hour recovery time point in those samples dosed with both Se and Pt. This drop in level of Se was not seen to the same extent in those samples containing MSA only at the 24 hour recovery time point, possibly suggesting that the Pt and Se played a role in the others decrease in concentration over time.

4.2.3.3 Single cell laser ablation ICP-MS

While the study of the properties of populations of cells has been frequently reported in the literature, little is known about the spread or variation within each cell population.[177] Analysis of single cells by techniques such as laser ablation are starting to be reported in the literature.[177–179]

Analysis of cell populations can provide useful information, however cell heterogeneity/variation is inescapable and therefore the analysis of single cells has the potential to offer new insights and more detailed studies of how cell systems can be affected. Single cell analysis comes with the enormous advantage of reduction in biological noise. Furthermore, as cancer is a heterogeneous disease, the possibility of investigating cell-to-cell variation could potentially lead to insights into tumour initiation, propagation, metastasis and therapeutic response. [177]

Therefore to investigate the effect of MSA on the uptake of Pt-drugs on colorectal cancer cells a small aliquot (approximately 50,000 cells) of the cells from each flask prepared in Section 4.2.3.2 were taken and spun down onto slides (as per Section 4.2.2.5). These cells were then analysed via LA-ICP-MS as described in Section 4.2.2.6.

Due to the large number of slides and different conditions it was decided to ablate 100 cells for Pt and Se on each slide as well as 25 slide blanks for each of the 15 slides. While laser ablation cannot provide accurate quantification of the concentration of elements within a single cell due to problems encountered with the creation of matrix matched standards, the distribution within a cell population can be determined, as can an approximate comparison between samples/slides run on the same day under the same conditions. As any data (cps) obtained on different days could not be directly compared due to slight differences in conditions experienced day to day, initially just one Se concentration (75µM) set was chosen for examination and comparison with oxaliplatin only and the control cells.

A problem often encountered with LA-ICP-MS is the accidental knocking out of the plasma when changing over samples from within the laser ablation cell which would make the direct comparison of samples impossible. Therefore to reduce the likelihood of this happening, a shard from several different slides and a small piece of NIST glass (used for tuning) were placed into the cell together so that cells from each shard could be ablated without having to disrupt the sample gas and risk the plasma going out.

Initially a test sample size of 10 cells for both Pt (using 1 hour oxaliplatin only slide) and Se (75uM MSA and 50 uM OxPt with 1 hour recovery) were chosen (see Figure 61 and Figure 62). Multiple Se isotopes were tested (including ^{77}Se, ^{78}Se and ^{82}Se) but the only isotope with clear Se signal was ^{77}Se (Figure 62). Screenshots of the other Se isotope responses can be found in Appendix C.

As each slide held a total of approximately 50,000 cells to ensure only a single cell was ablated each time a 30µm spot size was used to encompass the entire cell. Furthermore only cells which were on their own were targeted and any cells found in a cluster or too close together were not used.

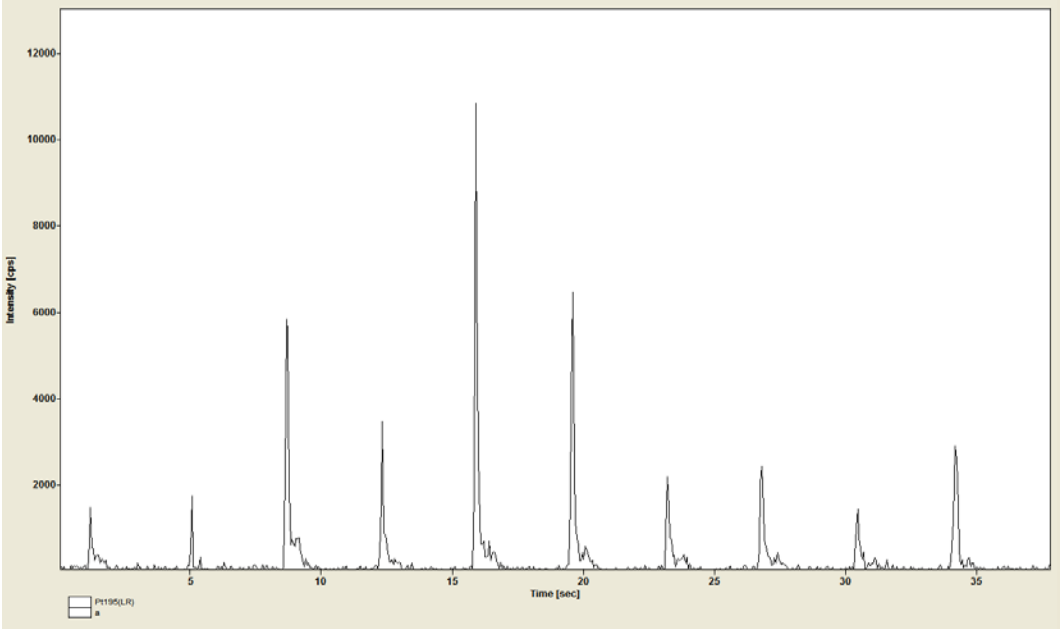

Figure 61 – ^{195}Pt signals obtained from 10 cells exposed to 50 µM oxaliplatin for 1 hour with 1 hour recovery time

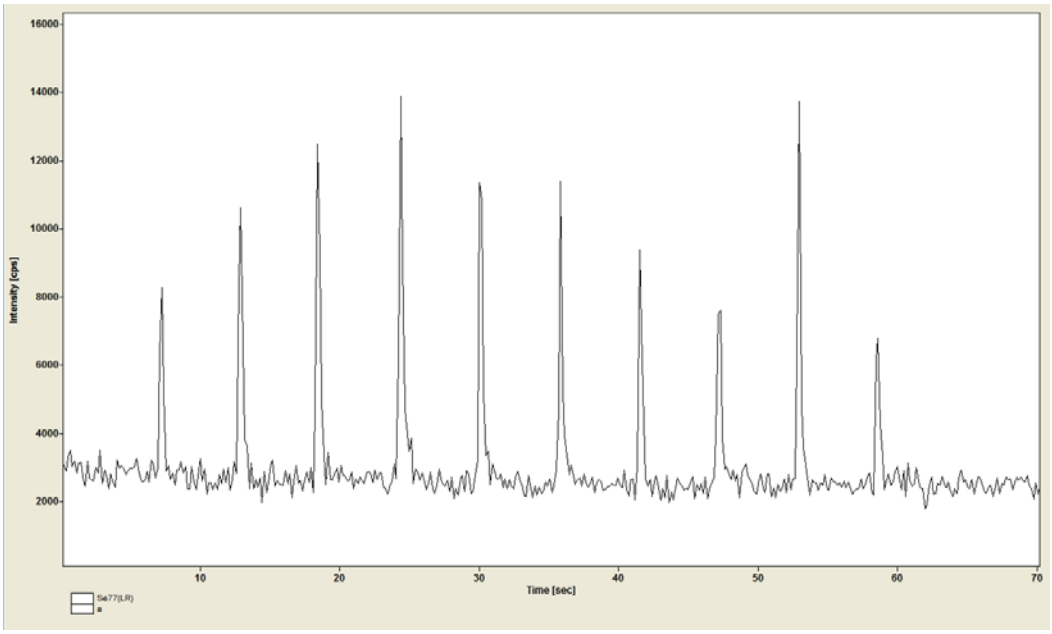

Figure 62 – ^{77}Se signals obtained from 10 cells exposed to 50 µM oxaliplatin and 75 µM MSA for 1 hour with 1 hour recovery time

While a good ^{77}Se signal was seen initially (as in Figure 62), when this was tested again (along with other isotopes), only the occasional spike above background was seen (see Appendix C). The reason for this remains unclear as several parameters were altered and other isotopes retested

but the signal constantly remained intermittent. It was theorised that the position of the slide shard within the cell could receive a different gas flow, and thus causing a reduced signal, or that the He ablation gas or heat from the lighting was causing the Se to be lost off the surface of the shard over the course of the day, however these factors were investigated thoroughly and still no constant signals were obtained.

A further complication was the level of crystallisation of media around the edges of the cells as observed using the laser microscope. Figure 63 shows some examples of the worst crystallisation observed.

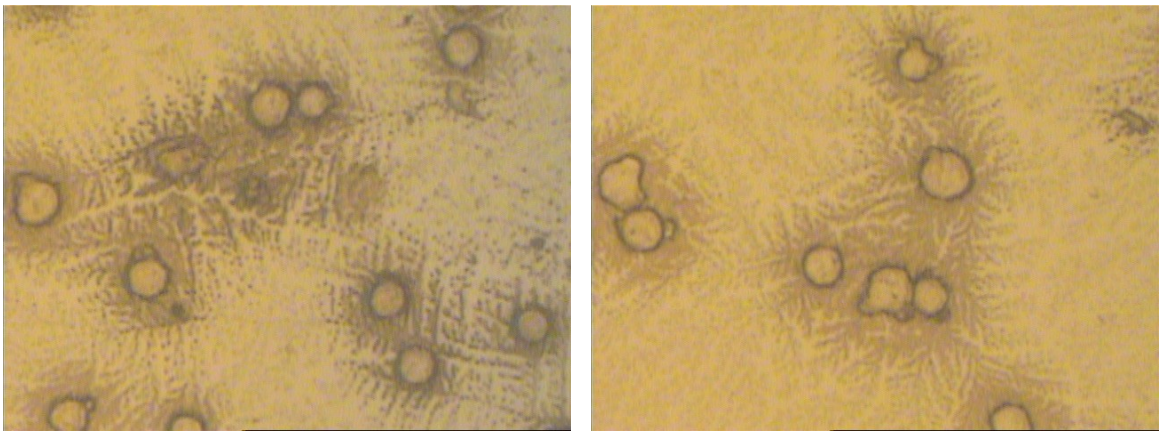

Figure 63 – Examples of HT-29 cells with crystallised media present on slides

The crystallisation was not consistent over the entire slide and was thought to possibly be due to the amount of media used to spin the cells onto the slides. This theory could not be tested as no fresh unspun samples remained at that point; however, a small amount (250 µL media) was added onto a couple of test slides (placed into the cytospin rotor buckets) and re-spun for 20 minutes at 4000 rpm in an attempt re-dissolve the remaining media off the slides before being adsorbed by the filter card. While this did remove a lot of the crystallised media, some still remained and a reduced number of cells on the slide were observed (see Figure 64).

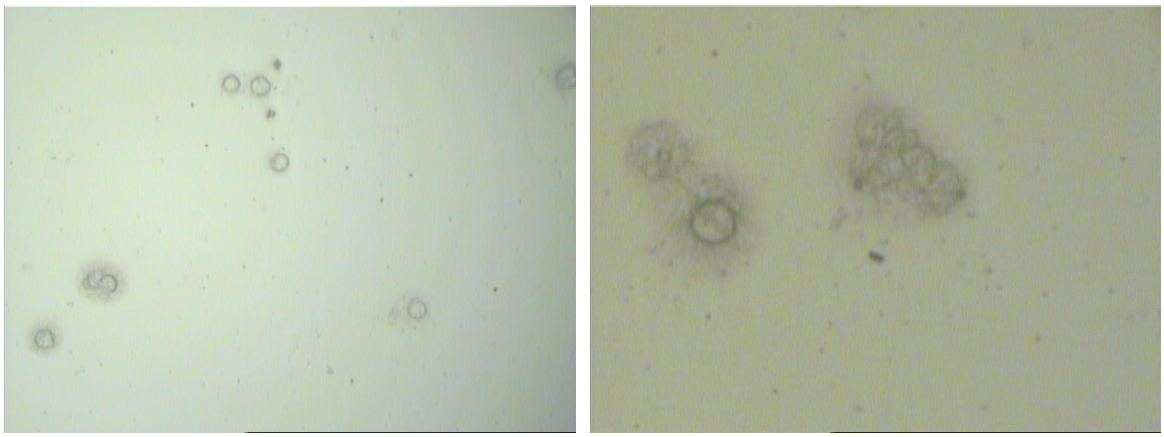

Figure 64 – Examples of HT-29 cells on slides having been re-spun

Due to the varying results and the fact that only whole slides (i.e. slides that had not already been cut down) could be washed using this method, only original and unwashed shards were used for the following work. Furthermore due to difficulties seeing selenium, it was therefore decided to look solely at the Pt signals. Initially, shards from slides containing oxaliplatin only and 75 µM MSA and 50 µM oxaliplatin both with 1 hour recovery time points as well as control were put into the ablation cell together and 100 cells on each shard was ablated looking at the platinum signal intensity as well as 25 slide blanks.

The data obtained from these three slides is presented below. The first observation is that the level of Pt taken up by the cells is not consistent as is evident in Figure 65 and Figure 66. These histograms depict the spread of the data which has been grouped into classes and plotted against the frequency. From Figure 65 (oxaliplatin only) a near Gaussian distribution is observed. However a slightly more distorted Gaussian distribution was observed in the cells dosed with both oxaliplatin and MSA (Figure 66), likely caused by the significantly lower intensities observed (often just above background). Both sets of data are slightly skewed from a normal Gaussian distribution with a slight tail on the right/ positive skew.

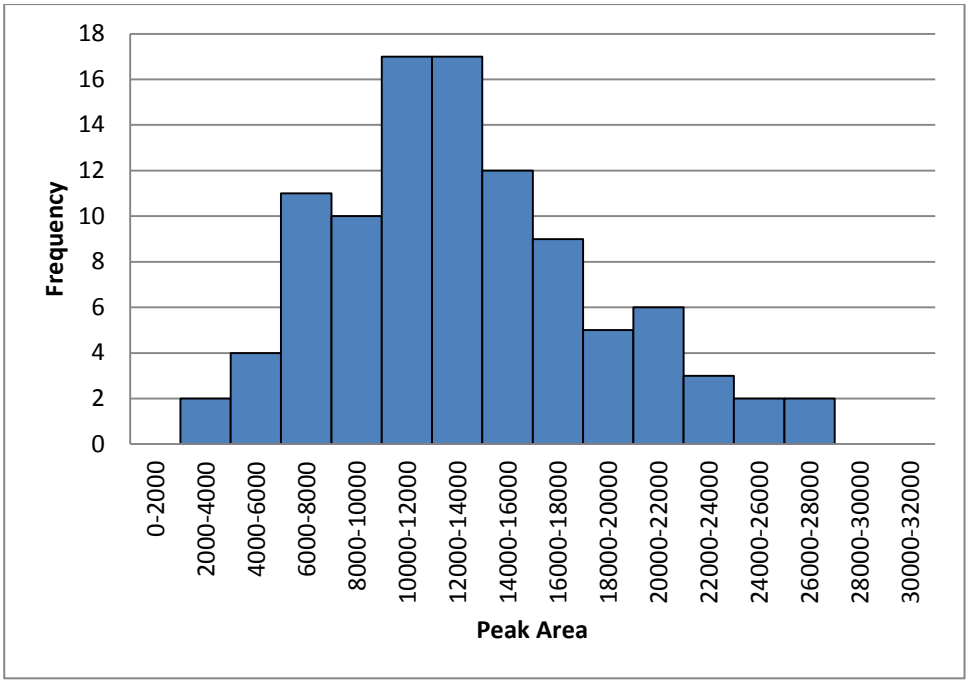

Figure 65 – Histogram depicting the distribution of Pt measured in 100 cells exposed to 50 µM oxaliplatin

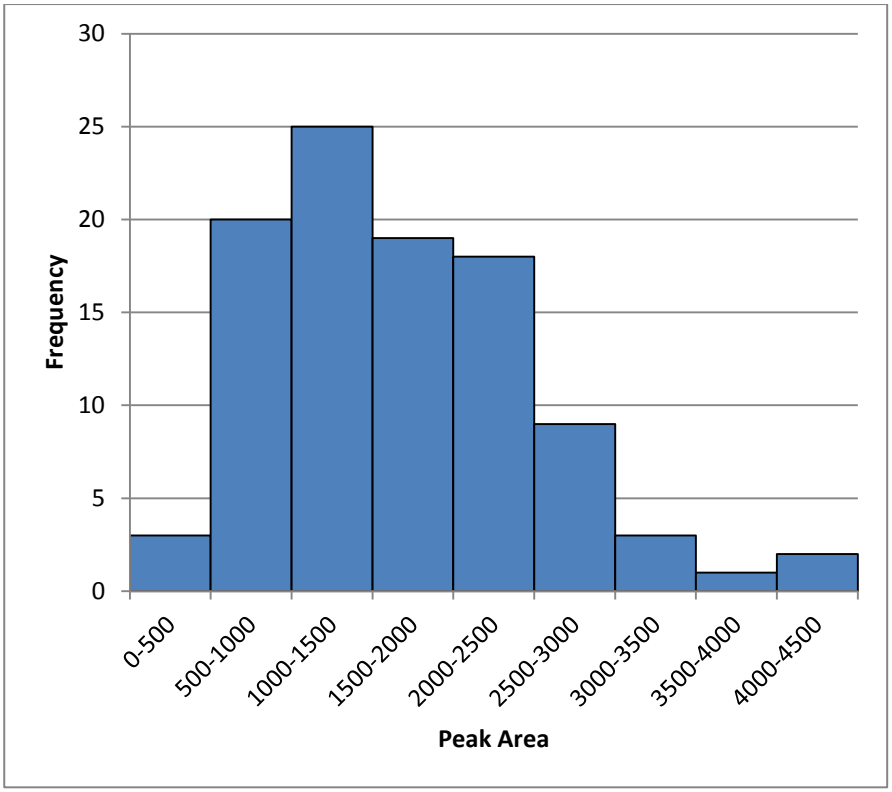

Figure 66 - Histogram depicting the distribution of Pt measured in 100 cells exposed to 50 µM oxaliplatin and 75 µM MSA

While the complete data set for all 100 cells on each slide can be found in Appendix C, differences in intensities for Pt measured in the first set of 25 cells from the control, oxaliplatin only and oxaliplatin and MSA at 1 hour recovery time points are illustrated in Figure 67.

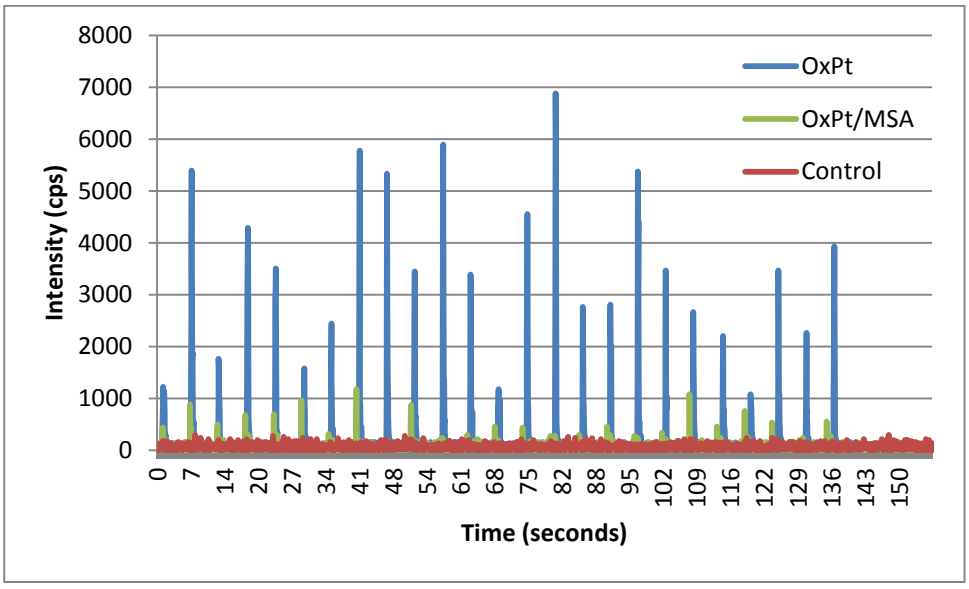

Figure 67 – ^{195}Pt intensities measured in 25 cells at three different dosing conditions

Figure 67 indicates a significant drop in Pt intensity between cells exposed to MSA and those which were not. The position of the shard within the ablation cell (see discussion below) could

have impacted this. However as the drop in intensity was at a significant level, and is supported in part by evidence of a slightly smaller decrease in Pt uptake by cells observed in the solution ICP-MS work, this was therefore thought to be a real effect.

A further data set was obtained allowing the comparison of Pt intensities observed for cells dosed with oxaliplatin only at 1 hour and 24 hour recovery. Figure 68 shows the variation in Pt intensities observed, while the full data sets can be found in Appendix C.

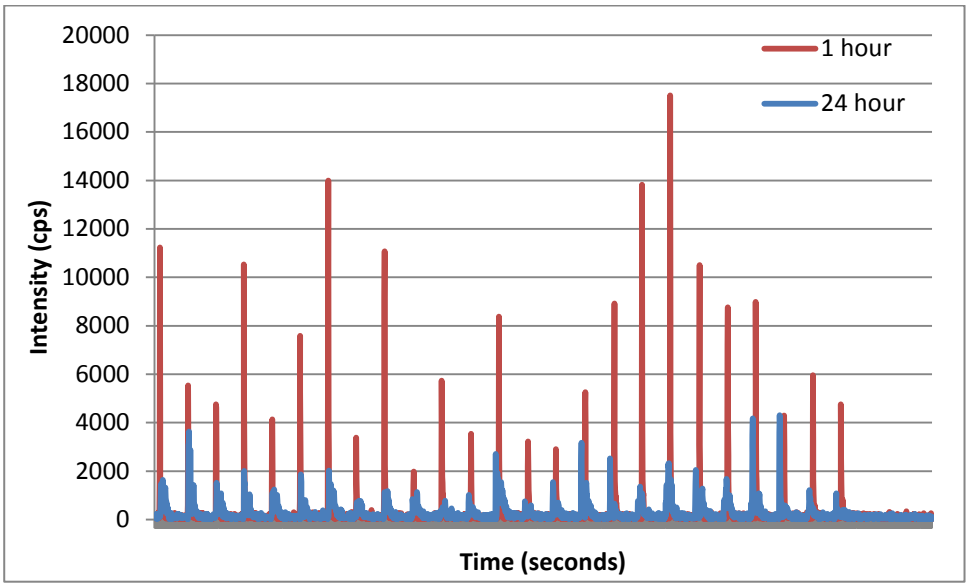

Figure 68 – Comparing the ^{195}Pt intensities measured in 25 cells with 1 and 24 hour recovery times

As with the solution based cell ICP-MS work, Figure 68 shows a decrease in the Pt intensities per cell at the 24 hour recovery time point, however the effect does seem to be exaggerated by LA-ICP-MS (as with the addition of MSA above). One potential explanation for this phenomenon is the effect of the position of the shards within the laser ablation cell which would ultimately receive a different gas flow thus influencing the transport efficiency to the ICP-MS for analysis.

To indicate how the effect of differing gas flows experienced at different parts within the ablation cell could cause a decrease in intensities measured, some gas flow modelling work of the ablation cell used in this experiment is shown below.[180] The flow modelling was done using a He gas flow of 0.6 L min^{-1}, which was slightly higher than that used in this experiment (0.55 L min^{-1}) but illustrates the differing gas flows as determined by number of samples in the cell clearly.

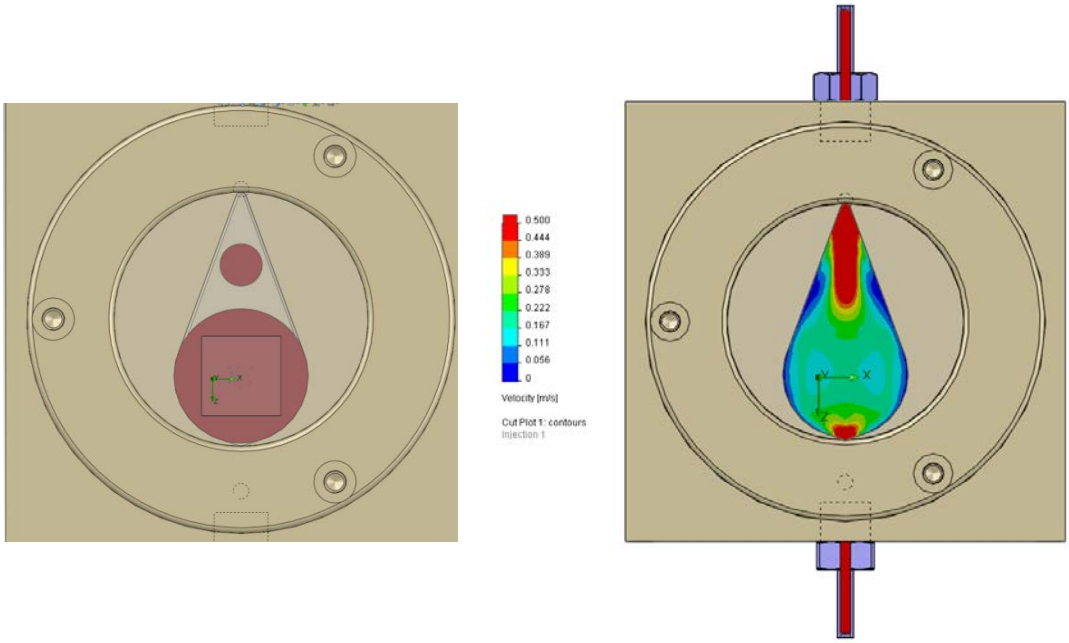

Figure 69 - Gas flow modelling in teardrop cell with a single square slide fragment

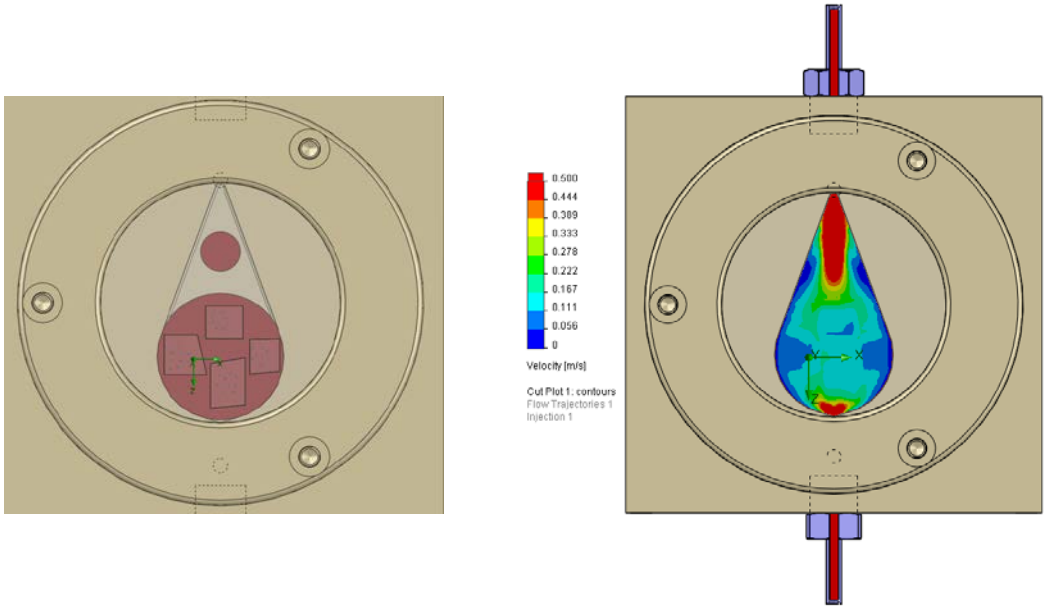

Figure 70 - Gas flow modelling in teardrop cell with 4 smaller shards

Firstly with a single square slide placed in the centre (Figure 69) a relatively uniform gas flow is observed around the slide, with the fastest flow in the centre. However, when four smaller slide fragments were used (as in Figure 70) a non-uniform gas flow with a swirling effect is observed, and would thus affect the intensity of the signals observed.

To overcome the non-uniform effect as observed in Figure 70, ideally each slide would be cut to the same size and placed in the chamber one at a time for analysis (as in Figure 69), however in this experiment this was not feasible. To reduce the impact of the gas flows as much as possible

in this experiment all shards of slides were placed as close the centre line of the cell where gas flows are at their best (a slightly different arrangement to that shown in Figure 70), however it is plausible to speculate that the exaggeration of the decrease in Pt signal observed by laser ablation is due to the position within the cell.

Overall it is clear that analysis of ^{195}Pt in single cells dosed with oxaliplatin is possible by LA-ICP-MS. Furthermore, while this data is not quantitative, a comparison of intensities at different conditions supports the findings from solution based analysis of cell populations where the level of Pt measured decreased when the cells had been dosed with MSA and when looking at cells dosed with oxaliplatin only there was a decrease in Pt taken up by cells at the 24 hour recovery time point when compared to the 1 hour.

It is also clear that the amount of Pt taken up by each cell is not the same and the spread is a slightly skewed Gaussian distribution. This distribution is similar to that observed in a study by Managh *et al*. where the distribution of gadolinium label was measured in cells.[178]

Assuming total ablation of a cell, it can be said that the signal obtained from each ablated cell would be representative of the total amount of Pt taken up per individual cell. However with the variable level of media crystallisation on and around the cells, total ablation of every cell may not have been achieved.

In conclusion, an attempt was made to measure Pt and Se in single cells. While initial success for measuring Se was made the signals were not seen consistently again and the reason for this remains unclear. With further method development and troubleshooting, it is feasible that Se, along with Pt, in single cells could be measured, which has not as yet been reported in the literature. Some success was achieved in measuring the Pt distribution within a cell population, however a full comparison at all dosing conditions was not possible. While this experiment encountered several problems throughout, and only limited Pt data was obtained there is potential for this technique to be useful in the study of Pt-based anti-cancer chemotherapy drugs. This work has shown the distribution in cellular uptake of Pt, and this work could potentially be expanded to investigate the minimum threshold for cell apoptosis. Furthermore, in larger cell types it has been observed that various labels and nanoparticles have centred around the nucleus within the cell, potentially making it possible to single out the nucleus and compare levels of Pt within the nucleus and the surrounding areas of the cell. [181,182]

4.3 Competitive binding of oxaliplatin and MSA

4.3.1 Introduction

As previously discussed, Pt-based anti-cancer drugs such as oxaliplatin enter cells from the bloodstream by active transport or passive diffusion through the cell membrane.[183] Once within a cell oxaliplatin, which had previously had its oxalate ligand substituted by chloride ions, undergoes hydrolysis and the resulting Pt species is believed to be the active form of the drug which forms adducts with the DNA.[132,184–186] However it is well known that oxaliplatin reacts with other species within the cells as they are filled with an abundance of ligands which only have to displace the weakly bound water molecules on the activated drug.

It is known that only around 1% of the drug ever reaches the DNA, and therefore it is these interactions of Pt complexes with non-DNA molecules that make up a substantial portion of the remaining interactions of the Pt-drugs. [3–5,71,187,188] One key intracellular component studied is the tri-peptide g-L-glutamyl-L-cysteinyl glycine (glutathione or GSH, Figure 71), which is the most abundant low molecular weight thiol containing molecule found within the cytosol. [16,174,189,190] Currently it is thought that Pt-GSH complexes could potentially be a major cellular sink for Pt-based drugs, with a reported approximation of 60% of the intracellular cisplatin being accounted for by Pt-GSH binding, thus potentially rendering much of the drug inactive.[191,192] Furthermore, it is thought to potentially play a role in increasing cell resistance, and elevated levels of glutathione were found in cisplatin resistant tumour cells. [16,192,193]

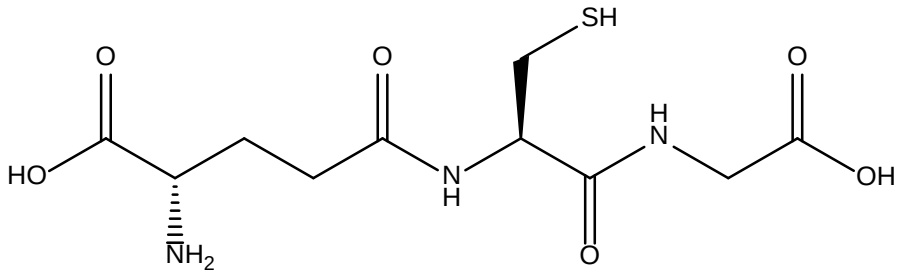

Figure 71 – Structure of glutathione

With a significant number of patients taking supplements during cancer treatment, an understanding of the ramifications of any interactions between these supplements and the Pt-based drugs is required. Selenium has been theorised to potentially have a role in reducing some of the side effects experienced by patients. Some side effects are thought to be caused by a decrease in antioxidant levels in the plasma which have a role in the prevention of oxidative

damage, while selenium (a dietary antioxidant) has the ability to scavenge free oxygen radicals thus reducing oxidative stress, and therefore potentially reducing the level of side effects experienced. [47,194,195] Furthermore, selenium compounds are known to bind to peptides and proteins in the cytosol (such as glutathione), thus potentially preventing as much Pt-based drugs (such as oxaliplatin) from binding to these proteins and leaving a greater amount free to bind with the DNA.[191,196,197]

While a previous study, both practical and computational, has been carried out to investigate the binding of oxaliplatin and glutathione, the work presented in this part of this chapter focusses on the competitive binding of MSA and oxaliplatin with glutathione.[134] While the previous work detailed in this chapter is suggestive that the presence of selenium has a slightly negative impact on the amount of Pt-based chemotherapy drugs taken up by cells, the reason for this effect hasn't as yet been determined. Furthermore, the consequence of having a raised level of intracellular Se on the binding sites of Pt remains uncertain. This work aimed to investigate the interaction of oxaliplatin and MSA, and in particular if a competitive binding scenario exists when in the presence of biological material, in this case the cytosolic protein glutathione.

4.3.2 Methodology

To investigate the competitive binding of MSA and oxaliplatin with glutathione (GSH), four different solutions were prepared and analysed as listed below:

- 20 mM glutathione solution (GSH)
- Glutathione and oxaliplatin mixture (GSH:OxPt, 2:1, 10 mM:5 mM)
- Glutathione and MSA mixture (GSH:MSA, 2:1, 20 mM:10 mM)
- Glutathione, oxaliplatin and MSA mixture (GSH:OxPt:MSA, 1:1:1, 5 mM)

All solutions were prepared in 50:50 methanol:water mixture with 0.1% formic acid. The glutathione, oxaliplatin, MSA, HPLC grade water, formic acid and methanol were all purchased from Sigma Aldrich (Poole, UK).

The samples were analysed on an LTQ linear ion trap mass spectrometer (Thermo Electron, San Jose, CA, USA) with an electrospray ionisation source (ESI). The LTQ was operated in the positive mode at 5.20 kV and 260°C. The instrument was calibrated prior to use with Ultramarks 1621, caffeine and Met-Arg-Phe-Ala (MRFA) in accordance with the manufacturer's recommendations. The resolving powers achieved were in the order of 1500 while the upper instrumental error limit in measurements was 0.2 m/z units. The LTQ auto-tune function was used following this to obtain lens, quadrupole and octapole voltages for maximum transmission of the ions of interest. Helium gas was used as a buffer gas within the ion trap (at approximately 10^{-3} Torr) to improve the trapping efficiency as well as the collision gas for collision induced dissociated experiments (CID).

Samples were introduced into the instrument at the rate of 10 µL min^{-1} into the electrospray source which utilised nitrogen as a nebulising gas. Auxiliary and sheath gases were tuned daily to enable maximum signal transmission.

4.3.3 Results and Discussion

The mass spectra for the first three conditions tested (GSH only, GSH and oxaliplatin and GSH and MSA) can be found in Appendix C, however the main peaks of interest are listed in Table 25 - Table 27.

Table 25 – Peaks of interest observed in GSH only solution

Most Abundant Isotope *m/z*	Assignment
308.17	$[GSH + H]^+$
615.00	$[(GSH)_2 + H]^+$
921.83	$[(GSH)_3 + H]^+$

Table 26 – Peaks of interest observed in GSH:OxPt (2:1) solution

Most Abundant Isotope *m/z*	Assignment
308.17	$[GSH + H]^+$
398.17	$[OxPt + H]^+$
614.92	$[(GSH)_2 + H]^+$
704.92	$[OxPt + GSH + H]^+$
795.17	$[(OxPt)_2 + H]^+$
922.08	$[(GSH)_3 + H]^+$
1012.17	$[OxPt + (GSH)_2 + H]^+$
1102.92	$[(OxPt)_2 + GSH + H]^+$
1499.83	$[(OxPt)_3 + GSH + H]^+$

Table 27 – Peaks of interest observed in GSH:MSA (2:1) solution

Most Abundant Isotope *m/z*	Assignment
308.17	$[GSH + H]^+$
402.17	$[(MSA + G) + H]^+$
613.25	$[(GSH)_2 + H]^+$
800.73	$[(MSA + G)_2 + H]^+$

As can be seen in Table 27, it is evident that under the conditions in this experiment the glutathione molecule is cleaved and loses fragments (represented as G in the tables as opposed to GSH), as was evident by the drop in the mass. However, it is not clear what this loss from the GSH molecule is, or if it remains constant. In some cases, a loss of *m/z* 32, which could indicate a loss of O_2, while in other scenarios there was loss of *m/z* 33 which could indicate the loss of –SH, or potentially O_2H.

To be able to identify which of oxaliplatin (OxPt) and MSA bound preferentially to the GSH, both chemicals were added to the GSH in equimolar concentrations and the mass spectrum recorded (see Figure 72 and Table 28).

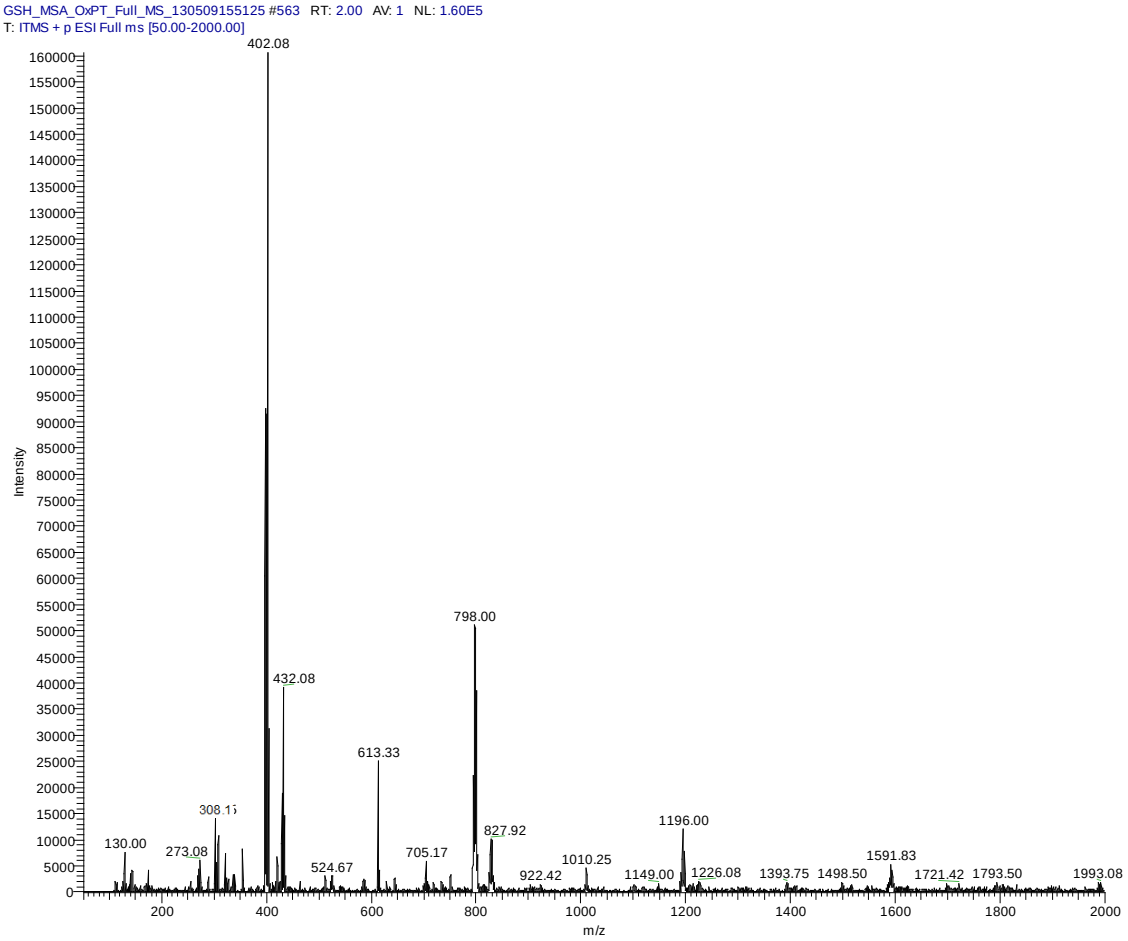

Figure 72 – Full mass spectrum of the competitive binding of MSA and OxPt to GSH

Table 28 – Peaks of interest observed in GSH:OxPt:MSA (1:1:1) solution

Most Abundant Isotope *m/z*	Assignment
308.17	$[GSH + H]^+$
402.08	$[(MSA + G) + H]^+$
432.08	$[MSA + GSH + H]^+$
613.33	$[(GSH)_2 + H]^+$
705.17	$[OxPt + GSH + H]^+$
798.00	$[G + OxPt + MSA + H]^+$
827.92	$[GSH + OxPt + MSA + H]^+$
1010.25	$[OxPt + (GSH)_2 + H]^+$
1196.00	$[G + (OxPt)_2 + MSA + H]^+$
1591.83	$[G + (OxPt)_3 + MSA + H]^+$

As can be seen in Figure 72 a range of binding occurred between GSH, oxaliplatin and MSA. The largest peak observed was that of MSA and glutathione at *m/z* 402 (having lost the thiol group). One noticeable difference in this spectrum is the addition of a peak at *m/z* 432 which is MSA and glutathione without the loss of the thiol which was not seen in previous spectra (Figure 128, Appendix C). However, while it appears that the primary binding of glutathione was with MSA, binding with oxaliplatin and a combination of oxaliplatin and MSA was present as well, and in fact little or no free oxaliplatin remained in solution.

With MSA, oxaliplatin and glutathione being present in solution at equimolar concentrations it was thought that not all MSA and oxaliplatin would be able to bind to the glutathione and thus would result in a competitive binding scenario. This however was found not to be the case as oxaliplatin dimers and trimers were found to interact with the glutathione and MSA such that little or no free oxaliplatin was found in solution. The presence of such oxaliplatin dimers and trimers is evidence of the high affinity oxaliplatin has for glutathione, as was previously reported by Shoeib *et al*.[134] As well as the variety of different ways oxaliplatin is able to bind with glutathione, it is worth noting that this binding is not prevented by the presence of an equimolar concentration of MSA.

However, it is also worth noting that the high levels of oxaliplatin, and MSA, as used in this experiment, would not be found in a true biological system, and therefore the results are not wholly representative of what would happen in the body. The presence of oxaliplatin dimers is unlikely to be seen within the body due to the plethora of binding sites which can be found within cells, however in an attempt to force a competitive binding scenario, high concentrations were used in this experiment.

While previously in this chapter it was observed that the amount of Pt in the cytosol did decrease slightly when MSA was also used to dose cells (Figure 53), the results from this work are not conclusive to say whether this was due to MSA binding preferentially to cytosolic proteins or peptides, such as glutathione. Despite the largest peak being observed being glutathione and MSA only, due to no peak for unbound oxaliplatin being observed it can be assumed that all oxaliplatin was bound to glutathione/glutathione and MSA in various combinations, as discussed above. Therefore, the presence of selenium did not conclusively appear to free up binding sites that could otherwise be taken up by oxaliplatin.

4.4 Conclusions

This chapter explored the effect of selenium supplementation on oxaliplatin and colorectal cancer cells. Firstly, when investigating the cells at a subcellular level, the most notable result was the decrease in the level of platinum in the cytosol in the presence of MSA. This was accompanied by a slight decrease of platinum within the nuclear fraction, however this change was not significant. Furthermore, a slight decrease in the level of Pt-DNA adducts was observed when MSA was present; however this was again deemed to not be a significant difference. However, while the platinum at the subcellular level was easily determined, selenium was not measured above background level.

Following this, the effect of selenium supplementation of the total cellular uptake of oxaliplatin was investigated. In cultured cells it was seen that the presence of selenium, in the form of MSA, did reduce the amount of oxaliplatin taken up by the cell. This was seen in analysis of populations of cells as well as by single cell analysis. In this work both selenium and platinum were successfully measured, suggesting that in the previous selenium was either at too low a concentration or being lost in the DNA or cell partitioning methods. While this work showed that when dosed with MSA, the cells did not take up the oxaliplatin as readily, this effect was not in a linear relationship with the MSA dosage concentration. Furthermore, the level of both oxaliplatin and selenium found in the cells had decreased when compared to the one hour recovery time point, possibly suggesting a level of repair. The platinum in whole cells was also examined using LA-ICP-MS, and while not quantitative, a comparison of the relative signal intensities also showed that less Pt was present within cells exposed to MSA than those which were not, thus confirming the results from the solution based work.

When investigating whether MSA and oxaliplatin competitively bound in the presence of glutathione, the dominant peak was that of glutathione and MSA potentially suggesting that MSA was preferentially bound. However, no free oxaliplatin was observed in the solution, and instead it bound in multiple other forms, both with glutathione on its own and in combination with glutathione and MSA. And therefore, no evidence was found to suggest that the presence of selenium freed up oxaliplatin for binding elsewhere.

5. Summary and further work

This thesis aimed at addressing just a few of the many potential areas of research surrounding the use of Pt-based chemotherapy drugs while utilising highly sensitive techniques such as ICP-MS, with a primary focus on the measurement of Pt in clinical samples, the effect of selenium supplementation on the distribution and adduct formation in *in-vitro* cell cultures, and the binding of platinum to cytosolic proteins.

Due to the different themes being explored in each experimental chapter the main conclusions can be found in the relevant chapters, however a brief summary of each section of work along with potential areas of further work is presented below.

5.1 Pt-DNA adduct comparison in blood and saliva samples from patients undergoing Pt-based chemotherapy

ICP-MS was successfully utilised in the measurement of Pt-DNA adducts in both blood leukocyte and saliva samples. This work highlighted some practical issues associated with patient sampling, and in particular with the collection of saliva samples. While one of the aims of the work was to investigate the feasibility of using a more patient friendly and less invasive sampling technique, problems obtaining patient adherence to the sampling protocol were experienced, suggesting that while in theory saliva collection is more favourable from the patient's perspective, from an analytical standpoint obtaining a useable sample was difficult. Furthermore, as is often the case when working with clinical patients a high dropout rate was experienced. Therefore collecting enough samples for a comparison study was challenging. When a comparison of the number of adducts in the two sample types was made, a limited correlation was observed in the pre-infusion samples, while a lack of correlation in the 1 hour post-infusion samples was found, suggesting that saliva is not, as used here, a viable alternative to leukocytes for the determination of Pt-DNA adducts. However, as platinum could be measured rapidly in the saliva as well as leukocyte samples at the 1 hour post-infusion time point, saliva may still have some potential for use as a clinical sample type.

While the research presented here in this thesis has made some interesting discoveries it has also highlighted some areas which would benefit from further research. While the work on saliva as a viable alternative source of Pt-DNA adducts to leukocytes proved unsuccessful, if a saliva sample could be cell sorted prior to DNA extraction, this could potentially provide a better correlation or help to illustrate why a poor correlation was observed in these samples. However, this would require a fresh saliva sample and not one stored as was the case in this investigation, thus

defeating the objective of having a sampling kit patients could use at home, and which could ultimately not provide any benefits over the current leukocyte sampling technique. Nevertheless, an extended time study (whether by blood, saliva or another sample type) which would allow the accurate tracking of Pt-DNA levels over the hours and days following treatments, and between cycles, would allow a more accurate comparison between adduct levels and toxicities experienced by patients which could help clinicians increase the quality of patient care and potentially aid in the personalisation of doses.

5.2 Binding of oxaliplatin to cytosolic proteins

ESI-MS was used in the investigation of the binding of platinum to cytosolic proteins. Platinum binding to both nitrogen and sulfur rich peptides was observed immediately after mixing, and with the samples being re-analysed after 24 hours no obvious effect of time was observed and the complexes observed appeared stable. Although reproducing biological conditions was beyond the scope of this experiment, and thus oxaliplatin bound to the peptides as a whole molecule, the fact that it bound to both sulfur and nitrogen rich peptides shows potential for these peptides to be binding sites within the cells.

The computational study demonstrated that, as observed from the experimental data, oxaliplatin would bind to both sulfur and nitrogen binding sites. The relative free energies of various peptide-oxaliplatin binding scenarios were examined and while often the nitrogen sites offered a lower relative free energy, the difference between the nitrogen and sulfur values tended to be very small, and thus binding to both sulfur and nitrogen would be found in the samples analysed. Initially only two peptides where selected for analysis via computational modelling, however this work could be extended to include the remaining 8 peptides.

The work presented here suggests that there is a large excess of potential binding sites for Pt in the cellular proteome and that no single species or functionality is likely to dominate. It follows that therapeutic intervention would be difficult as there doesn't appear to be a single therapeutic target that could be modified to improve the efficiency of Pt binding to its target, the DNA. However, given recent improvement in UHPLC and nano-LC for the analysis of peptides it would be appropriate to reinvestigate a direct top-down analysis of the Pt-cytosol-proteome.

5.3 Effect of selenium on the cellular distribution and uptake of oxaliplatin in cultured cells

ICP-MS was used in the investigation into the effect of selenium supplementation on platinum-based chemotherapy in cultured colorectal cancer cells. Firstly attempts were made to determine the effect of selenium on the number of Pt-DNA adducts as well as the subcellular distribution of platinum, but as the selenium was not successfully measured only the effect of selenium on platinum could be determined. The work showed there appeared to be a slight shift of the platinum away from the nucleus when selenium was present, as evident by a small reduction in Pt-DNA adducts and a lower amount of Pt in the nuclear fraction. When the cells were studied as a whole, it was evident that selenium did reduce the overall amount of platinum being taken up by the cells. Cells were incubated with selenium for 24 hours prior to being washed and then dosed with platinum, thus ensuring that any change in platinum uptake observed was due to the selenium and not any Pt-Se interactions. Furthermore an attempt was made to measure the selenium and platinum in single cell analysis via LA-ICP-MS, and while this work was not quantitative a comparative look at platinated cells with and without selenium supported the findings of an overall reduction in the level of platinum per cell when selenium was present. And finally, a competitive binding study found that both selenium and platinum bound to glutathione, and no preferential binding was observed. While the predominant peak observed was that of GSH-MSA, it is worth noting that no free oxaliplatin was observed due to dimeric and trimeric binding of oxaliplatin to the peptide which was present.

The work performed on cell cultures showed a great deal of promise but more work is required. Firstly, some of the experiments could be repeated in order to confirm the results observed and to obtain better average results. However, the primary interest would be to extend the work and look further at dosing levels of both oxaliplatin and MSA, and to attempt to find a DNA extraction procedure and subcellular fractionation technique which would allow the measurement of selenium as well as the platinum.

LA-ICP-MS uniquely provided a means of studying platinum distribution at the single cell level. Further research is required to establish a robust methodology for selenium so that the effect of selenium on platinum could be measured at the single cell level which has never been done before. But perhaps the most significant application which LA-ICP-MS could be applied to is its use in the measurement of platinum in patient samples, such as leukocytes or tumour cells. Gaining clinical patient sample data is always useful due to the natural variability in humans,

however to be able to investigate how the platinum-based drugs are taken up by and affect individual cells is of prime interest.

6. References

1. P. D. Sasieni, J. Shelton, N. Ormiston-Smith, C. S. Thomson, and P. B. Silcocks, *Br. J. Cancer*, 2011, **105**, 460–465.

2. E. E. M. Brouwers, M. Tibben, H. Rosing, J. H. M. Schellens, and J. H. Beijnen, *Mass Spectrom. Rev.*, 2008, **27**, 67–100.

3. C. R. Centerwall, K. A. Tacka, D. J. Kerwood, J. Goodisman, B. B. Toms, R. L. Dubowy, and J. C. Dabrowiak, *Mol. Pharmacol.*, 2006, **70**, 348–355.

4. J. Reedijk, *Chem. Rev.*, 1999, **99**, 2499–2510.

5. A. Zayed, T. Shoeib, S. E. Taylor, G. D. D. Jones, A. L. Thomas, J. P. Wood, H. J. Reid, and B. L. Sharp, *Int. J. Mass Spectrom.*, 2011, **307**, 70–78.

6. H. Varmus and R. A. Weinberg, *Genes and the Biology of Cancer*, W. H. Freeman and Company, New York, 1993.

7. B. C. Baguley and D. J. Kerr, *Anticancer Drug Development*, Academic Press, London, 2002.

8. A. V Klein and T. W. Hambley, *Chem. Rev.*, 2009, **109**, 4911–4920.

9. L. Kelland, *Nat. Rev. Cancer*, 2007, **7**, 573–584.

10. C. A. Rabik and M. E. Dolan, *Cancer Treat. Rev.*, 2007, **33**, 9–23.

11. C. F. Harrington, R. C. Le Pla, G. D. D. Jones, A. L. Thomas, and P. B. Farmer, *Chem. Res. Toxicol.*, 2010, **23**, 1313–1321.

12. J. L. Misset, H. Bleiberg, W. Sutherland, M. Bekradda, and E. Cvitkovic, *Crit. Rev. Oncol. Hematol.*, 2000, **35**, 75–93.

13. C. R. Culy, D. Clemett, and L. R. Wiseman, *Drugs*, 2000, **60**, 895–924.

14. E. Å. Lundqvist, *Int. J. Gynaecol. Obstet.*, 2012, **119**, 151–154.

15. N. J. Wheate, S. Walker, G. E. Craig, and R. Oun, *Dalt. Trans.*, 2010, **39**, 8113–8127.

16. D. Gibson, *Dalt. Trans.*, 2009, **48**, 10681–10689.

17. M. E. Bosch, a J. R. Sánchez, F. S. Rojas, and C. B. Ojeda, *J. Pharm. Biomed. Anal.*, 2008, **47**, 451–459.

18. M. S. Davies, S. J. Berners-Price, and T. W. Hambley, *J. Inorg. Biochem.*, 2000, **79**, 167–172.

19. F. Arnesano and G. Natile, *Coord. Chem. Rev.*, 2009, **253**, 2070–2081.

20. A. M. Fichtinger-Schepman, J. L. van der Veer, J. H. den Hartog, P. H. Lohman, and J. Reedijk, *Biochemistry*, 1985, **24**, 707–713.

21. D. Wang and S. J. Lippard, *Nat. Rev.*, 2005, 4, 307–320.

22. R. A. Alderden, M. D. Hall, and T. W. Hambley, *J. Chem. Educ.*, 2006, **83**, 728–734.

23. E. Raymond, S. Faivre, S. Chaney, J. Woynarowski, and E. Cvitkovic, *Mol. Cancer Ther.*, 2002, **1**, 227–235.

24. J. M. Woynarowski, S. Faivre, M. C. Herzig, B. Arnett, W. G. Chapman, a V Trevino, E. Raymond, S. G. Chaney, A. Vaisman, M. Varchenko, and P. E. Juniewicz, *Mol. Pharmacol.*, 2000, **58**, 920–927.

25. S. Dawood and B. Leyland-Jones, *Cancer Invest.*, 2009, **27**, 482–488.

26. K. Schwarz and C. M. Foltz, *J. Am. Chem.*, 1957, **79**, 3292–3293.

27. S. Dodig and I. Cepelak, *Acta. Pharm.*, 2004, **54**, 261–276.

28. J. J. R. Frausto da Silva and R. J. P. Williams, *The biological chemistry of the elements*, OU, Oxford, 2nd edn., 2001.

29. H. G. Infante, R. Hearn, and T. Catterick, *Anal. Bioanal. Chem.*, 2005, **382**, 957–967.

30. M. Fakih, S. Cao, F. A. Durrani, and Y. M. Rustum, *Clin. Colorectal Cancer*, 2005, **5**, 132–135.

31. R. J. Shamberger and D. V Frost, *Can. Med. Assoc. J.*, 1969, **100**, 682.

32. G. F. Combs and W. P. Gray, *Pharmcol. Ther.*, 1998, **79**, 179–192.

33. G. N. Schrauzer, D. A. White, and C. J. Schneider, *Bioinorg. Chem.*, 1977, **34**, 23–34.

34. L. C. Clark, K. P. Cantor, and W. H. Allaway, *Arch. Environ. Health*, 1991, **46**, 37–42.

35. P. D. Whanger, *Br. J. Nutr.*, 2004, **91**, 11–28.

36. J. A. Milner, *Fed. Proc.*, 1985, **44**, 2568–2572.

37. W. J. Blot, J. Li, P. R. Taylor, W. Guo, S. Dawsey, G. Wang, C. S. Yang, S. Zheng, M. Gail, G. Li, Y. Yu, B. Liu, J. Tangrea, Y. Sun, F. Liu, J. F. Fraumeni, and B. Li, *J. Natl. Cancer Inst.*, 1993, **85**, 1483–1492.

38. B. K. Dunn, E. S. Richmond, L. M. Minasian, A. M. Ryan, and L. G. Ford, *Nutr. Cancer*, 2010, **62**, 896–918.

39. L. Auerbach, *J. Men's Heal. Gend.*, 2006, **3**, 397–403.

40. C. Ip, Y. Dong, and H. E. Ganther, *Cancer Metastasis Rev.*, 2002, **21**, 281–289.

41. H. E. Ganther and J. R. Lawrence, *Tetrahedron*, 1997, **53**, 12299–12310.

42. C. Ip, H. J. Thompson, Z. Zhu, and H. E. Ganther, *Cancer Res.*, 2000, **60**, 2882–2886.

43. G. Li, H.-J. Lee, Z. Wang, H. Hu, J. D. Liao, J. C. Watts, G. F. Combs, and J. Lü, *Carcinogenesis*, 2008, **29**, 1005–1012.

44. G. F. Combs, *Med. Klin.*, 1999, **94**, 18–24.

45. E. N. Drake, *Med. Hypotheses*, 2006, **67**, 318–322.

46. A. Molassiotis, P. Fernadez-Ortega, D. Pud, G. Ozden, J. a Scott, V. Panteli, A. Margulies, M. Browall, M. Magri, S. Selvekerova, E. Madsen, L. Milovics, I. Bruyns, G. Gudmundsdottir, S. Hummerston, a M. Ahmad, N. Platin, N. Kearney, and E. Patiraki, *Ann. Oncol.*, 2005, **16**, 655–663.

47. N. I. Weijl, G. D. Hopman, E. G. W. M. Lentjes, H. M. Berger, F. J. Cleton, and S. Osanto, *Ann. Oncol.*, 1998, **9**, 1331–1337.

48. N. I. Weijl, T. J. Elsendoorn, E. G. W. M. Lentjes, G. D. Hopman, A. Wipkink-Bakker, a H. Zwinderman, F. J. Cleton, and S. Osanto, *Eur. J. Cancer*, 2004, **40**, 1713–1723.

49. T. J. Elsendoorn, N. I. Weijl, S. Mithoe, A. H. Zwinderman, F. Van Dam, F. A. De Zwart, A. D. Tates, and S. Osanto, *Mutat. Res.*, 2001, **498**, 145–158.

50. D. N. D. Seely, D. Stempak, and S. Baruchel, *J. Pediatr. Hematol. Oncol.*, 2007, **29**, 32–47.

51. B. Olas and B. Wachowicz, *Postep. Hyg. Med. Dos.*, 1997, **51**, 95–108.

52. K. Seija and M. Talerczyk, *Gynecol. Oncol.*, 2004, **93**, 320–327.

53. Y. J. Hu, Y. Chen, Y. Q. Zhang, M. Z. Zhou, X. M. Song, B. Z. Zhang, L. Luo, P. M. Xu, Y. N. Zhao, Y. B. Zhao, and G. Cheng, *Biol. Trace Elem. Res.*, 1997, **56**, 331–341.

54. K. Altundag, Y. S. Silay, O. Altundag, O. G. Yigitbasi, O. Gundeslioglu, and M. Gunduz, *Med. Hypotheses*, 2005, **64**, 1162–1165.

55. V. Vaccaro, I. Sperduti, and M. Milella, *N. Engl. J. Med.*, 2011, **365**, 768–769.

56. J. L. Fischer, E. M. Mihelc, K. E. Pollok, and M. L. Smith, *Mol. Cancer Ther.*, 2007, **6**, 355–361.

57. W. D. Graf, O. E. Oleinik, T. A. Glauser, P. Maertens, D. N. Eder, and C. E. Pippenger, *Neuropediatrics*, 1998, **29**, 195–201.

58. C. S. Muniz, J. M. Marchante-Gayon, J. Ignacio-Garcia-Alonso, and A. Sanz-Medel, *J. Anal. At. Spectrom.*, 1998, **13**, 283–287.

59. S. Vouillamoz-Lorenz, J. Bauer, F. Lejeune, and L. A. Decosterd, *J. Pharm. Biomed. Anal.*, 2001, **25**, 465–475.

60. R. J. Motzer, E. Reed, F. Perera, D. Tang, H. Shamkhani, M. C. Poirier, W. Y. Tsai, R. J. Parker, and G. J. Bosl, *Cancer*, 1994, **73**, 465–475.

61. H. Vanhoe, J. Goossens, L. Moens, and R. Dams, *J. Anal. At. Spectrom.*, 1994, **9**, 177–185.

62. E. H. Larsen and S. Sturup, *J. Anal. At. Spectrom.*, 1994, **9**, 1099–1105.

63. J. J. Thompson and R. S. Houk, *Appl. Spectrosc.*, 1987, **41**, 801–806.

64. J. W. Ferguson and R. S. Houk, *Spectrochim. Acta Part B At. Spectrosc.*, 2006, **61**, 905–915.

65. S. Zimmermann, C. M. Menzel, Z. Berner, J.-D. Eckhardt, D. Stüben, F. Alt, J. Messerschmidt, H. Taraschewski, and B. Sures, *Anal. Chim. Acta*, 2001, **439**, 203–209.

66. K. E. Jarvis, G. A. L, and R. S. Houk, *Handbook of Inductively Coupled Plasma Mass Spectrometery*, Blackie, London, First., 1992.

67. J. S. Becker, M. Zoriy, J. S. Becker, J. Dobrowolska, and A. Matusch, *J. Anal. At. Spectrom.*, 2007, **22**, 736–744.

68. N. Jakubowski, T. Prohaska, F. Vanhaecke, P. H. Roos, T. Lindemann, and L. Rottmann, *J. Anal. At. Spectrom.*, 2011, **26**, 693–726.

69. N. Jakubowski, T. Prohaska, F. Vanhaecke, P. H. Roos, and T. Lindemann, *J. Anal. At. Spectrom.*, 2011, **26**, 727–757.

70. Z. Yang, X. Hou, and B. T. Jones, *Appl. Spectrosc. Rev.*, 2002, **37**, 57–88.

71. E. E. M. Brouwers, M. M. Tibben, D. Pluim, H. Rosing, H. Boot, A. Cats, J. H. M. Schellens, and J. H. Beijnen, *Anal. Bioanal. Chem.*, 2008, **391**, 577–585.

72. M. Guillong, I. Horn, and D. Gunther, *J. Anal. At. Spectrom.*, 2003, **18**, 1224–1230.

73. D. J. Douglas and J. B. French, *J. Anal. At. Spectrom.*, 1988, **3**, 742–747.

74. Thermo-Finnigan, *Element 2XR Hardware Manual*, 2005.

75. R. Thomas, *Spectroscopy*, 2002, **17**, 24–31.

76. S. J. Hill, *Inductively Coupled Plasma Spectrometry and its Applications*, Blackwell Publishing, 2nd edn., 2007.

77. Thermo-Finnigan, *Finnigan LTQ Hardware Manual*, 2003.

78. J. B. Fenn, M. Mann, C. K. Meng, S. F. Wong, and C. M. Whitehouse, *Science (80-.).*, 1989, **246**, 64–71.

79. J. B. Fenn, *J. Biomol. Tech.*, 2006, **13**, 101–118.

80. P. Kebarle and M. Peschke, *Anal. Chim. Acta*, 2000, **406**, 11–35.

81. A. Gomez and K. Tang, *Phys. Fluids*, 1994, **6**, 404–414.

82. T. C. Rohner, N. Lion, and H. H. Girault, *Phys. Chem. Chem. Phys*, 2004, **6**, 3056–3068.

83. D. Wang and S. J. S. J. Lippard, *Nat. Rev. Drug Discov. 4*, 2005, **4**, 307–320.

84. A. Ghezzi, M. Aceto, C. Cassino, E. Gabano, and D. Osella, *J. Inorg. Biochem.*, 2004, **98**, 73–78.

85. L. E. Ta, L. Espeset, J. Podratz, and A. J. Windebank, *Neurotoxicology*, 2006, **27**, 992–1002.

86. J. H. Schellens, J. Ma, A. S. Planting, M. E. van der Burg, E. van Meerten, M. de Boer-Dennert, P. I. Schmitz, G. Stoter, and J. Verweij, *Br. J. Cancer*, 1996, **73**, 1569–1575.

87. E. S. McDonald, K. R. Randon, A. Knight, and A. J. Windebank, *Neurobiol. Dis.*, 2005, **18**, 305–313.

88. F. A. Blommaert, B. G. Floot, H. C. van Dijk-Knijnenburg, F. Berends, R. A. Baan, J. H. Schornagel, L. den Engelse, and A. M. Fichtinger-Schepman, *Chem. Biol. Interact.*, 1998, **108**, 209–225.

89. J. T. Lam, A. Kanerva, G. J. Bauerschmitz, K. Takayama, K. Suzuki, M. Yamamoto, S. M. Bhoola, B. Liu, M. Wang, M. N. Barnes, R. D. Alvarez, G. P. Siegal, D. T. Curiel, and A. Hemminki, *J. Gene Med.*, 2004, **6**, 1333–1342.

90. W. P. Petros, G. Broadwater, D. Berry, R. B. Jones, J. J. Vredenburgh, C. J. Gilbert, J. P. Gibbs, O. M. Colvin, and W. P. Peters, *Clin. Cancer Res.*, 2002, **8**, 698–705.

91. P. Bin, A. V. Boddy, M. W. English, A. D. Pearson, L. Price, M. J. Tilby, and D. R. Newell, *Anticancer Res.*, 1994, **14**, 2279–2283.

92. G. J. Veal, J. Errington, M. J. Tilby, a D. J. Pearson, a B. M. Foot, H. McDowell, C. Ellershaw, B. Pizer, G. M. Nowell, D. G. Pearson, and a V Boddy, *Br. J. Cancer*, 2007, **96**, 725–731.

93. R. J. Parker, I. Gill, R. Tarone, J. a Vionnet, S. Grunberg, F. M. Muggia, and E. Reed, *Carcinogenesis*, 1991, **12**, 1253–1258.

94. E. Reed, R. J. Parker, I. Gill, A. Bicher, M. Dabholkm, J. A. Vionnet, F. Bostick-bruton, R. Tarone, and F. M. Muggia, *Cancer Res.*, 1993, **53**, 3694–3699.

95. G. J. Veal, C. Dias, L. Price, A. Parry, J. Errington, J. Hale, A. D. J. Pearson, A. V Boddy, D. R. Newell, and M. J. Tilby, *Clin. Cancer Res.*, 2001, **7**, 2205–2212.

96. E. Reed, R. F. Ozols, R. Tarone, S. H. Yuspa, and M. C. Poirier, *Proc. Natl. Acad. Sci. U. S. A.*, 1987, **84**, 5024–5028.

97. A. C. Pieck, A. Drescher, K. G. Wiesmann, J. Messerschmidt, G. Weber, D. Strumberg, R. A. Hilger, M. E. Scheulen, and U. Jaehde, *Br. J. Cancer*, 2008, **98**, 1959–1965.

98. J. Will, D. A. Wolters, and W. S. Sheldrick, *ChemMedChem*, 2008, **3**, 1696–1707.

99. R. C. Deconti, B. R. Toftness, R. C. Lange, and W. A. Creasey, *Cancer Res.*, 1973, **33**, 1310–1315.

100. G. Weber, J. Messerschmidt, a C. Pieck, a M. Junker, A. Wehmeier, and U. Jaehde, *Anal. Bioanal. Chem.*, 2004, **380**, 54–58.

101. J. Liu, E. Kraut, J. Bender, R. Brooks, S. Balcerzak, M. Grever, H. Stanley, S. D'Ambrosio, R. Gibson-D'Ambrosio, and K. K. Chan, *Cancer Chemother. Pharmacol.*, 2002, **49**, 367–374.

102. D. García Sar, M. Montes-Bayón, L. Aguado Ortiz, E. Blanco-González, L. M. Sierra, and A. Sanz-Medel, *Anal. Bioanal. Chem.*, 2008, **390**, 37–44.

103. G. M. Almeida, T. L. Duarte, P. B. Farmer, W. P. Steward, and G. D. D. Jones, *Int. J. Cancer*, 2008, **122**, 1810–1819.

104. P. L. Olive and J. P. Banáth, *Nat. Protoc.*, 2006, **1**, 23–29.

105. G. M. Almeida, T. L. Duarte, W. P. Steward, and G. D. D. Jones, *DNA Repair (Amst).*, 2006, **5**, 219–225.

106. I. W. H. Jarvis, *PhD Thesis*, 2011, Newcastle University.

107. D. G. Sar, M. Montes-Bayón, E. Blanco-González, and A. Sanz-Medel, *TrAC Trends Anal. Chem.*, 2010, **29**, 1390–1398.

108. R. Clough, L. R. Drennan-Harris, C. F. Harrington, S. J. Hill, and J. F. Tyson, *J. Anal. At. Spectrom.*, 2012, **27**, 1185–1224.

109. P. Winship, *PhD Thesis*, 2006, Department of Chemistry, Loughborough University.

110. S. L. Kerr, *PhD Thesis*, 2008, Department of Chemistry, Loughborough University.

111. A. Zayed, *PhD Thesis*, 2012, Department of Chemistry, Loughborough University.

112. R. G. Schipper, E. Silletti, and M. H. Vingerhoeds, *Arch. Oral Biol.*, 2007, **52**, 1114–1135.

113. N. Spielmann and D. T. Wong, *Oral Dis.*, 2011, **17**, 345–354.

114. P. Gassó, M. Pagerols, I. Flamarique, J. Castro-Fornieles, N. Rodriguez, S. Mas, S. Curran, K. Aitchison, P. Santosh, and A. Lafuente, *Am. J. Hum. Biol.*, 2014, **26**, 859–862.

115. A. P. Athanasoulia, C. Sievers, M. Ising, A. C. Brockhaus, A. Yassouridis, G. K. Stalla, and M. Uhr, *Eur. J. Endocrinol.*, 2012, **167**, 327–335.

116. S. Söderqvist, H. Matsson, M. Peyrard-janvid, and J. Kere, *J. Cogn. Neurosci.*, 2012, **26**, 54–62.

117. E. E. Davis, J. H. Savage, J. R. Willer, Y.-H. Jiang, M. Angrist, A. Androutsopoulos, and N. Katsanis, *Clin. Genet.*, 2014, **85**, 359–364.

118. R. M. Iwasiow, A. Desbois, and H. C. Birnboim, *Oragene*, 2011, 1–2.

119. DNA GenotechInc, *http://www.dnagenotek.com/ROW/pdf/PD-PR-015.pdf (Accessed:16/04/2014)*, 2012.

120. K. Yamada, N. Kato, A. Takagi, M. Koi, and H. Hemmi, *Anal. Bioanal. Chem.*, 2005, **382**, 1702–1707.

121. C. Thiede, G. Prange-Krex, J. Freiberg-Richter, M. Bornhauser, and G. Ehninger, *Bone Marrow Transplant.*, 2000, **25**, 575–577.

122. G. W. Burnett and H. W. Scherp, *Oral Microbiology and Infectious Disease*, Williams & Wilkins Co, Baltimore, 1962.

123. F. A. Blommaert, C. Michael, and P. M. A. B. Terheggen, *Cancer Res.*, 1993, **53**, 5669–5675.

124. E. S. Kim, J. J. Lee, G. He, C.-W. Chow, J. Fujimoto, N. Kalhor, S. G. Swisher, I. I. Wistuba, D. J. Stewart, and Z. H. Siddik, *J. Clin. Oncol.*, 2012, **30**, 3345–3352.

125. P. J. van de Vaart, J. Belderbos, D. de Jong, K. C. Sneeuw, D. Majoor, H. Bartelink, and a C. Begg, *Int. J. Cancer*, 2000, **89**, 160–166.

126. A. Bonetti, P. Apostoli, M. Zaninelli, F. Pavanel, M. Colombatti, G. L. Cetto, T. Franceschi, L. Sperotto, and R. Leone, *Clin. Cancer Res.*, 1996, **2**, 1829–1835.

127. E. Reed, Y. Ostchega, S. M. Steinberg, S. H. Yuspa, R. C. Young, R. F. Ozols, and M. C. Poirier, *Cancer Res.*, 1990, **50**, 2256–2260.

128. D. Maxwell Parkin, F. Bray, J. Ferlay, and P. Pisani, *Int. J. Cancer*, 2001, 153–156.

129. L. P. Rivory, *Aust. Prescr.*, 2002, **25**, 108–110.

130. D. Simpson, C. Dunn, M. Curran, and K. L. Goa, *ADIS Drug Eval.*, 2003, **63**, 2127–2156.

131. D. Hagrman, J. Goodisman, and A. Souid, *J. Pharmacol. Exp. Ther.*, 2004, **308**, 658–666.

132. E. Jerremalm, I. Wallin, J. Yachnin, and H. Ehrsson, *Eur. J. Pharm. Sci.*, 2006, **28**, 278–283.

133. A. Broomand, E. Jerremalm, J. Yachnin, H. Ehrsson, and F. Elinder, *J. Negat. Results Biomed.*, 2009, **8**, 2–9.

134. T. Shoeib and B. L. Sharp, *Metallomics*, 2012, **4**, 1308–1320.

135. E. M. Moustafa, C. L. Camp, A. S. Youssef, A. Amleh, H. J. Reid, B. L. Sharp, and T. Shoeib, *Metallomics*, 2013, **5**, 1537–1546.

136. C. L. Camp, *PhD Thesis*, 2014, Department of Chemistry, Loughborough University.

137. D. M. Mallawaaratchy, S. Mactier, K. L. Kaufman, K. Blomfield, and R. I. Christopherson, *J. Proteomics*, 2012, **75**, 1590–1599.

138. Z. El Fajoui, F. Toscano, G. Jacquemin, J. Abello, J.-Y. Scoazec, O. Micheau, and J.-C. Saurin, *Gastroenterology*, 2011, **141**, 663–673.

139. B. Michalke, *J. Trace Elem. Med. Biol.*, 2010, **24**, 69–77.

140. C. R. Jimenez, J. C. Knol, G. A. Meijer, and R. J. A. Fijneman, *J. Proteomics*, 2010, **73**, 1873–1895.

141. C. Leroy, C. Fialin, A. Sirvent, V. Simon, S. Urbach, J. Poncet, B. Robert, P. Jouin, and S. Roche, *Cancer Res.*, 2009, **69**, 2279–2286.

142. P. Heffeter, M. A. Jakupec, W. Körner, P. Chiba, C. Pirker, and R. Dornetshuber, *Biochem. Pharmacol.*, 2007, **73**, 1873–1886.

143. S. S. de Oliveira, I. M. de Oliveira, W. De Souza, and J. A. Morgado-Díaz, *FEBS Lett.*, 2005, **579**, 6179–6185.

144. J. Kim, S. Park, N. Y. Tretyakova, and C. R. Wagner, *Mol. Pharm.*, 2005, **2**, 233–241.

145. F. Nicholas, *Medicinal Inorganic Chemistry*, American Chemical Society, 2005.

146. J. Kim, H. Crooks, T. Dracheva, T. G. Nishanian, B. Singh, J. Jen, and T. Waldman, *Cancer Res.*, 2002, **62**, 2744–2748.

147. D. Lebwohl and R. Canetta, *Eur. J. Cancer*, 1998, **34**, 1522–1534.

148. K. Rikova, A. Guo, Q. Zeng, A. Possemato, J. Yu, H. Haack, J. Nardone, K. Lee, C. Reeves, Y. Li, Y. Hu, Z. Tan, M. Stokes, L. Sullivan, J. Mitchell, R. Wetzel, J. Macneill, J. M. Ren, J. Yuan, C. E. Bakalarski, J. Villen, J. M. Kornhauser, B. Smith, D. Li, X. Zhou, S. P. Gygi, T.-L. Gu, R. D. Polakiewicz, J. Rush, and M. J. Comb, *Cell*, 2007, **131**, 1190–1203.

149. A. Sreekumar, M. K. Nyati, S. Varambally, T. R. Barrette, D. Ghosh, T. S. Lawrence, and A. M. Chinnaiyan, *Cancer Res.*, 2001, **61**, 7585–7593.

150. Y. Kuramitsu and K. Nakamura, *Proteomics*, 2006, **6**, 5650–5661.

151. J. Kim, S. R. Tannenbaum, and F. M. White, *J. Proteome Res.*, 2005, **4**, 1339–1346.

152. S. Hector and J. H. M. Prehn, *Biochim. Biophys. Acta*, 2009, **1795**, 117–129.

153. G. S. Gorman, J. P. Speir, C. A. Turner, and I. J. Amster, *J. Am. Chem. Soc.*, 1992, **114**, 3986–3988.

154. T. Falta, P. Heffeter, A. Mohamed, W. Berger, S. Hann, and G. Koellensperger, *J. Anal. At. Spectrom.*, 2011, **26**, 109–115.

155. G. Hermann, P. Heffeter, T. Falta, W. Berger, S. Hann, and G. Koellensperger, *Metallomics*, 2013, **5**, 636–647.

156. C. Lee, W. Yang, and R. G. Parr, *Phys. Rev. B Condens. Matter Mater. Phys.*, 1988, **37**, 785–789.

157. A. D. Becke, *Phys. Rev. A*, 1988, **38**, 3098–3100.

158. A. D. Becke, *J. Chem. Phys.*, 1993, **98**, 5648–5652.

159. American Cancer Society, *http://www.cancer.org/cancer/cancerbasics/cancer-prevalence (Accessed: 17/02/2014)*.

160. R. Abdulah, K. Miyazaki, M. Nakazawa, and H. Koyama, *J. Trace Elem. Med. Biol.*, 2005, **19**, 141–50.

161. H. Goenaga-Infante, *Personal Communication*, 2009.

162. M. P. Rayman, *Proc. Nutr. Soc.*, 2007, **64**, 527–542.

163. R. Brigelius-Flohé, *Chem. Biodivers.*, 2008, **5**, 389–395.

164. S. E. Taylor, *MChem Report*, 2010, Loughborough University.

165. C. Cooper, *MChem Report*, 2013, Loughborough University.

166. C. Bokemeyer, I. Bondarenko, A. Makhson, J. T. Hartmann, J. Aparicio, F. de Braud, S. Donea, H. Ludwig, G. Schuch, C. Stroh, A. H. Loos, A. Zubel, and P. Koralewski, *J. Clin. Oncol.*, 2009, **27**, 663–671.

167. D. L. Hatfield and M. J. Berry, *Selenium: Its molecular biology and role in human health*, Springer, New York, 3rd edn., 2012.

168. Qiagen, *QIAGEN Genomic DNA Handbook*, 2012.

169. Calbiochem and Merck, *ProteoExtract® Subcellular Proteome Extraction Kit*, 2007.

170. A. T. Townsend, *Fresenius. J. Anal. Chem.*, 1999, **364**, 521–526.

171. C. E. Sieniawska, R. Mensikov, H. T. Delves, and R. Meniskov, *J. Anal. At. Spectrom.*, 1999, **14**, 109–112.

172. M. S. A. Horstwood, G. L. Foster, R. R. Parrish, S. R. Noble, and G. M. Nowell, *J. Anal. At. Spectrom.*, 2003, **18**, 837–846.

173. M. P. Molloy, E. E. Brzezinski, J. Hang, M. T. McDowell, and R. A. Van Bogelen, *Proteomics*, 2003, **3**, 1912–1919.

174. Y. Kasherman, S. Sturup, and D. Gibson, *J. Med. Chem.*, 2009, **52**, 4319–4328.

175. C. Chen, P. Zhang, X. Hou, and Z. Chai, *Biochim. Biophys. Acta*, 1999, **1427**, 205–215.

176. M. P. Rayman, *Lancet*, 2000, **356**, 233–241.

177. D. Wang and S. Bodovitz, *Trends Biotechnol.*, 2010, **28**, 281–290.

178. A. J. Managh, S. L. Edwards, A. Bushell, K. J. Wood, E. K. Geissler, J. A. Hutchinson, R. W. Hutchinson, H. J. Reid, and B. L. Sharp, *Anal. Chem.*, 2013, **85**, 10627–10634.

179. B. Shrestha and A. Vertes, *Anal. Chem.*, 2009, **81**, 8265–8271.

180. A. J. Managh, *Personal Communication*, 2014.

181. D. Drescher, C. Giesen, H. Traub, U. Panne, J. Kneipp, and N. Jakubowski, *Anal. Chem.*, 2012, **84**, 9684–9688.

182. C. Giesen, L. Waentig, T. Mairinger, D. Drescher, J. Kneipp, P. H. Roos, U. Panne, and N. Jakubowski, *J. Anal. At. Spectrom.*, 2011, **26**, 2160–2165.

183. R. C. Todd and S. J. Lippard, *Metallomics*, 2009, **1**, 280–291.

184. D. Esteban-Fernández, E. E. Moreno-gordaliza, B. Cañas, M. A. Palacios, M. M. Gómez-Gómez, B. Can, and D. Esteban-ferna, *Metallomics*, 2010, **2**, 19–38.

185. S. Arnould, I. Hennebelle, P. Canal, R. Bugat, and S. Guichard, *Eur. J. Cancer*, 2003, **39**, 112–119.

186. M. A. Graham, G. F. Lockwood, D. Greenslade, S. Brienza, M. Bayssas, and E. Gamelin, *Clin. Cancer Res.*, 2000, **6**, 1205–1218.

187. V. Brabec and J. Kasparkova, *Drug Resist. Updat.*, 2002, **5**, 147–161.

188. S. Akiyama, Z. S. Chen, T. Sumizawa, and T. Furukawa, *Anticancer. Drug Des.*, 1999, **14**, 143–151.

189. Q. Liu, H. Wei, J. Lin, L. Zhu, and Z. Guo, *J. Inorg. Biochem.*, 2004, **98**, 702–712.

190. K. Bracht, R. Boubakaria, R. Grünert, and P. J. A. Bednarski, *Anticancer. Drugs*, 2006, **17**, 41–51.

191. T. Ishikawas and F. Ali-Osman, *J. Biol. Chem.*, 1993, **268**, 20116–20125.

192. P. Mistry, L. R. Kelland, G. Abel, S. Sidhar, and K. R. Harrap, *Br. J. Cancer*, 1991, **64**, 215–220.

193. A. K. Godwin, A. Meister, P. J. O'Dwyer, C. S. Huang, T. C. Hamilton, and M. E. Anderson, *Proc. Natl. Acad. Sci. U. S. A.*, 1992, **89**, 3070–3074.

194. Y. Chen, P. Jungsuwadee, M. Vore, D. A. Butterfield, and D. K. St Clair, *Mol. Interv.*, 2007, **7**, 147–156.

195. G. L. Nicolson and R. Settineri, *Funct. Foods Heal. Dis.*, 2011, **4**, 135–160.

196. H. Goenaga Infante, G. O'Connor, M. Rayman, R. Hearn, and K. Cook, *J. Anal. At. Spectrom.*, 2006, **21**, 1256–1263.

197. H. Goenaga Infante, G. O'Connor, M. Rayman, R. Wahlen, J. Entwisle, P. Norris, R. Hearn, and T. Catterick, *J. Anal. At. Spectrom.*, 2004, **19**, 1529–1538.

7. Publications

Published papers

S. E. Taylor, J. P. Wood, G. D. D. Jones, A. L. Thomas, H. J. Reid and B. L. Sharp, A feasibility study of the use of saliva as an alternative to leukocytes as a source of DNA for the study of Pt-DNA adducts in cancer patients receiving platinum-based chemotherapy, *Anal. Bioanal. Chem*., 406 (2014), 8033-8036

A. Zayed, T. Shoeib, S. E. Taylor, G. D. D. Jones, A. L. Thomas, J. P. Wood, H. J. Reid and B. L. Sharp, Determination of Pt–DNA adducts and the sub-cellular distribution of Pt in human cancer cell lines and the leukocytes of cancer patients, following mono- or combination treatments, by inductively-coupled plasma mass spectrometry, *Int. J. Mass Spectrom.*, 307 (2011), 70-78.

A. Zayed, G. D. D. Jones, H. J. Reid, T. Shoeib, S. E. Taylor, A. L. Thomas, J. P. Wood, and B. L. Sharp, Speciation of Oxaliplatin adducts with DNA Nucleotides, *Metallomics,* 3 (2011), 991-1000.

Publications in preparation

S. E. Taylor, C. Camp, T. Shoeib, J. Pugh, H. J. Reid and B. L. Sharp, Interaction of oxaliplatin with cytosolic proteins.

S. E. Taylor, J. Pugh, K. Bowman, J.P. Wood, G. D. D. Jones, H. J. Reid, B. L. Sharp, The effect of selenium supplementation of the cellular uptake of oxaliplatin.

Conference proceedings

The work presented in this thesis has also been presented at the conferences listed below in poster format:

- Health and Life Sciences Conference, Loughborough University, 14/03/2011
- School of Science conference, Science Matters 2012, Loughborough University, 21/03/2012
- Department of Chemistry Network Meeting, Loughborough University, 25/04/2012
- 11th East Midlands Proteomics Workshop, 28/11/2012
- Metallomics 2013, Oviedo, Spain, 08/07/2013-11/07/2013

8. Appendices

Appendix A – Chapter 2 supplementary information

Table 29 - Patient saliva sample condition details

Patient ID	Saliva		
	Pre	1 hour post	24 hours post
033	IC	✓	✓
035	✓	✓	✓
034	✓	✓	✓
036	✓	IC	IC
037	✓	X	X
038	IC	✓	✓
039	✓	✓	✓
040	✓	✓	X
041	IC	X	X
044	IC	✓	X
045	✓*	✓	✓
042	✓	✓	IC
043	IC	✓	IC
047	✓	✓	IC
046	✓	✓	X
048	✓	✓	✓
049	✓	✓	✓
050	✓	✓	✓
051	✓	✓	✓
052	IC	✓	✓
053	✓	✓	✓
054	✓	✓	✓
055	✓	✓	✓

Note: Patient 045 – Pre sample not taken till end of treatment due. 1 hour sample was done 1 hour following this.

Key

IC	Incomplete sample (too little given)
✓	Sample given, correct volume
X	Missing sample
	Complete set of 3 saliva samples
	Pre and 1 hour set complete

Table 30 - Clinical study patient details

Patient ID	Chemotherapy regime	Cycle Number	Diagnosis	Age	Sex	Best response	Grade 3/4 Toxicities	Cycles received (intended)	Dose reduction of platinum (cycle number)	PFS (days)	OS (days)	Additional comments
33	EOX	2	SCC Oesophagus	71	F	PR	Lethargy cycle 1	6 (6-8)	75% 2 50% 3 onwards	474	822 (still alive)	
34	EOX	4	Adeno ca oesophagus	67	M	PR		6 (6-8)	75 % 3 onwards	161	333	
35	FOLFOX and Bev	10	CRC	65	M	PR	Diarrhoea cycle 1	12 (12)	75% 2 onwards	398	848	
36	ECF	5	Gastric	70	F	PR		8 (6-8)	50% cycle 1 onwards (poor baseline renal function)	273	279	
37	FOLFOX	4	CRC	29	F	NA	Thrombocytopenia cycle 7	8 (12)	80% cycle 8 onwards	629	836 (still alive)	Adjuvant - post surgical resection of mets
38	FOLFOX and Bev	11	CRC	64	M	PR	Neutropenia cycle2	12 (12)	75% cycle 3 onwards 50% cycle 10 onwards	472	941 (still alive)	Neo-adjuvant
39	FOLFOX and Bev	8	CRC	64	M	PR	Neuropathy cycle 3	12 (12)	70% cycle 4 onwards 0% cycle 10 onwards	433	874 (still alive)	
40	FOLFOX	3	Small bowel adeno	67	F	NA	Diarrhoea and fatigue cycle 5	6 (12)	80% cycle 6 onwards	277	463	
41	EOX	1	Gastric	69	M	PR		8 (6-8)		354	375	
42	FOLFOX and Bev	2	CRC	71	F	SD		12 (12)		291	297	
43	XELOX	11	CRC	46	F	PR	Diarrhoea cycle 2	9 (12)	80% cycle 3 onwards 70% cycle 5 onwards	735 (not progressed yet)	735 (still alive)	
44	EOX	1	Gastric	78	M	PR	Neutropaenia and neuropathy cycle 1	6 (6-8)	80% cycle 2 onwards	389	419	
45	EOX	1	Gastric	62	M	CR		6 (6-8)		238	277	
46	ECX	3	GOJ	64	M	PR		3 (6-8)		308	609	

47	FOLFOX	3	CRC	58	F	NA		6 (12)		369	481 (still alive)	Adjuvant
48	FOLFOX	2	CRC	65	F	NA	Neutropaenia and neuropathy cycle 2	8 (12)	75% cycle 3 onwards	144	261	Adjuvant
49	FOLFOX and Bev	7	CRC	47	F	PR	Neuropathy cycle 3	12 (12)	80% cycle 4 onwards 75% cycle 8 onwards Stopped cycle 12	433	651 (still alive)	Neo-adj
50	FOLFOX	2	CRC	56	M	SD	Neuropathy cycle 1	8 (12)	75% cycle 2 onwards 50% cycle 7 onwards 0% cycle 8	102	171	Neo Adj
51	FOLFOX and Bev	11	CRC	60	F	PR		12 (12)		398	665 (still alive)	
52	FOLFOX	5	CRC	62	M	NA		9 (12)		504 (no PD yet)	504 (still alive)	Adjuvant
53	ECX	2	GOJ	67	M	PR		3 (3)		307	445	Neo- Adj
54	Cis / etop	3	Small cell oesophagus	53	M	PR	Deterioration in hearing cycle 3	4 (6)	85% cycle 4	350	483 (still alive)	
55	EOX	2	Gastric	72	M	PR	Fatigue, diarrhoea, neutropenia, vomiting, neuropathy cycle 1	7 (6-8)	75% cycle 2 onwards 50% cycle 4 onwards	490 (no PD yet)	490 (still alive)	

Table Key and Notes

SCC = Squamous cell carcinoma
CRC= colorectal cancer
GOJ = gastric oesophageal junction adeno ca
PR= partial response
SD= stable disease
PD = progressive disease
NA = Not assessable Or not assessed
CR = Complete radiological response
Adeno ca. SCCs and GOJ could all be lumped as Upper GI
Dose reduction = % of full dose given – if 100% implies they tolerated it well. The earlier on in the cycle number they had a reduction the more prone they were to toxicities

Blood calibration graphs

Table 31 - Patient blood batch details

Batch Number	Patient ID numbers
1	36, 37, 38, 40
2	41, 44, 45, 42
3	43, 46, 47, 52
4	35, 34, 39, 48, 49
5	50, 51, 53, 54

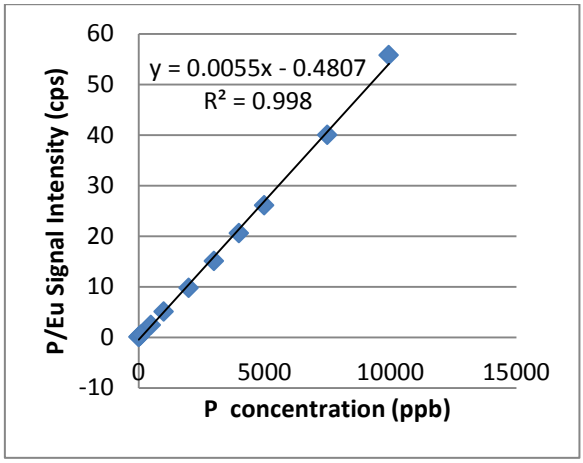

Figure 73 - Blood batch 1 - P calibration graph

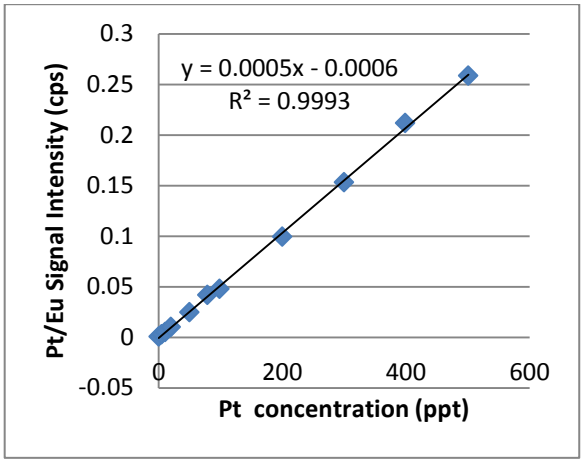

Figure 74 - Blood batch 1 - Pt calibration graph

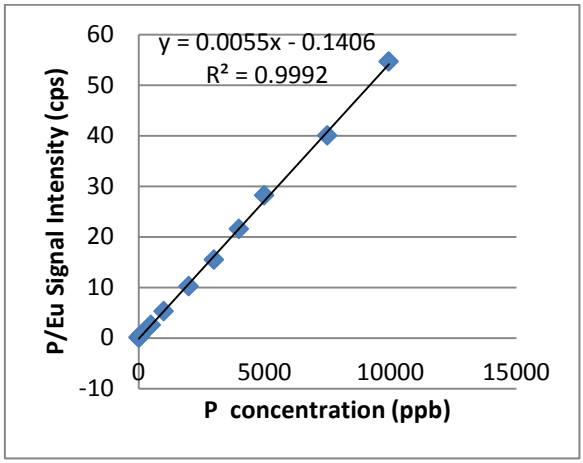

Figure 75 - Blood batch 2 - P calibration graph

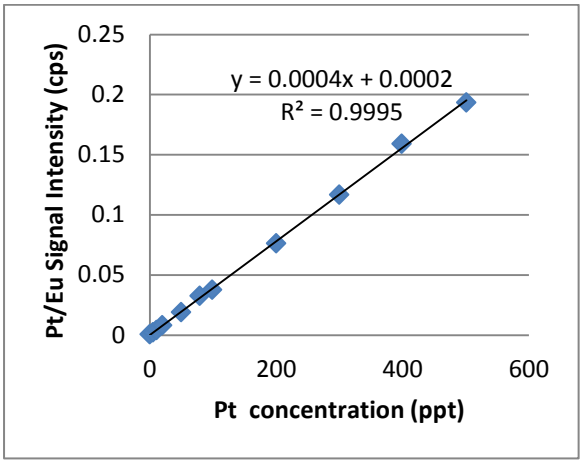

Figure 76 - Blood batch 2 - Pt calibration graph

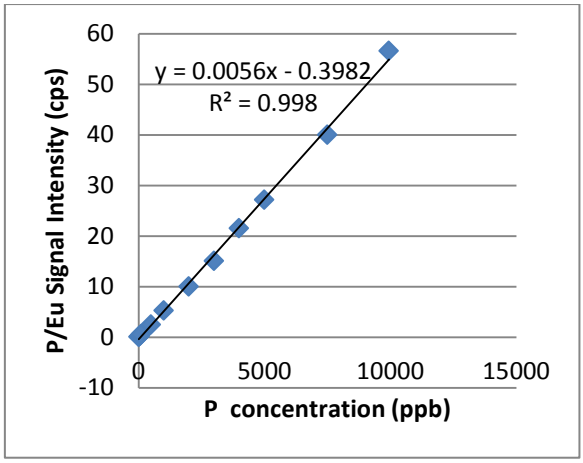

Figure 77 - Blood batch 3 - P calibration graph

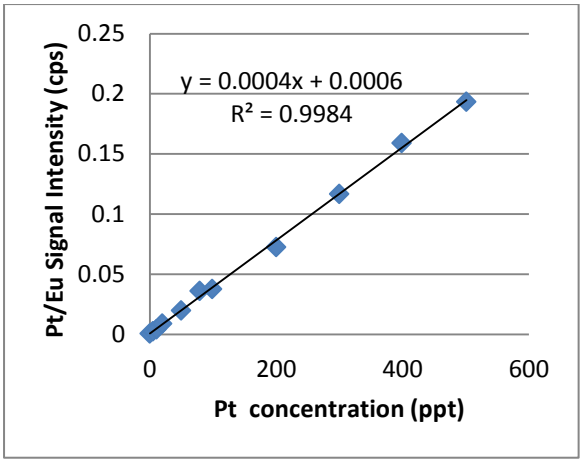

Figure 78 - Blood batch 3 - Pt calibration graph

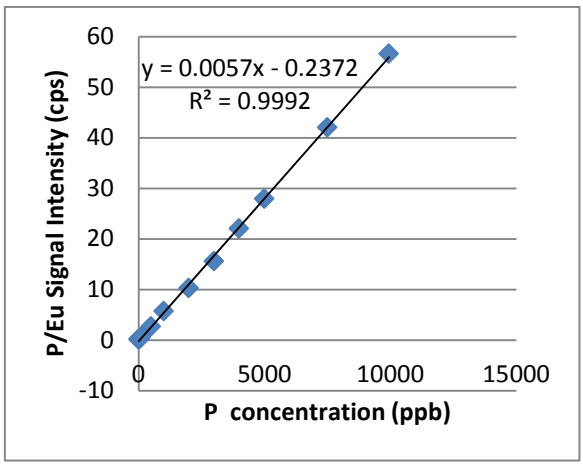

Figure 79 - Blood batch 4 - P calibration graph

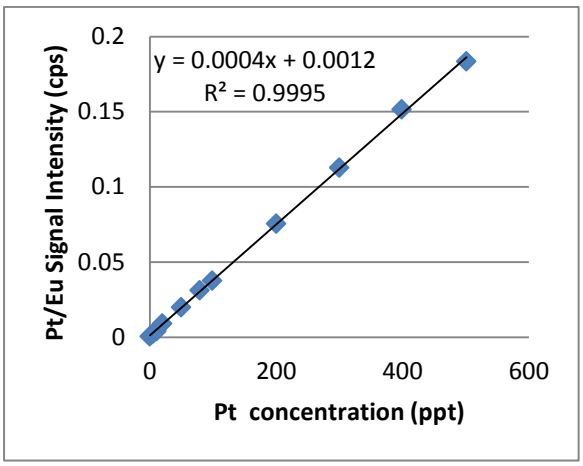

Figure 80 - Blood batch 4 - Pt calibration graph

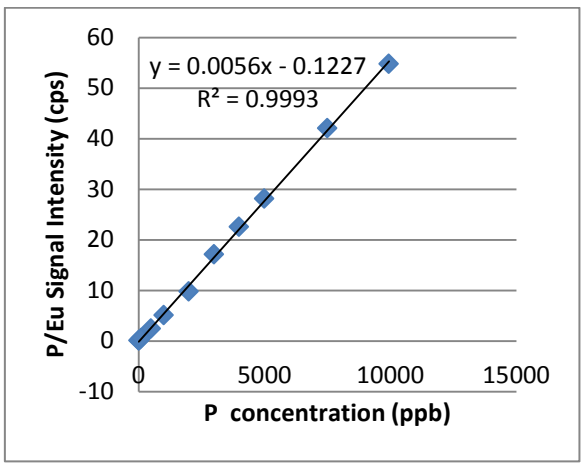

Figure 81 - Blood batch 5 - P calibration graph

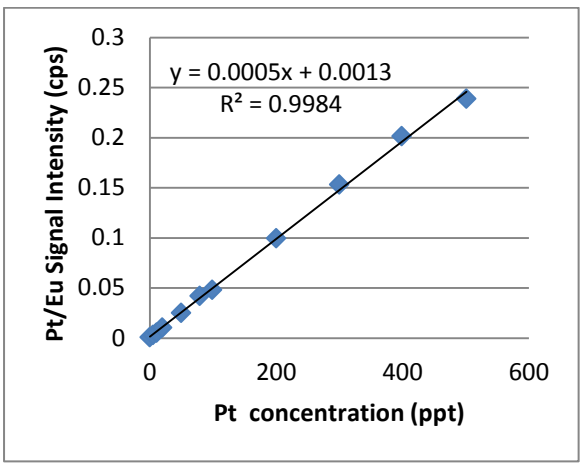

Figure 82 - Blood batch 5 - Pt calibration graph

Saliva calibration graphs

Table 32 - Patient saliva batch details

Batch Number	Patient ID numbers
1	36, 37, 38, 40, 41, 44, 45
2	42, 43, 46, 47, 52
3	35, 34, 39, 48, 49
4	50, 51, 53, 54

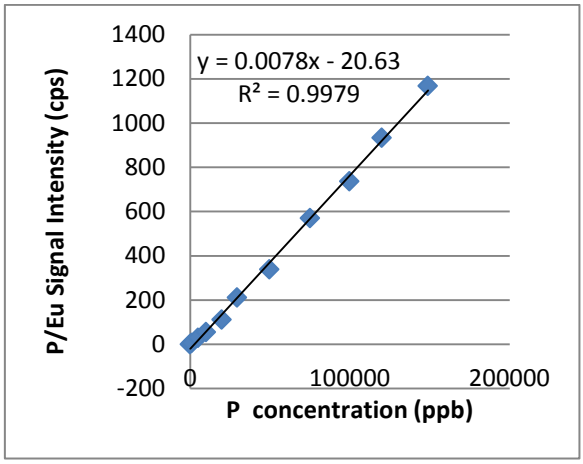

Figure 83 - Saliva Batch 1 - P calibration graph

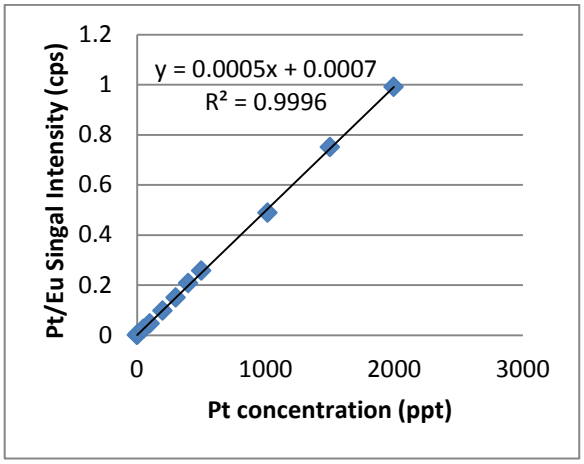

Figure 84 - Saliva Batch 1 - Pt calibration graph

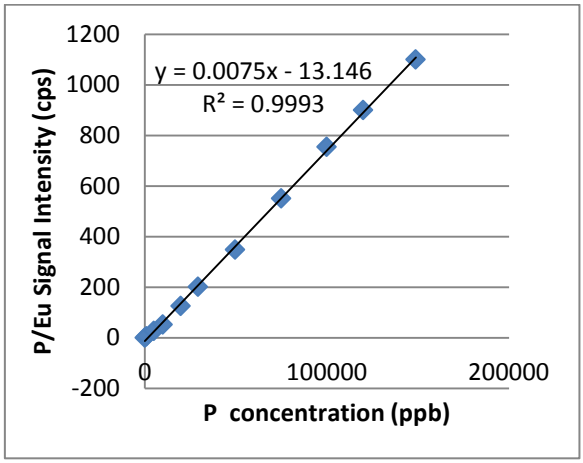

Figure 85 - Saliva Batch 2 - P calibration graph

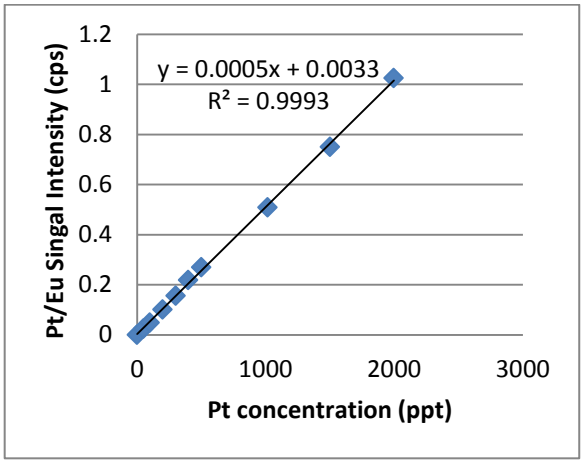

Figure 86 - Saliva Batch 2 - Pt calibration graph

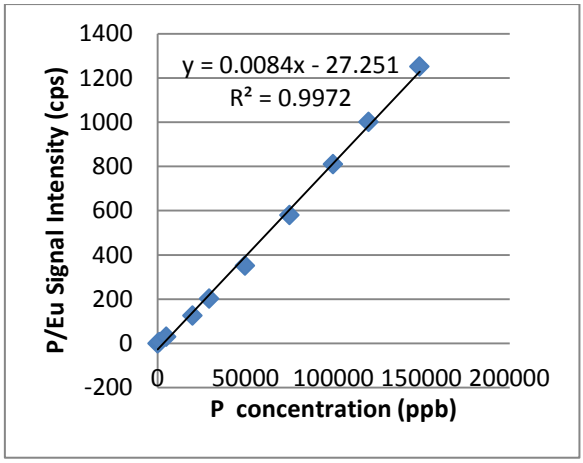

Figure 87 - Saliva Batch 3 - P calibration graph

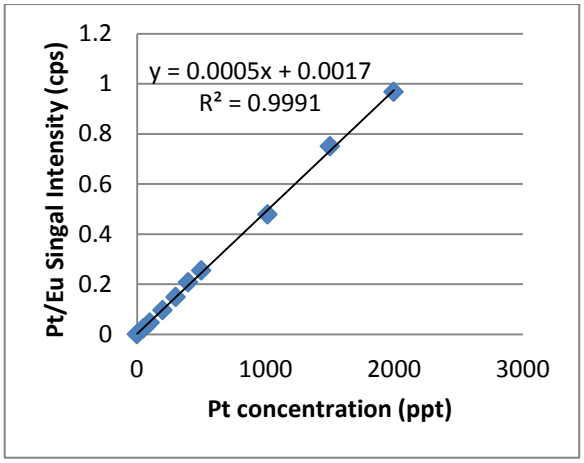

Figure 88 - Saliva Batch 3 - Pt calibration graph

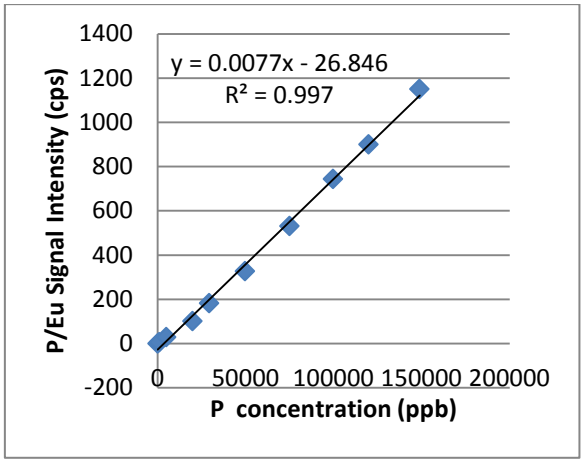

Figure 89 - Saliva batch 4 - P calibration graph

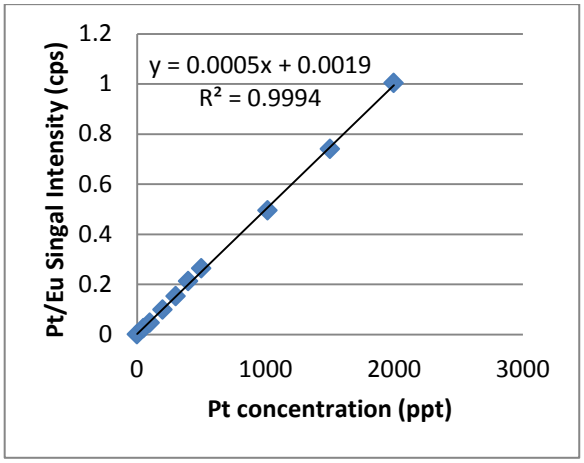

Figure 90 - Saliva batch 4 - Pt calibration graph

Table 33 - Blood Pt-DNA adduct replicates

Patient ID	Time point	Replicate Number	P conc (ppb)	Pt conc (ppb)	Number of adducts per 10^6 nucleotides	Average adducts (per 10^6 nucleotides)
35	Pre	1	3306	0.009	0.417	0.424
		2	3764	0.010	0.407	
		3	3549	0.010	0.447	
	1 hour	1	3458	0.081	3.695	3.840
		2	3840	0.095	3.931	
		3	3082	0.076	3.894	
34	Pre	1	3972	0.005	0.197	0.205
		2	4188	0.006	0.212	
		3	3643	0.005	0.208	
	1 hour	1	3485	0.113	5.128	4.098
		2	3451	0.080	3.681	
		3	4196	0.092	3.485	
	24 hour	1	3660	0.109	4.744	5.098
		2	3378	0.114	5.357	
		3	3438	0.113	5.195	
39	Pre	1	3326	0.012	0.561	0.562
		2	4098	0.015	0.581	
		3	3201	0.011	0.543	
	1 hour	1	3620	0.072	3.157	3.349
		2	3988	0.088	3.500	
		3	4145	0.089	3.390	
48	Pre	1	3644	0.008	0.328	0.376
		2	3515	0.009	0.399	
		3	3510	0.009	0.402	
	1 hour	1	3953	0.131	5.267	5.317
		2	3445	0.116	5.348	
		3	3251	0.109	5.337	
49	Pre	1	3897	0.016	0.632	0.651
		2	3486	0.015	0.684	
		3	3782	0.015	0.638	
	1 hour	1	3050	0.144	7.494	7.107
		2	3306	0.145	6.963	
		3	3702	0.160	6.863	
50	Pre	1	3536	0.002	0.100	0.134
		2	3641	0.004	0.164	
		3	3142	0.003	0.139	
	1 hour	1	3366	0.093	4.376	4.534
		2	3610	0.101	4.429	
		3	3153	0.095	4.798	
51	Pre	1	4193	0.007	0.263	0.275
		2	3193	0.006	0.293	
		3	3487	0.006	0.269	
	1 hour	1	4138	0.086	3.304	3.355
		2	3212	0.065	3.200	

		3	4024	0.090	3.560	
53	Pre	1	3845	0.011	0.444	0.437
		2	3835	0.011	0.453	
		3	3057	0.008	0.414	
	1 hour	1	4080	0.086	3.357	3.347
		2	3072	0.066	3.428	
		3	3921	0.080	3.256	
54	Pre	1	3781	0.007	0.305	0.274
		2	3030	0.005	0.252	
		3	3666	0.006	0.264	
	1 hour	1	3518	0.046	2.091	1.678
		2	3278	0.030	1.440	
		3	3997	0.038	1.504	
55	Pre	1	3068	0.007	0.347	0.368
		2	3989	0.010	0.376	
		3	4106	0.010	0.381	
	1 hour	1	3799	0.071	2.961	2.867
		2	3340	0.055	2.608	
		3	3226	0.062	3.032	

Table 34 - Saliva Pt-DNA adduct replicates

Patient ID	Time point	Replicate Number	P conc (ppb)	Pt conc (ppb)	Number of adducts per 10^6 nucleotides	Average adducts (per 10^6 nucleotides)
35	Pre	1	17662	0.050	0.446	0.447
		2	17044	0.048	0.447	
	1 hour	1	15567	0.549	5.600	5.602
		2	14560	0.514	5.604	
	24 hour	1	10007	0.393	6.235	6.223
		2	10322	0.404	6.212	
34	Pre	1	34011	0.084	0.391	0.395
		2	28509	0.072	0.398	
	1 hour	1	7833	0.184	3.732	3.741
		2	7575	0.179	3.749	
	24 hour	1	8567	0.127	2.349	2.360
		2	8612	0.129	2.370	
39	Pre	1	11936	0.044	0.581	0.593
		2	12064	0.046	0.605	
	1 hour	1	10129	0.285	4.463	4.437
		2	11379	0.316	4.411	
	24 hour	1	9297	0.084	1.432	1.435
		2	11256	0.102	1.437	
48	Pre	1	11057	0.053	0.759	0.761
		2	13213	0.063	0.762	
	1 hour	1	9489	0.199	3.329	3.336
		2	8976	0.189	3.343	
	24 hour	1	15221	0.268	2.792	2.781
		2	14709	0.257	2.769	
49	Pre	1	11547	0.080	1.098	1.170
		2	11194	0.088	1.241	
	1 hour	1	7327	0.195	4.229	4.240
		2	7674	0.206	4.251	
	24 hour	1	8914	0.183	3.250	3.244
		2	8834	0.180	3.238	
50	Pre	1	26880	0.048	0.284	0.287
		2	24460	0.045	0.290	
	1 hour	1	11290	0.284	3.992	4.002
		2	11289	0.285	4.012	
	24 hour	1	26605	0.263	1.571	1.574
		2	27385	0.272	1.576	
51	Pre	1	139028	0.665	0.759	0.765
		2	120872	0.586	0.770	
	1 hour	1	60356	1.140	2.997	3.041
		2	54505	1.059	3.084	
	24 hour	1	11404	0.384	5.339	5.346
		2	11398	0.384	5.352	
53	Pre	1	22865	0.087	0.603	0.602
		2	24131	0.091	0.601	

	1 hour	1	21177	0.420	3.149	3.165
		2	19831	0.397	3.181	
	24 hour	1	37837	0.953	3.996	3.990
		2	36420	0.914	3.984	
54	Pre	1	13230	0.057	0.680	0.681
		2	13197	0.057	0.682	
	1 hour	1	37533	1.375	5.814	5.812
		2	37188	1.361	5.810	
	24 hour	1	18000	0.733	6.461	6.471
		2	17460	0.713	6.480	
55	Pre	1	20359	0.046	0.362	0.367
		2	15585	0.036	0.371	
	1 hour	1	16157	0.414	4.069	4.075
		2	16578	0.426	4.081	
	24 hour	1	10582	0.278	4.169	4.165
		2	10846	0.284	4.160	

Table 35- Blood and Saliva adduct values for incomplete patient sets

Patient ID	Time point	Replicate number	Blood		Saliva	
			Adducts (per 10^6 nucleotides)	Average adducts (per 10^6 nucleotides)	Adducts (per 10^6 nucleotides)	Average adducts (per 10^6 nucleotides)
33	Pre	1	0.348	0.348	0.345	0.356
		2	0.344		0.367	
		3	0.351		-	
	1 hour	1	2.622	2.627	4.542	4.537
		2	2.631		4.531	
		3	2.630		-	
	24 hour	1	-	-	3.813	3.803
		2	-		3.793	
		3	-		-	
36	Pre	1	0.348	0.345	0.413	0.404
		2	0.342		0.394	
		3	0.345		-	
	1 hour	1	2.230	2.233	1.245	1.255
		2	2.238		1.264	
		3	2.230		-	
	24 hour	1	-	-	1.467	1.460
		2	-		1.452	
		3	-		-	
37	Pre	1	0.351	0.344	0.421	0.411
		2	0.342		0.401	
		3	0.339		-	
	1 hour	1	5.012	5.006	-	-
		2	4.993		-	
		3	5.012		-	
	24 hour	1	-	-	-	-
		2	-		-	
		3	-		-	
38	Pre	1	0.345	0.331	0.437	0.431
		2	0.315		0.425	
		3	0.334		-	
	1 hour	1	2.461	2.454	4.361	4.357
		2	2.442		4.354	
		3	2.458		-	
	24 hour	1	-	-	3.710	3.715
		2	-		3.719	
		3	-		-	
40	Pre	1	0.436	0.438	0.259	0.261
		2	0.433		0.263	
		3	0.443		-	
	1 hour	1	4.964	5.014	3.413	3.414
		2	5.012		3.414	
		3	5.065		-	
	24 hour	1	-	-	-	-

		2	-		-	
		3	-		-	
41	Pre	1	0.009	0.009	0.008	0.009
		2	0.009		0.009	
		3	0.009		-	
	1 hour	1	2.357	2.361	-	-
		2	2.364		-	
		3	2.361		-	
	24 hour	1	-	-	-	-
		2	-		-	
		3	-		-	
42	Pre	1	0.451	0.455	0.354	0.353
		2	0.461		0.353	
		3	0.454		-	
	1 hour	1	4.325	4.328	6.531	6.513
		2	4.322		6.495	
		3	4.337		-	
	24 hour	1	-	-	4.315	4.321
		2	-		4.326	
		3	-		-	
43	Pre	1	0.485	0.475	0.403	0.399
		2	0.462		0.395	
		3	0.476		-	
	1 hour	1	3.113	3.107	2.465	2.456
		2	3.102		2.447	
		3	3.107		-	
	24 hour	1	-	-	2.846	2.858
		2	-		2.869	
		3	-		-	
44	Pre	1	0.007	0.007	0.010	0.010
		2	0.008		0.010	
		3	0.008		-	
	1 hour	1	3.254	3.256	4.894	4.899
		2	3.264		4.903	
		3	3.251		-	
	24 hour	1	-	-	-	-
		2	-		-	
		3	-		-	
45	Pre	1	1.023	1.029	1.345	1.353
		2	0.997		1.362	
		3	1.065		-	
	1 hour	1	4.651	4.632	1.846	1.840
		2	4.642		1.834	
		3	4.601		-	
	24 hour	1	-	-	2.345	2.351
		2	-		2.357	
		3	-		-	
46	Pre	1	0.235	0.227	0.174	0.171
		2	0.234		0.168	
		3	0.213		-	

	1 hour	1	1.974	2.983	3.824	3.809
		2	2.013		3.794	
		3	1.961		-	
	24 hour	1	-	-	-	-
		2	-		-	
		3	-		-	
47	Pre	1	0.321	0.338	0.684	0.678
		2	0.358		0.671	
		3	0.335		-	
	1 hour	1	4.325	4.328	3.154	3.178
		2	4.330		3.201	
		3	4.330		-	
	24 hour	1	-	-	3.022	3.008
		2	-		2.995	
		3	-		-	
52	Pre	1	0.294	0.279	0.354	0.354
		2	0.262		0.354	
		3	0.280		-	
	1 hour	1	3.644	3.634	4.355	4.344
		2	3.624		4.332	
		3	3.634		-	
	24 hour	1	-	-	4.684	4.673
		2	-		4.662	
		3	-		-	

Appendix B – Chapter 3 supplementary information

Nitrogen rich peptides

Peptide 1 – NNIK

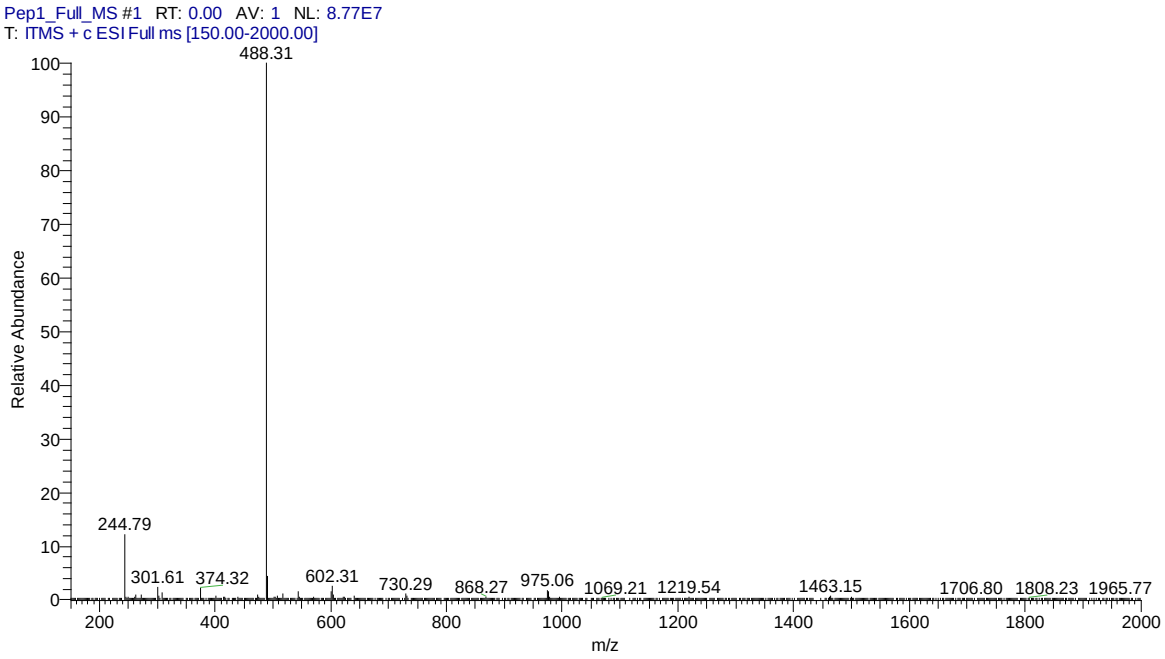

Figure 91 – Full mass spectrum for peptide 1 (NNIK)

Table 36 – Peak assignments for peptide 1 (NNIK)

Most abundant isotope *m/z*	Assignment
244.79	$[NNIK + 2H]^{2+}$
301.61	$[(NNIK+N) + 2H]^{2+}$
374.32	$[(NNIK – N) + H]^{+}$
488.25	$[NNIK + H]^{+}$
602.31	$[(NNIK+N) + H]^{+}$
975.06	$[(NNIK)_2 + H]^{+}$

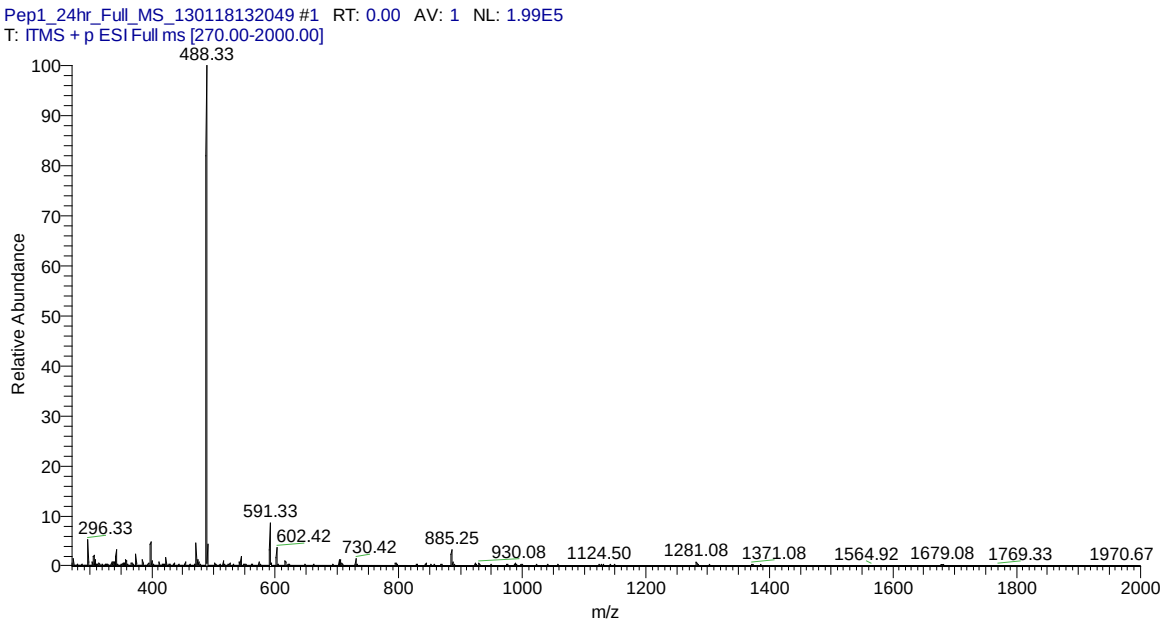

Figure 92 – Full mass spectrum for peptide 1 (NNIK) and oxaliplatin after 24 hours

Table 37 – Peak assignments for peptide 1 (NNIK) and oxaliplatin after 24 hours incubation

Most abundant isotope *m/z*	Assignment
398.17	$[OxPt + H]^+$
488.25	$[NNIK + H]^+$
602.45	$[(NNIK+N) + H]^+$
885.25	$[NNIK+ OxPt + H]^+$
1281.08	$[NNIK + (OxPt)_2 + H]^+$
1371.08	$[(NNIK)_2 + OxPt + H]^+$
1679.08	$[NNIK + (OxPt)_3 + H]^+$
1769.33	$[(NNIK)_2 + (OxPt)_2 + H]^+$

Peptide 2 – ENQK

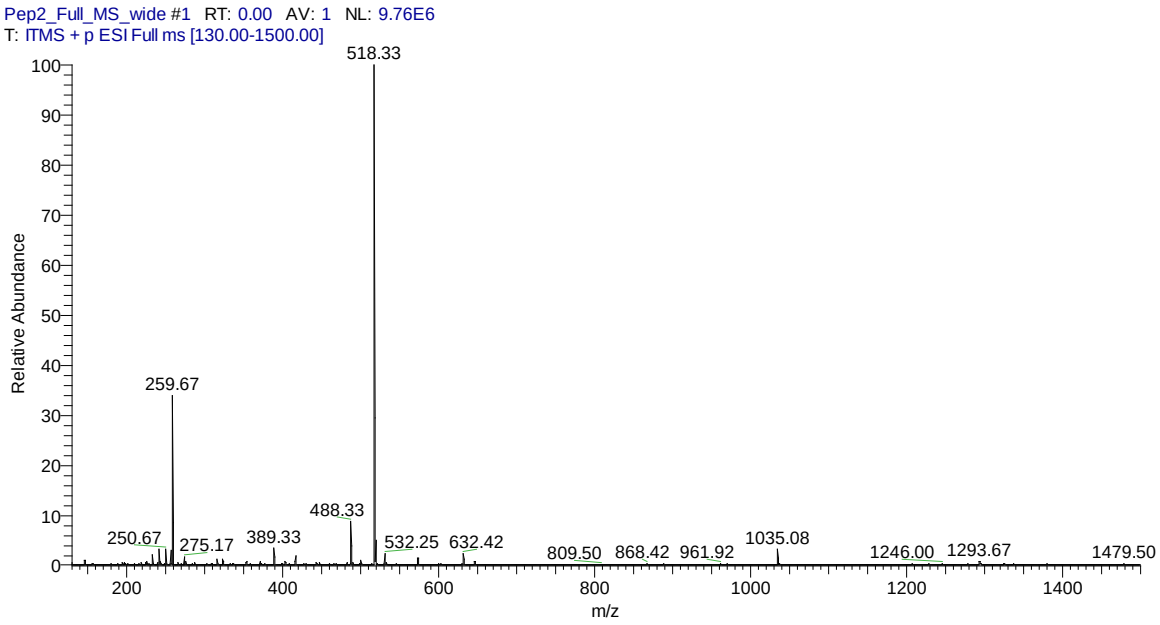

Figure 93 – Full mass spectrum for peptide 2 (ENQK)

Table 38 – Peak assignments for peptide 2 (ENQK)

Most abundant isotope *m/z*	Assignment
259.67	$[ENQK + 2H]^{2+}$
389.33	$[(ENQK-K) + H]^{+}$
488.33	$[(ENQK-CH_2NH_3) + H]^{+}$
518.33	$[ENQK + H]^{+}$
632.42	$[ENQK + (ENQK-C_4H_{11}N) + H]^{+}$
1035.08	$[(ENQK)_2 + H]^{+}$

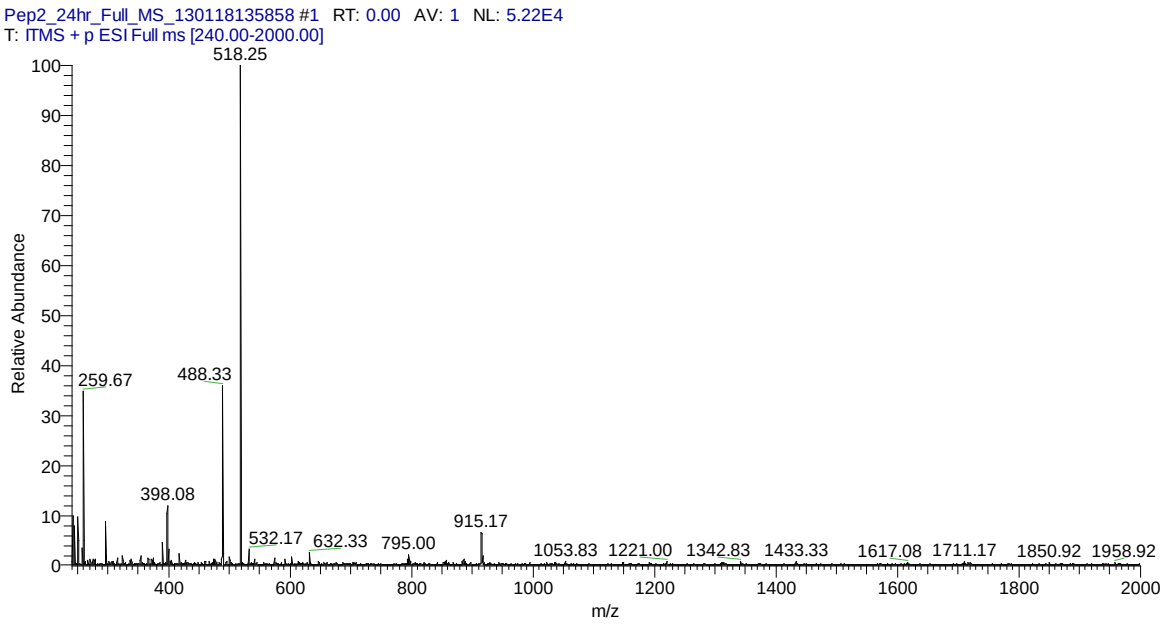

Figure 94 – Full mass spectrum for peptide 2 (ENQK) and oxaliplatin after 24 hours incubation

Table 39 – Peak assignments for peptide 2 (ENQK) and oxaliplatin after 24 hours incubation

Most abundant isotope *m/z*	Assignment
259.67	$[ENQK + 2H]^{2+}$
398.08	$[OxPt + H]^{+}$
488.33	Peptide 1 carryover
518.25	$[ENQK + H]^{+}$
532.17	$[(ENQK - C_{14}H_{19}N_6O_7) + OxPt + H]^{+}$
632.33	$[ENQK + (ENQK\text{-}C_4H_{11}N) + H]^{+}$
795.00	$[(OxPt)_2 + H]^{+}$
915.17	$[ENQK + OxPt + H]^{+}$
1035.83	$[(ENQK)_2 + H]^{+}$
1311.92	$[ENQK + (OxPt)_2 + H]^{+}$
1433.33	$[(ENQK)_2 + OxPt + H]^{+}$
1711.17	$[ENQK + (OxPt)_3 + H]^{+}$

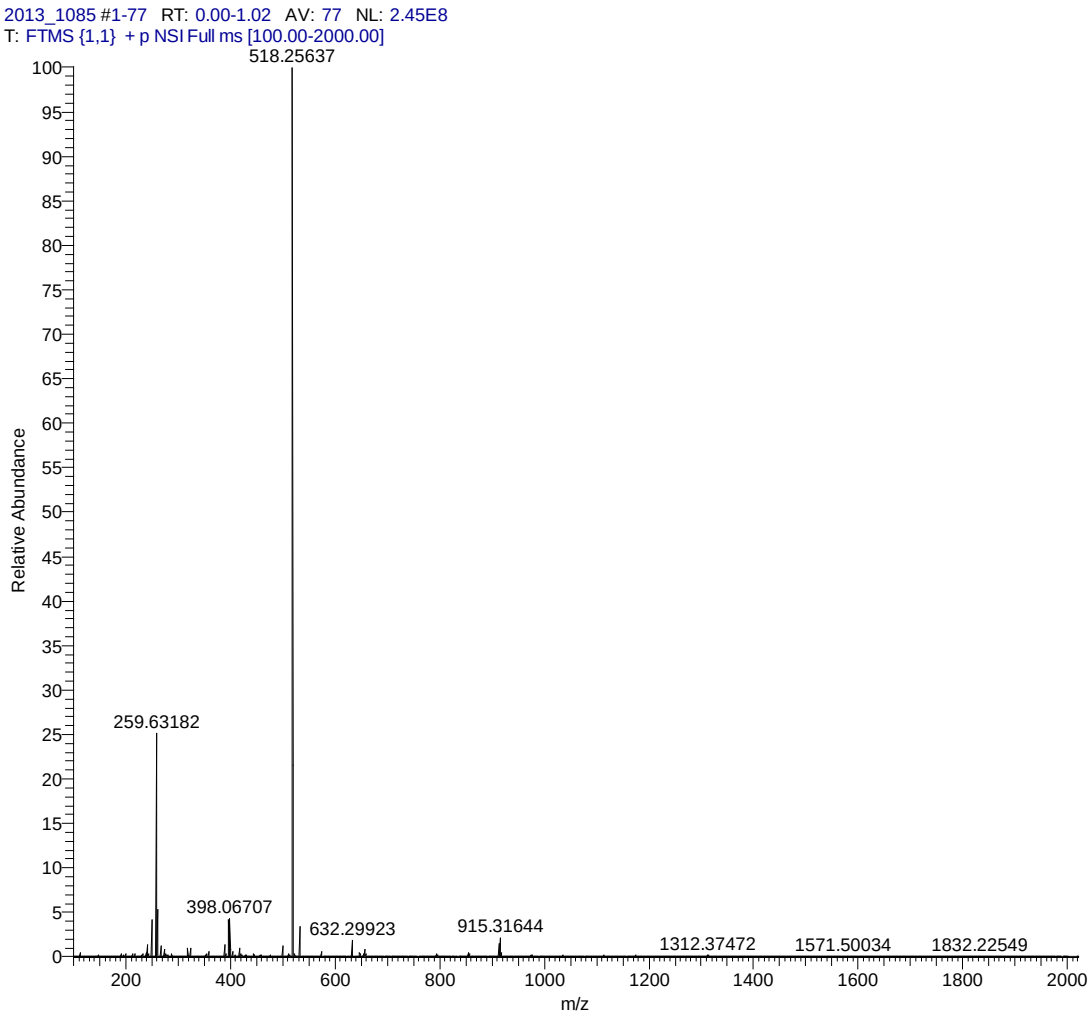

Figure 95 - Orbitrap spectrum of peptide 2 (ENQK) and oxaliplatin

Peptide 3 – QHEK

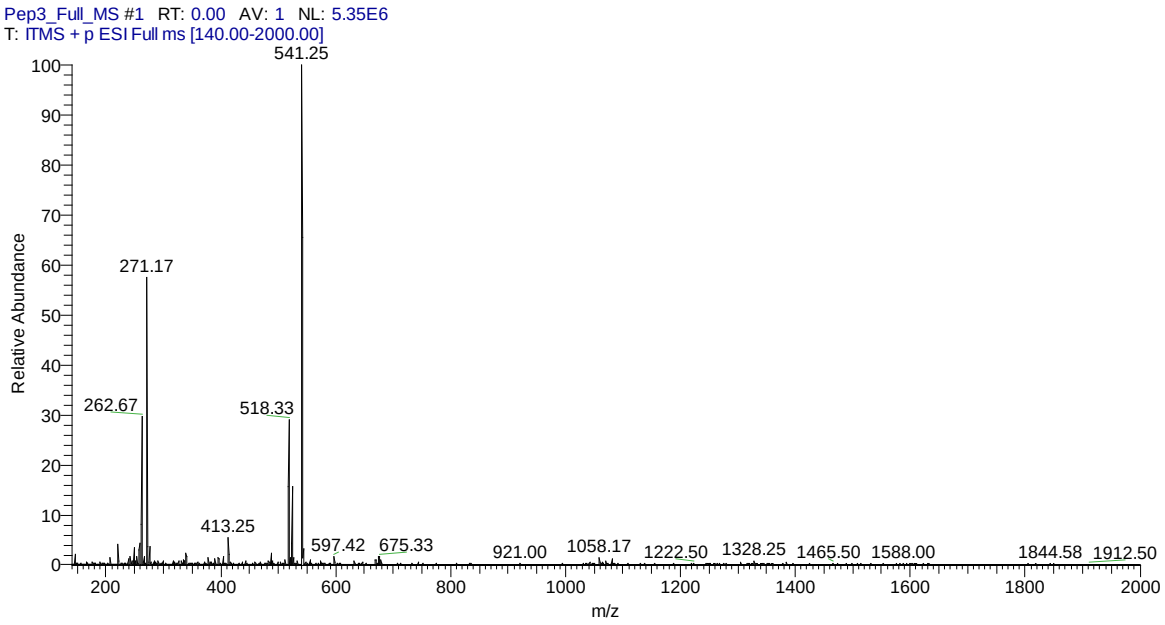

Figure 96 – Full mass spectrum for peptide 3 (QHEK)

Table 40 – Peak assignments for peptide 3 (QHEK)

Most abundant isotope *m/z*	Assignment
262.67	$[QHEK - NH_3 + 2H]^{2+}$
271.17	$[QHEK + 2H]^{2+}$
413.25	$[(QHEK\text{-}Q) + H]^{+}$
541.25	$[QHEK + H]^{+}$
1081.17	$[(QHEK)_2 + H]^{+}$

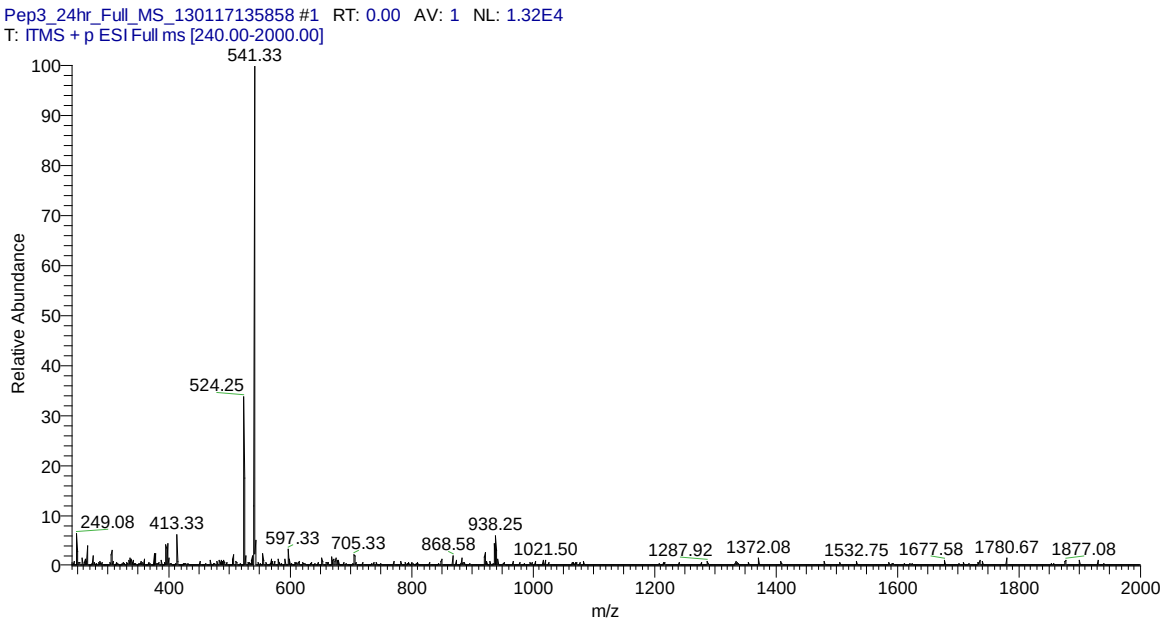

Figure 97 – Full mass spectrum for peptide 3 (QHEK) and oxaliplatin after 24 hours incubation

Table 41 – Peak assignments for peptide 3 (QHEK) and oxaliplatin after 24 hours incubation

Most abundant isotope *m/z*	Assignment
397.17	$[OxPt + H]^+$
413.33	$[(QHEK\text{-}Q) + H]^+$
524.25	$[(QHEK\text{-}NH_3) + H]^+$
541.33	$[QHEK + H]^+$
793.17	$[(OxPt)_2 + H]^+$
938.25	$[QHEK + OxPt + H]^+$
1082.68	$[(QHEK)_2 + H]^+$
1335.08	$[QHEK + (OxPt)_2 + H]^+$
1480.42	$[(QHEK)_2 + OxPt + H]^+$
1877.08	$[(QHEK)_2 + (OxPt)_2 + H]^+$

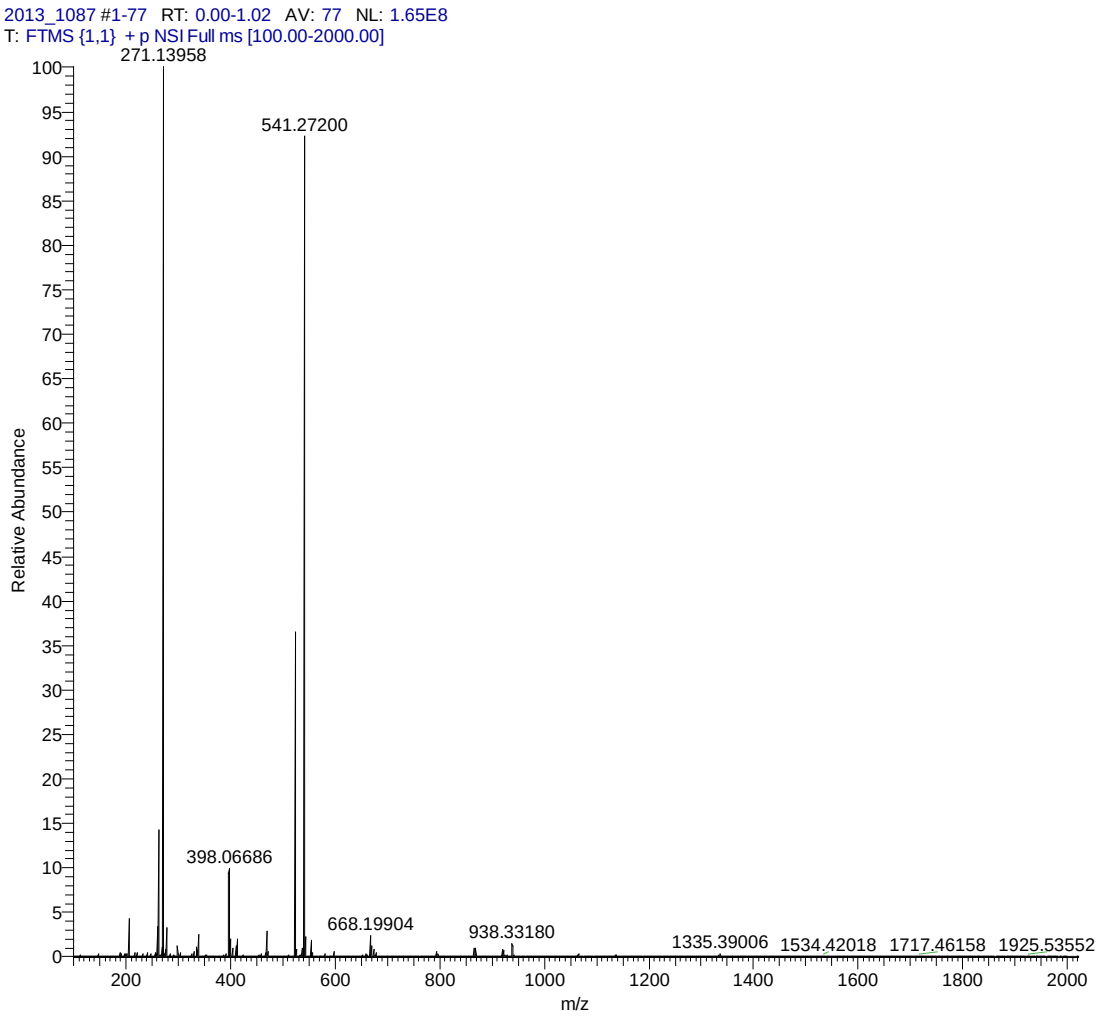

Figure 98 - Orbitrap spectrum of peptide 3 (QHEK) and oxaliplatin

Peptide 4 – YRPR

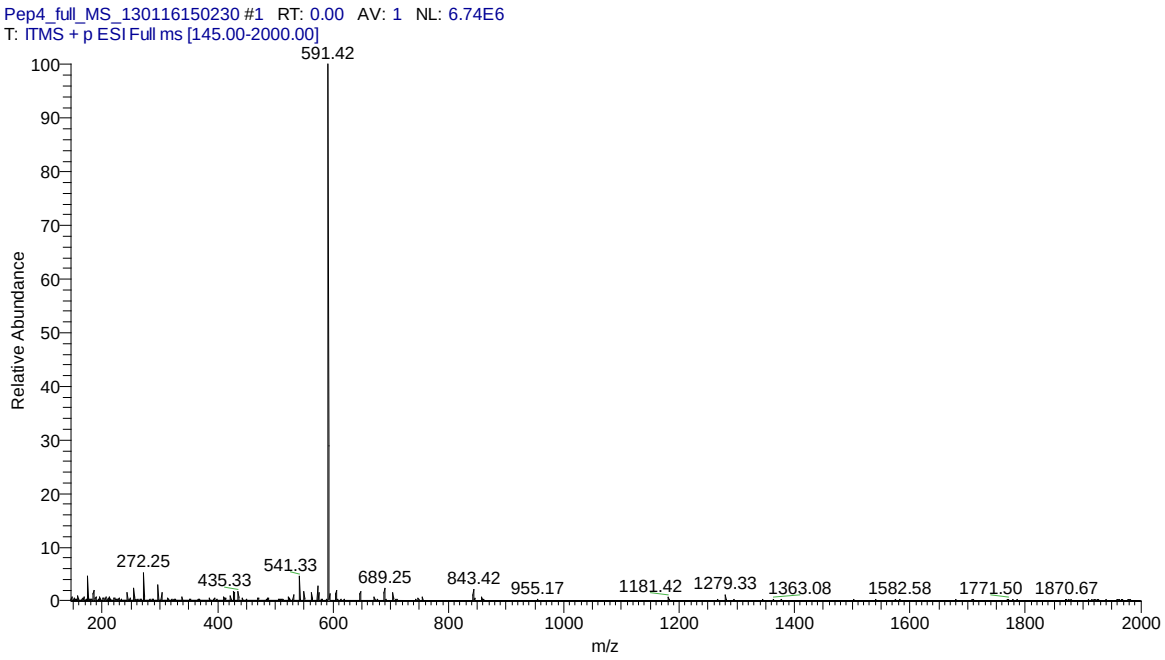

Figure 99 – Full mass spectrum for peptide 4 (YRPR)

Table 42 – Peak assignments for peptide 4 (YRPR)

Most abundant isotope *m/z*	Assignment
435.33	$[(YRP + H]^+$
541.33	Peptide 3 carry over
591.42	$[YRPR + H]^+$
1181.42	$[(YRPR)_2 + H]^+$
1771.50	$[(YRPR)_3 + H]^+$

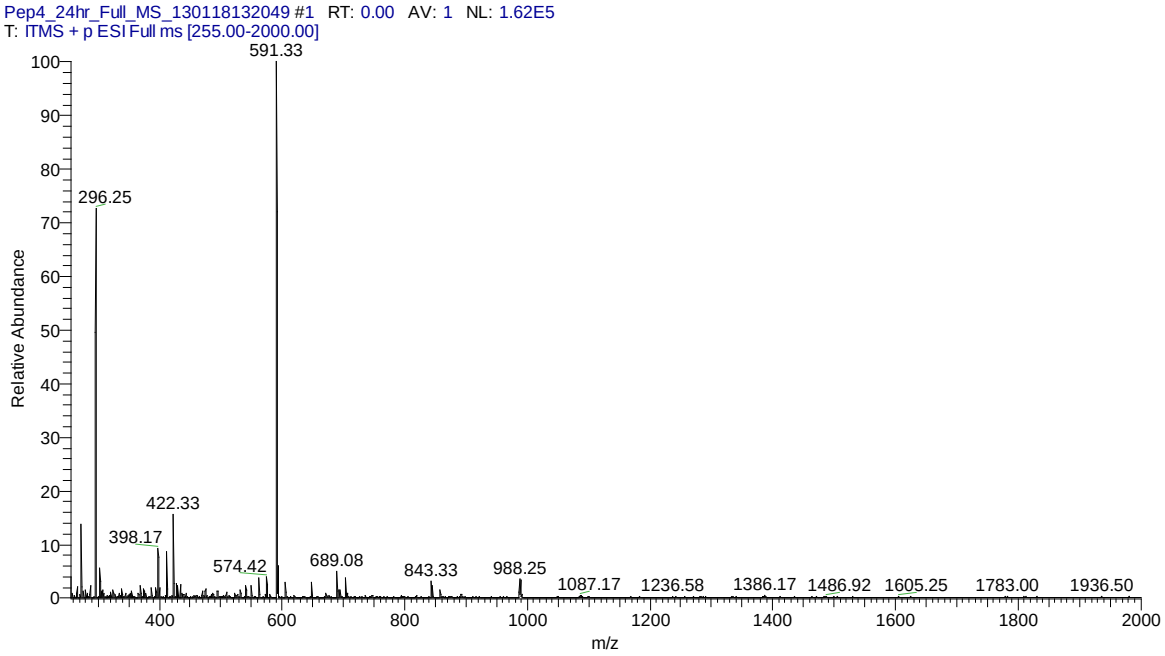

Figure 100 – Full mass spectrum for peptide 4 (YRPR) and oxaliplatin after 24 hours incubation

Table 43 – Peak assignments for peptide 4 (YRPR) and oxaliplatin after 24 hours incubation

Most abundant isotope *m/z*	Assignment
296.25	$[YRPR + 2H]^{2+}$
398.17	$[OxPt + H]^{+}$
591.33	$[YRPR + H]^{+}$
988.25	$[YRPR + OxPt + H]^{+}$
1386.17	$[YRPR + (OxPt)_2 + H]^{+}$

Sulfur rich peptides

Peptide 5 – GCMR

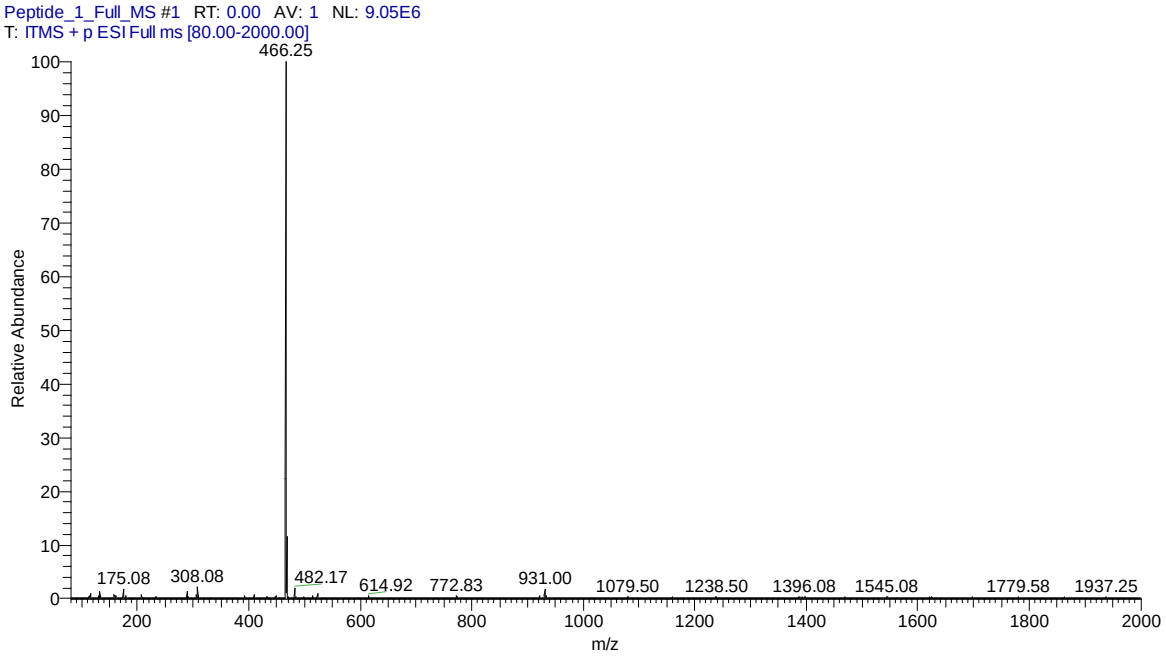

Figure 101 – Full mass spectrum for peptide 5 (GCMR)

Table 44 – Peak assignments for peptide 5 (GCMR)

Most abundant isotope *m/z*	Assignment
175.08	$[R + H]^+$
233.08	$[GCMR + 2H]^{2+}$
308.08	$[(GCMR\text{-}R) + H]^+$
466.25	$[GCMR + H]^+$
482.17	$[GCMR + NH_2 + H]^+$
772.83	$[GCMR + GCM + H]^+$
931.00	$[(GCMR)_2 + H]^+$
1396.08	$[(GCMR)_3 + H]^+$

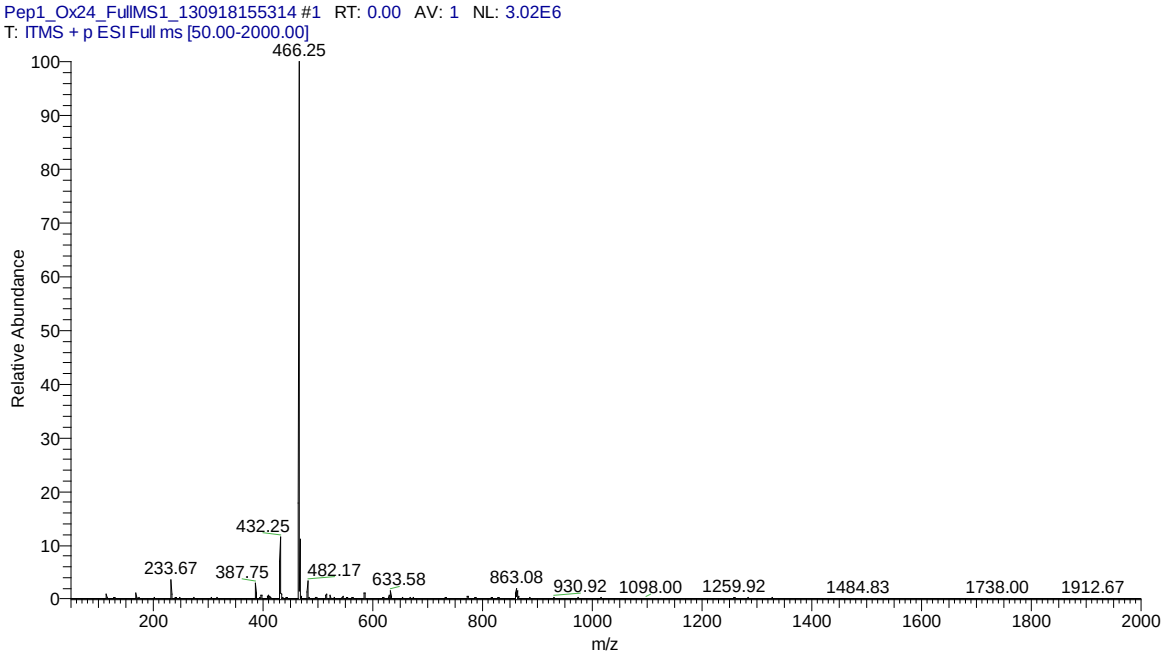

Figure 102 – Full mass spectrum for peptide 5 (GCMR) and oxaliplatin after 24 hours incubation

Table 45 – Peak assignments for peptide 5 (GCMR) and oxaliplatin after 24 hours incubation

Most abundant isotope *m/z*	Assignment
233.67	$[GCMR + 2H]^{2+}$
398.08	$[OxPt + H]^{+}$
432.25	$[(GCMR\text{-}SH) + H]^{+}$
466.25	$[GCMR + H]^{+}$
482.17	$[GCMR + NH_2 + H]^{+}$
633.58	$[(GCMR)_2 + OxPt + 2H]^{2+}$
863.08	$[GCMR + OxPt + H]^{+}$
930.92	$[(GCMR)_2 + H]^{+}$

Peptide 6 – AMMK

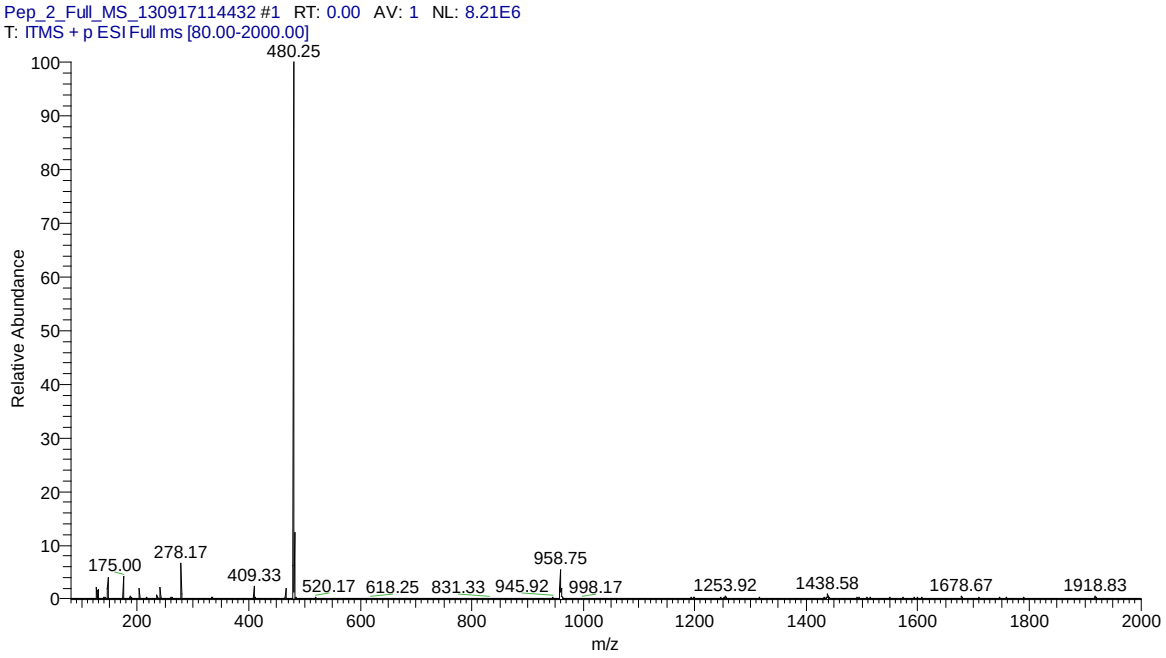

Figure 103 – Full mass spectrum for peptide 6 (AMMK)

Table 46 – Peak assignments for peptide 6 (AMMK)

Most abundant isotope *m/z*	Assignment
175.00	$[(AMMK- C_7H_{15}N_2OS) + H]^+$
240.58	$[AMMK + 2H]^{2+}$
278.17	$[(AMMK-C_8H_{20}N_3O_2S) + H]^+$
409.33	$[(AMMK-A) + H]^+$
480.25	$[AMMK + H]^+$
958.75	$[(AMMK)_2 + H]^+$
1438.58	$[(AMMK)_3 + H]^+$
1918.33	$[(AMMK)_4 + H]^+$

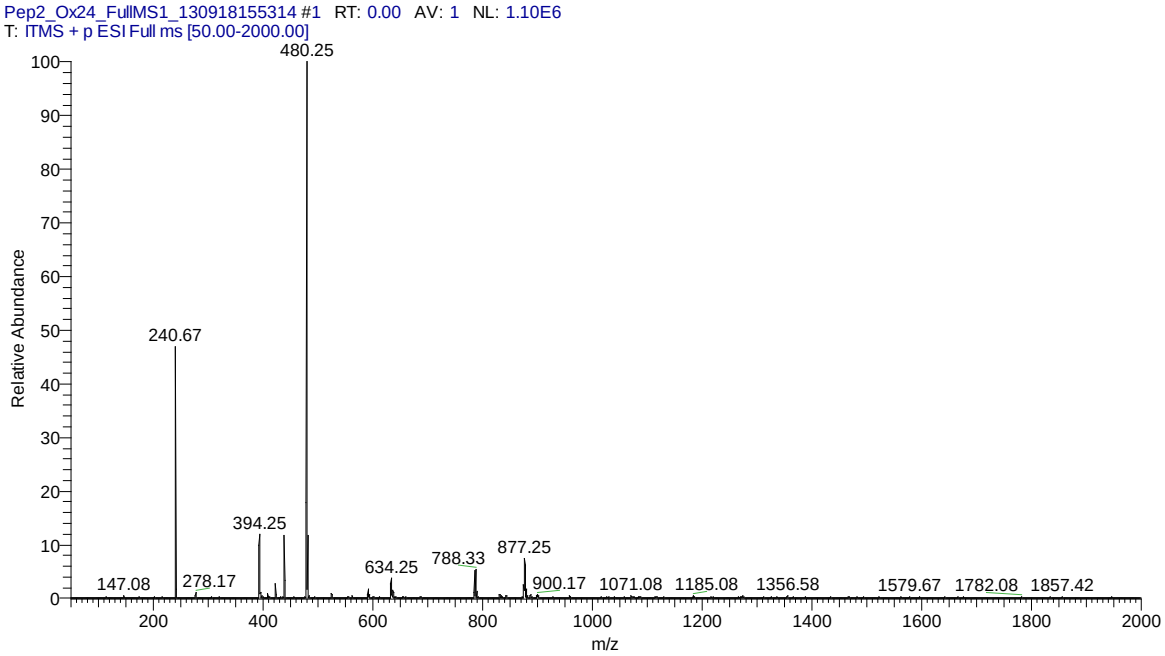

Figure 104 – Full mass spectrum for peptide 6 (AMMK) and oxaliplatin after 24 hours incubation

Table 47 – Peak assignments for peptide 6 (AMMK) and oxaliplatin after 24 hours incubation

Most abundant isotope *m/z*	Assignment
240.67	$[AMMK + 2H]^{2+}$
394.25	$[(AMMK\text{-}A) - H_2O + OxPt + 2H]^{2+}$
438.62	$[AMMK + OxPt + 2H]^{2+}$
480.25	$[AMMK + H]^{+}$
634.25	$[AMMK + (OxPt)_2 + 2H]^{2+}$
788.33	$[(AMMK\text{-}A) - H_2O + OxPt + H]^{+}$
877.25	$[AMMK + OxPt + H]^{+}$
958.75	$[(AMMK)_2 + H]^{+}$
1274.17	$[AMMK + (OxPt)_2 + H]^{+}$
1356.56	$[(AMMK)_2 + OxPt + H]^{+}$

Peptide 7 – MSMK

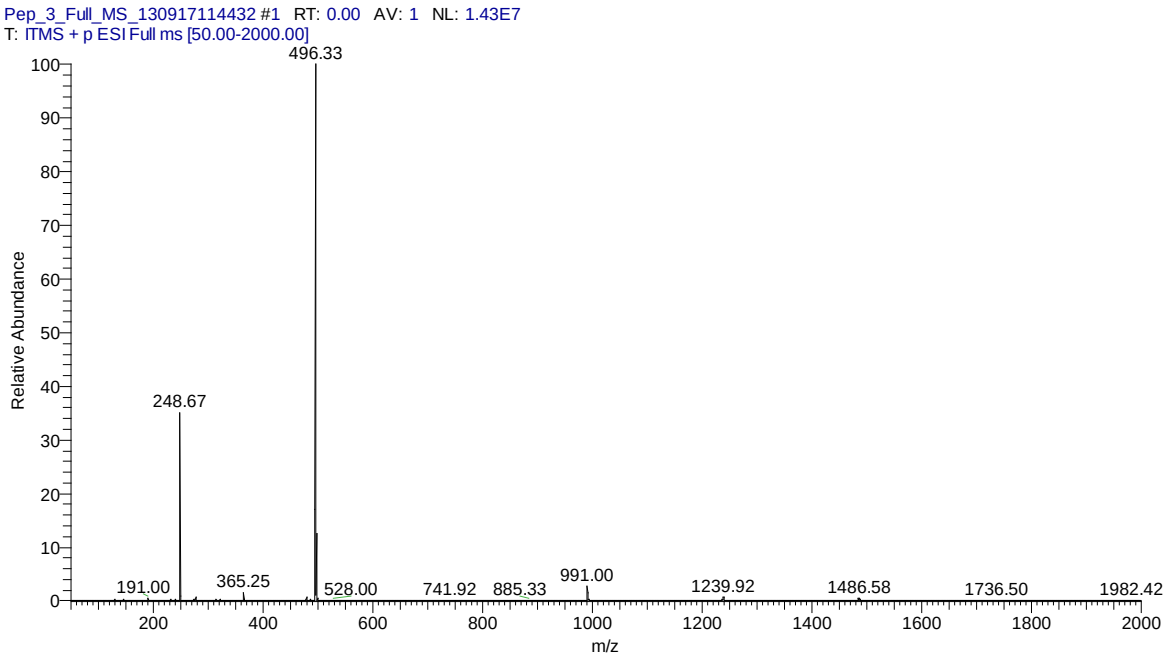

Figure 105 – Full mass spectrum for peptide 7 (MSMK)

Table 48 – Peak assignments for peptide 7 (MSMK)

Most abundant isotope *m/z*	Assignment
248.67	$[MSMK + 2H]^{2+}$
365.25	$[(MSMK-M) + H]^{+}$
496.33	$[MSMK + H]^{+}$
991.00	$[(MSMK)_2 + H]^{+}$
1486.58	$[(MSMK)_3 + H]^{+}$
1987.42	$[(MSMK)_4 + H]^{+}$

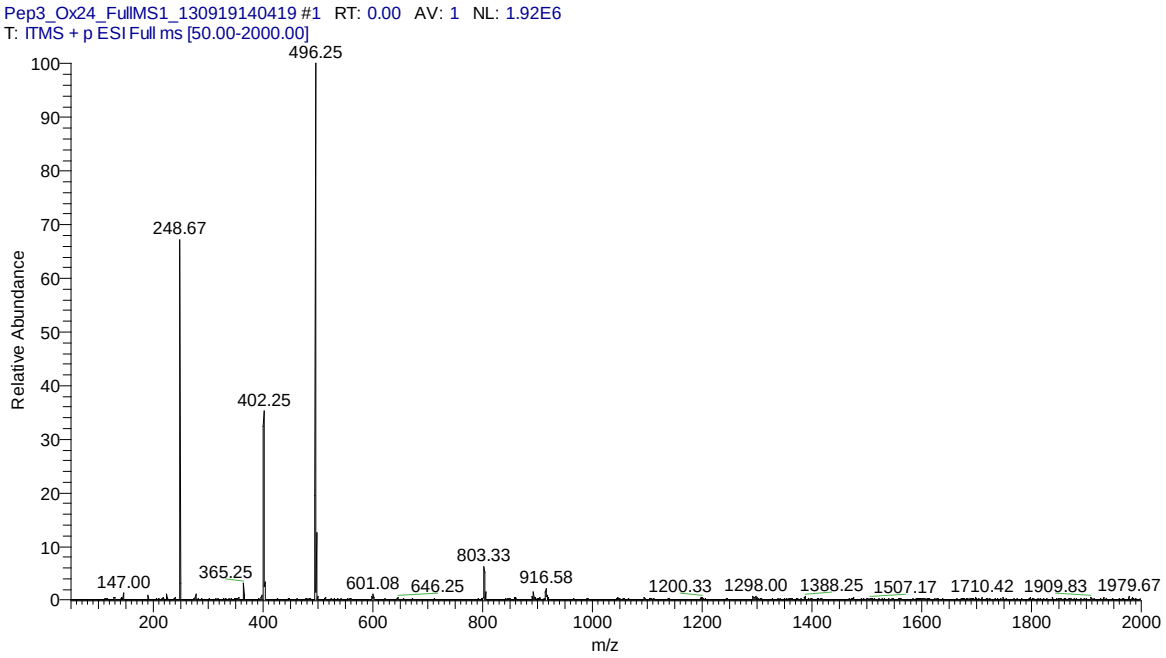

Figure 106 – Full mass spectrum for peptide 7 (MSMK) and oxaliplatin after 24 hours incubation

Table 49 – Peak assignments for peptide 7 (MSMK) and oxaliplatin after 24 hours incubation

Most abundant isotope *m/z*	Assignment
147.00	$[M + NH_2 + H]+$
248.67	$[MSMK + 2H]^{2+}$
365.25	$[(MSMK-M) + H]^{+}$
398.17	$[OxPt + H]^{+}$
402.25	$[MSMK + (OxPt\text{-}C_2O_4) + 2H]^{2+}$
496.25	$[MSMK + H]^{+}$
803.33	$[MSMK + (OxPt\text{-}C_2O_4) + H]^{+}$
892.92	$[MSMK + OxPt + H]^{+}$
992.08	$[(MSMK)_2 + H]^{+}$
1289.00	$[MSMK + (OxPt)_2 + H]^{+}$
1388.25	$[(MSMK)_2 + OxPt + H]^{+}$

Peptide 8 – MMTK

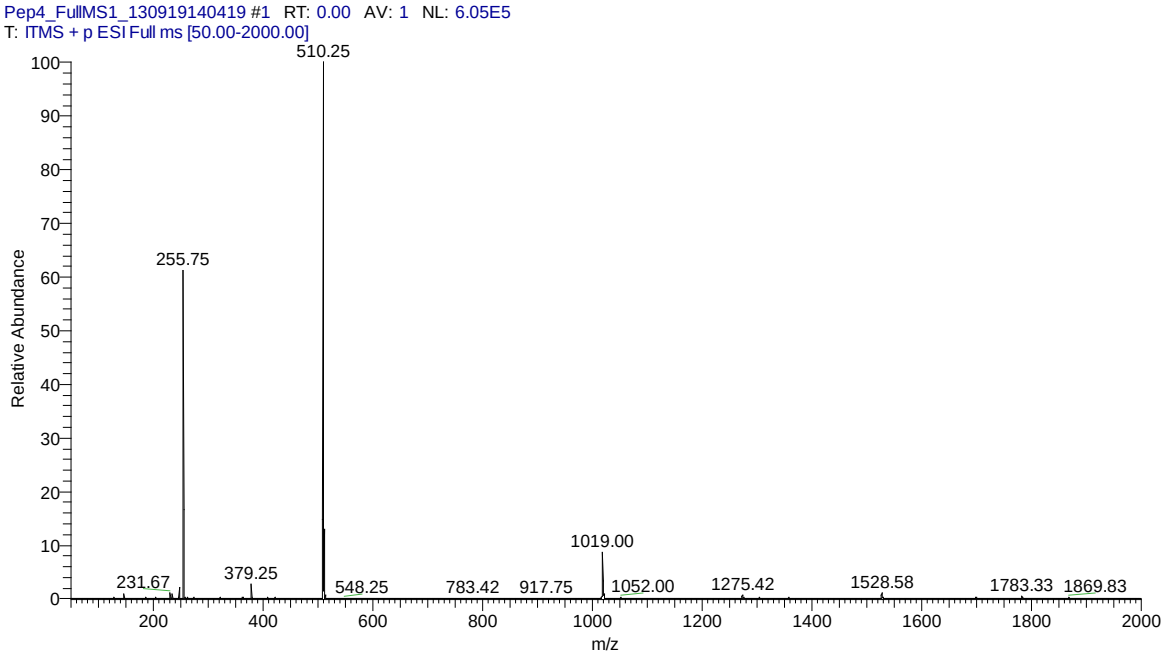

Figure 107 – Full mass spectrum for peptide 8 (MMTK)

Table 50 – Peak assignments for peptide 8 (MMTK)

Most abundant isotope *m/z*	Assignment
231.67	$[(MMTK – MM -NH_3) + H]^+$
255.75	$[MMTK + 2H]^{2+}$
379.25	$[(MMTK-M) + H]^+$
510.25	$[MMTK + H]^+$
1019.00	$[(MMTK)_2 + H]^+$
1528.58	$[(MMTK)_3 + H]^+$

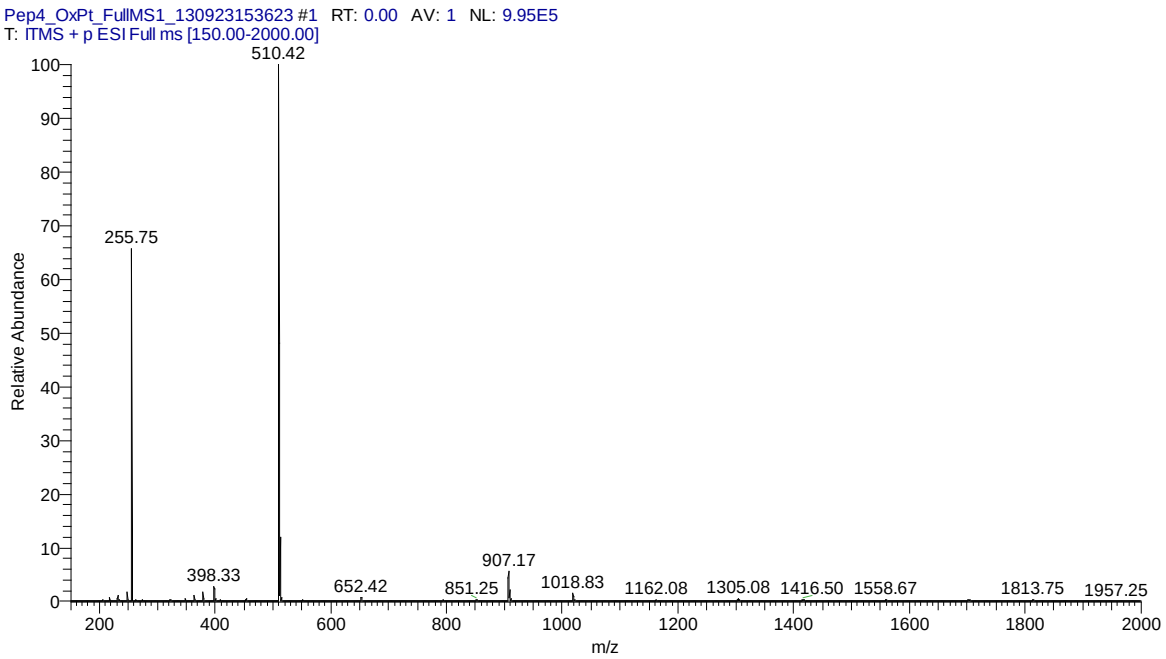

Figure 108 – Full mass spectrum for peptide 8 (MMTK) and oxaliplatin after 24 hours incubation

Table 51 – Peak assignments for peptide 8 (MMTK) and oxaliplatin after 24 hours incubation

Most abundant isotope *m/z*	Assignment
255.75	$[MMTK + 2H]^{2+}$
379.33	$[(MMTK\text{-}M) + H]^{+}$
398.33	$[OxPt + H]^{+}$
454.17	$[MMTK + OxPt + 2H\ ]^{2+}$
510.33	$[MMTK + H]^{+}$
907.17	$[MMTK + OxPt + H\ ]^{+}$
1018.83	$[(MMTK)_2 + H]^{+}$
1305.08	$[MMTK + (OxPt)_2 + H]^{+}$
1416.50	$[(MMTK)_2 + OxPt + H]^{+}$

Peptide 9 – MCAAR

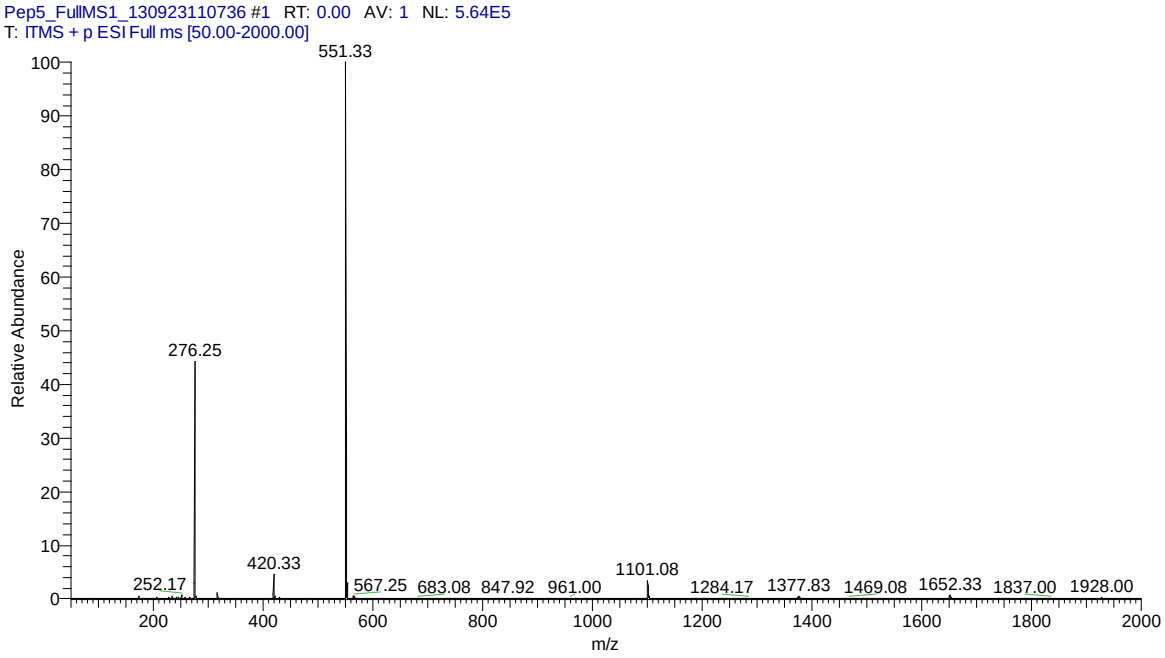

Figure 109 – Full mass spectrum for peptide 9 (MCAAR)

Table 52 – Peak assignments for peptide 9 (MCAAR)

Most abundant isotope *m/z*	Assignment
276.25	$[MCAAR + 2H]^{2+}$
420.33	$[(MCAAR)-M + H]^{+}$
551.33	$[MCAAR + H]^{+}$
567.25	$[MCAAR + NH_2 + H]^{+}$
1101.08	$[(MCAAR)_2 + H]^{+}$
1652.33	$[(MCAAR)_3 + H]^{+}$

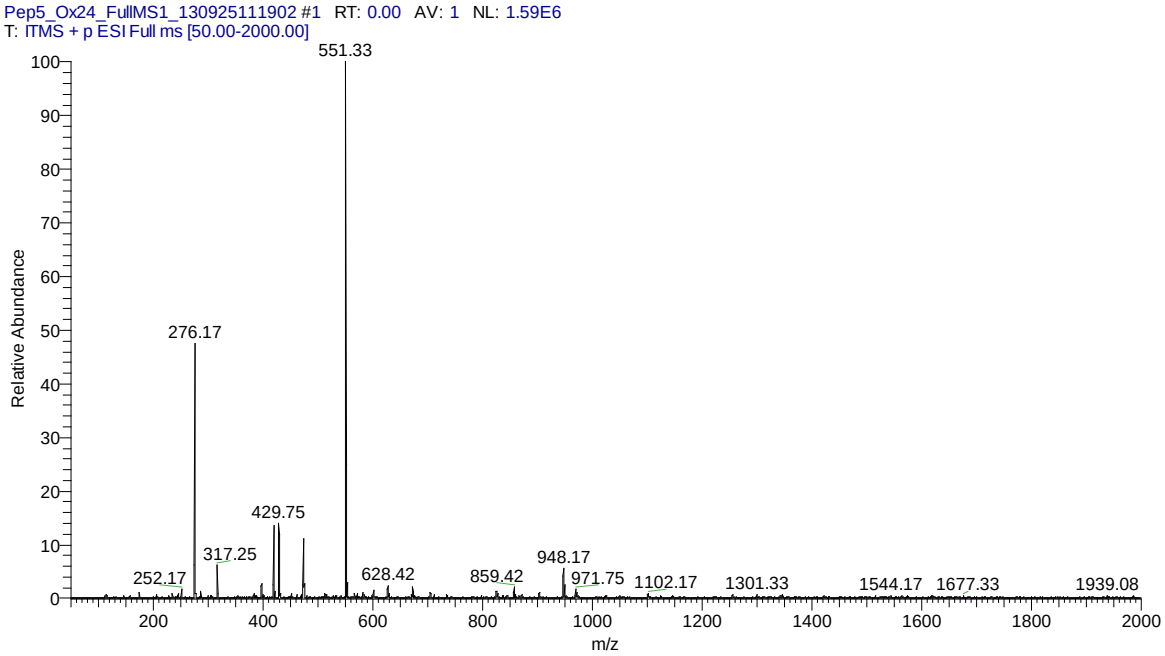

Figure 110 – Full mass spectrum for peptide 9 (MCAAR) and oxaliplatin after 24 hours incubation

Table 53 – Peak assignments for peptide 9 (MCAAR) and oxaliplatin after 24 hours incubation

Most abundant isotope *m/z*	Assignment
252.14	$[(MCAAR\text{-}C_8H_{17}N_3O_2S_2) + H]^+$
276.17	$[MCAAR + 2H]^{2+}$
317.25	$[(MCAAR\text{-}C_8H_{16}N_2O_2S_2) + H]^+$
398.17	$[OxPt + H]^+$
420.33	$[(MCAAR\text{-}M) + H]^+$
551.33	$[MCAAR + H]^+$
673.50	$[MCAAR + OxPt + 2H]^{2+}$
948.17	$[MCAAR + OxPt + H]^+$
1102.17	$[(MCAAR)_2 + H]^+$
1347.83	$[MCAAR + (OxPt)_2 + H]^+$

Peptide 10 – CVK

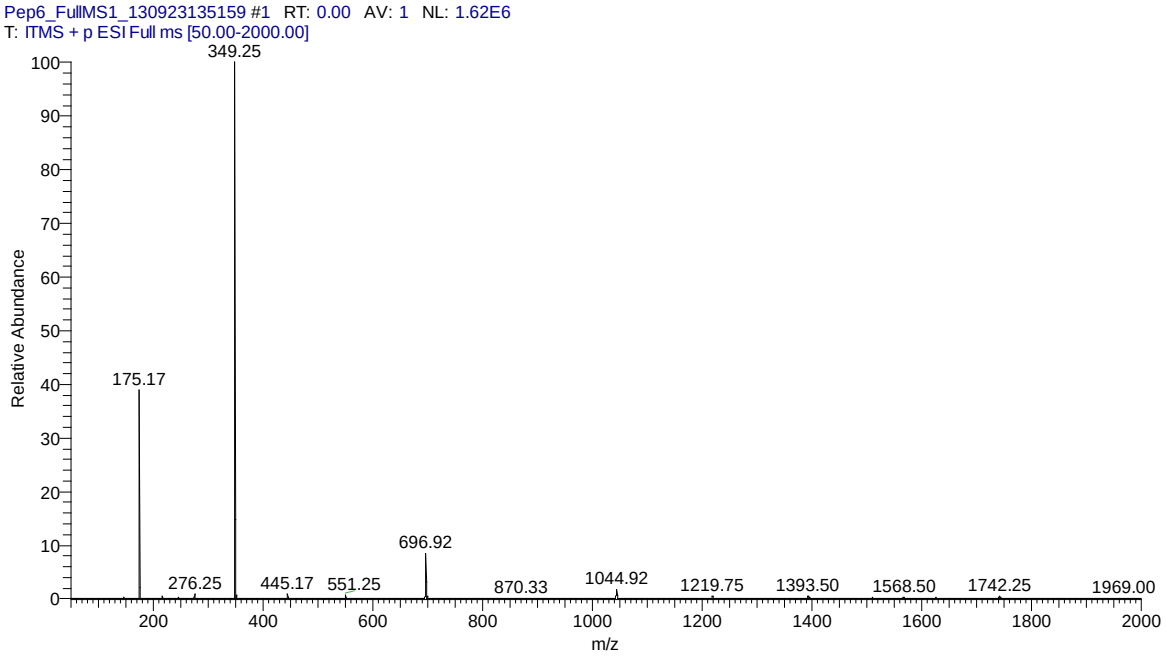

Figure 111 – Full mass spectrum for peptide 10 (CVK)

Table 54 – Peak assignments for peptide 10 (CVK)

Most abundant isotope *m/z*	Assignment
175.17	$[CVK + 2H]^{2+}$
349.25	$[CVK + H]^{+}$
696.92	$[(CVK)_2 + H]^{+}$
1044.92	$[(CVK)_3 + H]^{+}$
1393.50	$[(CVK)_4 + H]^{+}$
1742.25	$[(CVK)_5 + H]^{+}$

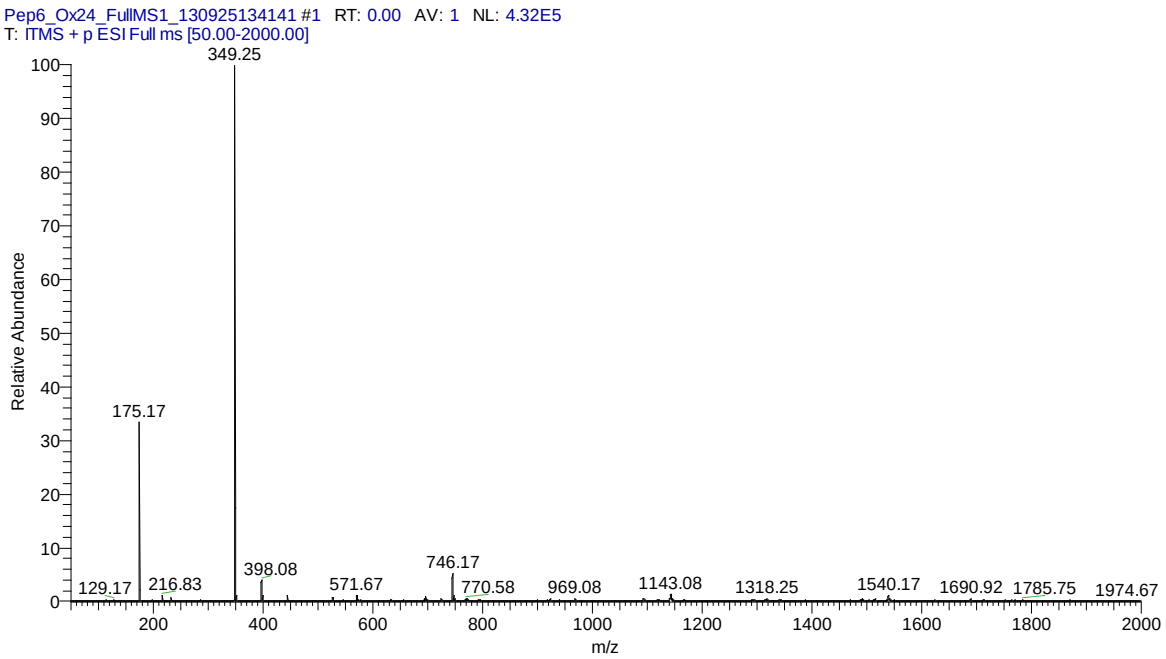

Figure 112 – Full mass spectrum for peptide 10 (CVK) and oxaliplatin after 24 hours incubation

Table 55 – Peak assignments for peptide 10 (CVK) and oxaliplatin after 24 hours incubation

Most abundant isotope *m/z*	Assignment
175.17	$[CVK + 2H]^{2+}$
349.25	$[CVK + H]^{+}$
398.08	$[OxPt + H]^{+}$
571.67	$[CVK + OxPt + 2H]^{2+}$
697.00	$[(CVK)_2 + H]^{+}$
746.17	$[CVK + OxPt + H]^{+}$
1093.25	$[(CVK)_2 + OxPt + H]^{+}$
1143.08	$[CVK + (OxPt)_2 + H]^{+}$
1540.17	$[CVK + (OxPt)_3 + H]^{+}$

Appendix C – Chapter 4 supplementary information

Cell culture: Whole cell population analysis

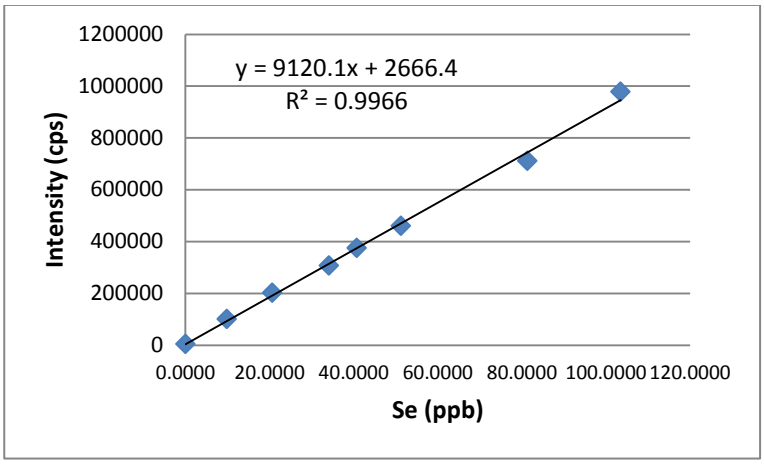

Figure 113 - ^{82}Se calibration graph for determining the level of Se in populations of whole cells

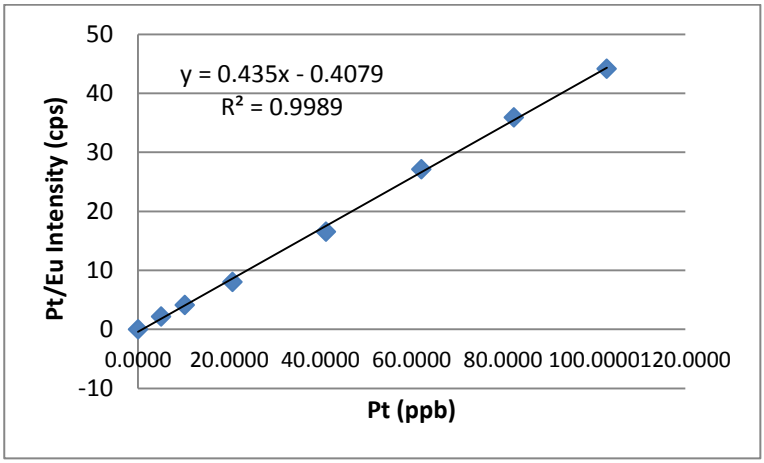

Figure 114 - ^{195}Pt calibration graph for determining the level of Pt in populations of whole cells

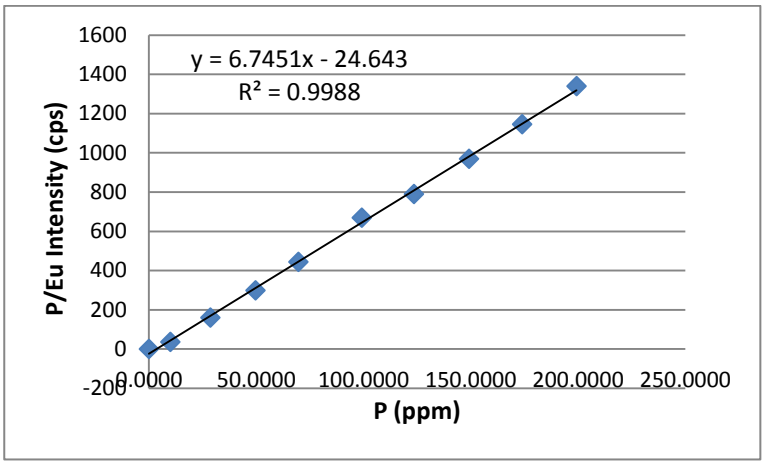

Figure 115 - ^{31}P calibration graph for determining the level of P in populations of whole cells

Table 56 - Replicate and average data for whole cell experiment

Sample code	Sample name	Pt (ppb) per million cells	Average	Se (ppb) per million cells	Average
C1.1	Control 1 5M	0.056	0.058	0.816	0.865
C1.2	Control 2 5M	0.049		0.823	
C1.3	Control 3 5M	0.052		0.737	
C1.4	Control 4 10M	0.076		1.085	
M1.1	25uM MSA 1 hr 1 5M	0.148	0.080	5.531	5.966
M1.2	25uM MSA 1 hr 2 5M	0.048		5.627	
M1.3	25uM MSA 1 hr 3 5M	0.048		6.114	
M1.4	25uM MSA 1 hr 4 10M	0.075		6.592	
M2.1	50uM MSA 1 hr 1 5M	0.048	0.056	7.859	8.132
M2.2	50uM MSA 1 hr 2 5M	0.049		8.353	
M2.3	50uM MSA 1 hr 3 5M	0.051		7.499	
M2.4	50uM MSA 1 hr 4 10M	0.074		8.816	
M3.1	75uM MSA 1 hr 1 5M	0.047	0.055	8.849	9.269
M3.2	75uM MSA 1 hr 2 5M	0.050		9.713	
M3.3	75uM MSA 1 hr 3 5M	0.049		9.649	
M3.4	75uM MSA 1 hr 4 10M	0.074		8.865	
P1.1	Pt 1 hr 1 5M	7.014	6.711	0.898	0.866
P1.2	Pt 1 hr 2 5M	6.931		0.843	
P1.3	Pt 1 hr 3 5M	6.860		0.842	
P1.4	Pt 1 hr 4 10M	6.041		0.882	
MP1.1	25uM MSA Pt 1 hr 1 5M	4.745	4.777	6.509	6.260
MP1.2	25uM MSA Pt 1 hr 2 5M	4.941		6.725	
MP1.3	25uM MSA Pt 1 hr 4 10M	4.645		5.545	
MP2.1	50uM MSA Pt 1 hr 1 5M	5.135	5.047	6.995	7.134
MP2.2	50uM MSA Pt 1 hr 2 5M	5.146		7.260	
MP2.3	50uM MSA Pt 1 hr 3 5M	5.148		7.341	
MP2.4	50uM MSA Pt 1 hr 4 10M	4.758		6.940	
MP3.1	75uM MSA Pt 1 hr 1 5M	4.704	4.554	9.687	9.606
MP3.2	75uM MSA Pt 1 hr 2 5M	4.651		9.869	
MP3.3	75uM MSA Pt 1 hr 3 5M	4.674		9.877	
MP3.4	75uM MSA Pt 1 hr 4 10M	4.187		8.992	
M4.1	25uM MSA 24 hr 1 5M	0.048	0.054	4.718	4.871
M4.2	25uM MSA 24 hr 2 5M	0.048		4.950	
M4.3	25uM MSA 24 hr 3 5M	0.047		4.873	
M4.4	25uM MSA 24 hr 4 10M	0.074		4.943	
M5.1	50uM MSA 24 hr 1 5M	0.047	0.054	8.226	7.686
M5.2	50uM MSA 24 hr 2 5M	0.047		7.589	
M5.3	50uM MSA 24 hr 3 5M	0.048		7.495	
M5.4	50uM MSA 24 hr 4 10M	0.074		7.433	
M6.1	75uM MSA 24 hr1 5M	0.047	0.056	8.500	8.515
M6.2	75uM MSA 24 hr 2 5M	0.047		8.819	

M6.3	75uM MSA 24 hr 4 10M	0.074		8.226	
P2.1	Pt 24 hr 1 5M	5.163	4.687	0.853	0.855
P2.2	Pt 24 hr 2 5M	4.366		0.869	
P2.3	Pt 24 hr 3 5M	4.324		0.870	
P2.4	Pt 24 hr 4 10M	4.894		0.829	
MP4.1	25uM MSA Pt 24 hr 1 5M	2.805	2.745	5.256	5.226
MP4.2	25uM MSA Pt 24 hr 2 5M	2.905		5.387	
MP4.3	25uM MSA Pt 24 hr 3 5M	2.917		5.393	
MP4.4	25uM MSA Pt 24 hr 4 10M	2.353		4.865	
MP5.1	50uM MSA Pt 24 hr 1 5M	3.330	3.401	6.965	6.705
MP5.2	50uM MSA Pt 24 hr 2 5M	3.320		6.864	
MP5.3	50uM MSA Pt 24 hr 3 5M	3.403		6.974	
MP5.4	50uM MSA Pt 24 hr 4 10M	3.550		6.018	
MP6.1	75uM MSA Pt 24 hr 1 5M	3.548	3.447	6.756	6.746
MP6.2	75uM MSA Pt 24 hr 2 5M	3.562		6.877	
MP6.3	75uM MSA Pt 24 hr 3 5M	3.676		7.012	
MP6.4	75uM MSA Pt 24 hr 4 10M	3.003		6.337	

Single cell LA-ICP-MS:

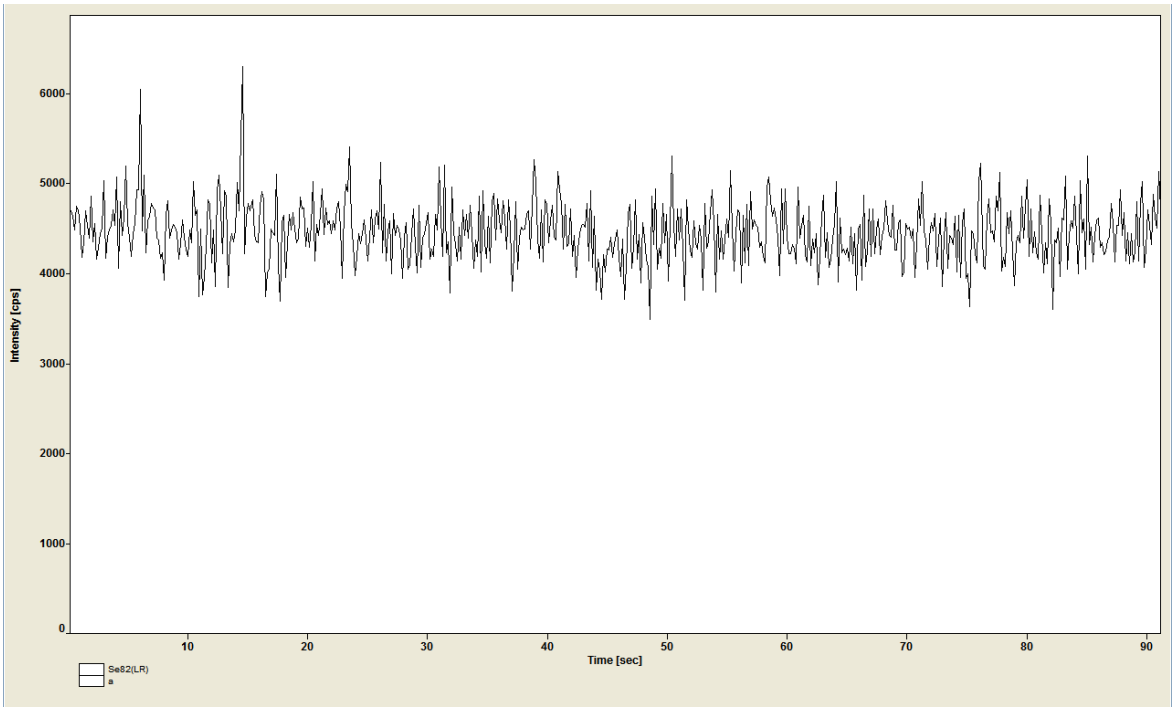

Figure 116 - Test ablation of 10 cells measuring ^{82}Se (LR)

Evidence of inconsistent ^{77}Se signals:

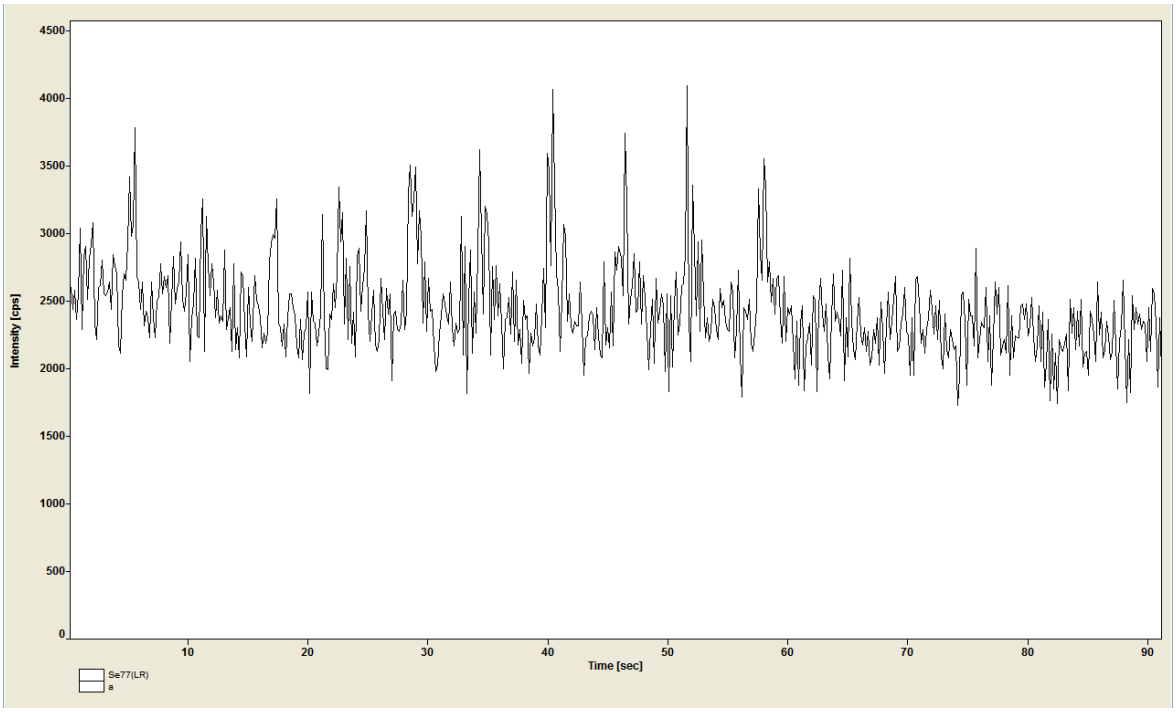

Figure 117 - Test ablation of 10 cells measuring ^{77}Se (LR)

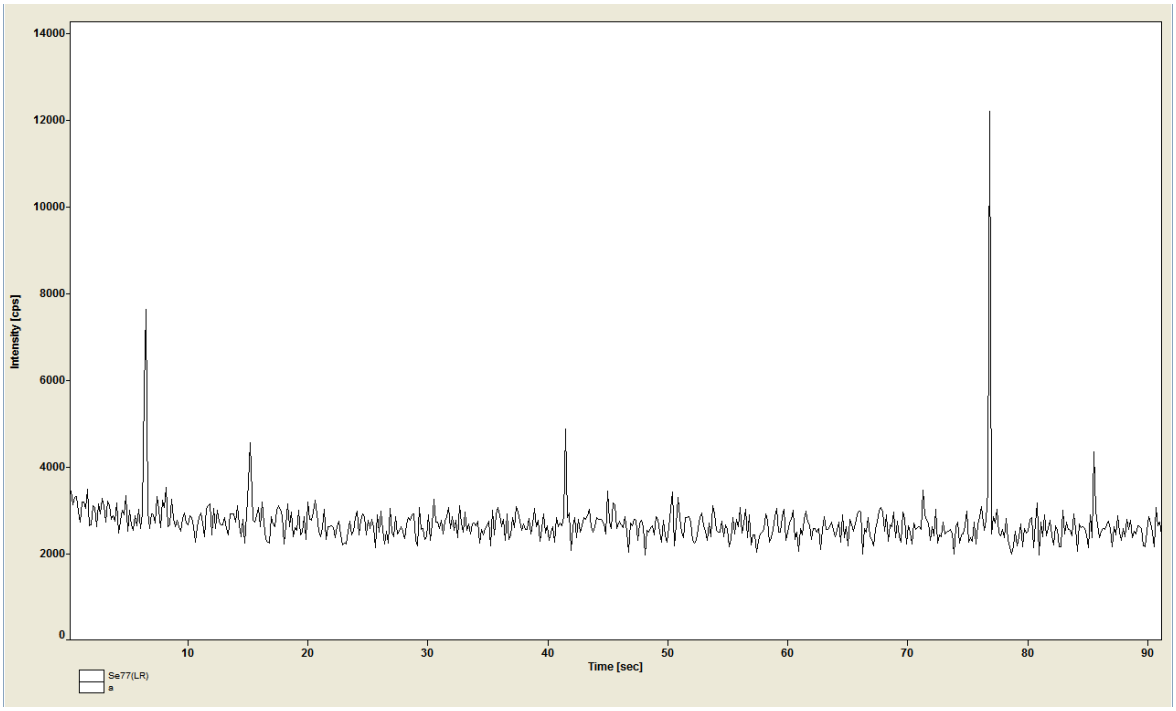

Figure 118 - Second test ablation of 10 cells measuring ^{77}Se (LR)

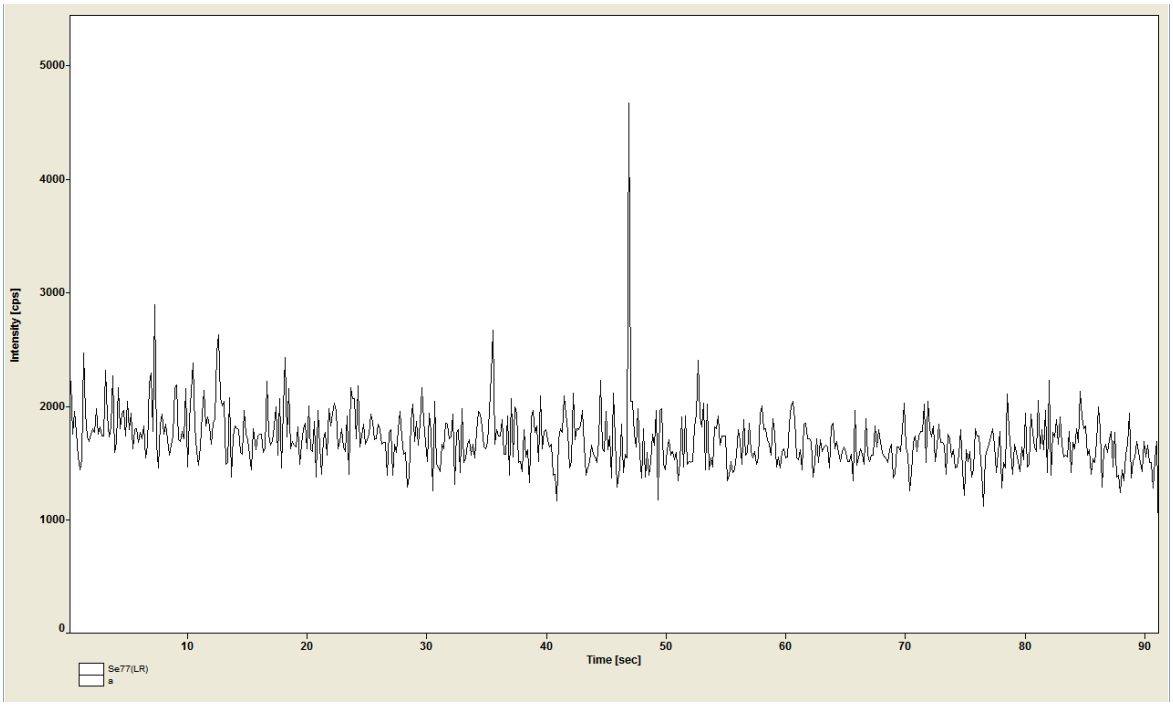

Figure 119 - Third test ablation of 10 cells measuring ^{77}Se (LR)

Slide background:

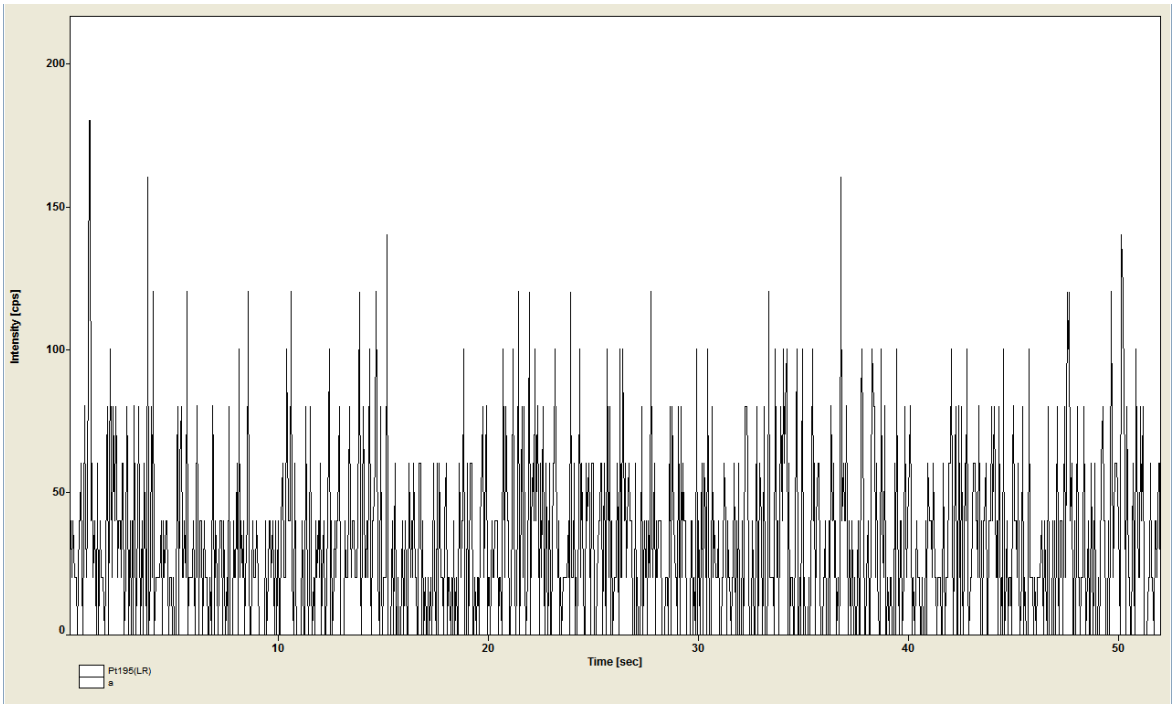

Figure 120 - ^{195}Pt slide background test ablation of 10 blank areas of slide

Platinum ablation results:

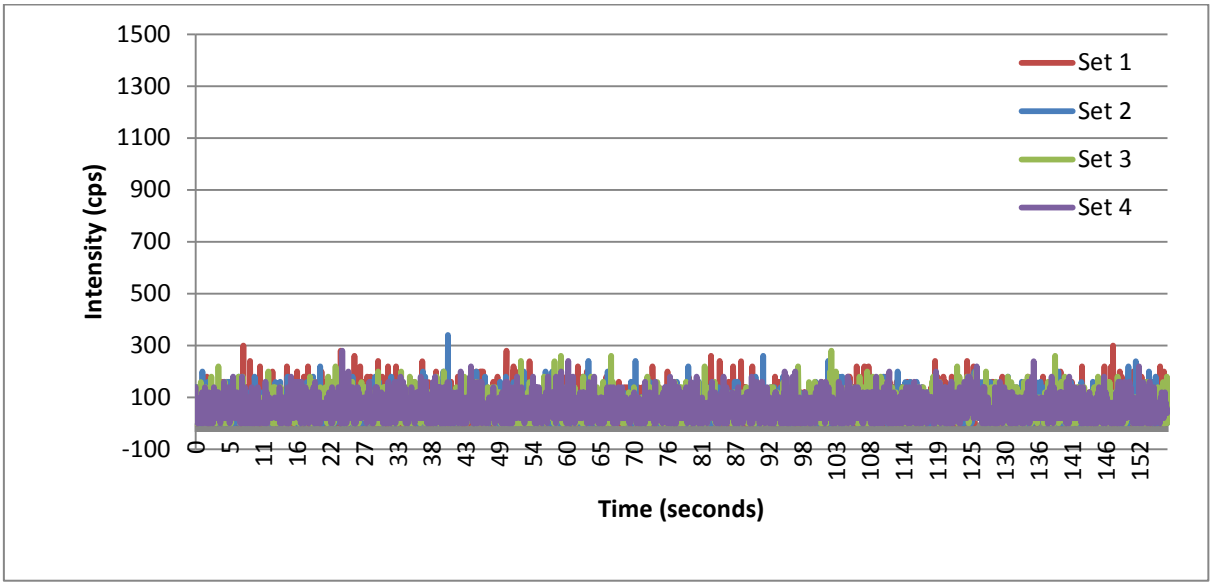

Figure 121 - Ablation of 100 (4 x 25) cells on control slide measuring ^{195}Pt

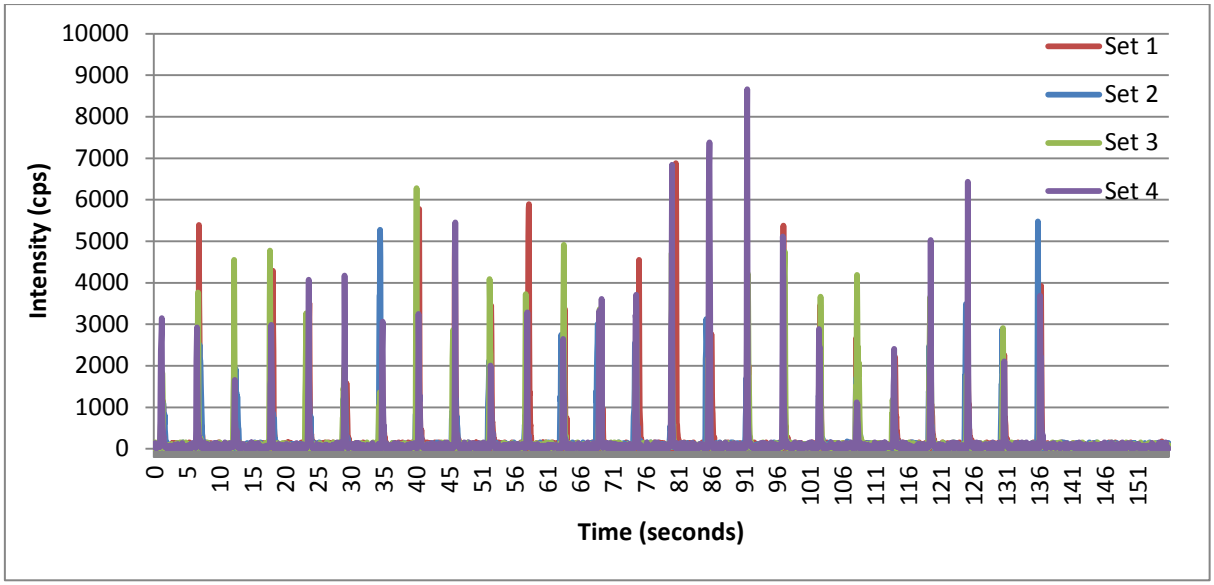

Figure 122 – Intensity of ^{195}Pt in 100 (4 x 25) ablated cells on slide containing cells exposed to 50 µM oxaliplatin with 1 hour recovery

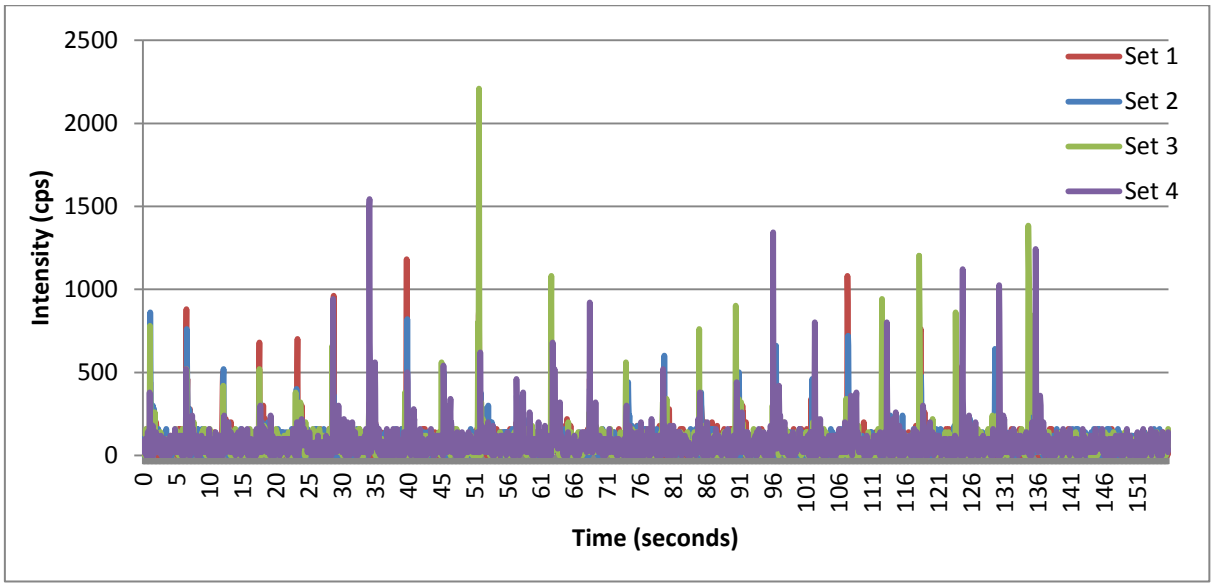

Figure 123 - Intensity of ^{195}Pt in 100 (4 x 25) ablated cells on slide containing cells exposed to 50 µM oxaliplatin and 75 µM MSA with 1 hour recovery

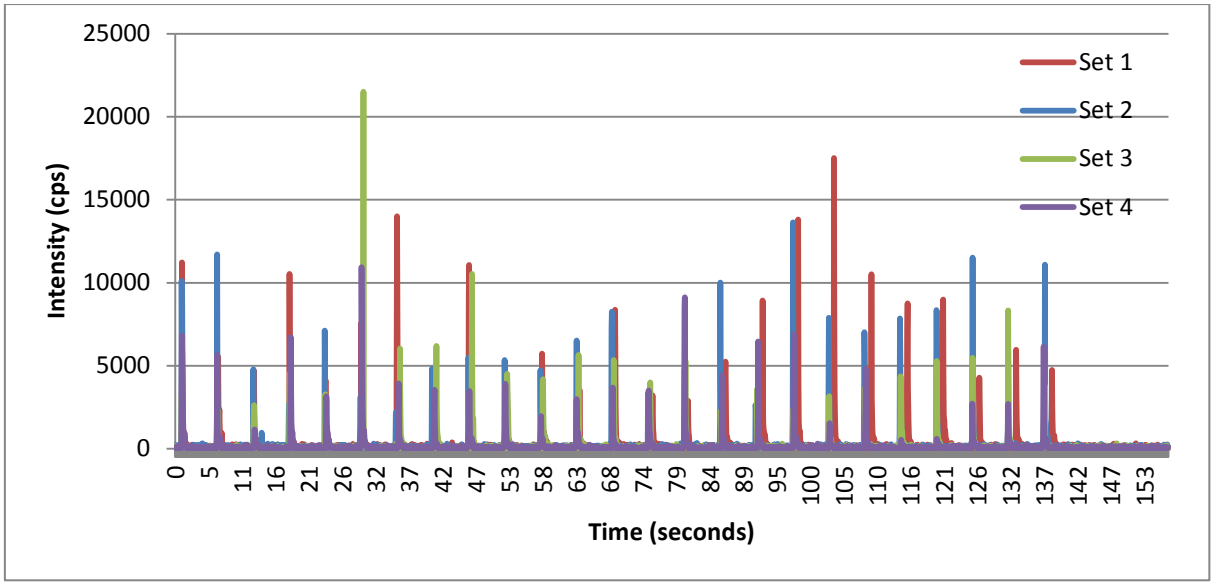

Figure 124 - Intensity of ^{195}Pt in 100 (4 x 25) ablated cells on slide containing cells exposed to 50 µM oxaliplatin with 1 hour recovery

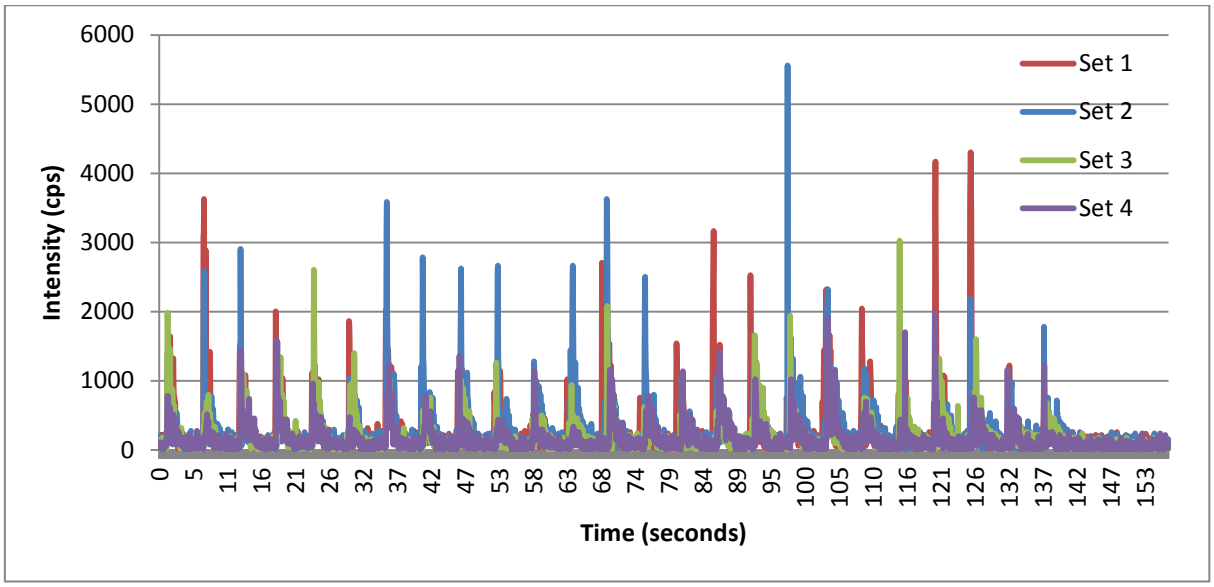

Figure 125 - Intensity of ^{195}Pt in 100 (4 x 25) ablated cells on slide containing cells exposed to 50 µM MSA with 24 hours recovery

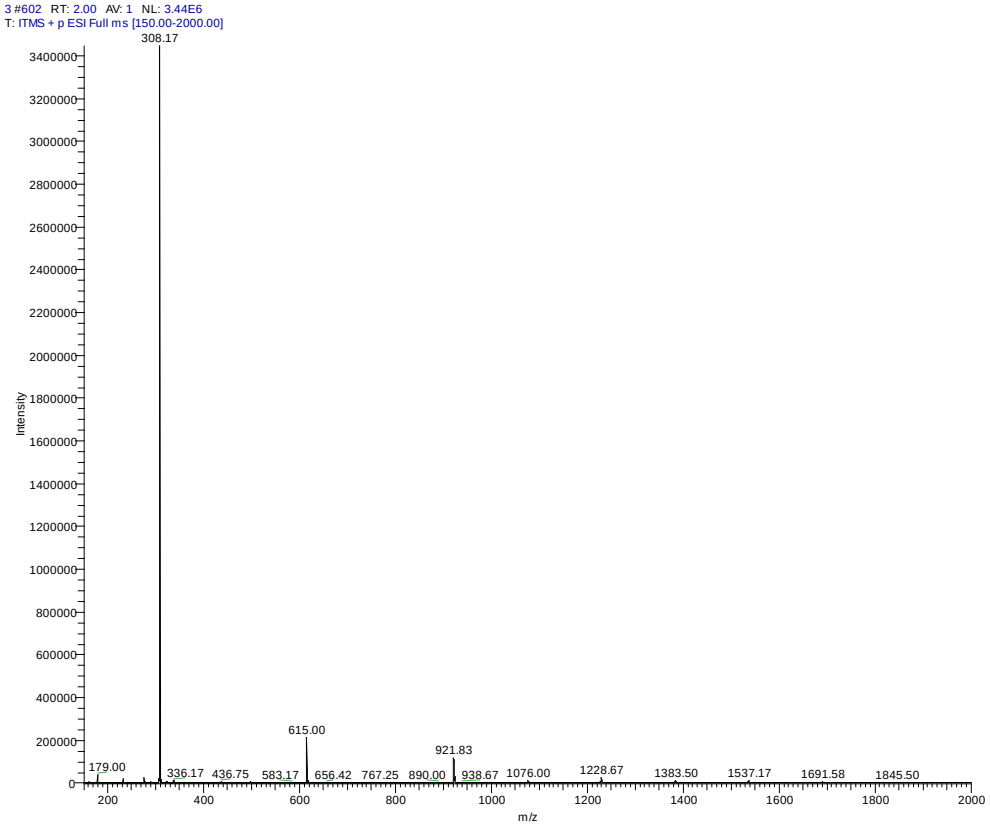

Figure 126 - Full mass spectrum for GSH solution

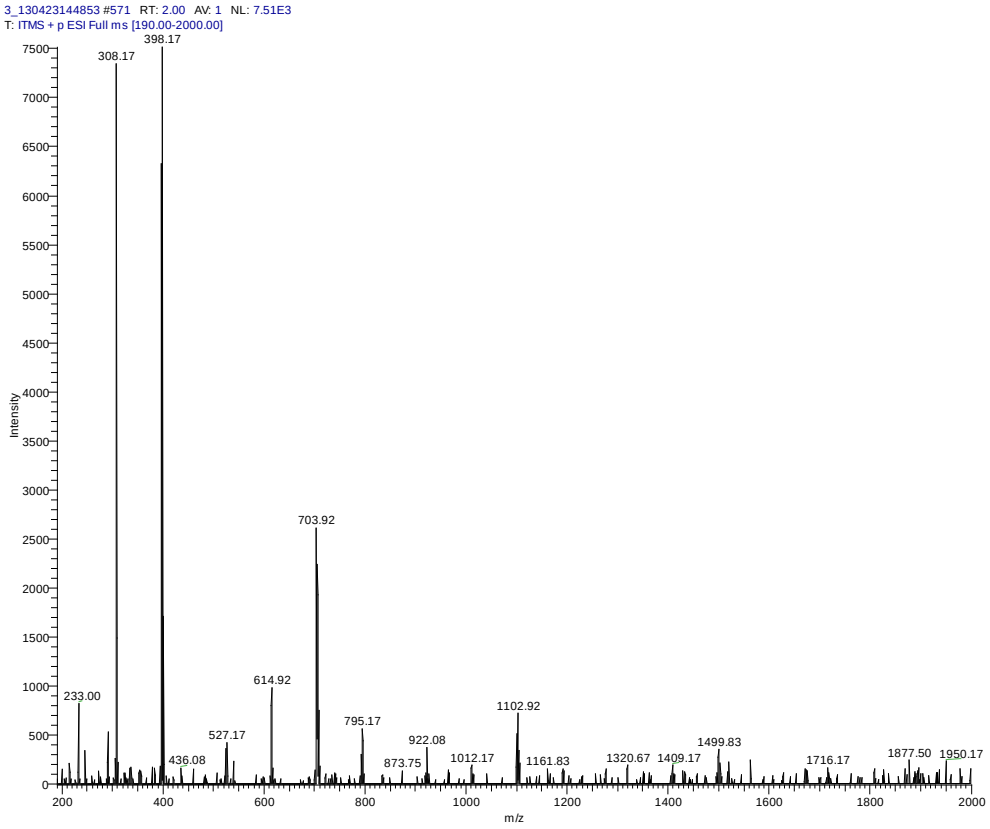

Figure 127 - Full mass spectrum for GSH:OxPt solution

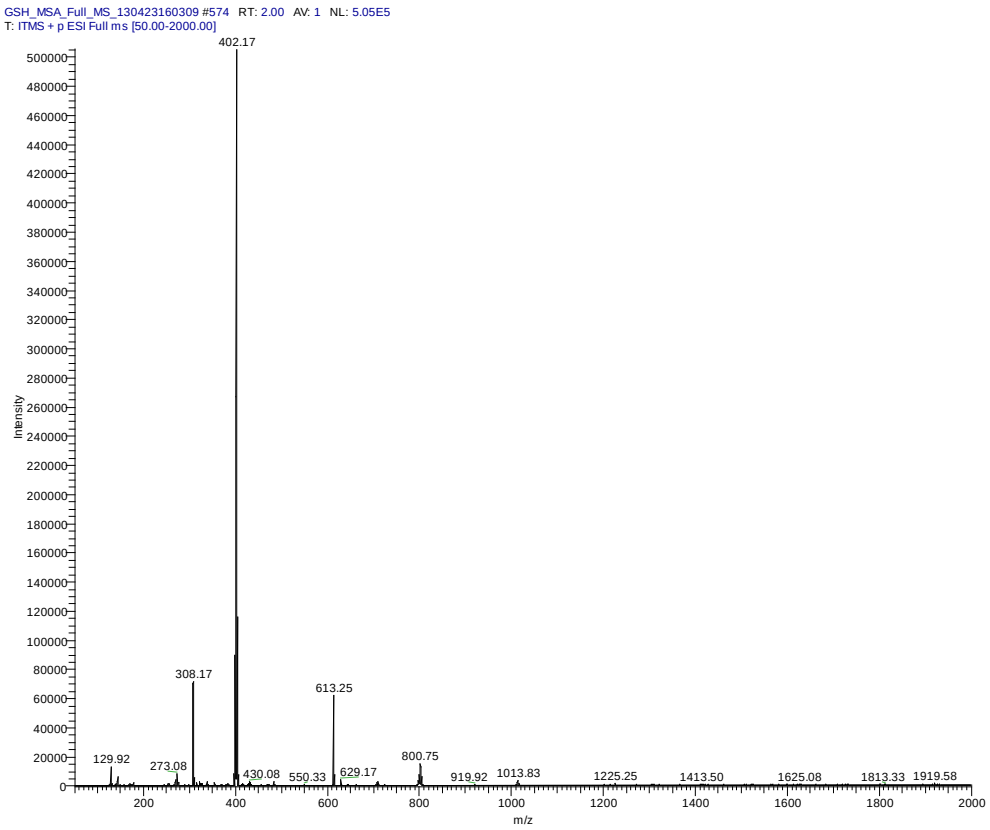

Figure 128 - Full mass spectrum for GSH:MSA solution

Appendix D – Published paper

The section contains a copy of the following paper, reproduced with the permission of Springer:

S. E. Taylor, J. P. Wood, G. D. D. Jones, A. L. Thomas, H. J. Reid and B. L. Sharp, A feasibility study of the use of saliva as an alternative to leukocytes as a source of DNA for the study of Pt-DNA adducts in cancer patients receiving platinum-based chemotherapy, *Anal. Bioanal. Chem*., 406 (2014), 8033-8036

Anal Bioanal Chem (2014) 406:8033–8036
DOI 10.1007/s00216-014-8274-x

NOTE

A feasibility study of the use of saliva as an alternative to leukocytes as a source of DNA for the study of Pt-DNA adducts in cancer patients receiving platinum-based chemotherapy

Sarah E. Taylor · Joanna P. Wood · Anne L. Thomas · George D. D. Jones · Helen J. Reid · Barry L. Sharp

Received: 4 August 2014 / Revised: 14 October 2014 / Accepted: 14 October 2014 / Published online: 6 November 2014

Abstract This note presents a comparison of the use of saliva versus leukocytes for the determination of Pt-DNA adducts obtained from patients undergoing platinum-based chemotherapy. Samples of both blood and saliva were taken pre- and post-treatment and were analysed via sector-field inductively coupled plasma mass spectrometry (SF-ICP-MS) to determine the level of Pt-DNA adducts formed. As expected, significant inter-patient variability was seen; however, a lack of correlation between the levels of adducts observed in saliva and blood samples was also observed (Pearson correlation coefficient r=−0.2598). A high yield of DNA was obtained from saliva samples, but significant difficulties were experienced in obtaining patient adherence to the saliva sampling procedure. In both leukocyte and saliva samples, not only was Pt from previous chemotherapy cycles detected, but the rapid appearance of Pt in the DNA was noted in both sample types 1 h after treatment.

Keywords ICP-MS · Oxaliplatin · Cisplatin · Clinical samples · Blood · Saliva · Pt-DNA adducts

S. E. Taylor · H. J. Reid · B. L. Sharp (✉)
Centre for Analytical Science, Department of Chemistry, Loughborough University, Loughborough LE11 3TU, UK
e-mail: B.L.Sharp@lboro.ac.uk

J. P. Wood · A. L. Thomas · G. D. D. Jones
Department of Cancer Studies and Molecular Medicine, Robert Kilpatrick Clinical Sciences Building, Leicester Royal Infirmary, University of Leicester, Leicester LE2 7LX, UK

Introduction

Since the first report of the chemotherapeutic action of cispatin (diamminedichloroplatinum(II)) in the late 1960s by Rosenberg, several new platinum-based drugs have come into use for the treatment of cancer, including oxaliplatin and carboplatin. Cisplatin and oxaliplatin form platinated intra-strand cross-links, primarily between two adjacent guanine bases or guanine-adenine bases, distorting the DNA structure and resulting in cell apoptosis if the damage is too great for repair [1].

The formation of these Pt-DNA adducts has been the focus of several studies. For example, Zayed et al. investigated the level of adducts in leukocyte samples, pre- and post-treatment at 1- and 4-h time points, in patients receiving platinum-based chemotherapy and also observed a level of carry-over of platinum between treatment cycles [2]. For such investigations, an alternative sampling method would be desirable as blood sampling requires trained personnel to obtain the sample as well as the need for rapid extraction of the leukocytes, so it is an unsuitable method for frequent sampling of patients unless they are hospitalised. The use of saliva would be advantageous as it is a non-invasive and more patient-friendly sampling technique and does not require trained personnel to obtain the sample. Furthermore, commercially available kits allow saliva sampling in the privacy of a patient's home and keep the sample stable for at least 5 years before the DNA needs to be extracted [3]. This study sets out to investigate the feasibility of using saliva as a viable alternative to blood sampling for quantitative investigation of the formation of platinum-associated DNA, "Pt-DNA adducts", in patients undergoing platinum-based chemotherapy. The data set presented is not designed to be statistically powered for clinical purposes, but rather to investigate the feasibility of using saliva samples.

Experimental

Materials

All chemicals and reagents used were purchased from Sigma (Poole, UK), unless otherwise stated. HNO_3 (70 %) was purchased from Romil Ltd. (Cambridge, UK). OG-500 saliva collection kits and PrepIT.L2P DNA extraction reagents were purchased from Oragene (Ontario, Canada), QIAGEN QiaAmp DNA Blood Mini Kit was purchased from Qiagen (Crawley, UK) and Ficoll-Paque PLUS from GE Healthcare (Chalfont, UK).

Collection of blood and saliva samples from patients

Informed consent was obtained from patients fulfilling the criteria stated on the ethical approval which was granted by the Leicestershire and Rutland Research Ethics Committee (no. 6106). Approximately 15 mL of blood and 2 mL saliva were collected from 10 patients undergoing platinum-based chemotherapy immediately prior to treatment and 1 h post treatment, with a further 24-h time point for saliva. The sampling time points were chosen for patient convenience, and therefore, a 24-h blood sampling time point was not possible (with the exception of patient number 34) and only saliva samples, which could be collected by the patient at home, were obtained. Samples were taken from patients on different cycles and on different combination treatment regimes, including epirubicin, oxaliplatin and capecitabine (EOX); 5-fluorouracil, folinic acid and oxaliplatin (FOLFOX); FOLFOX and bevacizumab (Bev); epirubicin, cisplatin and capecitabine (ECX); and cisplatin and etopside (Cis/etop).

Leukocyte isolation and DNA extraction

Blood samples were stored at room temperature in vials containing potassium EDTA (SARSTEDT, Germany), giving a concentration of 1.2–2 mg EDTA/mL of blood. The leukocytes from the blood samples were isolated as quickly as possible, typically within 2 h of the sample being taken. Leukocytes were extracted from the blood samples using Ficoll-Paque PLUS following the manufacturer's guidelines, before cell counting and separation into aliquots of 4–5 million cells/mL which were frozen at −80 °C in RPMI 1640 media containing 20 % FCS and 10 % DMSO. The QiaAmp DNA Blood Mini Kit was used in conjunction with an automated system for the DNA extraction, QIAcube (Qiagen, Crawley, UK). The manufacturer's guidelines were followed, and the extracted DNA was dissolved in water.

DNA extraction from saliva

Patients were asked to abstain from food, drink, chewing gum and smoking for 1 h prior to donating 2 mL of saliva. Patients were encouraged to allow the saliva to form naturally and to pool at the front of the mouth and then to deposit the sample as opposed to forcing the saliva production. A stabilising solution, provided as part of the kit, was added to the saliva and mixed thoroughly with the sample to give a final volume of 4 mL before a leak-free secure lid sealed the container. This allowed the final 24-h sample to be collected by the patient at home and posted securely back to the laboratory. Samples were stored upright at room temperature until the DNA extraction was performed as per the manufacturer's protocol. The extracted DNA was dissolved in water, and both saliva and leukocyte DNA were quantified using UV absorbance at 260 nm before being stored at −20 °C for analysis via sector-field inductively coupled plasma mass spectrometry (SF-ICP-MS).

Sample preparation, instrumentation and statistical analysis

A digestion method originally described by Yamada et al. and modified by Kerr was used on the extracted DNA samples for both blood and saliva [4, 5]. Briefly, 0.8 volume of 70 % nitric acid was added to 1 volume of sample and heated at 70 °C for 1 h; 0.8 volume of 30 % hydrogen peroxide was then added to each sample and heated at 70 °C for a further 4 h. The digested samples were evaporated to dryness while being heated at 70 °C under a gentle stream of oxygen-free nitrogen gas before being reconstituted in 350 μL of 2 % nitric acid with 0.5 ppb Eu internal standard [2]. Replicate analyses of blood and saliva samples were performed as follows: DNA extracted from three individual leukocyte aliquots were analysed, while, as only one saliva sample was obtained at each time point, the extracted DNA was divided into two equal aliquots before analysis.

The digested DNA clinical samples were analysed using SF-ICP-MS (Thermo Scientific, Element 2 XR, Bremen, Germany). The instrument was operated with a sample uptake rate of approximately 80 μL/min using a PFA nebuliser (PFA-ST Elemental Scientific, Omaha, USA) fitted to a cyclonic spray chamber (Glass Expansion, Victoria, Australia). Three elements, Eu, Pt and P, were determined in each sample by monitoring the singly charged isotopes $^{153}Eu^{+}$, $^{195}Pt^{+}$ (in low resolution) and $^{31}P^{+}$ (in medium resolution). The data obtained via SF-ICP-MS was used to calculate the level of Pt associated with DNA (Pt-DNA adducts per 10^6 nucleotides). Statistical analysis of the data was performed using the statistical package R (version 3.0.2).

Results

Figures 1 and 2 show the levels of Pt-DNA adducts measured in each sample at the different sampling time points for blood and saliva samples respectively for all 10 patients on the various platinum-based chemotherapies. Furthermore, the figures highlight the good reproducibility observed from the replicate samples. Figure 3 depicts the data for both sample types for easier comparison at each time point. A large amount of variability in adduct formation was observed between patients which can, at least in part, be attributed to the different combination treatments, doses and types of cancer of the patients in this study. Variability in adduct formation is well known, reflecting the fact that patient-specific factors are involved in determining how a patient reacts to chemotherapy treatment [2, 6].

A low number of Pt-DNA adducts were observed in each pre-drug infusion sample; however, this was expected as none of the patients were on their first cycle of chemotherapy and a carry-over effect between cycles has been seen before, indicating that a low level of platinum persists in the patients' DNA between cycles, which are typically between 2 and 3 weeks apart [2]. The level of Pt-DNA adducts increases rapidly after drug infusion, not only in leukocyte samples but also in the DNA derived from saliva. Figure 2 also shows that in some cases, the number of adducts at the 24-h time point had increased, when compared to the 1-h sample; in other patients, this level had decreased, potentially due to depurination, or an indication of adduct repair and/or enhanced drug clearance, an effect previously observed in leukocyte samples [1, 2, 7].

While it is clear from Figs. 1 and 2 that it was possible to measure Pt-DNA adducts in clinical blood and saliva samples, the number of adducts recorded for saliva and blood did not correlate. The pre- and 1-h post-infusion time points were directly compared, and the Pearson correlation coefficients were calculated as 0.6143 and −0.2598, respectively. While

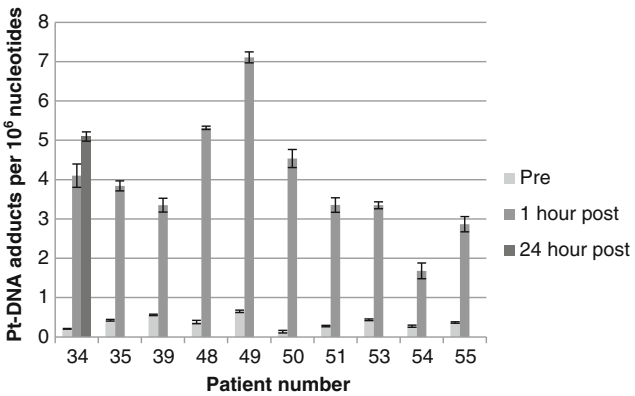

Fig. 1 Number of Pt-DNA adducts formed in pre- and post-infusion blood leukocyte samples in patients (error bars produced using 2×standard deviation, n=3)

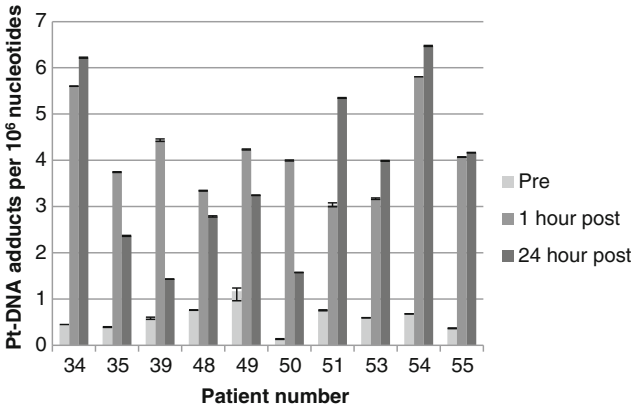

Fig. 2 Number of Pt-DNA adducts formed in pre- and post-infusion saliva samples in patients (error bars represent the range of sample values)

there was some positive correlation between the pre-infusion samples for the blood and saliva samples, there was a lack of correlation between the number of adducts per 10^6 nucleotides recorded in the 1-h post-infusion blood and saliva samples. However, with the exception of patient 54, the range of adducts per 10^6 nucleotides recorded was within a factor of 2 at the 1-h time point. Furthermore, a paired t test was performed on the two data sets, and the results were not found to be significantly different (t=0.32, t_{crit}=2.26, P=0.05). This suggests that any correlation in the data should have been evident, but the differences are distributed about the mean and show no obvious trend.

Previous work has shown that saliva DNA does not come exclusively from buccal epithelial cells, but rather is a mixture of a range of cells depending on the condition of the mouth. One study found that the number of leukocyte cells in saliva varied greatly from 2 to 136,000 cells/mL up to 1.1×10^6 cells/mL where a patient had an inflamed oral cavity [8]. Oral mucositis, a common side effect of chemotherapy experienced by some chemotherapy patients, can result in sores and ulcers, leading to an increased level of blood in the mouth. While the extent of oral mucositis is not fully known for the patient group in this investigation, it is feasible that a potential reason for the poor correlation observed in this study is due to an unknown and variable level of leukocyte contamination in each saliva sample, and potentially that the mechanism of the uptake of platinum by buccal cells is different to that of blood cells.

Only 10 patients were chosen for this investigation as this was an initial feasibility study to investigate whether saliva was a viable alternative to leukocyte sampling. The study was not extended to a larger patient cohort for two reasons: the lack of correlation with leukocyte data and poor patient compliance with the sampling protocol. While in theory the saliva kits were easy to use and could be used at home, frequently samples were returned incomplete (either too little saliva or stabilising solution not used) and, thus, could not be used as part of this study. Had the collection of samples met with

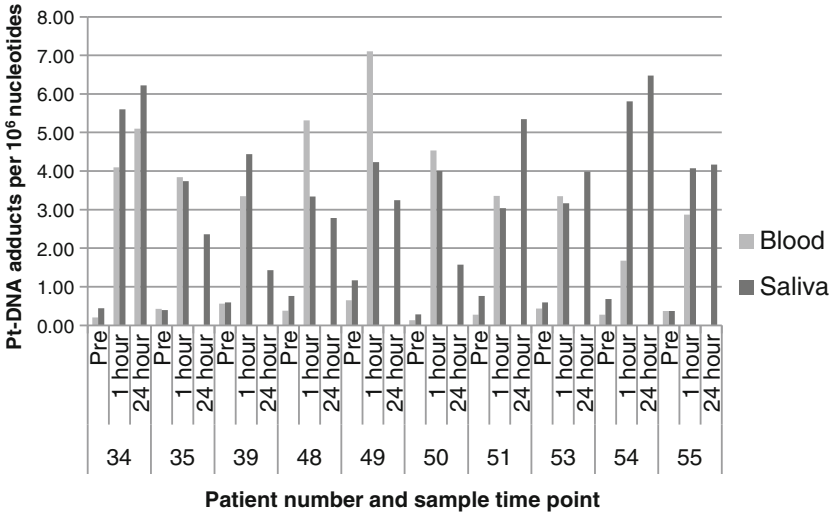

Fig. 3 Comparison of Pt-DNA adduct formation levels in saliva and leukocyte patient samples

greater patient acceptance, replicate samples would have been included in this study. A further difficulty is that samples should be from 'drool' and not 'forced' saliva, and so replicates at a single time point were not practical. Best results were obtained under supervision in the clinic but here blood sampling is a viable alternative.

For saliva to be considered as an alternative to leukocytes for the measurement of Pt-DNA adducts, it is clear that a cell-sorting step prior to the DNA extraction would be required; however, this would likely have to be done on a fresh saliva sample (i.e. not lysed and stabilised in a kit such as was the case in this experiment), and thus it is impractical for the collection of clinical samples at regular intervals outside the hospital environment. Ultimately, it may not have significant advantages over blood sampling.

Conclusion

This investigation has shown that it is possible to determine the level of Pt-DNA adducts in DNA extracted from both white blood cells and saliva clinical samples using SF-ICP-MS; significant inter-patient variability was observed in both data sets. Platinum from previous chemotherapy cycles was readily observed in both sample types. To the best of our knowledge, this was the first time that Pt-DNA adducts obtained from both saliva and leukocyte samples from the same patients have been successfully recorded by ICP-MS.

The purpose of this investigation was to determine whether saliva could be used as a less invasive and more patient-friendly sampling technique for the measurement of Pt-DNA adducts. DNA adducts were quantified, but the correlation found between sample types was poor. A surprising finding was the practical problems encountered in obtaining patient compliance with the saliva sampling protocol. More work is required before saliva can be validated as an alternative sample for the measurement of Pt-DNA adducts in cancer patients.

References

1. Brouwers EMM, Tibben MM, Pluim D, Rosing H, Boot H, Cats A, Schellens JHM, Beijnen JH (2008) Anal Bioanal Chem 391:577–585
2. Zayed A, Shoeib T, Taylor SE, Jones GDD, Thomas AL, Wood JP, Reid HJ, Sharp BL (2011) Int J Mass Spectrom 307:70–78
3. Long-term stability of DNA from saliva samples stored in the Oragene self-collection kit (2011) DNAgenotek Ltd http://www.dnagenotek.com/US/pdf/PD-WP-005.pdf. Accessed 15 Mar 2012
4. Yamada K, Kato N, Takagi A, Koi M, Hemm H (2005) Anal Bioanal Chem 382:1702–1707
5. Kerr SL (2008) PhD Thesis, Loughborough University
6. Harris CC (1989) Carcinogenesis 10:1563–1566
7. Weber G, Messerschmidt J, Pieck AC, Junker AM, Wehmeirer A, Jaedhe U (2004) Anal Bioanal Chem 380:54–58
8. Thiede C, Prange-Krex G, Freiberg-Richter J, Bornhauser M, Ehninger G (2000) Bone Marrow Transplant 25:575–577